Magnetic Resonance Imaging of the Paediatric Respiratory Tract

Magnetic Resonance Imaging van het ademhalingsstelsel bij kinderen

Bernadette Brigitte Louise Josephine Elders

Layout: Dennis Hendriks || ProefschriftMaken.nl
Cover: Studio Anne Ligtenberg
Printed by: ProefschriftMaken.nl

ISBN: 978-94-6423-710-8

The printing of this thesis was financially supported by:
Erasmus University Rotterdam, Department of Radiology and Nuclear Medicine Erasmus MC and ABN AMRO BANK N.V.

Magnetic Resonance Imaging of the Paediatric Respiratory Tract

Magnetic Resonance Imaging van het ademhalingsstelsel bij kinderen

Proefschrift

ter verkrijging van de graad van doctor aan de
Erasmus Universiteit Rotterdam
op gezag van de
rector magnificus

Prof. dr. A.L. Bredenoord

en volgens besluit van het College voor Promoties.
De openbare verdediging zal plaatsvinden op

dinsdag 10 mei 2022 om 10:30 uur

door

Bernadette Brigitte Louise Josephine Elders
geboren te Amsterdam

Erasmus University Rotterdam

Promotiecommissie

Promotor:	Prof. dr. H.A.W.M. Tiddens
Overige leden:	Prof. dr. J.G.J.V. Aerts Prof. dr. C.M. Schaefer - Prokop Dr. P.J.F.M. Merkus
Copromotor:	Dr. P. Ciet

Content

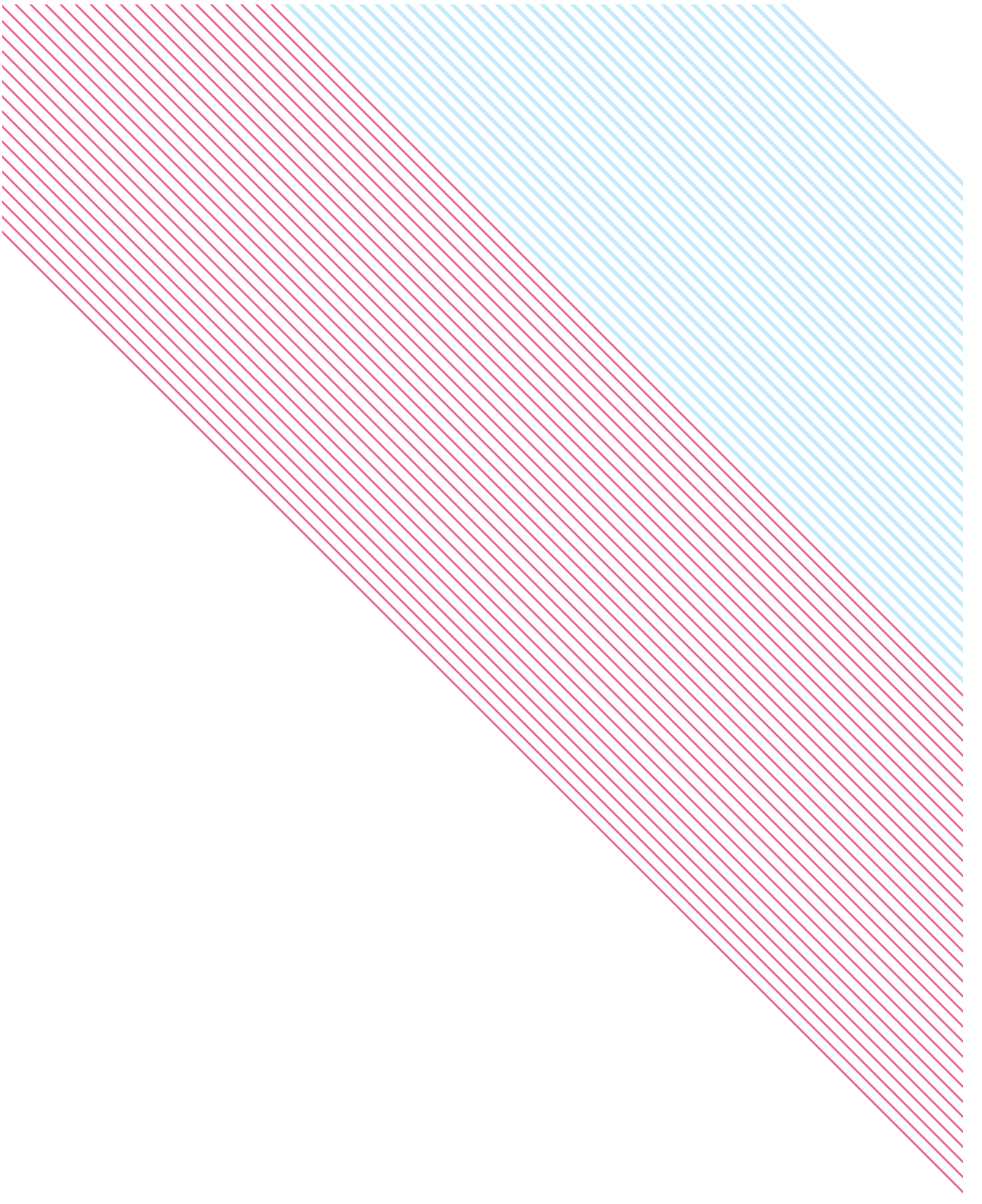

Chapter 1

General introduction

The respiratory tract plays a vital role in the body: facilitating the conduction and conditioning of air, phonation, swallowing and gas exchange. For this reason, diseases of the respiratory tract can have a great impact on the life of patients. Examples are frequent hospital admissions leading to school absenteeism, exercise intolerance leading to the inability to play with friends and dysphonia leading to declined mental health. Paediatric patients with diseases of the respiratory tract should therefore be closely monitored to identify those patients at risk for later morbidity, and in need of further follow up and/or treatment. Radiological imaging, in specific Magnetic Resonance Imaging (MRI), can play an important role in monitoring these patients. In this introduction we give an overview of three specific respiratory tract diseases: laryngotracheal stenosis (LTS), bronchopulmonary dysplasia (BPD) and congenital lung abnormalities (CLA). We will discuss the current monitoring options and we will highlight the opportunities and challenges of MRI for the follow up of respiratory tract diseases. With this introduction, the aims of this thesis are outlined.

The (diseased) paediatric respiratory tract

The respiratory tract can be divided into an upper and lower segment (figure 1).
The upper respiratory tract includes the nasal cavity, the pharynx and the larynx down to the subglottis. The upper respiratory tract is formed from the embryological pharyngeal apparatus between the 4th and 10th week of gestation. The larynx is formed by canalization of the sixth branchial arch, and if recanalization of this arch fails, a congenital atresia or stenosis can occur.(1) After birth the upper respiratory tract, and especially its mucosa, remains a structure sensitive to damage. An example of this susceptibility to damage is acquired LTS, occurring in up to 2% of patients after prolonged intubation and therefore mostly seen in prematurely born children, in which damage by a tracheal tube can cause stenosis of the larynx.(2-4)

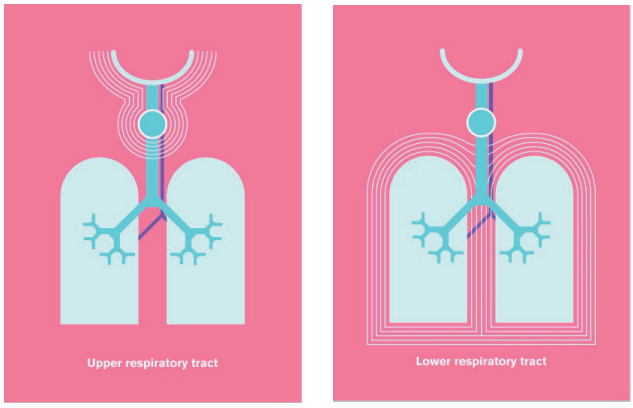

Figure 1: Schematic overview of the upper respiratory tract (left) with the thin lines highlighting the nasal cavity, pharynx and larynx and the lower respiratory tract (right) with the thin lines highlighting the trachea, bronchi and lungs. (*Studio Anne Ligtenberg*)

The lower respiratory tract consists of the trachea, bronchi and lung parenchyma. The trachea is formed from the embryological laryngotracheal tube, and from the respiratory bud. At the end of the laryngotracheal tube the lungs will form starting from the 4th week of gestation. Development of the lungs consists of four stages.(5, 6) During the pseudoglandular stage, between the 6th and 16th week of gestation, all the major components of the lower respiratory tract are formed except for those involved in gas exchange. During the canalicular stage, between 16 and 26 weeks of gestation, respiratory bronchioles and some vascularized terminal sacs are formed. During the terminal sac stage, between 26 weeks of gestation and birth, terminal sacs proliferate and develop a thin epithelium that enables gas exchange. During the alveolar stage, between 32 weeks of gestation and 8 years of age, the alveoli further mature to enable efficient gas exchange. If during any of these developmental stages an error occurs, CLA can develop. Common CLA are congenital pulmonary airway malformation (CPAM), bronchopulmonary sequestration (BPS), bronchial atresia (BA), bronchogenic cyst (BC) and congenital lobar overinflation (CLO)(figure 2).(7) In addition to CLA, pulmonary diseases can also develop before all developmental stages of the lung have been completed, for example when children are born prematurely. This is the case in BPD, where a combination of premature birth and exposure to mechanical ventilation can lead to altered and delayed development of normal alveoli and pulmonary vascularization.(5, 8)

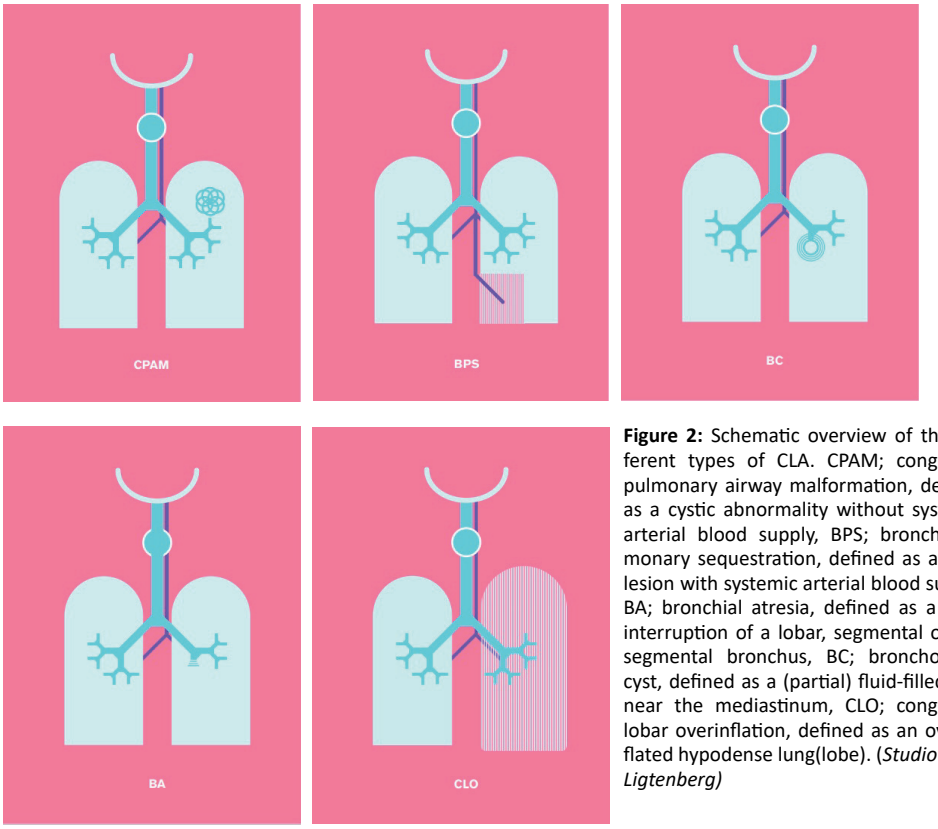

Figure 2: Schematic overview of the different types of CLA. CPAM; congenital pulmonary airway malformation, defined as a cystic abnormality without systemic arterial blood supply, BPS; bronchopulmonary sequestration, defined as a solid lesion with systemic arterial blood supply, BA; bronchial atresia, defined as a focal interruption of a lobar, segmental of sub segmental bronchus, BC; bronchogenic cyst, defined as a (partial) fluid-filled cyst near the mediastinum, CLO; congenital lobar overinflation, defined as an overinflated hypodense lung(lobe). (*Studio Anne Ligtenberg)*

The follow up of respiratory tract diseases

During the paediatric age, diseases of the upper and lower respiratory tract can result in a variety of symptoms, such as stridor, respiratory distress and dysphonia. Also more general symptoms, such as recurrent infections and failure to thrive can be related to respiratory tract diseases. In addition, these diseases can have consequences later in life including the risk of hospital admissions and inability to perform daily tasks, such as playing with friends and exercising, and therefore have a great impact on the quality of life of patients.(9-11) Long term follow up of respiratory tract diseases is essential to keep track of symptoms, to understand the course of disease and to identify those patients in need of treatment. However, since multiple problems can co-exist, follow up can be complex. For instance a premature born patient with an LTS and BPD or a patient with CLA and recurrent infections.

At the Erasmus MC- Sophia these complex respiratory tract diseases have a dedicated follow-up program within the paediatric chest centre (PCC) by a multidisciplinary team, consisting of general paediatricians, pulmonologists, othorhinolaryngologists, paediatric radiologists, surgeons, anaesthesiologists and neonatologists. In the PCC imaging plays an important role, providing vital information for the management team of the patient on both structure and function of the respiratory tract, which is important to understand the impact of the disease and to guide treatment.

Laryngotracheal stenosis

Follow up of diseases of the upper respiratory tract, such as LTS, is mainly done through physical examination, pulmonary function tests and laryngotracheoscopy, which is the current gold standard to assess the upper respiratory tract.(12) Although laryngotracheoscopy is broadly available and offers direct visualization of the upper respiratory tract, important downsides of this technique exist. A thorough laryngotracheoscopy requires general anaesthesia and the evaluation of the airways is subjective, as precise measurements are not possible. This results in poor intra and inter- observer agreement. Moreover, it is not possible to reproduce physiological manoeuvres (i.e. hyperventilation during exercise) during the procedure relevant for understanding the cause of the symptoms.(12-16) Direct laryngoscopy without anaesthesia is possible in the outpatient clinic, but can be an invasive procedure in children and only offers assessment limited up to the level of the vocal cords. Hence, objective quantitative data are lacking which are needed for a more efficient management of children with diseases of the upper respiratory tract. Because of the aforementioned limitations, laryngotracheoscopy is only used to evaluate the most severely affected patients. Extensive and less invasive imaging can be achieved by using Computed Tomography (CT). With CT it is possible to visualize the anatomy of the upper respiratory tract in three dimensions (3D) and it enables quantitative analyses of the airway geometry.(17-19) However, the use of CT to visualize the upper respiratory tract is hampered by exposure to ionizing radiation in the

sensitive region of the thyroid. The frequency and dose of medical radiation exposure in the thyroid region is associated with the risk of developing thyroid cancer.(20, 21) Moreover, CT has inferior tissue characterization and limited dynamic assessment with a small region of interest varying according to CT scanner, that provides even higher dose than static images. For these reasons, to date CT is scarcely used to image the paediatric upper respiratory tract.(19, 22)

Bronchopulmonary dysplasia

The gold standard for imaging the lower respiratory tract is chest CT, with the exception of the trachea which is still mostly imaged through bronchoscopy in children.(23-26) CT is a fast imaging method with good image resolution for several important lung structures, such as the airways and pulmonary vasculature. However, the cumulative exposure to ionizing radiation restricts the use of chest CT for paediatric patients, especially in those patients in need of frequent and long term follow up.(27)

At our institution patients with BPD are assessed with chest CT at 6 months and 8 years of age. Symptomatic patients can require more frequent imaging to detect possible complications and to monitor progression of structural abnormalities. However, the clinical usefulness of imaging in relatively asymptomatic BPD patients is still not clear. For these reasons, the European Respiratory Society (ERS) Task Force on long-term management of BPD has recently suggested the use of lung imaging only in subgroups of children with clinically severe BPD.(10)

Congenital lung abnormalities

CLA are prenatally diagnosed and followed up by ultrasonography and MRI.(28) The gold standard for postnatal follow up is CT. The ability of contrast enhancement to visualize the vascular component of CLA being the most important reason.(29) However, this comes at the cost of higher radiation exposure and risks related to contrast enhancement, such as the negative effect on brain development.(30) The downsides of CT for the follow up of CLA are even harder to justify as it remains unclear when CLA patients should undergo imaging to follow-up disease progression and possible complications, such as the rare malignant potential of some CLA entities.(31-33)

MRI of the paediatric respiratory tract

Despite all the aforementioned methods, an optimal method to image the paediatric respiratory tract is currently lacking. We believe that MRI could be a solution to this, as MRI offers the ability of combined evaluation of structure and function of the respiratory tract in a single examination. However, for the broad implementation of MRI for the follow up of paediatric respiratory tract disease, challenges have to be overcome (table 1).

Opportunities

Technical developments over the last decade have made MRI into a potential feasible imaging modality with many opportunities for the paediatric respiratory tract.(34, 35) Firstly, MRI is free of ionizing radiation and can therefore be used for repeated imaging, even in the youngest and most sensitive patients.(36)

Secondly, MRI has greater soft tissue characterization than CT. This could for instance be of aid in differentiating between normal lung and cystic lung tissue, and discriminating between consolidated lung and malignant degeneration of CLA.(37)

Thirdly, MRI enables combined structural and functional imaging in a single examination, such as dynamic imaging of the airways. This is highly relevant for diagnosing diseases, such as LTS and tracheobronchomalacia related to BPD, for which the severity may only be elicited during certain breathing manoeuvres.(38-40) In addition, imaging of ventilation and perfusion of the lungs is possible. Ventilation imaging can be done using oxygen MRI, hyperpolarized or fluorinated gas MRI.(41) Perfusion imaging can be done using contrast enhanced or non-contrast enhanced techniques. Though imaging with gases and contrast enhancement is limited by high hardware costs and patient safety issues related to contrast deposition, respectively.(30, 41, 42) Newly emerging techniques aim to overcome these limitations, such as Fourier Decomposition (FD), which enable safe imaging of ventilation and perfusion on MRI without using gaseous or intravenous contrast.(43, 44)

Table 1: MRI of the paediatric respiratory tract

Opportunities	Challenges
No ionizing radiation	Low proton density of the lung
Superior soft tissue contrast	Rapid signal decay
Dynamic imaging	Time consuming
Imaging of ventilation and perfusion	Sensitive to motion artefacts
Vascular imaging without contrast enhancement	Higher costs

Challenges

Before MRI can be used to image paediatric respiratory tract diseases, however, important challenges still have to be overcome.(34) First, visualization of lung tissue on MRI should be improved. Currently, the visualization of the lung on MRI is hard due to low proton density and rapid signal decay of lung tissue.(37) Although this is less of a problem for some lung pathologies, such as mucus and atelectasis, which have a higher proton density and are therefore easily identified on MRI. A solution may be offered by novel sequences such as ultra-short (UTE) and zero echo time (ZTE) which substantially improve the signal of the lung, with the additional benefit of it being silent sequences.(37, 45-48) These sequences show promising image quality comparable to CT for the imaging of neonatal BPD patients.

(49-54) However, these results refer to studies conducted at Cincinnati Children's Hospital and were obtained in a research setting with the use of a customized scanner, and can therefore not be directly applied in clinical practice using standard MRI scanners.

Second, MRI should be made less time consuming and (thereby) less sensitive to motion artefacts. Motion artefacts are a major problem within the paediatric population, due to their high respiratory and cardiac rate, especially in combination with respiratory disease.(34) But also fear for the MRI investigation and the exciting environment of the MRI can lead to poor patient compliance and general movement. Patient compliance and motion artefact reduction can be achieved by using anaesthesia or moderate sedation, but this is a burden for the patient and can induce atelectasis, which can obscure lung pathology.(34, 55-57) Below six months, anaesthesia can be omitted by using the feed-and-swaddle technique. With this technique the child is fed and tightly wrapped in a blanket or in a vacuum mattress, which restricts movement and which often results in the child sleeping through the imaging procedure.(58) From the age of six years and above, anaesthesia can be omitted by training and coaching of the child and parents and by distracting the patient during the MRI with an audio-visual system.(59, 60) Another option to reduce motion artefacts is to reduce scan time, leading to improved patient compliance. The duration of the MRI can be reduced by refinement of sequences as well as novel sequences, such as ZTE. This sequence has the additional benefit of being silent and therefore less burdensome for young patients.(37, 45-48, 50) Triggering and regularity of the respiration rate also has a great impact on scan time and motion artefacts.(34, 37) In older children respiratory regulation can be improved by spirometer guided training and scanning, to ensure that images are obtained at optimal breath hold in- and expiratory volume.(61) In addition, ECG triggering can reduce pulsation artefacts from the heart but it significantly increases scan time.(37)

A third challenge of chest MRI is the high cost, with a chest MRI costing two to three times more than a chest CT. Creating optimal MRI protocols will probably reduce costs of the MRI, but also novel techniques such as low-field MRI are promising for cost-reduction.(62, 63)

Aims of this thesis

Further exploration of these novel MRI techniques is needed before they can be used in clinical practice for the follow up of paediatric respiratory tract diseases. Therefore, the aim of this thesis is to contribute to the development and validation of MRI protocols to image structure and function of the paediatric respiratory tract. Hereby, we aim to apply these MRI techniques in the clinical practice of a tertiary care centre - the Erasmus MC –Sophia Children's hospital - for the diagnosis and management of paediatric patients with diseases related to the respiratory tract.

The specific primary aims of this thesis are:

The upper respiratory tract

- to develop an MRI protocol to image structure and function of the upper airways in children post open airway surgery for LTS

The lower respiratory tract

- to develop an MRI protocol to image structure and function in preterm born children with and without BPD at school age
- to develop an MRI protocol to image structure and function in neonatal BPD patients
- to develop an MRI protocol to image structure and function for the follow up of patients with CLA

And the secondary aim was:

- to compare these findings to clinical outcome in LTS, BPD and CLA

Outline of this thesis

Chapter 1 is an introduction to the research that is described in this thesis.

Part 1 The upper respiratory tract

Chapter 2 reviews previous studies on MRI of the upper airways in the paediatric population.

In **chapter 3,** we describe our results on static and dynamic MR imaging of the upper airways in paediatric and young adult patients after open airway surgery for LTS.

In **chapter 4,** we describe the use of a static and dynamic MRI of the vocal cords in paediatric and young adult patients after open airway surgery for LTS in relation to voice outcome.

Chapter 5 describes our findings on Computational Fluid Dynamic modelling of the upper airways in patients after LTS repair.

Part 2 The lower respiratory tract

Chapter 6 describes a pilot study in which we image the lungs of preterm born children with and without BPD at school age on MRI.

In **Chapter 7,** we make a comparison between the use of different short echo time sequences to image the lungs.

In **Chapter 8,** we describe our preliminary results on the development of a chest MRI protocol to image lung diseases in neonates.

Chapter 9 reviews previous studies on the reporting of CLA to develop a uniform radiological reporting system.

In **Chapter 10,** we present our findings on the development and implementation of a non-contrast chest MRI protocol for long term follow up of CLA, and our MRI findings to postnatal CT in a cohort of school age CLA patients .

References

1. Jefferson ND, Cohen AP, Rutter MJ. Subglottic stenosis. Semin Pediatr Surg. 2016;25(3):138-43.
2. Stephenson KA, Wyatt ME. Glottic stenosis. Semin Pediatr Surg. 2016;25(3):132-7.
3. Marston AP, White DR. Subglottic Stenosis. Clin Perinatol. 2018;45(4):787-804.
4. Walner DL, Loewen MS, Kimura RE. Neonatal subglottic stenosis--incidence and trends. Laryngoscope. 2001;111(1):48-51.
5. Smith LJ, McKay KO, van Asperen PP, Selvadurai H, Fitzgerald DA. Normal development of the lung and premature birth. Paediatr Respir Rev. 2010;11(3):135-42.
6. Mullassery D, Smith NP. Lung development. Semin Pediatr Surg. 2015;24(4):152-5.
7. Wong KKY, Flake AW, Tibboel D, Rottier RJ, Tam PKH. Congenital pulmonary airway malformation: advances and controversies. Lancet Child Adolesc Health. 2018;2(4):290-7.
8. Baraldi E, Filippone M. Chronic lung disease after premature birth. N Engl J Med. 2007;357(19):1946-55.
9. Pullens B, Dulfer K, Buysse CM, Hoeve LJ, Timmerman MK, Joosten KF. Long-term quality of life in children after open airway surgery for laryngotracheal stenosis. Int J Pediatr Otorhinolaryngol. 2016;84:88-93.
10. Duijts L, van Meel ER, Moschino L, Baraldi E, Barnhoorn M, Bramer WM, et al. European Respiratory Society guideline on long-term management of children with bronchopulmonary dysplasia. Eur Respir J. 2020;55(1).
11. Hijkoop A, van Schoonhoven MM, van Rosmalen J, Tibboel D, van der Cammen-van Zijp MHM, Pijnenburg MW, et al. Lung function, exercise tolerance, and physical growth of children with congenital lung malformations at 8 years of age. Pediatr Pulmonol. 2019;54(8):1326-34.
12. Monnier P. Pediatric Airway Surgery Management of Laryngotracheal Stenosis in Infants and Children. Berlin, Heidelberg: Springer Berlin Heidelberg; 2011.
13. Balakrishnan K, Sidell DR, Bauman NM, Bellia-Munzon GF, Boesch RP, Bromwich M, et al. Outcome measures for pediatric laryngotracheal reconstruction: International consensus statement. Laryngoscope. 2019;129(1):244-55.
14. Parkes WJ, Propst EJ. Advances in the diagnosis, management, and treatment of neonates with laryngeal disorders. Semin Fetal Neonatal Med. 2016;21(4):270-6.
15. van der Pol RJ, Singendonk MM, Konig AM, Hoeve H, Kammeijer Q, Pullens B, et al. Development of the reflux finding score for infants and its observer agreement. J Pediatr. 2014;165(3):479-84.
16. Singendonk MM, Pullens B, van Heteren JA, de Gier HH, Hoeve HL, Konig AM, et al. Reliability of the reflux finding score for infants in flexible versus rigid laryngoscopy. Int J Pediatr Otorhinolaryngol. 2016;86:37-42.
17. Becker M, Burkhardt K, Dulguerov P, Allal A. Imaging of the larynx and hypopharynx. Eur J Radiol. 2008;66(3):460-79.
18. Lin EL, Bock JM, Zdanski CJ, Kimbell JS, Garcia GJM. Relationship between degree of obstruction and airflow limitation in subglottic stenosis. Laryngoscope. 2018;128(7):1551-7.

19. Zdanski C, Davis S, Hong Y, Miao D, Quammen C, Mitran S, et al. Quantitative assessment of the upper airway in infants and children with subglottic stenosis. Laryngoscope. 2016;126(5):1225-31.
20. Mazonakis M, Tzedakis A, Damilakis J, Gourtsoyiannis N. Thyroid dose from common head and neck CT examinations in children: is there an excess risk for thyroid cancer induction? Eur Radiol. 2007;17(5):1352-7.
21. Lubin JH, Adams MJ, Shore R, Holmberg E, Schneider AB, Hawkins MM, et al. Thyroid Cancer Following Childhood Low-Dose Radiation Exposure: A Pooled Analysis of Nine Cohorts. J Clin Endocrinol Metab. 2017;102(7):2575-83.
22. Huang BY, Solle M, Weissler MC. Larynx: anatomic imaging for diagnosis and management. Otolaryngol Clin North Am. 2012;45(6):1325-61.
23. Lee EY, Restrepo R, Dillman JR, Ridge CA, Hammer MR, Boiselle PM. Imaging evaluation of pediatric trachea and bronchi: systematic review and updates. Semin Roentgenol. 2012;47(2):182-96.
24. van Straten M, Brody AS, Ernst C, Guillerman RP, Tiddens H, Nagle SK. Guidance for computed tomography (CT) imaging of the lungs for patients with cystic fibrosis (CF) in research studies. J Cyst Fibros. 2019.
25. van Mastrigt E, Logie K, Ciet P, Reiss IK, Duijts L, Pijnenburg MW, et al. Lung CT imaging in patients with bronchopulmonary dysplasia: A systematic review. Pediatr Pulmonol. 2016;51(9):975-86.
26. Oppenheim C, Mamou-Mani T, Sayegh N, de Blic J, Scheinmann P, Lallemand D. Bronchopulmonary dysplasia: value of CT in identifying pulmonary sequelae. AJR Am J Roentgenol. 1994;163(1):169-72.
27. Sodhi KS, Lee EY. What all physicians should know about the potential radiation risk that computed tomography poses for paediatric patients. Acta Paediatr. 2014;103(8):807-11.
28. Stocker LJ, Wellesley DG, Stanton MP, Parasuraman R, Howe DT. The increasing incidence of foetal echogenic congenital lung malformations: an observational study. Prenat Diagn. 2015;35(2):148-53.
29. Baez JC, Ciet P, Mulkern R, Seethamraju RT, Lee EY. Pediatric Chest MR Imaging: Lung and Airways. Magn Reson Imaging Clin N Am. 2015;23(2):337-49.
30. Gulani V, Calamante F, Shellock FG, Kanal E, Reeder SB, International Society for Magnetic Resonance in M. Gadolinium deposition in the brain: summary of evidence and recommendations. Lancet Neurol. 2017;16(7):564-70.
31. Casagrande A, Pederiva F. Association between Congenital Lung Malformations and Lung Tumors in Children and Adults: A Systematic Review. J Thorac Oncol. 2016;11(11):1837-45.
32. Stanton M. The argument for a non-operative approach to asymptomatic lung lesions. Semin Pediatr Surg. 2015;24(4):183-6.
33. Singh R, Davenport M. The argument for operative approach to asymptomatic lung lesions. Semin Pediatr Surg. 2015;24(4):187-95.

34. Ciet P, Tiddens HA, Wielopolski PA, Wild JM, Lee EY, Morana G, et al. Magnetic resonance imaging in children: common problems and possible solutions for lung and airways imaging. Pediatr Radiol. 2015;45(13):1901-15.
35. Hatabu H, Ohno Y, Gefter WB, Parraga G, Madore B, Lee KS, et al. Expanding Applications of Pulmonary MRI in the Clinical Evaluation of Lung Disorders: Fleischner Society Position Paper. Radiology. 2020;297(2):286-301.
36. Miglioretti DL, Johnson E, Williams A, Greenlee RT, Weinmann S, Solberg LI, et al. The use of computed tomography in pediatrics and the associated radiation exposure and estimated cancer risk. JAMA Pediatr. 2013;167(8):700-7.
37. Sodhi KS, Ciet P, Vasanawala S, Biederer J. Practical protocol for lung magnetic resonance imaging and common clinical indications. Pediatr Radiol. 2021:1-17.
38. Faust RA, Remley KB, Rimell FL. Real-time, cine magnetic resonance imaging for evaluation of the pediatric airway. Laryngoscope. 2001;111(12):2187-90.
39. Ciet P, Boiselle PM, Heidinger B, Andrinopoulou ER, O'Donnel C, Alsop DC, et al. Cine MRI of Tracheal Dynamics in Healthy Volunteers and Patients With Tracheobronchomalacia. AJR Am J Roentgenol. 2017;209(4):757-61.
40. Gunatilaka CC, Hysinger EB, Schuh A, Gandhi DB, Higano NS, Xiao Q, et al. Neonates With Tracheomalacia Generate Auto-Positive End-Expiratory Pressure via Glottis Closure. Chest. 2021.
41. Kruger SJ, Nagle SK, Couch MJ, Ohno Y, Albert M, Fain SB. Functional imaging of the lungs with gas agents. J Magn Reson Imaging. 2016;43(2):295-315.
42. Tiddens H, Kuo W, van Straten M, Ciet P. Paediatric lung imaging: the times they are a-changin'. Eur Respir Rev. 2018;27(147).
43. Veldhoen S, Weng AM, Knapp J, Kunz AS, Stäb D, Wirth C, et al. Self-gated Non-Contrast-enhanced Functional Lung MR Imaging for Quantitative Ventilation Assessment in Patients with Cystic Fibrosis. Radiology. 2017;283(1):242-51.
44. Bauman G, Scholz A, Rivoire J, Terekhov M, Friedrich J, de Oliveira A, et al. Lung ventilation- and perfusion-weighted Fourier decomposition magnetic resonance imaging: in vivo validation with hyperpolarized 3He and dynamic contrast-enhanced MRI. Magn Reson Med. 2013;69(1):229-37.
45. Gibiino F, Sacolick L, Menini A, Landini L, Wiesinger F. Free-breathing, zero-TE MR lung imaging. Magma. 2015;28(3):207-15.
46. Roach DJ, Cremillieux Y, Fleck RJ, Brody AS, Serai SD, Szczesniak RD, et al. Ultrashort Echo-Time Magnetic Resonance Imaging Is a Sensitive Method for the Evaluation of Early Cystic Fibrosis Lung Disease. Ann Am Thorac Soc. 2016;13(11):1923-31.
47. Dournes G, Menut F, Macey J, Fayon M, Chateil JF, Salel M, et al. Lung morphology assessment of cystic fibrosis using MRI with ultra-short echo time at submillimeter spatial resolution. Eur Radiol. 2016;26(11):3811-20.

48. Bae K, Jeon KN, Hwang MJ, Lee JS, Ha JY, Ryu KH, et al. Comparison of lung imaging using three-dimensional ultrashort echo time and zero echo time sequences: preliminary study. Eur Radiol. 2019;29(5):2253-62.
49. Critser PJ, Higano NS, Tkach JA, Olson ES, Spielberg DR, Kingma PS, et al. Cardiac MRI Evaluation of Neonatal Bronchopulmonary Dysplasia Associated Pulmonary Hypertension. Am J Respir Crit Care Med. 2019.
50. Hahn AD, Higano NS, Walkup LL, Thomen RP, Cao X, Merhar SL, et al. Pulmonary MRI of neonates in the intensive care unit using 3D ultrashort echo time and a small footprint MRI system. J Magn Reson Imaging. 2017;45(2):463-71.
51. Higano NS, Fleck RJ, Spielberg DR, Walkup LL, Hahn AD, Thomen RP, et al. Quantification of neonatal lung parenchymal density via ultrashort echo time MRI with comparison to CT. J Magn Reson Imaging. 2017;46(4):992-1000.
52. Higano NS, Hahn AD, Tkach JA, Cao X, Walkup LL, Thomen RP, et al. Retrospective respiratory self-gating and removal of bulk motion in pulmonary UTE MRI of neonates and adults. Magn Reson Med. 2017;77(3):1284-95.
53. Higano NS, Spielberg DR, Fleck RJ, Schapiro AH, Walkup LL, Hahn AD, et al. Neonatal Pulmonary Magnetic Resonance Imaging of Bronchopulmonary Dysplasia Predicts Short-Term Clinical Outcomes. Am J Respir Crit Care Med. 2018;198(10):1302-11.
54. Walkup LL, Tkach JA, Higano NS, Thomen RP, Fain SB, Merhar SL, et al. Quantitative Magnetic Resonance Imaging of Bronchopulmonary Dysplasia in the Neonatal Intensive Care Unit Environment. Am J Respir Crit Care Med. 2015;192(10):1215-22.
55. Liszewski MC, Ciet P, Lee EY. MR Imaging of Lungs and Airways in Children:: Past and Present. Magn Reson Imaging Clin N Am. 2019;27(2):201-25.
56. Lee JH, Zhang J, Wei L, Yu SP. Neurodevelopmental implications of the general anesthesia in neonate and infants. Exp Neurol. 2015;272:50-60.
57. Barton K, Nickerson JP, Higgins T, Williams RK. Pediatric anesthesia and neurotoxicity: what the radiologist needs to know. Pediatr Radiol. 2018;48(1):31-6.
58. Knudsen LM, Moen A. Practical planning to maintain premature infants' safety during magnetic resonance imaging: a systematic review. Adv Neonatal Care. 2015;15(1):23-37; quiz E1-2.
59. Harned RK, 2nd, Strain JD. MRI-compatible audio/visual system: impact on pediatric sedation. Pediatr Radiol. 2001;31(4):247-50.
60. Lemaire C, Moran GR, Swan H. Impact of audio/visual systems on pediatric sedation in magnetic resonance imaging. J Magn Reson Imaging. 2009;30(3):649-55.
61. Salamon E, Lever S, Kuo W, Ciet P, Tiddens HA. Spirometer guided chest imaging in children: It is worth the effort! Pediatr Pulmonol. 2017;52(1):48-56.
62. Campbell-Washburn AE, Ramasawmy R, Restivo MC, Bhattacharya I, Basar B, Herzka DA, et al. Opportunities in Interventional and Diagnostic Imaging by Using High-Performance Low-Field-Strength MRI. Radiology. 2019;293(2):384-93.
63. Campbell-Washburn AE, Suffredini AF, Chen MY. High-Performance 0.55-T Lung MRI in Patient with COVID-19 Infection. Radiology. 2021;299(2):E246-E7.

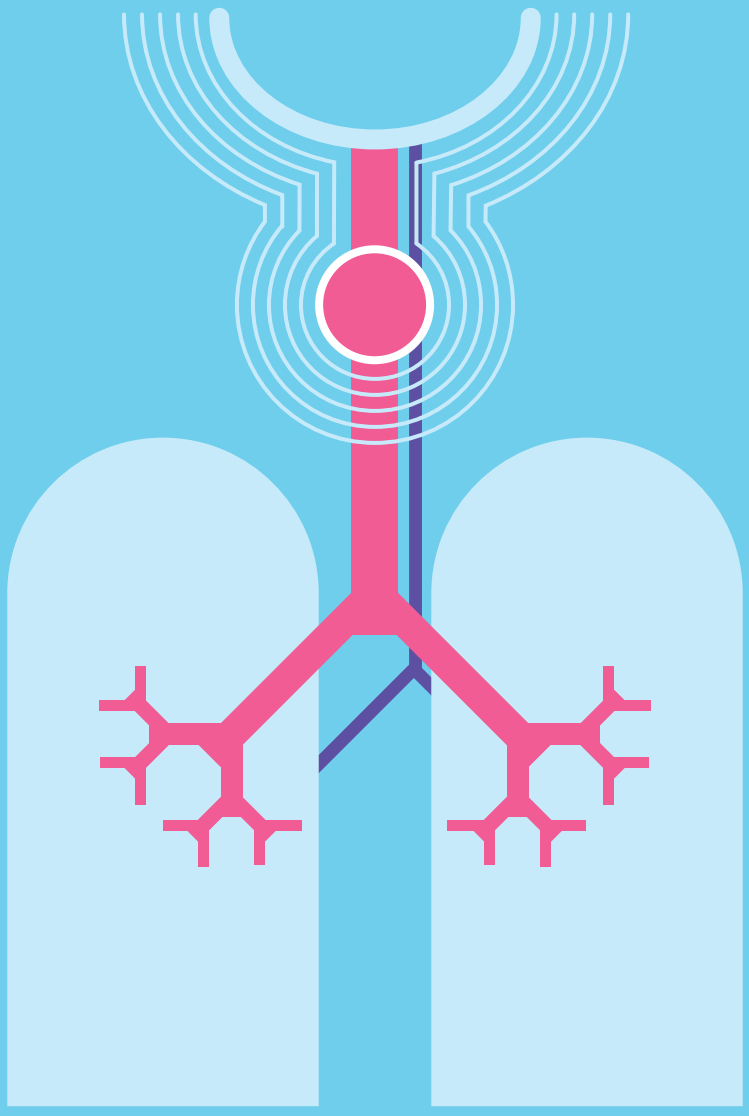

Upper respiratory tract

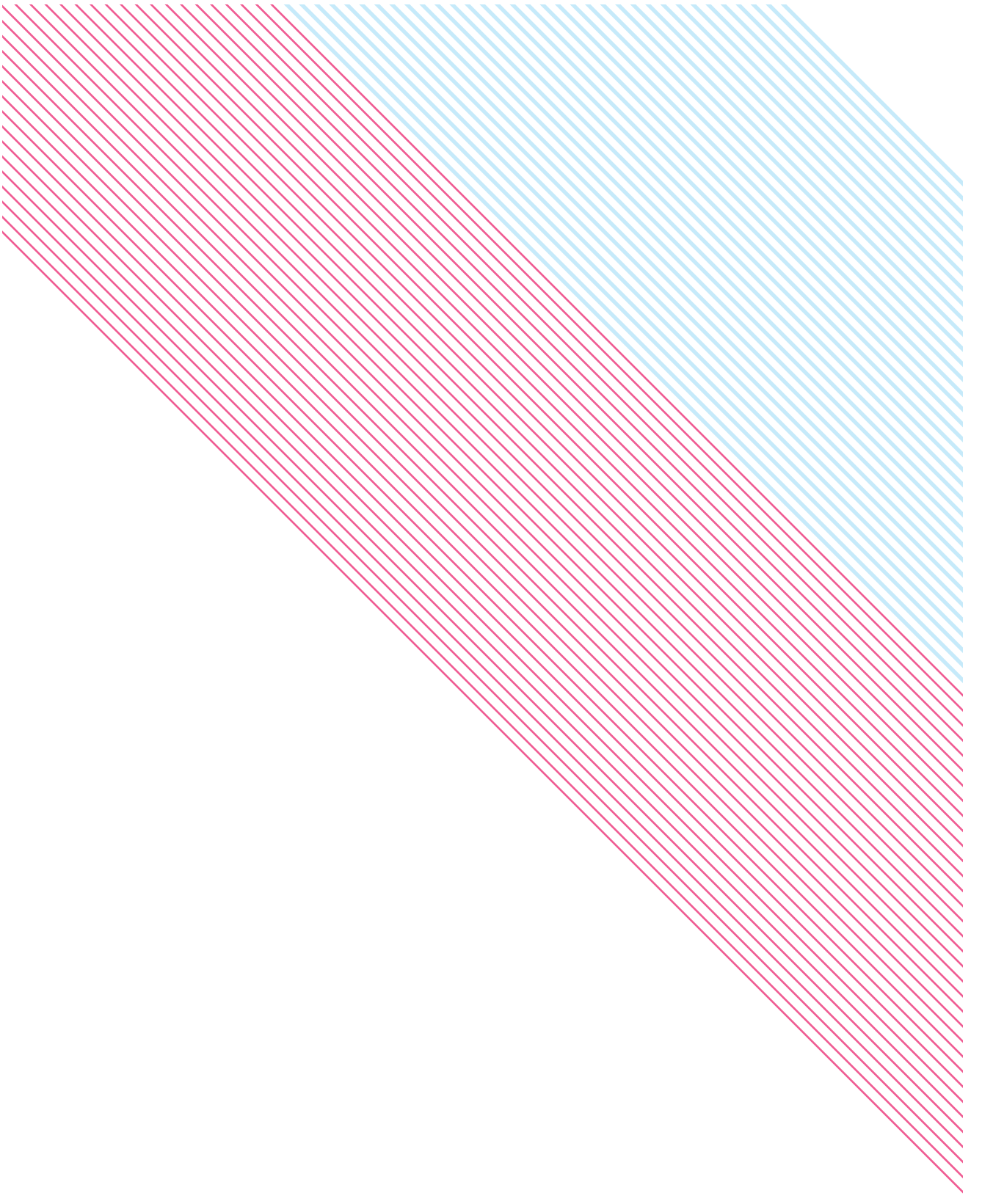

Chapter 2

Magnetic resonance imaging of the larynx in the paediatric population: a systematic review

Bernadette BLJ Elders, Sergei M Hermelijn, Harm AWM Tiddens, Bas Pullens, Piotr A Wielopolski, Pierluigi Ciet

Pediatric Pulmonology 2019;54(4):478-486

Abstract

Background: Magnetic Resonance Imaging (MRI) techniques to image the larynx have evolved rapidly into a promising and safe imaging modality, without need for sedation or ionising radiation. MRI is therefore of great interest to image paediatric laryngeal diseases. Our aim was to review MRI developments relevant for the paediatric larynx and to discuss future imaging options.

Methods: A systematic search was conducted to identify all morphological and diagnostic studies in which MRI was used to image the paediatric larynx, laryngeal disease or vocal cords.

Results: Fourteen articles were included: three studies on anatomical imaging of the larynx, two studies on Diffusion Weighted Imaging (DWI), four studies on vocal cord imaging and five studies on the effect of anaesthesiology on the paediatric larynx. MRI has been used for paediatric laryngeal imaging since 1991. MRI provides excellent soft tissue contrast and good visualisation of vascular diseases such as haemangiomas. However, visualisation of cartilaginous structures, with varying ossification during childhood, and tissue differentiation remain challenging. The latter has been partly overcome with DWI, differentiating between benign and malignant masses with excellent sensitivity (94-94.4%) and specificity (91.2-100%). Vocal cord imaging evolved from static images focussed on vocal tract growth to dynamic images able to detect abnormal vocal cord movement.

Conclusion: MRI is promising to evaluate the paediatric larynx, but studies using MRI as diagnostic imaging modality are scarce. New static and dynamic MR imaging techniques could be implemented in the paediatric population. Further research on imaging of paediatric laryngeal diseases should be conducted.

Introduction

Pathologies of the larynx in children are rare but severe conditions, and can have life-long consequences. The development of the larynx, normally completed around the 10th week of gestation, can fail at various time-points resulting in a variety of congenital laryngeal diseases.(1) After birth, the paediatric larynx is sensitive to acquired laryngeal insults, such as infectious diseases, inflammatory processes and traumatic injuries(table 1).(1) Severe cases might be in need for surgical intervention, such as micro- laryngeal surgery, laryngotracheal reconstruction or tracheostomy.(1) In the adult population, the most common diseases in the laryngeal region are of neoplastic origin.(2)

To understand the nature of laryngeal pathologies, multiple imaging modalities can be used.(1, 3, 4) In the paediatric population, the choice of the right modality should be carefully considered according to the wide variety of pathologies and the patient's age. Direct laryngoscopy is the gold standard for early diagnostics of the paediatric larynx and vocal cords, but its disadvantages are the operator-dependant diagnostic accuracy, the absence of objective measurements, limited detailed imaging and the need for anaesthetics to get a clear view of the subglottis.(5-7) Computed Tomography (CT) is used for extensive imaging of the larynx after surgical intervention. A limitation of CT is the exposure to radiation, which is especially important in laryngeal imaging because it exposes the thyroid, one of the most sensitive organs, to radiation.(8) This explains the limited use of CT for dynamic imaging of the larynx.

Over the past decades, Magnetic Resonance Imaging (MRI) techniques have rapidly evolved into a promising and safe modality to image the larynx, with the availability of faster sequences and specialised surface coils.(3, 9-11) However, most studies have been conducted in the adult population and are focussed on laryngeal malignancies. There is a dearth of paediatric MR laryngeal imaging. Though, MRI is of great interest for imaging paediatric laryngeal diseases, as sedation is not needed in older children and the use of MRI is not accompanied by exposure to radiation. This makes MRI ideal for dynamic evaluation of the larynx and vocal cords.

The aim of this study is to review the existing literature for recent developments in MR imaging of the paediatric larynx and discuss future innovative MR imaging.

Methods

Search strategy

A systematic search was developed to identify all morphological and diagnostic studies in which MRI was used to image the paediatric larynx. The search protocol was set up according to the Preferred Reporting Items for Systematic Reviews and Meta- Analysis (PRISMA) statement.(12) A search was conducted on 'paediatric' and 'larynx' or 'laryngeal disease' or 'vocal cords' and 'magnetic resonance imaging', the detailed search strategy is attached in supplementary material 1. Data bases used were: EMBASE, Medline Ovid, Web of Science, Cochrane and Google Scholar. In addition, the reference lists of the included articles were searched for additional articles of interest. Only original papers were included in this review. Reviews and case reports on less than ten patients were excluded due to risk of bias. The search was conducted in October 2017 and updated in December 2018.

Article selection

The article selection was done by two independent reviewers (BE, SH). Each reviewer evaluated the abstracts on the type of article, the imaged anatomic region and cohort size ($n \geq 10$) and age (≤18 years). Selected full-text articles were again read on the type of article, imaged anatomic region and the cohort size and age, and sufficient MR imaging data. ''Sufficient'' was defined as the following elements; MR scanner type and field strength, imaging parameters used, contrast and/or sedation requirements. Disagreement on inclusion/exclusion based on abstract or full text of the articles was resolved by consensus.

Results

Study selection

Eight hundred and sixty-three articles were identified. Duplicate studies were eliminated and 860 articles were screened for title and abstract based on article type, anatomical area imaged and number of patients included. The full text of 76 selected articles was reviewed for sufficient methodological information. Five articles were excluded based on incorrect article type, 18 on incorrect anatomic region, 12 on cohort size, 9 on cohort age, and 18 on insufficient MRI data, resulting in a final inclusion of 14 articles. The flowchart of the article selection is shown in figure 1. Table 2 shows the final 14 articles selected for this review, supplementary material 2 shows technical MRI information on the articles selected.

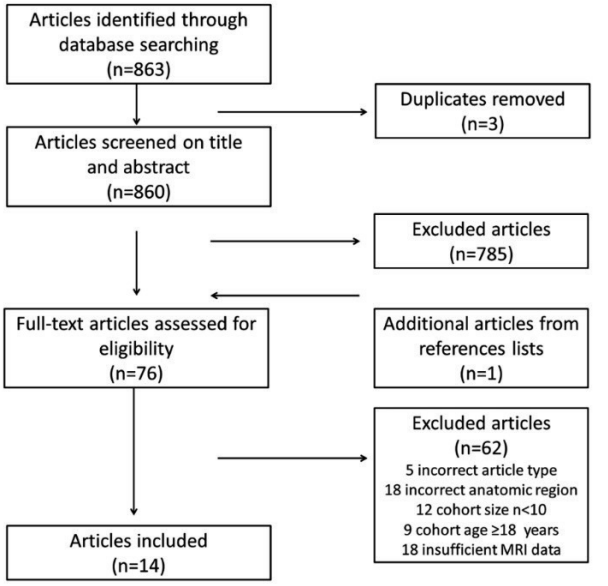

Figure 1: Flowchart of the article selection

Anatomical imaging

The first description of the paediatric larynx on MRI dates from 1991.(13) On 53 MRIs of patients aged between 1 day and 18 years, various laryngeal lesions, such as haemangioma, were evaluated and compared to CT in 25 cases. The images were evaluated by looking at four lesion characteristics: tissue contrast, detectability, extent and origin. All MRIs were made on a 0.5 or 1.5T scanner, and at least one T1 weighted image and one T2 weighted image were obtained. Despite the use of these early scanning techniques, good anatomical visualisation of mainly soft tissue was achieved. MRI was found to be excellent for all four lesion characteristics. T1 weighted images showed the best anatomical detail and T2 weighted images showed the best image contrast. Disadvantages of MRI were the difficulty to distinguish between inflammatory and malignant lesions, and difficulty to identify bony involvement due to changing ossification of cartilaginous structures in the developing paediatric larynx. Despite these disadvantages, MRI was proposed as an imaging tool to be superior to CT for the visualisation of complex laryngeal structures, because of its excellent anatomical visualisation.

In 1997 a 1.5T scanner was used to compare differences in anatomy and pathologies of the larynx between children and adults.(14) Despite the increased field strength of the MRI scanner, difficulties in the visualisation of bony involvement, motion artefacts, poor spatial resolution compared to CT and the inability to generate thin slices were seen as disadvantages for the clinical use of MRI.

However, in 2001 Mahboubi *et al.*, using a 1.5T scanner, managed to produce remarkably good images of paediatric laryngeal lesions, such as haemangiomas and lymphangiomas, and their surrounding structures.(15) Although visualisation of bony involvement remained superior on CT, this study confirmed the great potential of MRI as a possible diagnostic modality for paediatric laryngeal lesions.

Diffusion Weighted Imaging

For use of MRI for the diagnostics of paediatric laryngeal lesions, the most important disadvantages had to be overcome, especially the visualisation of bony structures and tissue characterisation. Inflammatory and malignant masses may have similar MRI signal intensity and the extent of mass can be hard to visualise, but is important to determine treatment options and prognosis. To overcome these difficulties Diffusion Weighted Imaging (DWI) of the laryngeal region was introduced in 2001 to characterise masses by their cellular density based on free motion of water protons.(16)(17) Structures with cellular swelling or a high cellular density, such as malignancies, have less free water proton movement. In the first study that used DWI to image the paediatric larynx, multiple benign and malignant masses, such as haemangioma, neurofibroma and non- Hodgkin lymphoma were visualised.(18) Benign masses could easily be discriminated from malignant masses with a sensitivity of 94.4% and a specificity of 91.2%.(18) Only two benign masses were falsely characterised as malignant due to the presence of high cellular compact bodies and fibrosis. In 2015 Taha *et al.* confirmed the feasibility of DWI to differentiate between benign and malignant laryngeal masses.(19) They were able to detect the nature of laryngeal masses with a sensitivity of 94% and a specificity of 100% in an adult and paediatric cohort.

Vocal cord imaging

The development of MRI sequences to visualise soft tissue allowed imaging of the vocal cords. The vocal cords were first imaged using MRI to define the differences in growth and maturation of the vocal tract between genders. In 129 children aged between 2 and 25 years the vocal tract was measured on MRI.(20) The laryngeal length increased over the years and its length correlated to body composition. Only small differences in vocal tract length were observed between boys and girls before puberty. However, in post pubertal boys a highly significant lengthening of the vocal tract was observed compared to girls. These differences were seen as a possible explanation for voice differences between the post pubertal genders.

In 2001 the first dynamic study of the vocal tract was conducted.(21) Faust *et al.* used cine-MRI to image the vocal tract in paediatric patients with impaired vocal function and healthy volunteers. The images, obtained during respiration and phonation, were viewed in a cine loop format. These cine-MRI images could easily identify impaired vocal cord movement and even showed patient-reported symptoms that could not be seen on endoscopy or static MRI. Figure 2 shows an axial MRI image of a healthy larynx during respiration(a) and phonation(b) from this study.(21)

Vorperian *et al*. imaged the vocal tract in 63 children aged between 2 weeks and 6.6 years old.(22) The MRIs were used to assess the effect of the development of soft and hard laryngeal structures on the vocal tract. During childhood the larynx descends from the spinal level C3-C4 to C6-C7.(23) This laryngeal descent was found to account for 45 to 65% of the vocal tract lengthening, depending on specific age ranges. These findings emphasised the contribution of the larynx on voice development and showed that MRI was able to visualise the laryngeal region in different age groups. Vorperian *et al*. also evaluated vocal tract differences between genders, by measuring the vocal tract length on 307 MRIs of children aged between 0 and 19 years.(24) The vocal tract length, measured on sagittal images as the length from the lips until the larynx, was significantly increased in boys compared to girls starting from an age of 12 years. This confirmed the gender differences shown in their earlier study.(22)

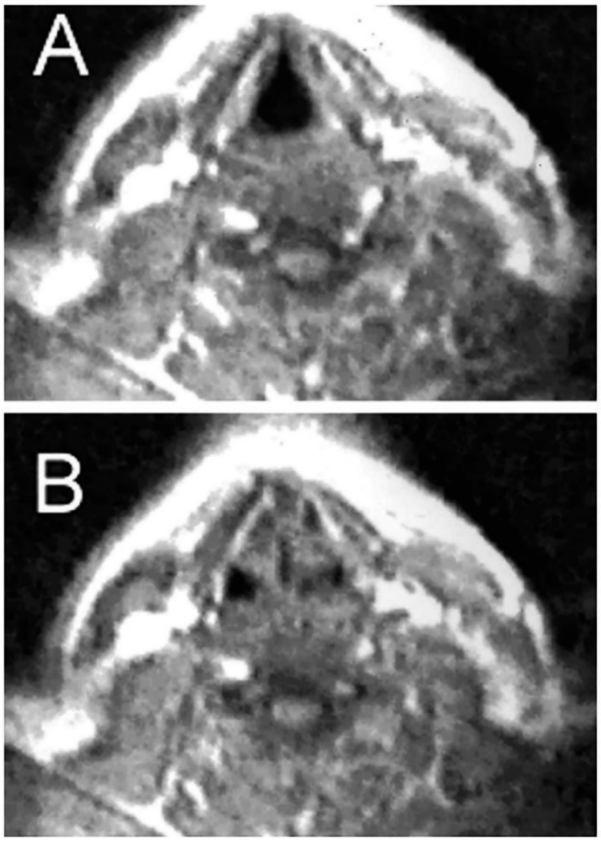

Figure 2: Axial TurboFLASH cine-MRI image (TR 2.5 ms, TE 1.2 ms, acquisition time 10 seconds per slice) with the use of a 1.5T MR imaging system (Siemens, Germany) of a healthy larynx during respiration (a) and phonation (b), showing bilateral symmetric vocal cord adduction during phonation.(21)(With permission)

Anaesthetics in imaging

An important advantage of MRI for imaging of the paediatric larynx is the limited need for anaesthetics. However, many of the earlier studies on MR imaging of the paediatric larynx had the primary aim to visualise the effects of anaesthesia and deep sedation on the airway.(25-29) A reported side effect of anaesthetics is respiratory distress, which in children is mainly caused by apnoea and upper airway collapse.(30) Despite multiple studies reporting on the anatomy of the sedated paediatric larynx, none of the studies made a direct comparison between sedated and non-sedated patients.

The effect of sedation on the paediatric larynx was first described by Litman *et al*, using MRI to study the effect of deep sedation on the airway in children between 0 and 14 years.(25) The most narrow part of the airway was at the level of the glottic opening in all age groups. In contrast to previous cadaver studies describing the cricoid ring as the most narrow part of the airway. This discrepancy might have been caused by the lack of volume standardisation during the MRIs, such as the use of a spirometer controlled MRI acquisition.(31) This might have resulted in images acquired during airway expiration, showing minor collapse of the laryngeal region. Another possible explanation is the use of propofol which can induce vocal cord tension, although this is not expected when sedation is maintained at a constant level.

Litman *et al.*, Vialet *et al*. and Bécret *et al*. further investigated the sedated laryngeal dimensions, concluding that the collapse of the paediatric airway during sedation can be partly overcome by positioning the child in either lateral or neutral position with a slight head extension.(26-28)

In the above mentioned studies, anaesthetics was used as part of the research protocol, aiming to image the sedated airway. In other studies, anaesthetics was used according to clinical protocols for scanning of non-cooperative young children.(14, 15, 18, 22, 24) In the study by Fitch *et al.*, where children as young as 2 years were instructed to lie still instead of using sedation, some images had to be excluded because of motion artefacts, which made it impossible to visualise the glottis.(20)

Discussion

Current MRI protocols are well capable of visualising soft tissue and vascular structures of the larynx (figure 3 and supplementary material 3). Fourteen publications on MR imaging of the larynx in the paediatric population were identified, mainly focussing on anatomy and anaesthetics, however these findings show that MRI can be a valuable imaging tool for the visualisation of several paediatric laryngeal diseases (table 1).

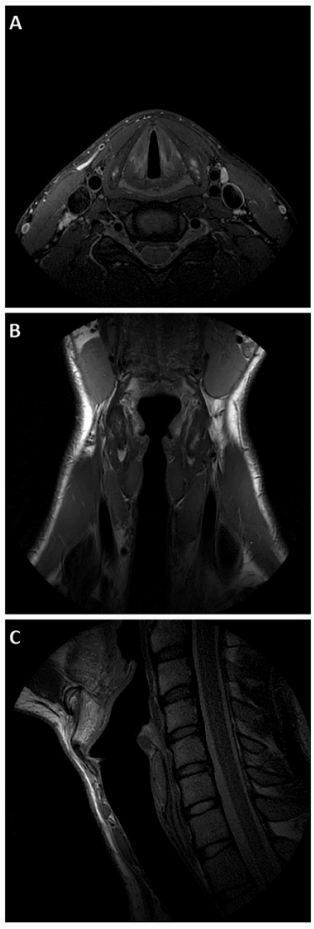

Figure 3: High-resolution T2 FSE weighted (PROPELLER) axial (A), coronal (B) and sagittal (C) images of the larynx of a healthy volunteer. Paediatric laryngeal MRI protocol developed at the Erasmus MC- Sophia Children's Hospital, with the use of a 3T MRI (GE Healthcare) using a 6 Chanel Carotid coil (spatial resolution 0.5x.0.5 (in plane) x 2mm.

Anatomical imaging

The studies found show that MRI is the best imaging modality for detailed anatomy of the healthy paediatric larynx(14), and laryngeal lesions such as haemangioma and cysts.(13, 15)

MR imaging of the paediatric larynx remains challenging due to the developing anatomy and the variety of laryngeal pathologies. Limitations of MRI include limited spatial resolution and longer scanning times when compared to CT. Images can be degraded by artefacts due to general patient movement or by swallowing or coughing.(32-34) Interestingly in this series of publications MR was described as an imaging technique that is relatively insensitive to motion and since the larynx stays in the same horizontal plane during respiration, the presence of respiratory artefacts is unlikely.(14, 20) Technical developments in recent years have resulted in improved spatial resolution and dedicated hardware, such as the availability

of 3T scanners and neck surface coils, are expected to further decrease scanning times and increase image quality.(35)

The findings described in paediatric studies are in line with studies conducted in the adult population, describing T1 and T2 sequences to provide excellent soft tissue characterisation of the larynx.(11, 32, 36) This is particularly important for laryngeal diseases with complex anatomy, such as laryngotracheal stenosis, laryngoceles and haemangioma which are easily identified on MRI.(3, 32) Most selected studies compared the anatomy as shown on MRI to CT. No paediatric studies comparing MRI to laryngoscopy were found, but a comparative study in the adult population shows promising results in favour of MRI.(6)

Tissue characterisation

The visualisation of cartilaginous structures of the paediatric larynx, with varying ossification stages during childhood, and the differentiation between inflammatory and malignant masses remain challenging on MRI(11), but these are considered important factors in disease treatment and prognosis.(9, 11, 32) In the paediatric population, malignant masses are extremely rare, but benign lesions such as cysts and haemangioma are more common.(37-39) Two studies on the imaging of paediatric laryngeal lesions with T1 and T2 sequences were identified. These studies both described the differentiation between benign and malignant lesions and bony involvement to be inferior on MRI compared to CT. However, studies by Abdel Razek *et al*. and Taha *et al.* showed that the latter can be partly overcome with DWI(18, 19), which is in line with adult studies.(9, 11, 40) Tissue characterisation over time has been shown in adult cohorts to be challenging, because inflammation and fibrosis after surgery or radiation is hard to distinguish from the primary lesion.(40) These challenges were not reviewed in this series, hence there is need for longitudinal studies in the paediatric population.

Another option to improve tissue characterisation is the use of intravenous contrast. In three of the studies identified, contrast enhanced MRI was used.(15, 18, 19) In the studies by Taha *et al.* and Abdel Razek *et al.* gadolinium contrast was used in a diagnostic setting, but the advantage of contrast enhancement is not described.(18, 19) Only the study by Mahboubi *et al.* described contrast administration to aid in the diagnosis of paediatric laryngeal lesions by enhancing vascular and malignant lesions.(15) It should be taken into account that intravenous contrast has important disadvantages related to costs, renal impairment, possible allergic reactions, and the need for an intravenous cannula. Moreover, recent publications related to deposition of MRI contrast in human tissue have compelled the European Medicines Agency (EMA) to ban the use of specific gadolinium contrast media limiting their use to specific oncological purposes.(41-44)

Vocal cord imaging

The imaging of the vocal cords has evolved from static images evaluating the growth of the vocal tract to dynamic cine-MRI for the visualisation of (impaired) vocal cord movement.

The studies identified show promising results of using MRI for dynamic imaging of vocal cord function. Studies in the adult population show that quantification of vocal cord function is possible using dynamic MRI.(10, 45)

Anaesthetics in imaging

The narrow and noisy environment of an MRI scanner, together with the need for a subject to lie still during the MRI examination often requires the use of anaesthetics for laryngeal MRI investigations in children younger than five years.(18, 24) Many of the studies identified in relation to anaesthetics were conducted primarily for the development of safer methods for paediatric airway management during sedation or anaesthesia.(25-29) These studies do not clearly answer the question if anaesthetics is a prerequisite for laryngeal MRI in the paediatric population. However, these studies do show that the dimensions of the larynx on MRI change due to the administration of anaesthetics and thus these images cannot be fully compared to the un-sedated airway. With the development of faster scanning protocols the need for anaesthetics is likely to be reduced. The studies identified report scanning times up to 10 minutes per sequence.(21, 25, 29) However, a paediatric laryngeal MRI protocol developed at the Erasmus MC- Sophia Children's Hospital shows the possibility of an extensive anatomical and dynamic evaluation within 30 minutes. In addition, in the neonatal population where laryngeal MRI would be of interest to image congenital lesions, increasing experience with the use of the 'feed and sleep'- method will make it possible to omit sedation. Likewise, dynamic laryngeal MRI techniques require full cooperation without the influence of anaesthetics.

Conclusion

MRI is a promising modality for the evaluation of paediatric laryngeal diseases (table 3). Most of the MRI studies on the anatomy of the paediatric larynx were conducted before 2001, so with the recent technological advancements of MRI, image quality has definitely improved. The most recent studies focussed on tissue characterisation and on the effect of anaesthesia in the larynx. Studies using MRI as a diagnostic imaging modality and longitudinal studies are scarce. In addition, although dynamic imaging of the vocal cords has been proven feasible in the adult population, implementation in the paediatric population is still lacking. Clinical studies on the technical use of MRI in the spectrum of paediatric laryngeal diseases, such as laryngeal stenosis and vocal cord dysfunction, are lacking. Further research should be conducted to explore these options.

Acknowledgements

We would like to acknowledge W.M. Bramer, from the Erasmus MC- medical library, for his assistance in the literature search.

Table 1: Paediatric laryngeal pathologies

Laryngomalacia	Trauma	Laryngotracheobronchitis	Benign	Vocal cord nodule
Laryngeal atresia	- Acquired glottic stenosis	Epiglottitis	- Haemangioma	Vocal cord polyp
Laryngeal web	- Mucosal trauma	Retropharyngeal abscess	- Papillomatosis	Vocal cord granuloma
Laryngeal cleft	- Blunt trauma	Diphtheria	- Laryngeal/saccular cysts	Vocal cord paralysis
Congenital glottic stenosis	- Penetrating trauma	Tuberculosis	- Laryngocele	- Acquired
	Gastro- pharyngeal reflux	Granulomatosis	- Subglottic cyst	- Congenital
		Sarcoidosis	- Neurofibroma	Paradoxic vocal cord motion
		Rheumatic disease	Malignant	
		Recurrent respiratory papillomatosis	- Sarcoma	
		Relapsing polychondritis	- Squamous cell carcinoma	
			- Lymphoma	
			- Mucoepidermoid carcinoma	
			- Neuroectodermal tumour	
			- Metastatic carcinoma	

Paediatric laryngeal pathologies for which MRI imaging of the laryngeal region could be of use, freely adapted from Cummings Otolaryngology (46)

Table 2: Key features for all selected articles that resulted from our systematic review

Study	Study population (n)	Age range (years)	Scanner	Sedation or anaesthetics	Contrast (yes/no)	Sequences	Study aim	Main study result
Yuh (1991) (13)	53	0-18	Picker International, 0.5T GE, 1.5T	No	Both	T1, T2	Characterisation of paediatric head/neck masses	MRI can accurately characterize pediatric head/neck masses
Hudgins (1997)(14)	15	0-16	Not defined, 1.5 T	No	No	T1, FSE T2	Visualisation of the normal paediatric larynx	The paediatric and adult larynx differ in size, position, consistency and shape as seen on MRI
Fitch (1999) (20)	129	2.8-25	GE, 1.5 T	No	No	T1	Quantification of vocal tract morphology during development	The post pubertal vocal tract is larger in males compared to females
Faust (2001) (21)	10	0-16	Siemens, 1.5 T	No	No	SE T1, SE T2, cine- MRI	Dynamic visualisation of the paediatric airway	Cine MRI can be used to visualize vocal cord movement in children (feasibility study)
Mahboubi (2001)(15)	45	0-2	Siemens, 1.5 T	No	Both	SE T1	Visualisation of paediatric upper airway obstruction	MRI can characterize paediatric airway abnormalities with high image quality

Litman (2003)(25)	99	0-14	GE, 1.5 T	Sedation	No	SE T1	Determination of the effect of age on paediatric laryngeal diameter	In sedated children of all ages the narrowest part of the airway is the glottic opening
Litman (2005)(26)	17	2-11	Siemens, 1.5 T	Anaesthesia	No	T1	Evaluation of the effect of lateral positioning on the paediatric laryngeal diameter	Lateral positioning increases the airway dimensions in children
Vorperian (2005)(22)	63	0-6.6	GE, 1.5T Resonex, T not specified	Sedation	No	T1, T2	Evaluation of the growth pattern of the vocal tract	The vocal tract continues to grow from birth until 6.6 years of age without gender differences
Vialet (2008)(27)	30	0-8.8	Siemens, 1.5T	Anaesthesia	No	SE T1	Evaluation of the effect of head extension on paediatric laryngeal diameter	Head extension increases the laryngeal visualization in paediatric patients
Abdel Razek (2009)(18)	78	0-15	Siemens, 1.5 T	Sedation	Both	T1, FSE T2, DWI	Characterisation of paediatric laryngeal masses with DWI	DWI can differentiate benign from malignant laryngeal masses with sensitivity 94.4% and specificity 91.2%
Vorperian (2011)(24)	307	0-19	GE, 1.5T Resonex, T not specified	Sedation	No	SE T1, FSE T2	Evaluation of developmental sex differences in vocal tract length	Sex differences in vocal tract length exist before puberty
Taha (2015) (19)	49	5-82	Philips, 1.5T	No	Yes	T1, T2, DWI	Characterisation of laryngeal masses with DWI	DWI can differentiate benign from malignant laryngeal masses with sensitivity 94% and specificity 100%
Bécret (2016)(28)	155	0-18.5	Siemens, 1.5 T	Anaesthesia	No	SE T1	Quantification of the effect of age on airway modifications due to head extension	In children of all ages head extension increases the visualization of the larynx
Aqil (2017) (29)	60	0-12	Siemens, 3T	Anaesthesia	No	RGE T1	Visualisation of anatomical changes caused by different paediatric airway devices	Supraglottic airway devices alter paediatric airway dimensions

FSE= fast spin- echo, DWI = diffusion weighted imaging, SE= spin-echo, RGE= rapid gradient echo, T = Tesla, T1= T1 weighted image, T2= T2 weighted imaging

Table 3: Advantages and disadvantages of paediatric laryngeal MRI

Advantages	Disadvantages
No sedation needed	Inferior spatial resolution to CT
Free of ionising radiation	Long scanning time compared to CT
Excellent soft tissue contrast	Differentiation between malignant and
Good visualization of vascular structures	inflammatory lesions can be challenging
Dynamic imaging possible	Bony involvement can be challenging

References

1. Stephenson KA, Wyatt ME. Glottic stenosis. Semin Pediatr Surg. 2016;25(3):132-7.
2. Kamangar F, Dores GM, Anderson WF. Patterns of cancer incidence, mortality, and prevalence across five continents: defining priorities to reduce cancer disparities in different geographic regions of the world. J Clin Oncol. 2006;24(14):2137-50.
3. Becker M, Burkhardt K, Dulguerov P, Allal A. Imaging of the larynx and hypopharynx. Eur J Radiol. 2008;66(3):460-79.
4. Huang BY, Solle M, Weissler MC. Larynx: anatomic imaging for diagnosis and management. Otolaryngol Clin North Am. 2012;45(6):1325-61.
5. Scott AD, Wylezinska M, Birch MJ, Miquel ME. Speech MRI: morphology and function. Phys Med. 2014;30(6):604-18.
6. Henes FO, Laudien M, Linsenhoff L, Bremer JP, Oqueka T, Adam G, et al. Accuracy of Magnetic Resonance Imaging for Grading of Subglottic Stenosis in Patients with Granulomatosis with Polyangiitis: Correlation with Pulmonary Function Tests and Laryngoscopy. Arthritis Care Res 2017;70(5):777-84.
7. Williamson JP, James AL, Phillips MJ, Sampson DD, Hillman DR, Eastwood PR. Quantifying tracheobronchial tree dimensions: methods, limitations and emerging techniques. Eur Respir J. 2009;34(1):42-55.
8. Mazonakis M, Tzedakis A, Damilakis J, Gourtsoyiannis N. Thyroid dose from common head and neck CT examinations in children: is there an excess risk for thyroid cancer induction? Eur Radiol. 2007;17(5):1352-7.
9. Preda L, Conte G, Bonello L, Giannitto C, Tagliabue E, Raimondi S, et al. Diagnostic accuracy of surface coil MRI in assessing cartilaginous invasion in laryngeal tumours: Do we need contrast-agent administration? Eur Radiol. 2017;27(11):4690-8.
10. Baki MM, Menys A, Atkinson D, Bassett P, Morley S, Beale T, et al. Feasibility of vocal fold abduction and adduction assessment using cine-MRI. Eur Radiol. 2017;27(2):598-606.
11. Agnello F, Cupido F, Sparacia G, Midiri F, Miroddi M, Grassedonio E, et al. Computerised tomography and magnetic resonance imaging of laryngeal squamous cell carcinoma: A practical approach. Neuroradiol J. 2017;30(3):197-204.
12. Liberati A, Altman DG, Tetzlaff J, Mulrow C, Gotzsche PC, Ioannidis JP, et al. The PRISMA statement for reporting systematic reviews and meta-analyses of studies that evaluate healthcare interventions: explanation and elaboration. BMJ. 2009;339:b2700.
13. Yuh WTC, Sato Y, Loes DJ, Kao SCS, Berbaum KS, Ryals TJ, et al. Magnetic-Resonance-Imaging and Computed-Tomography in Pediatric Head and Neck Masses. Ann Otol Rhinol Laryngol.100(1):54-62.
14. Hudgins PA, Siegel J, Jacobs I, Abramowsky CR. The normal pediatric larynx on CT and MR. Am j neuroradiol. 1997;18(2):239-45.
15. Mahboubi S, Gheyi V. MR imaging of airway obstruction in infants and children. Int J Pediatr Otorhinolaryngol. 2001;57(3):219-27.

16. Wang J, Takashima S, Takayama F, Kawakami S, Saito A, Matsushita T, et al. Head and neck lesions: characterization with diffusion-weighted echo-planar MR imaging. Radiology. 2001;220(3):621-30.
17. Chavhan GB, Alsabban Z, Babyn PS. Diffusion-weighted imaging in pediatric body MR imaging: principles, technique, and emerging applications. Radiographics. 2014;34(3):E73-88.
18. Abdel Razek AA, Gaballa G, Elhawarey G, Megahed AS, Hafez M, Nada N. Characterization of pediatric head and neck masses with diffusion-weighted MR imaging. Eur Radiol. 2009;19(1):201-8.
19. Taha MS, Amir M, Hassan O, Sabra R, Taha T, Riad MA. Pre-treatment apparent diffusion coefficient mapping: Differentiation of benign from malignant laryngeal lesions. J Laryngol Otol. 2015;129(1):57-62.
20. Fitch WT, Giedd J. Morphology and development of the human vocal tract: A study using magnetic resonance imaging. J Acoust Soc Am. 1999;106(3):1511-22.
21. Faust RA, Remley KB, Rimell FL. Real-time, cine magnetic resonance imaging for evaluation of the pediatric airway. Laryngoscope. 2001;111(12):2187-90.
22. Vorperian HK, Kent RD, Lindstrom MJ, Kalina CM, Gentry LR, Y., et al. Development of vocal tract length during early childhood: A magnetic resonance imaging study. J Acoust Soc Am. 2005;117(1):338-50.
23. Adewale L. Anatomy and assessment of the pediatric airway. Paediatr Anaesth. 2009;19 Suppl 1:1-8.
24. Vorperian HK, Wang S, Schimek EM, Durtschi RB, Kent RD, Gentry LR, et al. Developmental sexual dimorphism of the oral and pharyngeal portions of the vocal tract: an imaging study. J Speech Lang Hear Res. 2011;54(4):995-1010.
25. Litman RS, Weissend EE, Shibata D, Westesson PL. Developmental changes of laryngeal dimensions in unparalyzed, sedated children. Anesthesiology. 2003;98(1):41-5.
26. Litman RS, Wake N, Chan LML, McDonough JM, Sin S, Mahboubi S, et al. Effect of lateral positioning on upper airway size and morphology in sedated children. Anesthesiology. 2005;103(3):484-8.
27. Vialet R, Nau A, Chaumoître K, Martin C. Effects of head posture on the oral, pharyngeal and laryngeal axis alignment in infants and young children by magnetic resonance imaging. Paediatr Anaesth. 2008;18(6):525-31.
28. Becret A, Vialet R, Chaumoitre K, Loundou A, Lesavre N, Michel F. Upper airway modifications in head extension during development. Anaesth Crit Care Pain Med. 2017;36(5):285-90.
29. Aqil M, Delvi B, Abujamea A, Alzahrani T, Alzahem A, Mansoor S, et al. Spatial relationship of i-gel® and Ambu® AuraOnceTM on pediatric airway: A randomized comparison based on three dimensional magnetic resonance imaging. Minerva Anestesiol. 2017;83(1):23-32.
30. Cote CJ, Notterman DA, Karl HW, Weinberg JA, McCloskey C. Adverse sedation events in pediatrics: a critical incident analysis of contributing factors. Pediatrics. 2000;105(4 Pt 1):805-14.

31. Salamon E, Lever S, Kuo W, Ciet P, Tiddens HA. Spirometer guided chest imaging in children: It is worth the effort! Pediatr Pulmonol. 2017;52(1):48-56.
32. Yousem DM, Tufano RP. Laryngeal imaging. Magn Reson Imaging Clin N Am. 2002;10(3):451-65.
33. Mannelli G, Cecconi L, Gallo O. Laryngeal preneoplastic lesions and cancer: challenging diagnosis. Qualitative literature review and meta-analysis. Crit Rev Oncol Hematol. 2016;106:64-90.
34. Kuno H, Onaya H, Fujii S, Ojiri H, Otani K, Satake M. Primary staging of laryngeal and hypopharyngeal cancer: CT, MR imaging and dual-energy CT. Eur J Radiol. 2014;83(1):e23-35.
35. Casselman J.W. High- Resolution Imaging of the Skull Base and Larynx. In: S.O. Schoenberg, O. Dietrich, M.F. Reiser. Parallel Imaging in Clinical MR Applications. Medical Radiology (Diagnostic Imaging). Berlin, Heidelberg: Springer; 2007.
36. Banko B, Dukic V, Milovanovic J, Kovac JD, Artiko V, Maksimovic R. Diagnostic significance of magnetic resonance imaging in preoperative evaluation of patients with laryngeal tumors. Eur Arch Otorhinolaryngol. 2011;268(11):1617-23.
37. Gindhart TD, Johnston WH, Chism SE, Dedo HH. Carcinoma of the larynx in childhood. Cancer. 1980;46(7):1683-7.
38. Parkes WJ, Propst EJ. Advances in the diagnosis, management, and treatment of neonates with laryngeal disorders. Semin Fetal Neonatal Med. 2016;21(4):270-6.
39. Ahmad SM, Soliman AM. Congenital anomalies of the larynx. Otolaryngol Clin North Am. 2007;40(1):177-91.
40. Maroldi R, Ravanelli M, Farina D. Magnetic resonance for laryngeal cancer. Curr Opin Otolaryngol Head Neck Surg. 2014;22(2):131-9.
41. Pullicino R, Radon M, Biswas S, Bhojak M, Das K. A Review of the Current Evidence on Gadolinium Deposition in the Brain. Clin Neuroradiol. 2018;28(2):159-69.
42. McDonald JS, McDonald RJ, Jentoft ME, Paolini MA, Murray DL, Kallmes DF, et al. Intracranial Gadolinium Deposition Following Gadodiamide-Enhanced Magnetic Resonance Imaging in Pediatric Patients: A Case-Control Study. JAMA Pediatr. 2017;171(7):705-7.
43. Young JR, Orosz I, Franke MA, Kim HJ, Woodworth D, Ellingson BM, et al. Gadolinium deposition in the paediatric brain: T1-weighted hyperintensity within the dentate nucleus following repeated gadolinium-based contrast agent administration. Clin Radiol. 2018;73(3):290-5.
44. Gulani V, Calamante F, Shellock FG, Kanal E, Reeder SB, International Society for Magnetic Resonance in M. Gadolinium deposition in the brain: summary of evidence and recommendations. Lancet Neurol. 2017;16(7):564-70.
45. Ahmad M, Dargaud J, Morin A, Cotton F. Dynamic MRI of larynx and vocal fold vibrations in normal phonation. J Voice. 2009;23(2):235-9.
46. Flint PW, Haughey BH, Lund VJ, Niparko JK, Robbins KT, Thomas JR, et al. Cummings Otolaryngology-head and neck surgery. Volume 3. Sixth edition.: Elsevier Health Sciences; 2014.

Supplementary materials

Supplementary materials 1: Systematic search strategy

Database	Search query	Findings
Embase	('nuclear magnetic resonance imaging'/exp OR 'nuclear magnetic resonance'/de OR 'nuclear magnetic resonance scanner'/de OR ((magnet* NEAR/3 resonan*) OR mri OR nmr OR mr OR dwi OR (diffus* NEAR/3 weight*)):ab,ti) AND ('larynx'/exp OR 'larynx disorder'/exp OR 'voice disorder'/exp OR ((laryn* NOT (laryn* NEAR/3 mask*)) OR cricoid* OR Arytenoid* OR vallecular OR glottis OR glottidi* OR glottic OR transglott* OR epiglott* OR subglott* OR supraglott* OR (vocal NEXT/1 (cord* OR tract* OR fold)) OR hoarseness* OR Dysphoni* OR Aphoni* OR Aphonia OR (voice* NEAR/3 (disorder* OR disturb*))):ab,ti) AND (child/exp OR adolescent/exp OR adolescence/exp OR pediatrics/exp OR childhood/exp OR 'child development'/de OR 'child growth'/de OR 'child health'/de OR 'child health care'/exp OR 'child care'/exp OR 'childhood disease'/exp OR 'pediatric ward'/de OR 'pediatric hospital'/de OR (adolescen* OR infan* OR newborn* OR (new NEXT/1 born*) OR baby OR babies OR neonat* OR child* OR kid OR kids OR toddler* OR teen* OR boy* OR girl* OR minors OR underag* OR (under NEXT/1 (age* OR aging)) OR juvenil* OR youth* OR kindergar* OR puber* OR pubescen* OR prepubescen* OR prepubert* OR pediatric* OR paediatric* OR school* OR preschool* OR highschool*):ab,ti) NOT ([Conference Abstract]/lim OR [Letter]/lim OR [Note]/lim OR [Editorial]/lim) NOT ('case report'/de OR ('case report'):ti) NOT ([animals]/lim NOT [humans]/lim) AND [english]/lim	481
Medline Ovid	(Magnetic Resonance Imaging/ OR ((magnet* ADJ3 resonan*) OR mri OR nmr OR mr OR dwi OR (diffus* ADJ3 weight*)).ab,ti.) AND (exp larynx/ OR exp Laryngeal Diseases/ OR ((laryn* NOT (laryn* ADJ3 mask*)) OR cricoid* OR Arytenoid* OR vallecular OR glottis OR glottidi* OR glottic OR transglott* OR epiglott* OR subglott* OR supraglott* OR (vocal ADJ (cord* OR tract* OR fold)) OR hoarseness* OR Dysphoni* OR Aphoni* OR (voice* ADJ3 (disorder* OR disturb*))).ab,ti.) AND (exp Child/ OR exp Infant/ OR exp Adolescent/ OR exp "Child Behavior"/ OR exp "Pediatrics"/ OR "Child Nutrition Sciences"/ OR "Infant nutritional physiological phenomena"/ OR exp "Child Welfare"/ OR "Child Development"/ OR exp "Child Health Services"/ OR exp "Child Care"/ OR "Hospitals, Pediatric"/ OR exp "Intensive Care Units, Pediatric"/ OR (adolescen* OR infan* OR newborn* OR (new ADJ born*) OR baby OR babies OR neonat* OR child* OR kid OR kids OR toddler* OR teen* OR boy* OR girl* OR minors OR underag* OR (under ADJ (age* OR aging)) OR juvenil* OR youth* OR kindergar* OR puber* OR pubescen* OR prepubescen* OR prepubert* OR pediatric* OR paediatric* OR school* OR preschool* OR highschool*).ab,ti.) NOT (letter OR news OR comment OR editorial OR congresses OR abstracts).pt. NOT (case report/ OR (case report).ti.) NOT (exp animals/ NOT humans/) AND english.la.	101
Web of science	TS=((((magnet* NEAR/2 resonan*) OR mri OR nmr OR mr OR dwi OR (diffus* NEAR/2 weight*))) AND (((laryn* NOT (laryn* NEAR/2 mask*)) OR cricoid* OR Arytenoid* OR vallecular OR glottis OR glottidi* OR glottic OR transglott* OR epiglott* OR subglott* OR supraglott* OR (vocal NEAR/1 (cord* OR tract* OR fold)) OR hoarseness* OR Dysphoni* OR Aphoni* OR Aphonia OR (voice* NEAR/2 (disorder* OR disturb*)))) AND ((adolescen* OR infan* OR newborn* OR (new NEAR/1 born*) OR baby OR babies OR neonat* OR child* OR kid OR kids OR toddler* OR teen* OR boy* OR girl* OR minors OR underag* OR (under NEAR/1 (age* OR aging)) OR juvenil* OR youth* OR kindergar* OR puber* OR pubescen* OR prepubescen* OR prepubert* OR pediatric* OR paediatric* OR school* OR preschool* OR highschool*)) NOT ((animal* OR rat OR rats OR mouse OR mice OR murine OR dog OR dogs OR canine OR cat OR cats OR feline OR rabbit OR cow OR cows OR bovine OR rodent* OR sheep OR ovine OR pig OR swine OR porcine OR veterinar* OR chick* OR zebrafish* OR baboon* OR nonhuman* OR primate* OR cattle* OR goose OR geese OR duck OR macaque* OR avian* OR bird*) NOT (human* OR patient*))) AND DT=(article) AND LA=(english) NOT TI=("case report")	110

Cochrane	(((magnet* NEAR/3 resonan*) OR mri OR nmr OR mr OR dwi OR (diffus* NEAR/3 weight*)):ab,ti) AND (((laryn* NOT (laryn* NEAR/3 mask*)) OR cricoid* OR Arytenoid* OR vallecular OR glottis OR glottidi* OR glottic OR transglott* OR epiglott* OR subglott* OR supraglott* OR (vocal NEXT/1 (cord* OR tract* OR fold)) OR hoarseness* OR Dysphoni* OR Aphoni* OR Aphonia OR (voice* NEAR/3 (disorder* OR disturb*))):ab,ti) AND ((adolescen* OR infan* OR newborn* OR (new NEXT/1 born*) OR baby OR babies OR neonat* OR child* OR kid OR kids OR toddler* OR teen* OR boy* OR girl* OR minors OR underag* OR (under NEXT/1 (age* OR aging)) OR juvenil* OR youth* OR kindergar* OR puber* OR pubescen* OR prepubescen* OR prepubert* OR pediatric* OR paediatric* OR school* OR preschool* OR highschool*):ab,ti)	2
Google scholar	"magnetic resonance"|mri|"diffusion weighted" larynx|laryngeal|glottis|"vocal cord|tract|fold"|hoarseness|Dysphonia|Aphonia|"voice disorder|disturbance" adolescents|infants|newborns|children -"laryngeal mask"	169
Total		863

Supplementary materials 2: Technical MRI information of all selected articles that resulted from the systematic search

Study	Scanner	T1			T2			DWI			Cine MRI		
		TR (ms)	TE (ms)	Slice thickness (mm)	TR (ms)	TE (ms)	Slice thickness (mm)	TR (ms)	TE (ms)	Slice thickness (mm)	TR (ms)	TE (ms)	Slice thickness (mm)
Yuh (1991)(13)	Picker International, 0.5T GE, 1.5T	350-680	20-26	5-10	1800-2500	80-100	5-10	-	-	-	-	-	-
Hudgins (1997)(14)	Not defined, 1.5 T	500-600	15-30	3-4	2000-3000	25-90	5	-	-	-	-	-	-
Fitch (1999)(20)	GE, 1.5 T	400	14	5	-	-	-	-	-	-	-	-	-
Faust (2001)(21)	Siemens, 1.5 T	n.a.	n.a.	n.a.	n.a.	n.a.	n.a.	-.	-	-	2.5	1.2	8
Mahboubi (2001)(15)	Siemens, 1.5 T	n.a.	n.a.	3-8	-	-	-	-	-	-	-	-	-
Litman (2003)(25)	GE, 1.5 T	n.a.	n.a.	3	-	-	-	-	-	-	-	-	-
Litman (2005)(26)	Siemens, 1.5 T	n.a.	n.a.	3	-	-	-	-	-	-	-	-	-
Vorperian (2005)(22)	GE, 1.5T Resonex, T not specified	350-700	14-30	n.a.	3000-5000	10-40	n.a.	-	-	-	-	-	-
Vialet (2008)(27)	Siemens, 1.5T	703	13	n.a.	-	-	-	-	-	-	-	-	-
Abdel Razek (2009)(18)	Siemens, 1.5 T	800	15	5	4500	80	5	10000	108	5	-	-	-
Vorperian (2011)(24)	GE, 1.5T Resonex, T not specified	350-700	14-30	n.a.	3000-5000	10-40	n.a.	-	-	-	-	-	-
Taha (2015)(19)	Philips, 1.5T	n.a.	n.a.	4	n.a.	n.a.	4.	5100	137	3	-	-	-
Bécret (2016)(28)	Siemens, 1.5 T	703	13	n.a.	-	-	-	-	-	-	-	-	-
Aqil (2017)(29)	Siemens, 3T	1700	3	n.a.	-	-	-	-	-	-	-	-	-

FSE= fast spin- echo, DWI = diffusion weighted imaging, n.a.. = information not available in article, SE= spin-echo, RGE= rapid gradient echo, T = Tesla, T1= T1 weighted image, T2= T2 weighted imaging, - = sequence not performed

Supplementary materials 3:

Dynamic axial 3D TRICKS cine-MRI of the larynx of a healthy volunteer during a respiration and phonation manoeuvre. Paediatric laryngeal MRI protocol developed at the Erasmus MC- Sophia Children's Hospital, with the use of a 3T MRI (GE Healthcare) using a 6 Chanel Carotid coil (temporal resolution 246 ms).

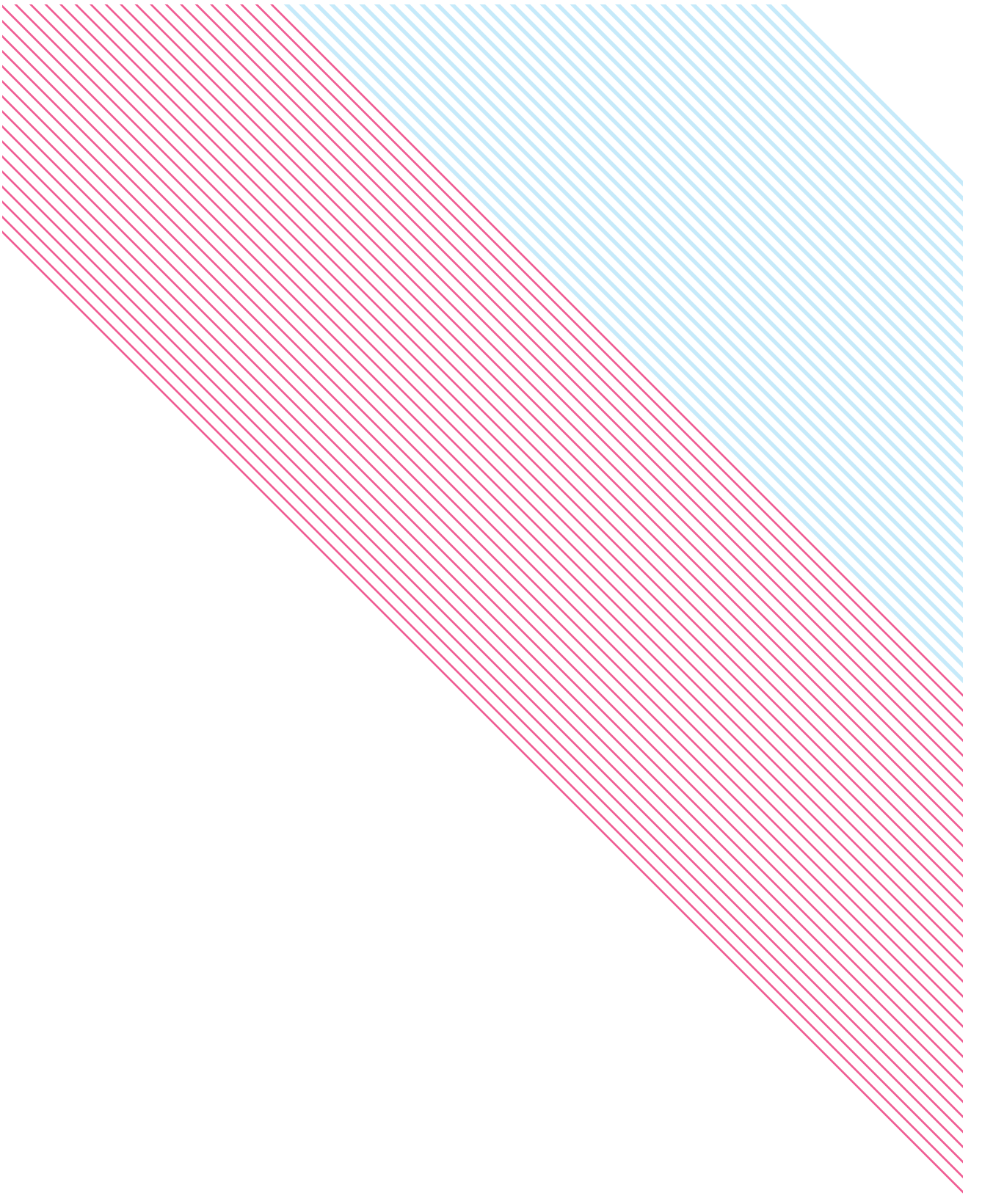

Chapter 3

Magnetic resonance imaging of the paediatric upper airways: the MUSIC study

Bernadette BLJ Elders, Pierluigi Ciet, Harm AWM Tiddens, Wytse B van den Bosch, Piotr A Wielopolski, Bas Pullens

Thorax 2021;76:44-51

Abstract

Rationale: Paediatric laryngotracheal stenosis (LTS) is often successfully corrected with open airway surgery. However, respiratory and vocal sequelae frequently remain. Clinical care and surgical interventions could be improved with better understanding of these sequelae.

Objective: The objective of this cross-sectional study was to develop an upper airway Magnetic Resonance Imaging (MRI) protocol to obtain information on anatomical and functional sequelae post-LTS repair.

Methods: Forty-eight patients (age 14.4 (range 7.5-30.7) years) and 11 healthy volunteers (15.9 (8.2-28.8) years) were included. Spirometry and static and dynamic upper airway MRI (3.0T, 30 min protocol) were conducted. Analysis included assessment of post-operative anatomy and airway lumen measurements during static and dynamic (inspiration and phonation) acquisitions.

Main results: Good image quality without artefacts was achieved for static and dynamic images in the majority of MRIs. MRI showed vocal cord thickening in 80.9% of patients and compared to volunteers, a significant decrease in vocal cord lumen area (22.0 (IQR 17.7-30.3) mm^2 vs. 35.1 (IQR 21.2-54.7) mm^2, p=0.03) but not cricoid lumen area (62.0 ± 27.3 mm^2 vs. 66.2 ± 34.8 mm^2, p=0.68). Furthermore, 53.2% of patients had an A-frame deformation at site of previous tracheal cannula, showing lumen collapse during inspiration. Dynamic imaging showed incomplete vocal cord abduction during inspiration in 42.6% and incomplete adduction during phonation in 61.7% of patients.

Conclusions: Static and dynamic MRI is an excellent modality to non-invasively image anatomy, tissue characteristics and vocal cord dynamics of the upper airways. MRI-derived knowledge on post-surgical LTS sequelae might be used to improve surgery.

Introduction

Paediatric laryngotracheal stenosis (LTS), mostly caused by prolonged intubation, can have life- long consequences.(1) Open airway surgery achieves decannulation in up to 95% of severe cases, but respiratory and vocal sequelae may occur.(1-4) Up to 70% of children have impaired in- and expiratory pulmonary function and the majority reports poor voice quality. (5-7)

The gold standard to assess the upper airways is direct laryngotracheoscopy under general anaesthesia.(2, 8) However, this method has important limitations, such as need for sedation, the semi-quantitative character of information obtained with possible substantial inter-observer variability, sub-optimal tissue characterisation and dynamic evaluation which can be limited by the depth of anaesthesia or the presence of the endoscope in the airway.(9) To broaden our knowledge on post-operative sequelae, we need a safe and comprehensive imaging method to visualise the upper airways in static and dynamic conditions. Computed Tomography (CT) has been used to image paediatric laryngeal stenosis(10, 11), but has the important downside of ionising radiation, especially in the region of the radiation- sensitive thyroid.(12) Thanks to improvements in Magnetic Resonance Imaging (MRI) technology, high-resolution images are achievable in paediatric patients and can be used to evaluate the upper airways.(13) Notably, the absence of ionising radiation, the improved tissue characterisation and the possibility of dynamic imaging make MRI suitable to image the upper airways after surgery. However, several challenges remain, such as image degradation from motion artefacts and long scan times. Consequently, to date MRI has only been used to detect and grade LTS in adult patients.(14, 15)

The aim of this cross-sectional study was to develop a static and dynamic upper airways MRI protocol to obtain information on anatomical and functional sequelae after open airway surgery for paediatric LTS.

Methods

We invited all patients with a history of open airway surgery for LTS to participate in the **M**agnetic resonance imaging of the **u**pper airways **i**n **c**hildren and young adults (**MUSIC**)-study. In- and exclusion criteria are shown in supplementary material 1. Patients were compared to healthy volunteers, consisting of patients' siblings or friends, without airway, vocal or pulmonary co- morbidities. A comparison between patients who did and did not participate in the MUSIC study is shown in supplementary material 2. Participating patients appeared to be significantly younger than those who did not participate (14.4 (11.7-19.4) vs. 19.1 (14.3-24.0) years, p=0.01). This study was approved by the local medical ethics review board (MEC-2018-013), written informed consent was obtained from all study participants.

Clinical status

The following data was collected from patients' electronic medical file: acquired or congenital stenosis, Cotton-Myer Grade of stenosis(16), location of stenosis (posterior glottis, subglottis, both), presence of a tracheal cannula before repair (Yes/No), type of surgery (single-stage (ss-), double stage laryngotracheal reconstruction (ds-LTR), cricotracheal reconstruction (CTR))(2), age at reconstruction and presence of comorbidities. Flow volume spirometry was obtained according to European Respiratory Society/American Thoracic Society guidelines by a certified researcher (B.E.).(17) Data are reported as percentage predicted or z-scores according to GLI index.(18, 19)

Magnetic resonance imaging

A paediatric upper airway MRI protocol was developed on a 3.0 Tesla scanner (*Discovery MR750, GE Healthcare, Milwaukee, WI, USA*) using a 6 channel dedicated carotid coil (*Machnet B.V., Rhoden, The Netherlands* and *Flick Engineering B.V., Winterswijk, The Netherlands)* (figure 1).(20) Total protocol duration was 30 minutes. The protocol consisted of static free breathing sequences to assess anatomy and tissue characterisation and dynamic sequences to assess upper airway movement. Dynamic sequences consisted of bi– (2D) and three-dimensional (3D) sequences, during which the following trained manoeuvres were performed: a manoeuvre of inspiration and 'AAA' phonation of 7 seconds each performed separately during two static 2D sequences and a manoeuvre of 2 second inspiration followed by 6 second 'AAA' phonation during the dynamic 3D sequence. These sequences were repeated until one of the manoeuvres was done correctly. Scan parameters are included in supplementary material 3A. The principal investigator (P.I.) (B.E.) trained participants the manoeuvres and was present during all MRI sessions. Image quality and presence and type of artefacts were recorded. Image analysis was done using Advantage Windows Server platform (*version 2.0, GE Healthcare, Milwaukee, WI, USA*), as shown in figure 2, details are provided in supplementary material 3B.

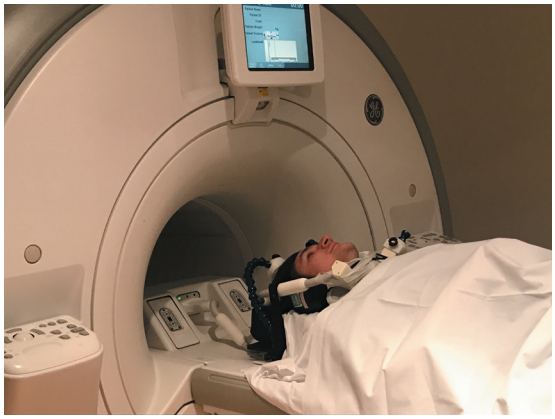

Figure 1: coil set-up, healthy volunteer demonstrating positioning of the 6CH carotid coil placed at the anterior side of the neck and secured with tape, the head is immobilized by the coil placement.

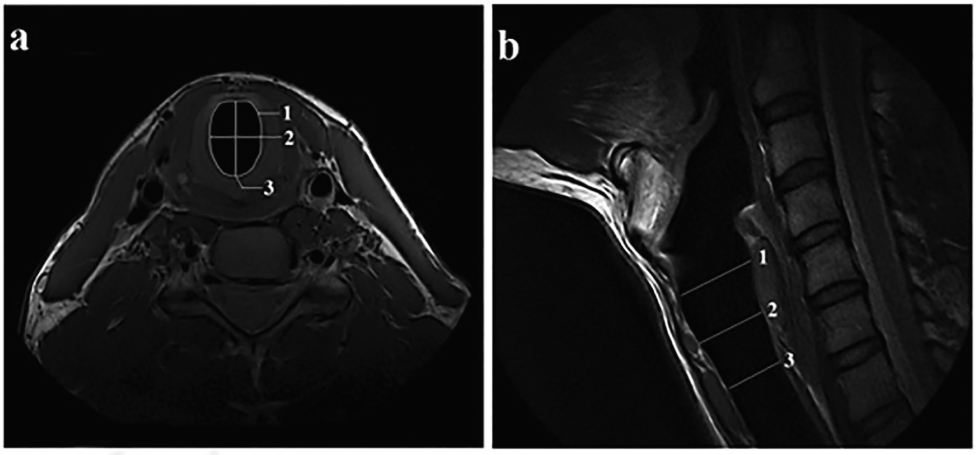

Figure 2: example of MRI analysis on a healthy volunteer (a) axial T2 weighted image showing the measurement of the lumen area (1), left-right (2) and transversal diameter (3) at the level of the cricoid, (b) sagittal T2 weighted image showing the location of the cricoid (1), the proximal trachea (2) and the most caudal slice (3).

We assessed anatomy on the T2 (T2-w) and Proton Density-weighted (PD-w) static scans and recorded the presence of arytenoid prolapse or vocal cord thickening, altered vocal cord positioning, presence and displacement of autologous cartilage grafts (anterior, posterior, none) and airway deformations. Airway lumen area, anterior-posterior and transversal diameters were measured on axial T2-w sequences at the level of the vocal cords, cricoid, tracheal deformation (if present) and proximal trachea and corrected for height in meters. Measurement of the proximal trachea was done at the axial slice midway between the cricoid and the most caudal slice. If this was the site of the tracheal deformation, a superior axial slice was used. We assessed tissue characteristics on T2-w and diffusion weighted imaging (DWI) to identify structural tissue alterations such as fibrosis, (chronic) oedema or a combination, at the following locations: arytenoids, vocal cords or cricoid.(21, 22) Tissue was characterized as described in table 1.

Table 1: Diffusion weighted imaging analysis methods

T2-w imaging		DWI	ADC	Tissue characterisation
Hyper intensity	**Thickening**			
+	+	Hyper	Hyper	Oedema and fibrosis
+	-	Hyper	Hyper	Oedema
-	+	Hyper	Hyper	Fibrosis
+	+	No signal	No Signal	Mild oedema and fibrosis
+	-	No signal	No signal	Mild oedema
-	+	No signal	No signal	Mild fibrosis
+/-	+/-	Hyper	Hypo	Unknown
+/-	+/-	Hypo	Hyper	Unknown
-	-	Hyper	Hyper	Artefact
-	-	No signal	No signal	Normal tissue

ADC; apparent diffusion coefficient, DWI; diffusion weighted imaging. +; present, -; absent, +/-; either present of absent

Movement of the upper airways was assessed on 2D and 3D dynamic imaging. Correct performance of the manoeuvres was evaluated in video format, defined as any vocal cord abduction during inspiration and any vocal cord adduction during phonation on 2D images, and any vocal cord movement on 3D images. Movement was evaluated on completeness and symmetry. Airway lumen areas were measured on axial 2D sequences at the vocal cords, cricoid, tracheal deformation (if present) and proximal trachea during inspiration and phonation. Quantitative measurements were only made if 2D manoeuvres were performed correctly.

Patients with a history of CTR, which is characterised by a partially absent cricoid cartilage, were excluded from measurements at the cricoid level. Analysis was done by the PI (B.E) with two years' experience in upper airways MRI. Intra and inter-observer reproducibility was tested by reanalysing 12 randomly selected MRIs by the PI and a second researcher appropriately trained in upper airways MRI (W.B.).

Statistics

The Shapiro- Wilk test was conducted to test data distribution. Normally distributed data are presented as mean ± standard deviation and non- normally distributed data are presented as median (range or interquartile range). Data were compared using the parametric t-test for normally distributed data, the Mann Whitney U test for not normally distributed data and the Chi square test for categorical data. Similarly, Pearson's and Spearman's rho correlations were calculated for normally and not normally distributed data respectively. Binary logistic regression was used for categorical data. Intra- and inter-observer agreement was calculated with the intra-class correlation coefficient. Correction for multiple testing was not performed and a 5% significance level was assumed. Data analysis was done using SPSS Statistics (*version 25, IBM SPSS, Chicago, IL, USA*).

Results

Patient and healthy volunteer characteristics are presented in table 2. Forty-eight patients and eleven healthy volunteers were included, with a mean age of 14.4 (range 7.5-30.7) and 15.9 (range 8.2-28.8) years. Three patients (6.3%) had a congenital LTS, and 45 patients (93.8%) had an acquired LTS. Patients most often underwent ss-LTR (87.5%). The most common comorbidity was bronchopulmonary dysplasia (BPD)(18.8%).

Table 2: Patient and healthy volunteer characteristics

	Patients (n= 48)	Volunteers (n=11)	p-value
Age at MRI (years)	14.4 (range 7.5-30.7)	15.9 (range 8.2-28.8)	0.92
Gender (n/% female)	25/52.1	4/36.4	0.37
Weight (kg)	45.2 (IQR 34.5-62.3)	60.8 (IQR 31.6-74.0)	0.34
Height (meter)	1.6 (IQR 1.4-1.7)	1.7 (IQR 1.4-1.8)	0.34
Type of stenosis (n/%)			
Congenital	3/6.3		
Acquired	45/93.8		
Cotton Myer grade of stenosis (n/%)			
Grade I	4/8.3		
Grade II	15/31.3		
Grade III	27/56.3		
Grade IV	2/4.2		
Location of stenosis (n/%)			
Posterior glottis			
Subglottis	11/22.9		
Posterior glottis and	17/35.4		
subglottis	20/41.7		
Tracheal cannula before repair (n/%)	38/79.2		
Type of reconstruction (n/%)			
ss-LTR	42/87.5		
ds- LTR	2/4.2		
CTR	4/8.3		
Age at reconstruction (years)	2.2 (IQR 1.1-4.5)		
Years since reconstruction	11.5 ± 4.6		
Comorbidities (n/%)	Asthma 2/4.2 BPD 9/18.8 Cardiac 3/6.3 DiGeorge syndrome 1/2.1 Oesophageal atresia 3/6.3 Kartagener syndrome 1/2.1 OSAS 1/2.1 PMR 6/12.5 Tracheomalacia 2/4.2		

BPD; bronchopulmonary dysplasia, CTR; cricotracheal resection, ds-LTR; double stage laryngotracheal reconstruction, IQR; interquartile range, ss-LTR; single stage laryngotracheal reconstruction, OSAS; obstructive sleep apnoea syndrome, PMR; psychomotor retardation. Data are presented as mean ± standard deviation, median (range or interquartile range) or absolute number (n) and percentage, *=p<0.05

Table 3 shows spirometry data for patients and healthy volunteers. Patients' expiratory and inspiratory (expressed as a decrease in forced inspiratory volume in 1 sec (FIV_1) divided by maximal vital capacity (VCmax) and an increase in Expiratory Disproportion Index (EDI)) spirometry outcomes were lower than those of healthy volunteers. Spirometry outcomes did not differ significantly between LTS patients with and without BPD (forced expiratory

volume in 1 sec (FEV_1) z-score=-1.9 ± 1.7 vs. -0.2 ± 1.00, p=0.88, FEV_1/ functional vital capacity (FVC) z-score=-2.3 (-2.9 - -0.7) vs. -1.2 (-2.0 - -0.3), p=0.34, FIV_1/VCmax=65.6 (49.8 - 80.0) vs. 63.2 (54.2 - 80.1) ,p=0.84, EDI= 67.6 ± 15.0% vs. 64.6 ± 15.4%, p=0.94).

Table 3: Flow- volume spirometry data

	Patients (n= 48)	**Volunteers (n=11)**	**p-value**
FVC			
% predicted	86.5 (80.5-100.0)	97.0 (91.0-110.0)	*0.02
z-score	-1.0 ± 1.3	0.1 ± 1.1	*0.02
FEV_1			
% predicted	80.5 (73.0-91.0)	97.0 (91.0-107.0)	*0.001
z-score	-1.6 (-2.3 - -0.8)	-0.3 (-0.8-0.6)	*0.001
FEV_1/FVC			
% predicted	91.0 (79.3-96.0)	100 (94.0-106.0)	*0.02
z-score	-1.4 ± 1.6	-0.3 ± 1.6	*0.04
PEF			
% predicted	58.5 (41.3-71.8)	111.0 (78.0-123.0)	*<0.001
z-score	-3.1 (-4.4 - - 2.2)	0.6 (-1.6-1.6)	*<0.001
FEF_{25}			
% predicted	61.5 (43.5-61.5)	109.0 (76.0-127.0)	*<0.001
z-score	-2.8 ± 1.4	-0.3 ± 2.2	*<0.001
FEF_{50}			
% predicted	62.1 ± 21.8	93.1 ± 44.8	*<0.001
z-score	-2.4 ± 1.5	-0.8 ± 2.3	*0.007
FEF_{75}			
% predicted	81.5 ± 36.2	104.4 ± 44.8	0.08
z-score	-0.8 ± 1.4	-0.1 ± 1.4	0.11
MEF			
% predicted	64.0 ± 23.0	92.8 ± 31.7	*0.001
z-score	-1.8 ± 1.3	-0.4 ± 1.5	*0.003
VCmax			
% predicted	89.1 ± 15.2	100.7 ± 12.7	*0.02
z-score	-1.1 (-1.53 – 0.0)	-0.3 (-0.8 – 0.9)	*0.02
FVCin			
% predicted	75.5 ± 15.0	85.7 ± 15.4	*0.05
FIV_1 (L)	1.7 (1.3-2.5)	2.7 (1.6-5.6)	0.47
FIV_1/FVC in (%)	78.5 (65.0-92.1)	99.8 (88.2-100.0)	*0.01
FIV_1/VCmax (%)	66.3 ± 16.5	80.9 ± 9.5	*0.007
FEV_1/FIV1 (%)	119.0 ± 25.8	105.3 ± 17.6	0.10
EDI (%)	62.6 (52.5-79.4)	45.3 (43.9-50.1)	*0.001

EDI; expiratory disproportion index, FEF_{25-75}; Forced Expiratory Flow at 25-75% of expiration, FEV_1; forced expiratory volume in 1 second, FIV_1; forced inspiratory volume in 1 second, FIV in; forced inspiratory volume, FVC; forced vital capacity, FVC in; forced vital capacity inspiratory, MEF; mean expiratory flow, PEF; peak expiratory flow, VC max; maximum vital capacity. Data are presented as mean ± standard deviation or median (interquartile range), *=p<0.05

Magnetic Resonance Imaging

MRI was successfully performed in 47 patients and 10 healthy volunteers (97%)(table 4). Two participants did not complete the MRI protocol due to claustrophobia. Image quality of the majority of the images was good, without artefacts in 66.7%. Excellent image resolution was achieved with best spatial resolution of 0.5 x 0.5 (in plane) x 2 mm (slice thickness) and best temporal resolution of 330 ms (3D dynamic scans).

Table 4: Magnetic Resonance Imaging results

General quality	**Patients and volunteers=59**		
Successful MRI (n/%)	57/97		
Quality static images (n/%)	Bad 0/0.0 Fair 2/3.5 Moderate 8/14.0 Good 35/61.4 Excellent 12/21.1		
Quality dynamic images (n/%)	Bad 2/3.5 Fair 5/8.8 Moderate 6/10.5 Good 40/70.2 Excellent 4/7.0		
Artefacts (n/%)	None 38/66.7 Coil 12/21.1 General motion 6/10.5 Respiratory motion 1/1.8		
Static	**Patients= 47◊**	**Volunteers=10**	**p-value**
Vocal cord thickening (n/%)	38/80.9	1/10	
Abnormal vocal cord positioning (n/%)	10/21.3	1/10	
Vocal cords			
Area (mm^2)	22.0 (17.7-30.3)	35.1 (21.2- 54.7)	*0.03
AP diameter (mm)	8.4 ± 2.0	9.0 ± 2.3	0.37
Transversal diameter (mm)	2.8 ± 1.0	3.8 ± 1.2	*0.01
Cricoid◊			
Area (mm^2)	62.3 ± 27.0	66.2 ± 34.8	0.70
AP diameter (mm)	8.4 ± 2.0	9.8 ± 2.1	0.05
Transversal diameter (mm)	6.3 ± 1.4	5.7 ± 0.8	0.16
Presence of tracheal deformation(n/%)	25/53.2	0/0	
Tracheal deformation			
Area (mm^2)	28.6 (20.8-41.9)	-	
AP diameter (mm)	6.6 ± 1.7	-	
Transversal diameter (mm)	4.4 ± 1.1	-	
Proximal trachea			
Area (mm^2)	61.0 (39.9-83.3)	86.1 (41.5-130.1)	0.19
AP diameter (mm)	7.3 ± 1.5	8.1 ± 2.1	0.16
Transversal diameter (mm)	7.3 ± 1.6	8.2 ± 1.3	0.10
Area decrease at deformation (area deformation/area trachea,%)	37.5 ± 23.5	-	-

Table 4: Continued

Dynamic			
Complete abduction during inspiration(n/%)	27/57.4	10/100	*0.01
Complete adduction during phonation(n/%)	18/38.3	10/100	*<0.01
2D	**Patients=35◊**	**Volunteers=9**	
Inspiration areas (mm^2)			
Vocal cords	43.7 ± 22.7	72.9 ± 42.3	*0.01
Cricoid	67.5 ± 26.9	84.3 ± 42.4	0.15
Tracheal deformation	38.4 ± 13.7	-	-
Trachea	79.5 ± 28.5	104.2 ± 50.5	0.07
Phonation areas (mm^2)			
Vocal cords	10.9 ± 9.3	7.2 ± 4.7	0.26
Cricoid	65.6 ± 30.4	90.5 ± 44.4	0.06
Tracheal deformation	46.9 ± 16.7	-	-
Trachea	77.0 ± 27.7	105.2 ± 49.9	*0.03
Difference in areas (%)			
Vocal cords	-72.1 ± 23.7	-88.9 ± 7.3	*0.04
Cricoid	-7.5 (-22.7-6.0)	-5.5 (-0.4-19.0)	*0.02
Tracheal deformation	27.0 ± 41.8	-	-
Trachea	-3.4 (-10.4-8.0)	2.2 (-4.6-10.5)	0.21

Data are presented as mean ± standard deviation, median (interquartile range) or absolute numbers (n) and percentages, *=p<0.05, data are corrected for height in meters. AP; anterior posterior. All areas and diameters are corrected for height in meters. ◊: Cricoid measurements conducted in n=43 for static and n=33 for dynamic images, due to exclusion of patients with history of CTR.

Figure 3 shows an example of a patient's static MR images. The outcomes of the static and dynamic MR analyses are shown in table 4. Thirty-eight patients (80.9%) and one healthy volunteer (10%) showed vocal cord thickening on MRI. This volunteer had a history of Tetralogy of Fallot, and had repeatedly been intubated during surgery, without any current complaints of respiratory distress. In patients with a history of LTR (n=43) autologous cartilage grafts could be identified on MRI in all but one patient, in whom the anterior graft could not be seen due to an artefact caused by a recently repaired tracheal fistula. Thirteen patients (30.2%) showed displacement of cartilage graft(s) into the airway lumen, namely displacement of the anterior cartilage graft in 3/39 (7.7%) and displacement of the posterior cartilage graft in 12/41 (29.3%) patients. Supplementary material 4 shows an example of displacement of a posterior cartilage graft.

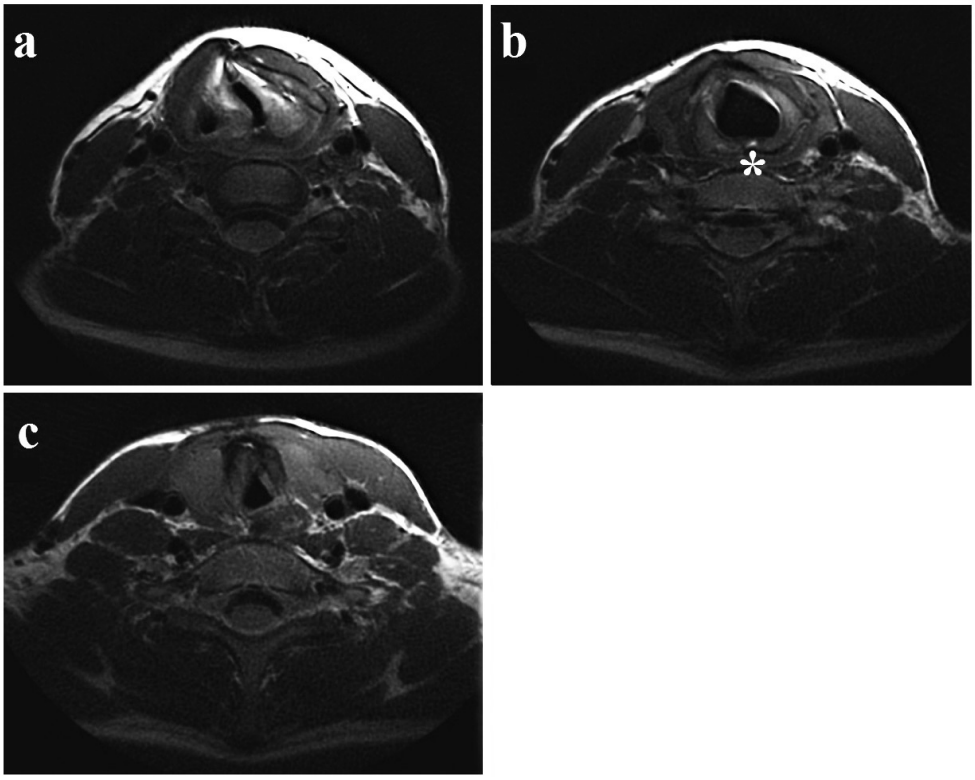

Figure 3: example of static MRI image of a patient with a history of LTS after prolonged intubation due to prematurity having undergone both a ss- and ds-LTR, showing deviation and thickening of the vocal cords (a), asterisk indicating the posterior cartilage graft placed during LTR (b) and the A-frame deformation of the trachea (c).

Patients' vocal cord lumen area was significantly smaller than that of healthy volunteers during free breathing. At the cricoid level, the location of LTR, the lumen area was comparable between patients and healthy volunteers. Additionally, in 25 patients (53.2%) an A-frame deformation at the level of previous tracheal cannula was found with an average lumen area reduction of 37.5% (range -9.3 – 74.5%) compared to the proximal trachea. Three patients showed other trachea deformations: one idiopathic saber-sheath deformation (an intra- thoracic tracheal deformation in which the transversal diameter of the trachea is smaller than the anterior-posterior diameter)(23), one saber-sheath deformation with an oesophageal pouch after oesophageal atresia repair, and one known malacia. In 78.3% of patients the narrowest point of the airway was located at the vocal cords, in 19.6% at the tracheal deformation, and in 2.2% at the trachea. In all healthy volunteers the narrowest point was located at the vocal cords. A significant correlation between vocal cord lumen area and both in- and expiratory spirometry was found (table 5, supplementary material 5).

Table 5: Correlations between areas at different levels of the upper airways on MRI and spirometry

	FEV_1 (%pred)		FEV_1/FVC (%pred)		FIV_1/VCmax (%)		EDI (%)	
Vocal cord area	r_s=0.30 (0.04-0.52)	**p=0.02**	r_s=0.33 (0.06-0.54)	**p=0.01**	r=0.34 (0.08-0.58)	**p=0.01**	r_s=-0.31 (^{s}0.53- -0.05)	**p=0.02**
Cricoid area	r=0.03 (-0.24-0.29)	p=0.85	r=-0.02 (-0.29-0.25)	p=0.88	r=0.03 (-0.24-0.29)	p=0.84	r=-0.08 (-0.19-0.35)	p=0.54
Tracheal deformation area	r_s=0.25 (^{s}0.16-0.59)	p=0.22	r_s=0.19 (^{s}0.23-0.54)	p=0.37	r=0.22 (-0.20-0.63)	p=0.30	r_s=-0.01 (^{s}0.19-0.35)	p=0.97
Trachea area	r_s=0.18 (^{s}0.09-0.42)	p=0.19	r_s=0.14 (^{s}0.13-0.39)	p=0.30	r=0.28 (0.01-0.53)	**p=0.04**	r_s=-0.06 (^{s}0.32-0.20)	p=0.65

EDI; Expiratory Disproportion Index, FEV_1; Forced Expiratory Volume in 1 second, FIV_1; Forced Inspiratory Volume in 1 second, FVC; Forced Vital Capacity. Data are presented as Pearson (r) or Spearman (r_s) correlation coefficient (95% confidence interval) and p- value. P values <0.05 are in bold.

As an incidental finding MRI showed hypointense regions on PD-w images in 40 patients (85.1%), and none of the healthy volunteers. Ultrasonography in four patients did not clarify the origin of this artefact (supplementary material 6), being either post-surgical artefacts from the use of metal surgical instruments, such as those detected in gradient-echo imaging of the post-surgical knee(24, 25), or subcutaneous emphysema, despite on physical examination no crackling could be felt on the neck.

A supplementary video shows an example of the dynamic MR images of a patient. Complete abduction during inspiration and complete adduction during phonation was seen in 57.4% and 38.3% of patients respectively, compared to 100% for both in healthy volunteers. In 11 patients (23.4%) asymmetrical vocal cord movement was observed. Quantitative analyses on the 2D dynamic images could be performed in 37 patients (78.7%) and 9 healthy volunteers (90%), due to correct execution of the manoeuvres. In two patients 2D dynamic scans were of insufficient quality to perform the area measurements. Patients showed a significantly smaller vocal cord lumen area during inspiration compared to healthy volunteers. Binary logistic regression did not show a correlation between posterior glottic involvement of the stenosis and the area between the vocal cords during inspiration (odds ratio 0.98 (CI 0.94-2.01),p=0.18) nor phonation (odds ratio 1.03 (CI 0.95-1.13),p=0.46) on MRI. A greater area between the vocal cords during inspiration was correlated to an increase in FIV_1/VCmax (r=0.38, CI 0.09-0.69, p=0.01) but not to the EDI (r=-0.23, CI -0.54-0.07,p=0.13).

In patients with an A-frame trachea deformation, an average decrease in airway lumen area of 27% during inspiration was observed. We did not find a correlation between the presence of a tracheal deformation and a decrease in inspiratory spirometry (FIV_1/VCmax odds ratio 0.98 (CI 0.94-1.02), p=0.35 and EDI 1.01 (CI 0.96-1.05),p=0.77)

On T2-w sequences thirty-seven (78.7%) patients showed signs of fibrosis or chronic oedema, located at the arytenoids in 59.6%, vocal cords in 57.4% and cricoid in 8.5%. Forty- six patients (95.8%) and ten healthy volunteers (90.9%) had DW images available for

analyses. On DWI 26.1% of patients showed signs of oedema, 6.5% of patients showed signs of fibrosis, and 17.4% of patients showed signs of a combination of oedema and fibrosis. One patient had a pattern on hyperintense signal on DWI with hypointense signal on ADC and one patient had a pattern of hypointense signal on DWI with hyperintense signal on ADC, both of unknown origin. Eighteen patients (39.1%) had signs of tissue alteration on T2-w imaging without signal abnormalities on DWI, corresponding to mild fibrosis and/or oedema. Tissue alteration according to the combination of T2-w and DW imaging did not correlate to previous glottic involvement (1.7 (CI 0.5-5.9) p=0.40) nor to impaired vocal movement on MRI (0.86 (CI 0.3-2.7) p=0.79). Tissue alteration according to T2-w images alone, therefore also including mild fibrosis and oedema, was significantly correlated to previous glottic involvement of the stenosis (odds ratio 9.5 (CI 1.7-53.4) p=0.01) as well as impaired vocal cord movement on MRI (3.5 (CI 1.0-11.6) p=0.04).

Intra- and inter variability analysis showed good to excellent consistency for all static (supplementary material 7) and dynamic MRI measurements, except for the subjective scoring of complete abduction and adduction.

Discussion

We used static and dynamic MRI to evaluate the upper airways after open airway surgery for paediatric LTS. MRI enabled visualisation of anatomical structures, tissue characterisation and quantification of vocal cord and airway dynamics and thereby provided a new imaging modality to assess post- surgical sequelae of LTS.

Static MRI permitted quantification of the post- surgical upper airway anatomy in an objective manner. Patients' vocal cord lumen area, but not cricoid lumen area, was smaller than that of healthy volunteers. These static measurements proved to be highly reproducible as shown by the excellent intra- and interobserver agreement. Furthermore, we could visualise the correct or incorrect position of autologous cartilage grafts in the cricoid.

Dynamic MR images of the vocal cords showed a high prevalence of impaired vocal cord movement. These sequences showed to be important to assess respiratory and vocal sequelae of LTS surgery and could be used as monitoring tool for different treatment options.(5) However, subjective scoring of impaired vocal cord ab- and adduction resulted in poor interobserver agreement, presumably because ab- and adduction is highly influenced by both thickening and abnormal positioning of the vocal cords. Therefore, we did not use subjective scoring of ab- and adduction for further analyses. To evaluate vocal cord movement, we recommend to use area measurements during inspiration and phonation. We furthermore recommend the use of both 2D and 3D sequences, with 2D best suitable

for quantitative measurements and 3D best suitable for the overall evaluation of upper airway dynamics.

Interestingly, dynamic MRI showed a high incidence of tracheal deformations with lumen collapse during inspiration. Previous studies have reported a lower incidence of A-frame deformations of 10% after tracheal cannula removal.(26) Likely the higher incidence in our study related to the ability to detect all A-frame deformations, irrespective of clinical symptoms. We did not observe a correlation between the presence of a tracheal deformation and impaired inspiratory spirometry outcomes. This could either be caused by a small sample size, or more likely by the malacic character of the tracheal deformation, where elastic recoil due to an increased negative pressure at the level of the stenosis (Bernoulli-Venturi effect) varies airway resistance at the level of the stenosis.(27, 28)

Tissue characterisation was evaluated on T2-w and DW imaging, showing good correlation between tissue alteration according to T2-w imaging and patient characteristics and outcome. Tissue alteration of airway mucosa (such as the presence of fibrosis) is currently subjectively diagnosed by laryngotracheoscopy, known to be sensitive to observer bias and poor interobserver correlations.(29, 30) T2-w MRI can be used as a replacement as it allows to visualise oedema and fibrosis. In addition, previous studies have shown the potential additional benefit of DWI to detect tissue with decreased free movement of hydrogen molecules due to cellular swelling or increased tissue density, as has been observed in post radiation fibrosis.(13, 31, 32) This is the first study using DWI to compare normal airway tissue to post- surgical tissue alterations. Although we did not have histology samples available for comparison, T2-w imaging seems to be able to characterise tissue of the upper airways. No added benefit of DWI compared to T2-w imaging was found, either because DWI does not detect mild tissue alterations or because DWI is highly sensitive to technical variations such as poor signal-to-noise ratios from poor coil fitting, inadequate fat suppression or motion artefacts in younger children. Contrast enhancement might be an alternative method to further improve tissue characterisation, but this would require intravenous access and could raise concerns related to the use of MRI contrast agents as tissue deposition in the brain has been reported.(33) In selected patients, a combination of MRI with Positron Emission Tomography (PET-MRI) might be used to detect active inflammation.(34)

Our overall findings suggest that MRI, when performed successfully, can supply highly relevant information for follow-up evaluation of LTS patients and provide similar information as laryngotracheoscopy. MRI can overcome important downsides of laryngotracheoscopy such as the need for anaesthesia, inter-observer variability issues and it allows objective tissue characterisation. A challenge of our MRI protocol is the need for patient cooperation, which precludes its use in children below the age of six years and in older non-cooperative children. Good correlations between spirometry outcomes and lumen areas suggest that

MRI measurements could aid in understanding the anatomical substrate causing airflow obstruction, as indicated by a previous study.(14) A more affordable and widely available alternative method could be flexible nasal endoscopy, however, this method is unsuitable to evaluate anatomy below the vocal cords, is non- quantitative and can be challenging in case of arytenoid prolapse. Therefore, we consider flexible nasal endoscopy not a realistic alternative to laryngotracheoscopy nor to MRI.(2)

Our findings also show the diversity and complexity of the post-surgical airway with patients presenting with a heterogeneity in the level(s) and severity of airway obstructions. The effect of obstructions at consecutive airway levels on airway dynamics and airway resistance is not entirely clear. We are currently working on computational fluid dynamic modelling studies to visualise airway mechanics in an attempt to determine the contributions of separate obstructions on airflow patterns and airway resistance.

The main limitation of our study is the lack of direct comparison with the gold standard, laryngotracheoscopy, because this is not routinely performed in our LTS follow up. However, in four patients we could compare MRI to a recent laryngotracheoscopy, showing that unilateral vocal cord movement on MRI corresponds to paralysis or asymmetrical fibrosis of the vocal cords on laryngotracheoscopy. This shows that these modalities are comparable, as seen in previous studies in paediatric OSAS and tracheomalacia(35, 36), as well as between CT and laryngoscopy in tracheomalacia.(37) Another important limitation to our study is the effect of co-morbidities on the lung function test. Co-morbidities might have influenced the airflow limitations in our cohort, as spirometry was technically challenging for some of these children. In addition z-scores for inspiratory spirometry values are not available. Lastly, because of the innovative character of our imaging analyses, we could not compare our data to reference values or other studies. We selected healthy volunteers first to get an impression of the healthy upper airways on MRI. For logistic reasons the chosen siblings and friends were not matched for sex and age and no sample size calculation was performed. Therefore correlations found should be interpreted cautiously and future studies should focus on obtaining MRI reference values at different ages in a larger cohort of healthy children.

In conclusion, this is the first study reporting follow-up MRI data of a large LTS population. MRI proved to be an excellent modality to non- invasively image anatomic structures, characterise tissue and quantify dynamics of the upper airways. Our observations of residual stenosis at consecutive airway levels, a high incidence of A-frame deformations of the trachea, and a high incidence of impaired vocal cord movement, contribute to the knowledge on post- surgical sequelae of LTS. The information provided by MRI might be useful to assess post-LTS sequelae in an out-patient setting. This can be especially helpful in cases of complex multi-level stenosis where imaging can provide the surgeon an objective

measurement of the different stenosis sites and can aid in the decision making for further surgery. Our study shows that MRI is a non-invasive safe and valuable image modality for the follow up of LTS patients.

Acknowledgements
We would like to acknowledged Eleni Rosalina Andrinopoulou for the statistical support on the article.

References

1. Jefferson ND, Cohen AP, Rutter MJ. Subglottic stenosis. Semin Pediatr Surg. 2016;25(3):138-43.
2. Monnier P. Pediatric Airway Surgery Management of Laryngotracheal Stenosis in Infants and Children. Berlin, Heidelberg: Springer Berlin Heidelberg; 2011.
3. Pullens B, Hoeve LJ, Timmerman MK, van der Schroeff MP, Joosten KF. Characteristics and surgical outcome of 98 infants and children surgically treated for a laryngotracheal stenosis after endotracheal intubation: excellent outcome for higher grades of stenosis after SS-LTR. Int J Pediatr Otorhinolaryngol. 2014;78(9):1444-8.
4. Padia R, Sjogren P, Smith M, Muntz H, Stoddard G, Meier J. Systematic review/meta-analysis comparing successful outcomes after single vs. double-stage laryngotracheal reconstruction. Int J Pediatr Otorhinolaryngol. 2018;108:168-74.
5. Pullens B, Hakkesteegt M, Hoeve H, Timmerman M, Joosten K. Voice outcome and voice-related quality of life after surgery for pediatric laryngotracheal stenosis. Laryngoscope. 2017;127(7):1707-11.
6. Pullens B, Pijnenburg MW, Hoeve HJ, Baatenburg de Jong RJ, Buysse CM, Timmerman MK, et al. Long-term functional airway assessment after open airway surgery for laryngotracheal stenosis. Laryngoscope. 2016;126(2):472-7.
7. Baker S, Kelchner L, Weinrich B, Lee L, Willging P, Cotton R, et al. Pediatric laryngotracheal stenosis and airway reconstruction: a review of voice outcomes, assessment, and treatment issues. J Voice. 2006;20(4):631-41.
8. Balakrishnan K, Sidell DR, Bauman NM, Bellia-Munzon GF, Boesch RP, Bromwich M, et al. Outcome measures for pediatric laryngotracheal reconstruction: International consensus statement. Laryngoscope. 2019;129(1):244-55.
9. Parkes WJ, Propst EJ. Advances in the diagnosis, management, and treatment of neonates with laryngeal disorders. Semin Fetal Neonatal Med. 2016;21(4):270-6.
10. Zdanski C, Davis S, Hong Y, Miao D, Quammen C, Mitran S, et al. Quantitative assessment of the upper airway in infants and children with subglottic stenosis. Laryngoscope. 2016;126(5):1225-31.
11. Huang BY, Solle M, Weissler MC. Larynx: anatomic imaging for diagnosis and management. Otolaryngol Clin North Am. 2012;45(6):1325-61.
12. Mazonakis M, Tzedakis A, Damilakis J, Gourtsoyiannis N. Thyroid dose from common head and neck CT examinations in children: is there an excess risk for thyroid cancer induction? Eur Radiol. 2007;17(5):1352-7.
13. Elders B, Hermelijn SM, Tiddens H, Pullens B, Wielopolski PA, Ciet P. Magnetic resonance imaging of the larynx in the pediatric population: A systematic review. Pediatr Pulmonol. 2019;54(4):478-86.
14. Henes FO, Laudien M, Linsenhoff L, Bremer JP, Oqueka T, Adam G, et al. Accuracy of Magnetic Resonance Imaging for Grading of Subglottic Stenosis in Patients with Granulomatosis with

Polyangiitis: Correlation with Pulmonary Function Tests and Laryngoscopy. Arthritis Care Res 2017;70(5):777-84.
15. Klink T, Holle J, Laudien M, Henes FO, Moosig F, Platzek C, et al. Magnetic resonance imaging in patients with granulomatosis with polyangiitis (Wegener's) and subglottic stenosis. Magma. 2013;26(3):281-90.
16. Myer CM, 3rd, O'Connor DM, Cotton RT. Proposed grading system for subglottic stenosis based on endotracheal tube sizes. Ann Otol Rhinol Laryngol. 1994;103(4 Pt 1):319-23.
17. Miller MR, Crapo R, Hankinson J, Brusasco V, Burgos F, Casaburi R, et al. General considerations for lung function testing. Eur Respir J. 2005;26(1):153-61.
18. Quanjer PH, Hall GL, Stanojevic S, Cole TJ, Stocks J, Global Lungs I. Age- and height-based prediction bias in spirometry reference equations. Eur Respir J. 2012;40(1):190-7.
19. Nouraei SA, Nouraei SM, Patel A, Murphy K, Giussani DA, Koury EF, et al. Diagnosis of laryngotracheal stenosis from routine pulmonary physiology using the expiratory disproportion index. Laryngoscope. 2013;123(12):3099-104.
20. Zhang Q, Coolen BF, van den Berg S, Kotek G, Rivera DS, Klomp DWJ, et al. Comparison of four MR carotid surface coils at 3T. PLoS One. 2019;14(3):e0213107.
21. Wang J, Takashima S, Takayama F, Kawakami S, Saito A, Matsushita T, et al. Head and neck lesions: characterization with diffusion-weighted echo-planar MR imaging. Radiology. 2001;220(3):621-30.
22. Chavhan GB, Alsabban Z, Babyn PS. Diffusion-weighted imaging in pediatric body MR imaging: principles, technique, and emerging applications. Radiographics. 2014;34(3):E73-88.
23. Ciccarese F, Poerio A, Stagni S, Attinà D, Fasano L, Carbonara P, et al. Saber-sheath trachea as a marker of severe airflow obstruction in chronic obstructive pulmonary disease. Radiol Med. 2014;119(2):90-6.
24. Haramati N, Penrod B, Staron RB, Barax CN. Surgical sutures: MR artifacts and sequence dependence. J Magn Reson Imaging. 1994;4(2):209-11.
25. Heindel W, Friedmann G, Bunke J, Thomas B, Firsching R, Ernestus RI. Artifacts in MR imaging after surgical intervention. J Comput Assist Tomogr. 1986;10(4):596-9.
26. Hysinger EB, Panitch HB. Paediatric Tracheomalacia. Paediatr Respir Rev. 2016;17:9-15.
27. Strohl KP, Butler JP, Malhotra A. Mechanical properties of the upper airway. Compr Physiol. 2012;2(3):1853-72.
28. Wilmott RW, Deterding RR, Li A, Ratjen FA, Sly P, Zar HJ, et al. Kendig's disorders of the respiratory tract in children 2019 [
29. van der Pol RJ, Singendonk MM, Konig AM, Hoeve H, Kammeijer Q, Pullens B, et al. Development of the reflux finding score for infants and its observer agreement. J Pediatr. 2014;165(3):479-84.
30. Singendonk MM, Pullens B, van Heteren JA, de Gier HH, Hoeve HL, Konig AM, et al. Reliability of the reflux finding score for infants in flexible versus rigid laryngoscopy. Int J Pediatr Otorhinolaryngol. 2016;86:37-42.

31. Abdel Razek AA, Gaballa G, Elhawarey G, Megahed AS, Hafez M, Nada N. Characterization of pediatric head and neck masses with diffusion-weighted MR imaging. Eur Radiol. 2009;19(1):201-8.
32. Taha MS, Amir M, Hassan O, Sabra R, Taha T, Riad MA. Pre-treatment apparent diffusion coefficient mapping: Differentiation of benign from malignant laryngeal lesions. J Laryngol Otol. 2015;129(1):57-62.
33. Young JR, Orosz I, Franke MA, Kim HJ, Woodworth D, Ellingson BM, et al. Gadolinium deposition in the paediatric brain: T1-weighted hyperintensity within the dentate nucleus following repeated gadolinium-based contrast agent administration. Clin Radiol. 2018;73(3):290-5.
34. Gatidis S, Bender B, Reimold M, Schafer JF. PET/MRI in children. Eur J Radiol. 2017;94:A64-A70.
35. Clark C, Ulualp SO. Multimodality assessment of upper airway obstruction in children with persistent obstructive sleep apnea after adenotonsillectomy. Laryngoscope. 2017;127(5):1224-30.
36. Hysinger EB, Bates AJ, Higano NS, Benscoter D, Fleck RJ, Hart C, et al. Ultrashort Echo-Time MRI for the Assessment of Tracheomalacia in Neonates. Chest. 2019.
37. Ngerncham M, Lee EY, Zurakowski D, Tracy DA, Jennings R. Tracheobronchomalacia in pediatric patients with esophageal atresia: comparison of diagnostic laryngoscopy/bronchoscopy and dynamic airway multidetector computed tomography. J Pediatr Surg. 2015;50(3):402-7.

Supplementary materials

Supplementary material 1: Flowchart of the patient and healthy volunteer selection

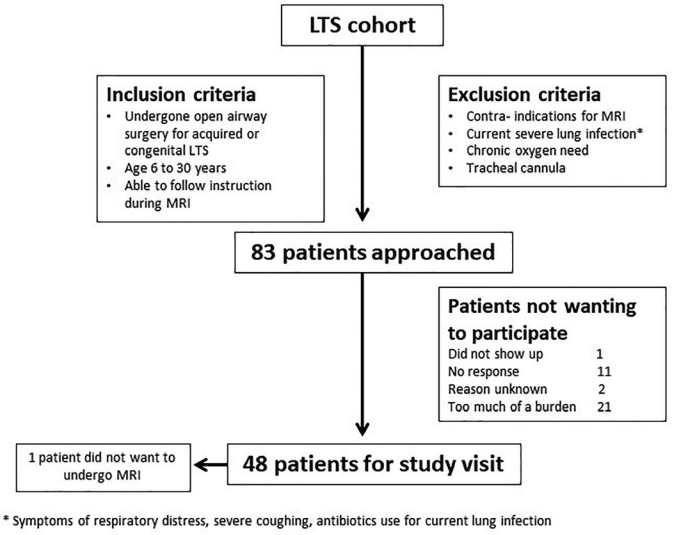

Supplementary material 2: Comparison between patients who did and did not participate in the MUSIC study

	Patients participating=48	Patients not participating=35	
Age (years)	14.4 (11.7-19.4)	19.1 (14.3-24.0)	*0.01
Gender (% female)	52.1	42.9	0.41
Type of stenosis (%)			0.12
Acquired	93.8	82.9	
Congenital	6.3	17.1	
CM grade of stenosis (%)			0.08
Grade I	8.3	-	
Grade II	31.3	20.6	
Grade III	56.3	79.4	
Grade IV	4.2	-	
Location of stenosis (%)			0.10
Posterior glottis	22.9	17.1	
Subglottis	35.4	57.1	
Posterior glottis and subglottis	41.7	22.9	
Tracheal cannula before repair (%)	79.2	74.3	0.60
Type of repair (%)			0.95
SS-LTP	87.5	85.7	
DS-LTP	4.2	5.7	
CTR	8.3	8.6	
Bronchopulmonary dysplasia (%)	18.8	22.9	0.65

CM; Cotton Myer, CTR; cricoid resection, ds-LTR; double stage laryngotracheal stenosis, ss-LTR; single stage laryngotracheal reconstruction. Data are presented as median (interquartile range) or percentage. *=p<0.05

Supplementary material 3A: Upper airways MRI protocol

Sequence	Plane	TR (ms)	TE (ms)	Flip (°)	BW (Hz)	NEX	pif	FOV (cm^2)	Matrix	Slices / thick (mm)	Actual Voxel resolution (mm^3)	Interp. resolution (mm^3)	Time
Anatomical													
2D T2w PROPELLER	Axial	4400	49	90/ 142	62.5	6	3	15.3 x 15.3	320 x 320	25 / 2.0	0.47 x 0.47 x 2.0	0.29 x 0.29 x 2.0	4 min 46 s
2D T2w FS PROPELLER	Axial	4570	50	90/ 142	62.5	6	3	15.3 x 15.3	320 x 320	25 / 2.0	0.47 x 0.47 x 2.0	0.29 x 0.29 x 2.0	4 min 57 s
2D T2w PROPELLER	Sagittal	3730	50	90/ 142	62.5	6	3	15.3 x 15.3	320 x 320	21 / 2.0	0.47 x 0.47 x 2.0	0.29 x 0.29 x 2.0	4 min 4 s
2D T2w PROPELLER	Coronal	3700	50	90/ 142	62.5	6	3	15.3 x 15.3	320 x 320	21 / 2.0	0.47 x 0.47 x 2.0	0.29 x 0.29 x 2.0	4 min 4 s
3D PDw SPGR Calc	Axial	3.8	2.1	3	90.9	5	1	15.3 x 15.3	320 x 224	68 / 0.8	0.47 x 0.68 x 0.8	0.29 x 0.29 x 0.4	4 min 3 s
Tissue Characterization													
2D Multi b-value DWI	Axial	2100	54.6	90/ 180	250.0	3 (b10) 5 (b100) 7 (b200) 11 (b400) 15 (b800)	1	18.0 x 4.5	90 x 180	16 / 3.2	2.0 x 1.0 x 3.2	0.70 x 0.70 x 3.2	4 min 17 s
Dynamic													
2D SSFSE Insp, AAAA	Axial	∞	47	90/ 110	62.5	0.5	2	15.3 x 10.7	160 x 128	25 / 2.0	0.95 x 0.68 x 0.8	0.29 x 0.29 x 0.4	7 s
3D TRICKS Cont. Insp-AAAA	Axial	2.0	0.9	3	90.9	1.0	2	21.0 x 12.6	160 x 98	18 / 3.0	1.31 x 2.14 x 3.0	0.82 x 0.82 x 1.5	8 s / 330 ms temporal resolution per volume

A/P; Anterior/Posterior, BW; Bandwidth, DWI; Diffusion Weighted Imaging, ETL; Echo Train Length, FOV; Field Of View, FS; fat saturated, PD; Proton Density, NEX; Number of Excitations, PROPELLER; Periodically Overlapping ParalLEL Lines with Enhanced Reconstruction , SPGR; Spoiled Gradient Echo Sequence, SSFSE; Single Shot Fast Spin Echo, TE; Echo Time, TR; Repetition Time, TRICKS; Time Resolved Imaging of Contrast Kinetics

Supplementary material 3B: MRI analyses protocol

Image quality
Bad: major artefacts and blurring, not suitable for analyses
Poor: moderate artefacts and blurring, partially suitable for analyses
Moderate: minor artefacts and blurring, suitable for analyses
Good: no artefacts or blurring, suitable for analyses
Excellent: no artefacts or blurring, excellent delineation of all structures

Artefacts
Coil, general motion or respiration related

Static images
Vocal cord thickening: protrusion of the vocal cords into the airway lumen at the vocal cords
Arytenoid prolapse: protrusion of the arytenoids into the airway lumen at the vocal cords
Vocal cord deviation: deviation from the triangular shape between anterior commissure and vocal cords
Airway deformations: disruption of the circular airway lumen (an A-frame deformation due to previous tracheal cannula placement or other deformations, such as due to esophageal atresia)
Displacement of cartilage grafts: protrusion of the cartilage grafts into the airway lumen
Fibrosis/chronic edema: tissue thickening or hyperintense signal on T2 weighted imaging

Dynamic images
Correct performance of the 2D dynamic maneuvers: any vocal cord abduction during inspiration and any vocal cord adduction during phonation
Correct performance of the 3D dynamic maneuvers: any vocal cord movement
Complete abduction: opening of the vocal cords into a triangular shape with a symmetrical 90 degree angle
Complete adduction: parallel closing of the vocal cords
Inspiration area: area between the vocal cords during inspiration measured on the axial 2D dynamic image
Phonation area: area between the vocal cords during phonation measured on the axial 2D dynamic image
Difference in area: area between the vocal cords during phonation divided by the area between the vocal cords during inspiration x 100%

Supplementary material 4: Example of displacement of a posterior cartilage piece

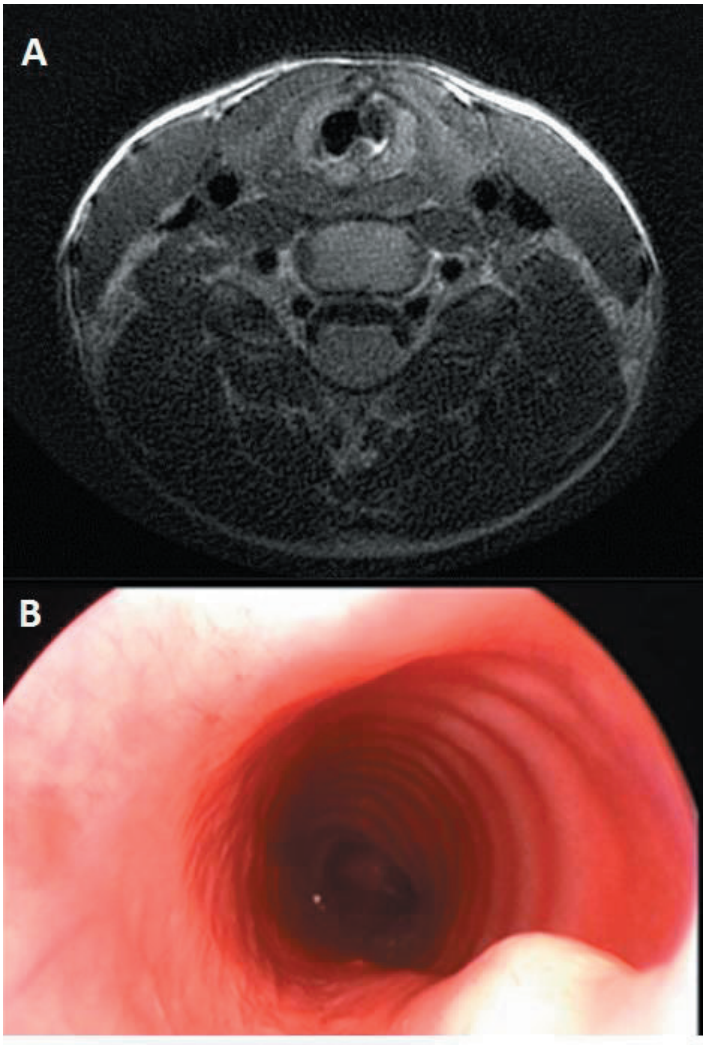

Supplementary material 4: axial T2-weighted PROPELLER image of a patient post-LTS repair at the level of the cricoid showing displacement of the posterior cartilage piece into the airway lumen (top image) and an image from a direct video laryngoscopy at the same location showing displacement of the posterior cartilage piece into the airway lumen (bottom image).

Supplementary material 5: Scatter plots of correlations between areas at different levels of the upper airways on MRI and spirometry

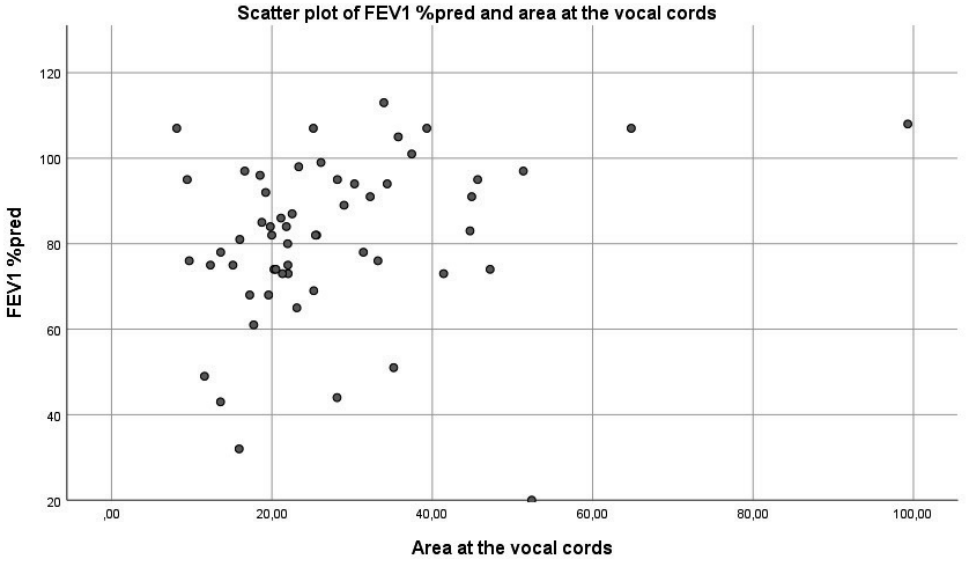

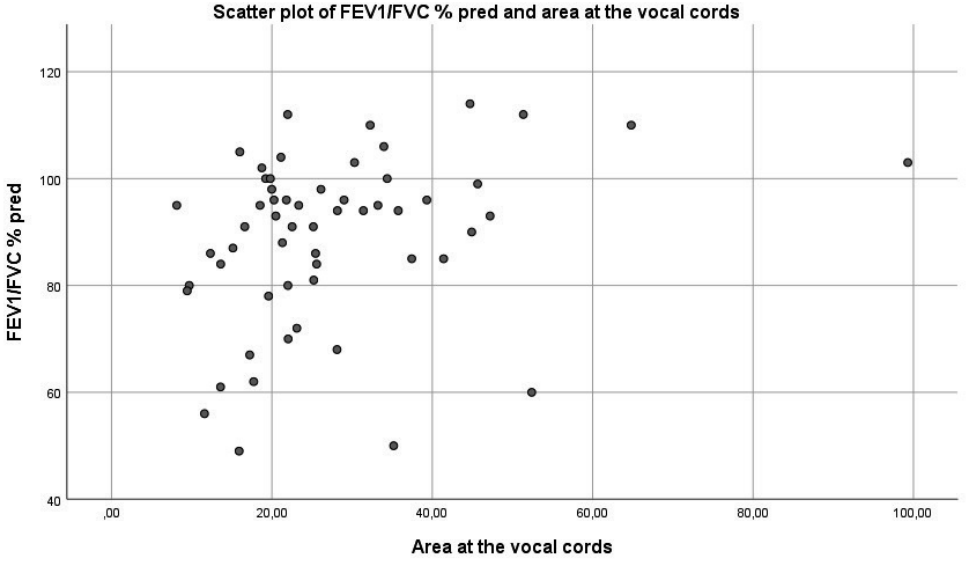

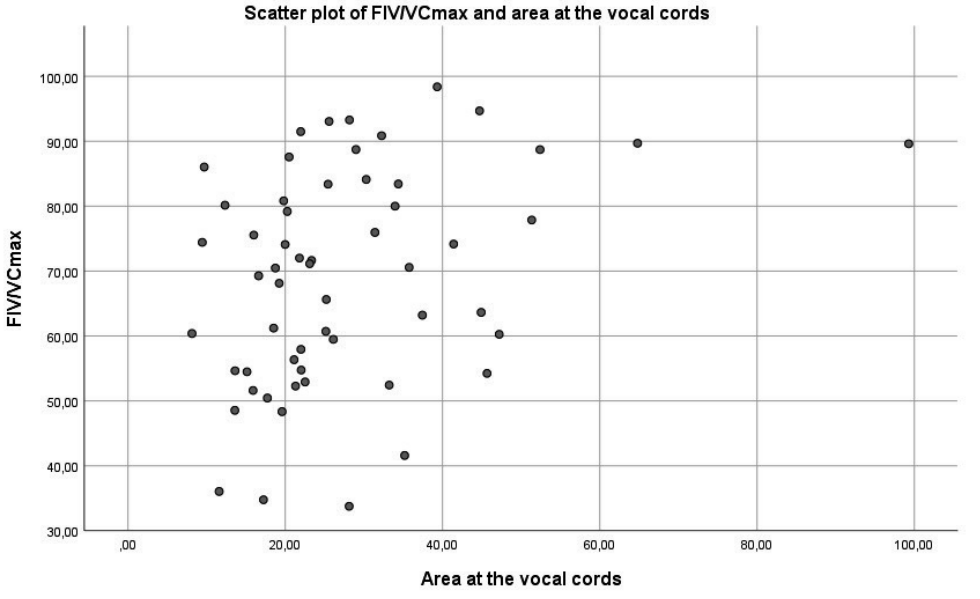
Scatter plot of FIV/VCmax and area at the vocal cords
FIV/VCmax
100,00
90,00
80,00
70,00
60,00
50,00
40,00
30,00
,00
20,00
40,00
60,00
80,00
100,00
Area at the vocal cords

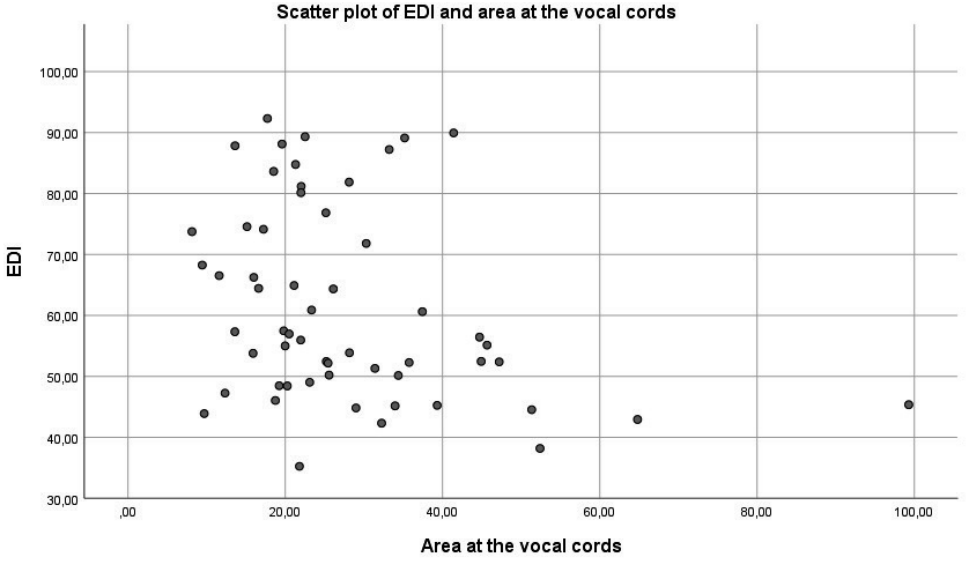
Scatter plot of EDI and area at the vocal cords
EDI
100,00
90,00
80,00
70,00
60,00
50,00
40,00
30,00
,00
20,00
40,00
60,00
80,00
100,00
Area at the vocal cords

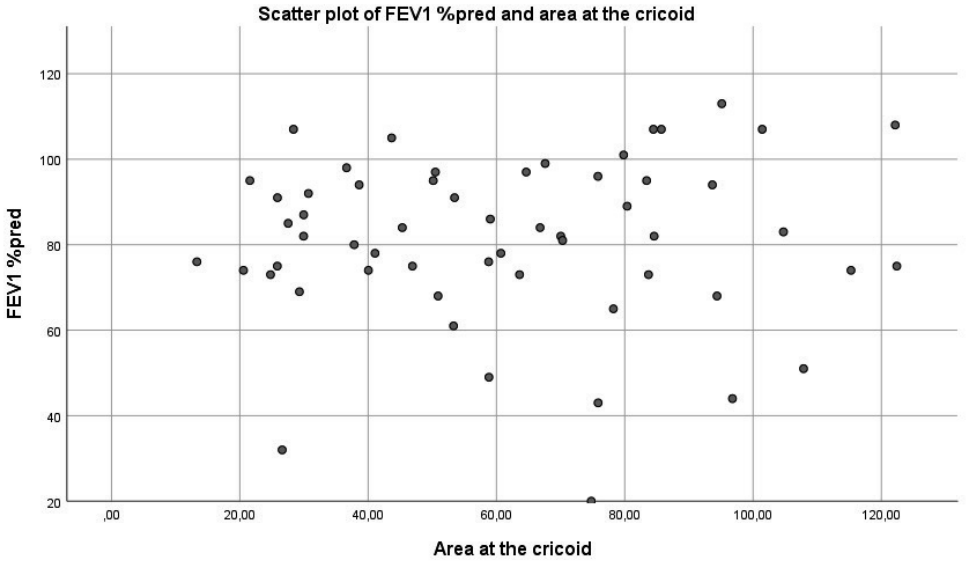
Scatter plot of FEV1 %pred and area at the cricoid
FEV1 %pred
120
100
80
60
40
20
,00
20,00
40,00
60,00
80,00
100,00
120,00
Area at the cricoid

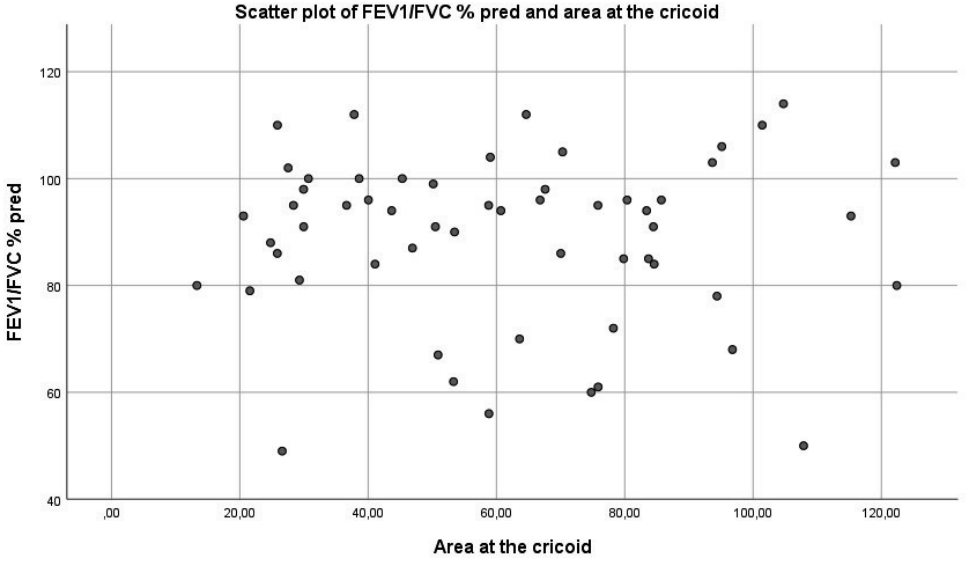
Scatter plot of FEV1/FVC % pred and area at the cricoid
FEV1/FVC % pred
120
100
80
60
40
,00
20,00
40,00
60,00
80,00
100,00
120,00
Area at the cricoid

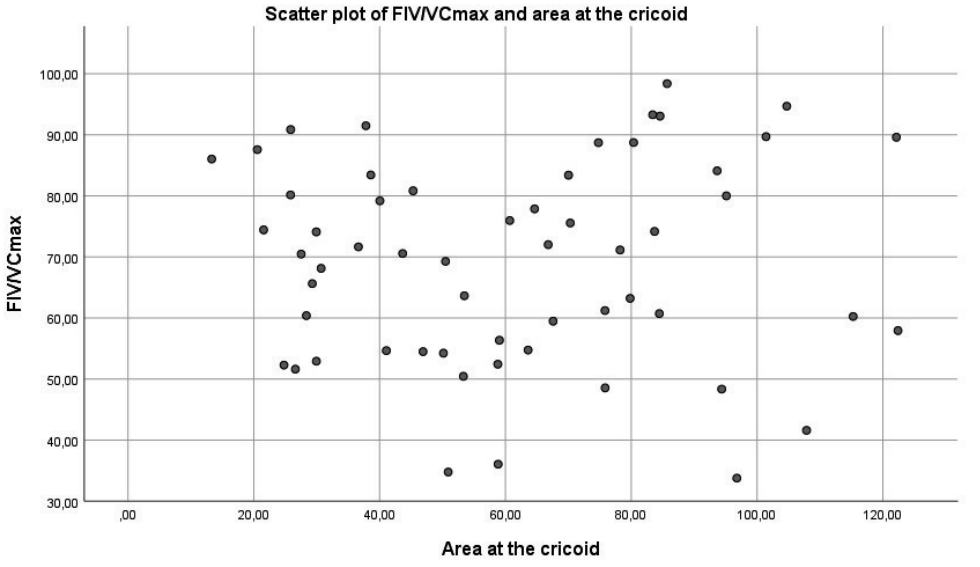
Scatter plot of FIV/VCmax and area at the cricoid
FIV/VCmax
100,00
90,00
80,00
70,00
60,00
50,00
40,00
30,00
,00
20,00
40,00
60,00
80,00
100,00
120,00
Area at the cricoid

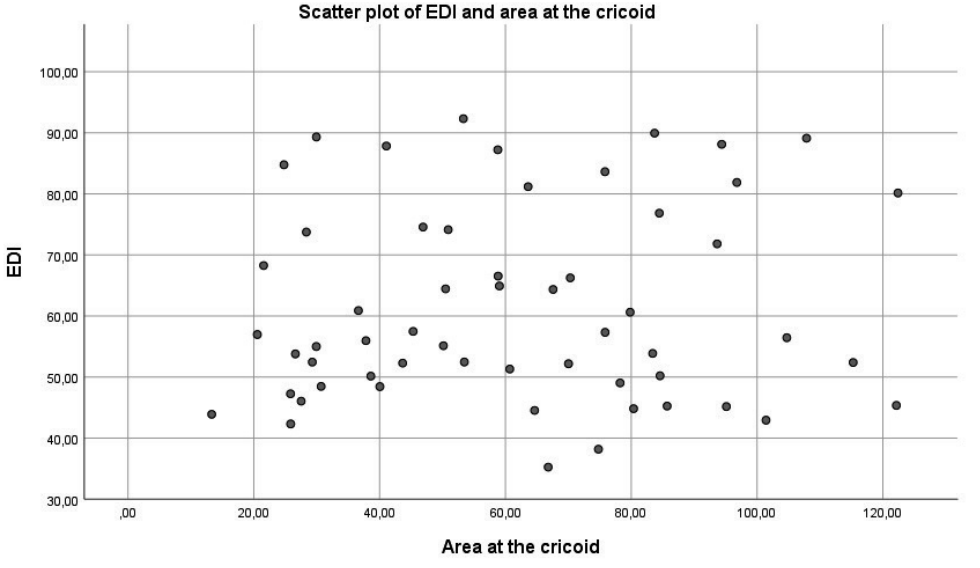
Scatter plot of EDI and area at the cricoid
EDI
100,00
90,00
80,00
70,00
60,00
50,00
40,00
30,00
,00
20,00
40,00
60,00
80,00
100,00
120,00
Area at the cricoid

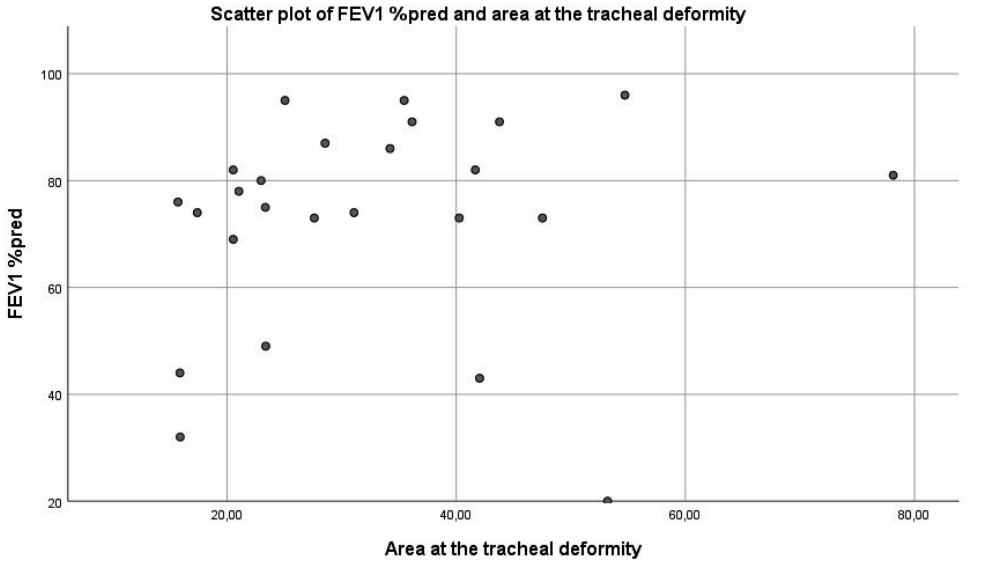
Scatter plot of FEV1 %pred and area at the tracheal deformity
FEV1 %pred
100
80
60
40
20
20,00
40,00
60,00
80,00
Area at the tracheal deformity

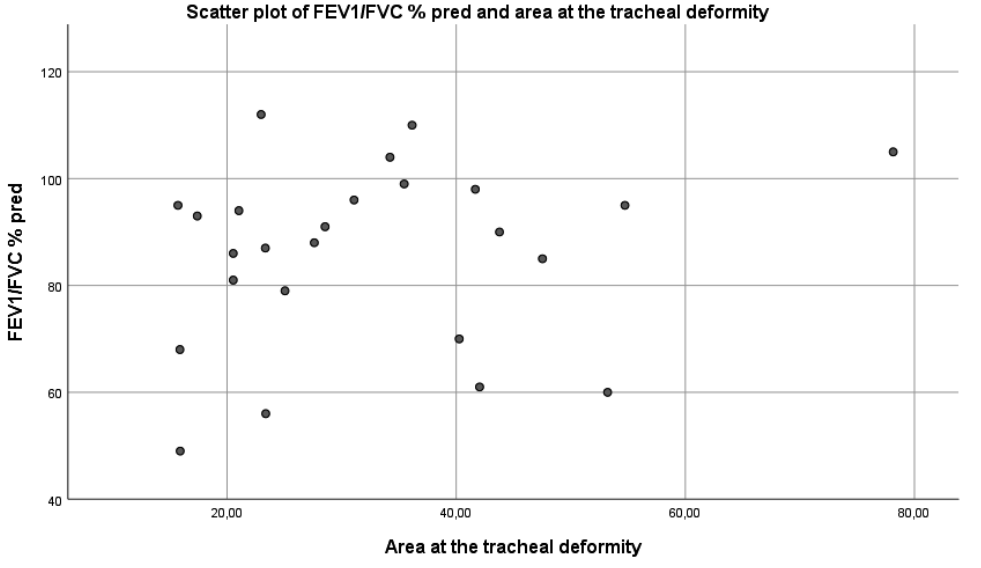
Scatter plot of FEV1/FVC % pred and area at the tracheal deformity
FEV1/FVC % pred
120
100
80
60
40
20,00
40,00
60,00
80,00
Area at the tracheal deformity

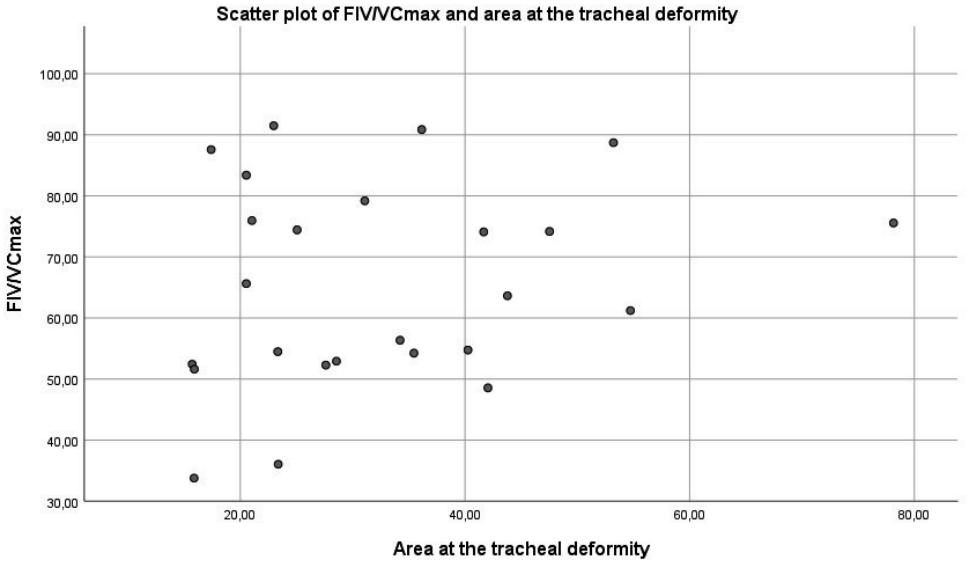
Scatter plot of FIV/VCmax and area at the tracheal deformity
FIV/VCmax
100,00
90,00
80,00
70,00
60,00
50,00
40,00
30,00
20,00
40,00
60,00
80,00
Area at the tracheal deformity

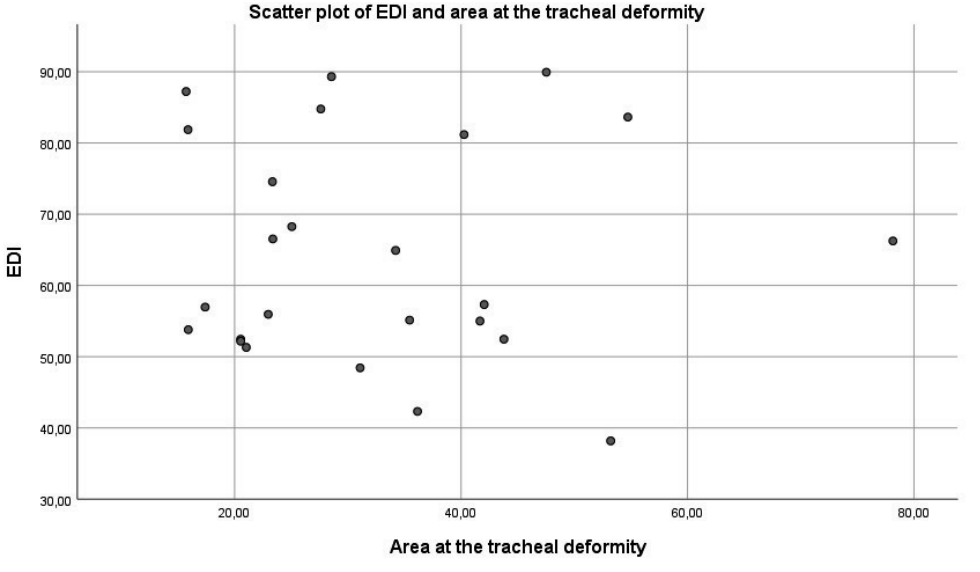
Scatter plot of EDI and area at the tracheal deformity
EDI
90,00
80,00
70,00
60,00
50,00
40,00
30,00
20,00
40,00
60,00
80,00
Area at the tracheal deformity

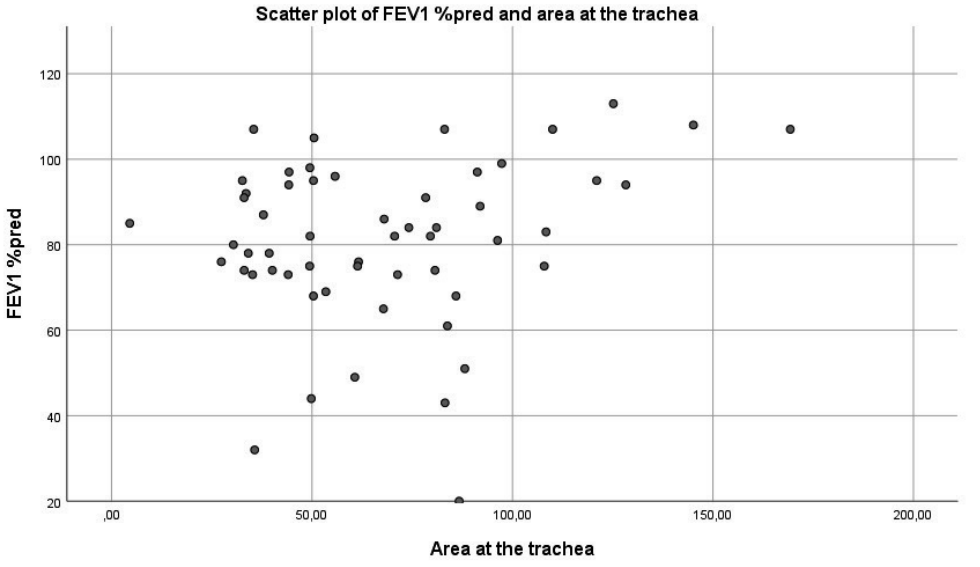
Scatter plot of FEV1 %pred and area at the trachea
FEV1 %pred
120
100
80
60
40
20
,00
50,00
100,00
150,00
200,00
Area at the trachea

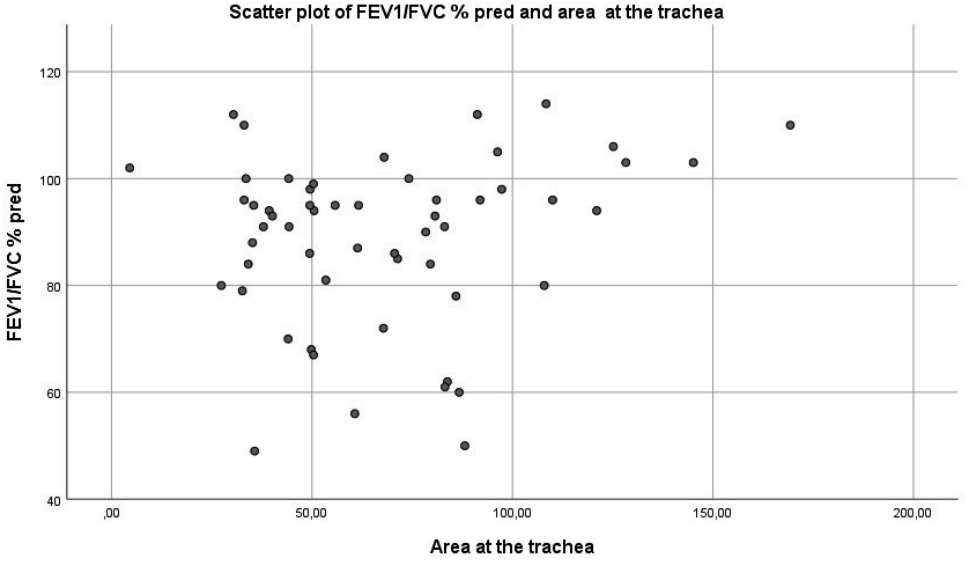
Scatter plot of FEV1/FVC % pred and area at the trachea
FEV1/FVC % pred
120
100
80
60
40
,00
50,00
100,00
150,00
200,00
Area at the trachea

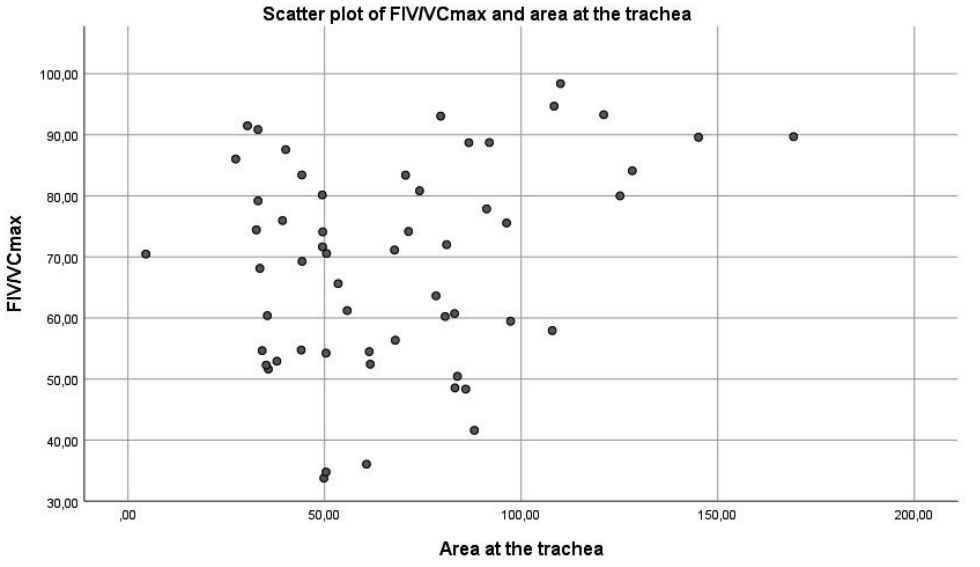
Scatter plot of FIV/VCmax and area at the trachea
FIV/VCmax
100,00
90,00
80,00
70,00
60,00
50,00
40,00
30,00
,00
50,00
100,00
150,00
200,00
Area at the trachea

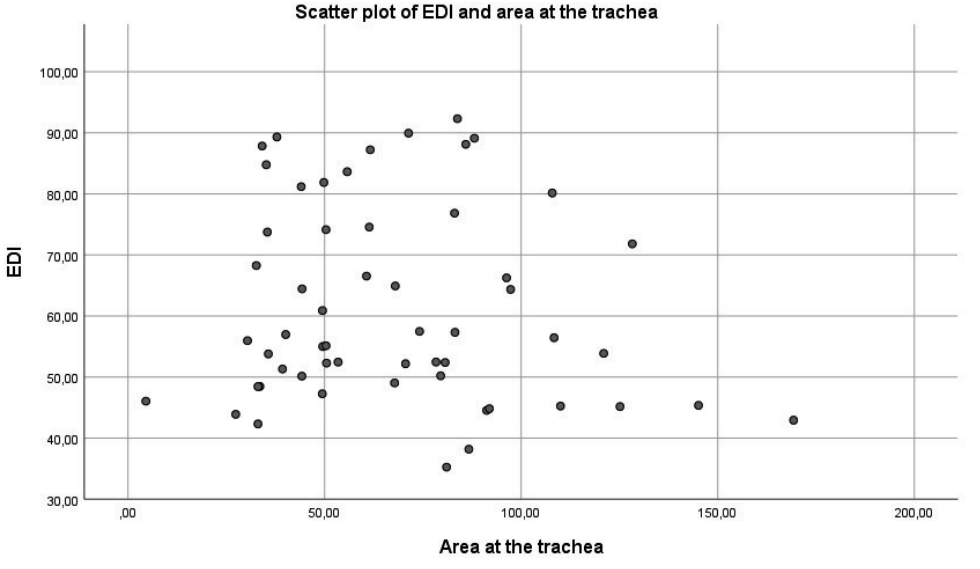
Scatter plot of EDI and area at the trachea
EDI
100,00
90,00
80,00
70,00
60,00
50,00
40,00
30,00
,00
50,00
100,00
150,00
200,00
Area at the trachea

Supplementary material 6: Incidental finding of hypodense regions on proton density imaging

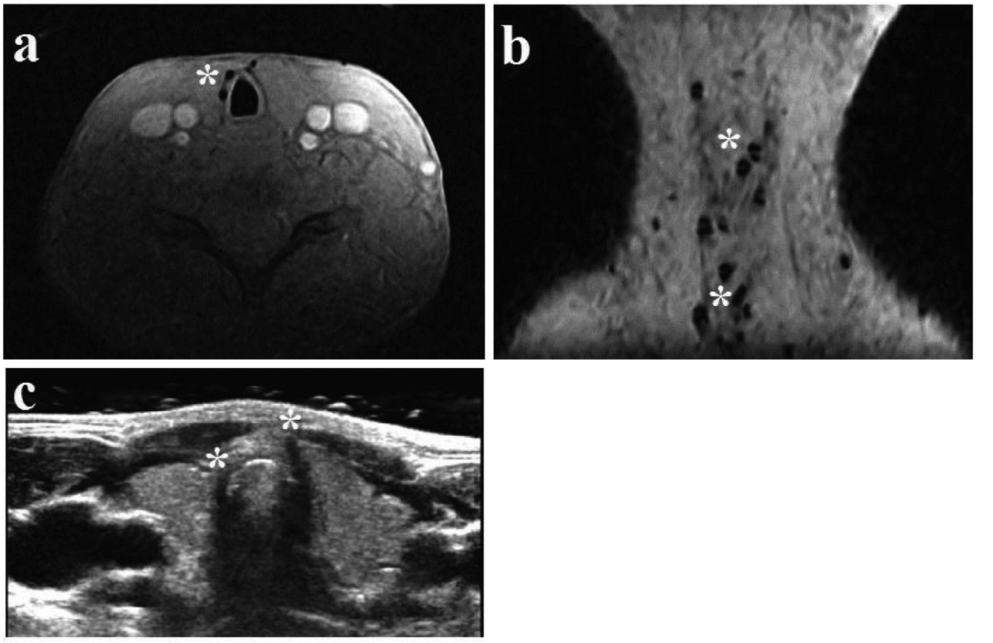

Supplementary material 6: example of a patient with history of LTS showing an incidental finding of hypodense regions (*) on axial (A) and sagittal (B) proton density weighted MRI and corresponding ultrasonography (C).

Supplementary material 7: Intra and interobserver variability results

A: Intra and inter observer variability of static MRI measurements

	Intraclass correlation	Interclass correlation
Presence of vocal cord thickening	0.92	0.67
Level of the vocal cords		
Area	0.99	0.95
AP diameter	0.99	0.91
Transversal diameter	0.98	0.89
Level of the cricoid		
Area	0.92	0.97
AP diameter	0.97	0.97
Transversal diameter	0.92	0.93
Presence of tracheal deformation	1.00	1.00
Level of tracheal deformation		
Area	0.93	0.99
AP diameter	0.61	0.99
Transversal diameter	0.89	0.99
Level of proximal trachea		
Area	0.99	0.98
AP diameter	1.00	0.91
Transversal diameter	0.97	0.95

Data are presented as intra class correlation coefficient (ICC). AP; anterior- posterior.

B: Intra and inter observer variability of dynamic MRI measurements

	Intraclass correlation	Interclass correlation
Complete abduction during inspiration	0.42	0.65
Complete adduction during phonation	0.91	0.00
Inspiration areas		
Vocal cords	0.91	0.97
Cricoid	0.99	0.93
Tracheal deformation	-	-
Trachea	0.98	0.98
Phonation areas		
Vocal cords	0.92	0.94
Cricoid	0.95	0.99
Tracheal deformation	-	-
Trachea	1.00	0.99

Data are presented as intra class correlation coefficient (ICC).

Supplementary video: Example of the dynamic MR images of a patient

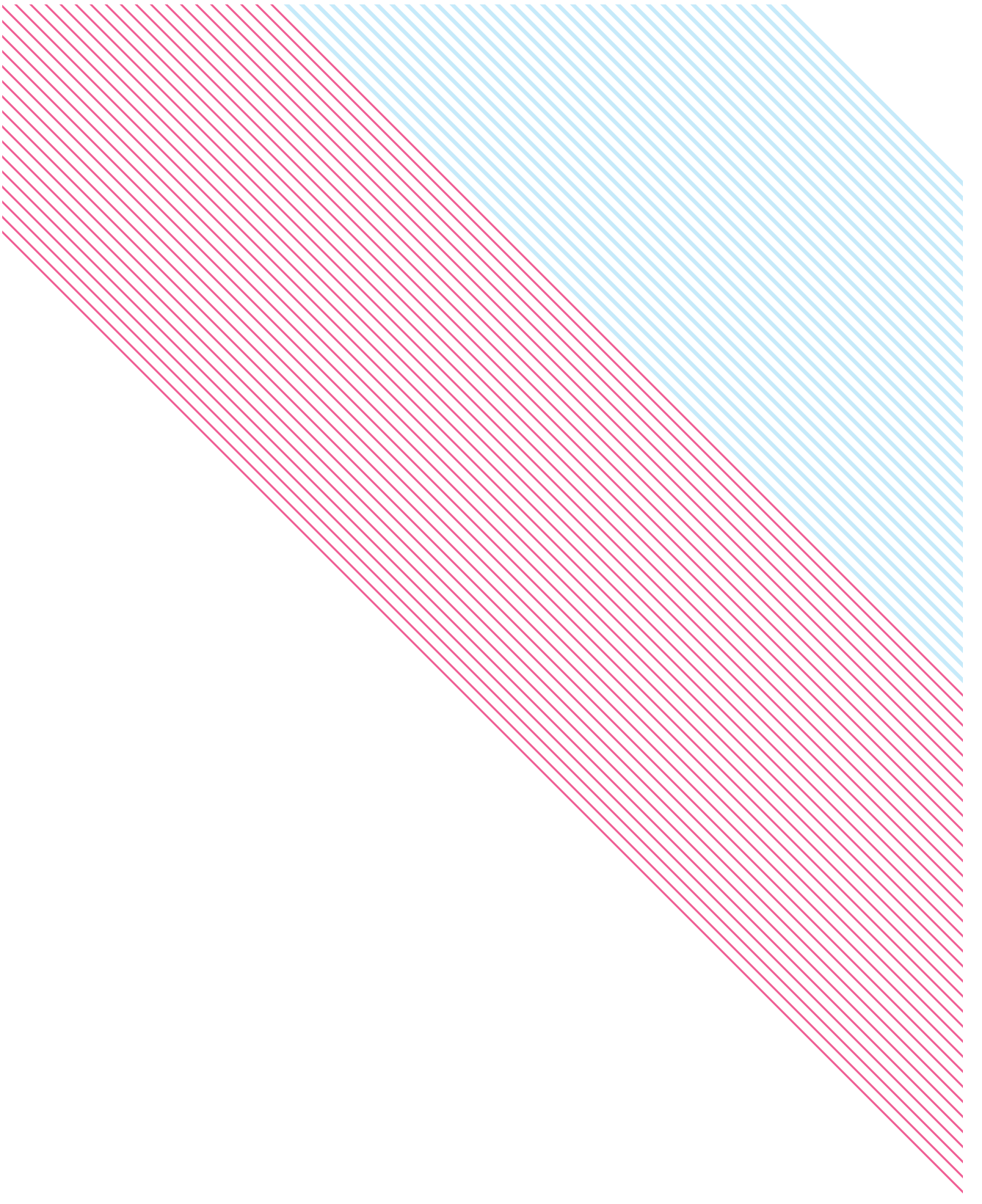

Chapter 4

Structure and function of the vocal cords after airway reconstruction on magnetic resonance imaging

Bernadette BLJ Elders, Marieke M Hakkesteegt, Pierluigi Ciet,
Harm AWM Tiddens, Piotr Wielopolski, Bas Pullens

Laryngoscope 2021;131:E2402-E2408

Abstract

Objectives: Dysphonia is a common problem at long-term follow up after airway surgery for laryngotracheal stenosis (LTS) with major impact on quality of life. Dysphonia after LTS can be caused by scar tissue from initial stenosis along with anatomical alterations after surgery. There is need for a modality to non-invasively image structure and function of the reconstructed upper airways including the vocal cords to assess voice outcome and possible treatment after LTS. Our objective was to correlate vocal cord structure and function of patients after airway reconstruction for LTS on static and dynamic Magnetic Resonance Imaging (MRI) to voice outcome.

Methods: Voice outcome was assessed by voice questionnaires ((pediatric) Voice Handicap Index (p)VHI)) and the Dysphonia Severity Index (DSI). Post-surgical anatomy, airway lumen and vocal cord thickness and movement on multi-planar static high-resolution MRI and dynamic acquisitions during phonation was correlated to voice outcome.

Results: Forty-eight patients (age 14.4 (range 7.5-30.7) years) and 11 healthy volunteers (15.9 (8.2-28.8) years) were included. Static MRI demonstrated vocal cord thickening in 80.9% of patients, correlated to a decrease in DSI (expected odds 0.75 [C.I. 0.58-0.96] p=0.02). Dynamic MRI showed impaired vocal cord adduction during phonation in 61.7% of patients, associated with a lower DSI score (0.65 [C.I. 0.48-0.88] p=0.006).

Conclusion: In LTS patients after airway reconstruction MRI can safely provide excellent structural and functional detail of the vocal cords correlating to DSI, with further usefulness expected from technical refinements. We therefore suggest MRI, as a tool for extensive imaging during LTS follow up.

Introduction

Laryngotracheal stenosis (LTS) is a rare disease of the pediatric upper airways.(1) Severe cases often need treatment with either a laryngotracheal reconstruction (LTR) or a cricotracheal resection (CTR) through open neck surgery.(2) In LTR the stenosis is enlarged with autologous cartilage grafts with (double stage, ds) or without (single stage, ss) a period of stenting, while in CTR (part of) the cricoid and/ or trachea is resected followed by a primary anastomosis.(2) Earlier outcome reports have mainly focused on the success rate of surgical airway repair, with up to 95% of patients relieved of their tracheal cannula. (3) However, surgery can result in respiratory and vocal sequelae, which can have a major impact on quality of life at long-term follow up.(4, 5)

Studies focusing on these sequelae show dysphonia and poor voice related quality of life in over 75% of pediatric patients after airway reconstruction for LTS.(4-9) Dysphonia in these patients possibly results from the initial stenosis at the level of the vocal cords and/or the crico-arytenoid joints, as well as from the airway surgery itself, which can result in scarring and disruption of the laryngeal framework. The placement of a posterior cartilage graft can cause a closure defect of the posterior glottis and scarring in that area, while a full laryngofissure can cause disruption of the anterior commissure.(10) The current gold standard to visualize the vocal cords is videostroboscopy, but downsides are that the images obtained are 2D and non- quantitative and tissue cannot objectively be characterized. Recent advances in Computed Tomography (CT) and Magnetic Resonance Imaging (MRI) make it possible to non-invasively image structure and function of the pediatric upper airways including the vocal cords.(11-16) However, no studies have been conducted to see if static and dynamic MR images of the vocal cords correspond to vocal function.

Therefore, we used static and dynamic MRI to image the vocal cords of patients in the long term follow up after open airway surgery for pediatric LTS, and correlated these MRI findings to voice parameters. We hypothesized that poor voice outcome would correlate to altered vocal cord structure and function on MRI.

Methods

All patients from the LTS outpatient follow-up clinic were approached to participate in this study. Inclusion criteria were: history of congenital or acquired LTS and history of LTR or CTR between 1994 (start of airway reconstructions at our institution) and 2018. Exclusion criteria were: age below 6 years, inability to undergo/ follow MRI instructions, current severe lung infection, oxygen usage and presence of a tracheal cannula. Healthy volunteers without airway, vocal or pulmonary co-morbidities were included to give an impression of

the healthy upper airways on MRI. Patients and healthy volunteers were not matched for age and gender. The study was approved by the local medical ethics committee (MEC2018-013) and written informed consent was obtained from all study participants. Anatomical data was previously reported.(17)

Clinical status

The following data was collected from the electronic patient file: acquired or congenital stenosis, Cotton- Myer Grade of stenosis(18), location of stenosis (posterior glottis/ subglottis/ both), tracheal cannula before repair (Yes/No), type of reconstruction (ss-LTR/ ds-LTR/ CTR, including use of anterior and/or posterior cartilage graft) and age at reconstruction.

(Pediatric)Voice Handicap Index

To assess voice related quality of life, all parents of patients younger than 16 years were asked to fill out the validated pediatric Voice Handicap Index (pVHI), while patients of 16 years and older filled out the VHI independently.(19-21) The (p)VHI includes questions on the functional (F), physical (P) and emotional (E) effects of dysphonia on daily life. In addition, the pVHI includes a question on the talkativeness of the child (0: quiet listener; to 7: very talkative) and a visual analogue scale (VAS) on voice quality (0: normal voice, to 10: severely affected voice). A higher (p)VHI score represents a worse voice related quality of life. Due to a difference in maximum scores between the pVHI and VHI, scores are also presented as a percentage of the maximum score (pVHI: percentage of 28(F), 36(P), 28(E) and 92 (total score), VHI: a percentage of 40 (F,P,E) and 120 (total score)).

Dysphonia Severity Index

Voice quality of patients and healthy volunteers was measured using the Dysphonia Severity Index (DSI), recorded with a head microphone and audio interface (*Focusrite Scarlett Solo, United Kingdom*), and the analysis was done using PRAAT software (*version 6.0, University of Amsterdam, The Netherlands*).(22) The DSI consists of: highest frequency (Hz), lowest intensity (dB), maximum phonation time (MPT)(s) and jitter(%). We used a head microphone, with a smaller mouth-to-microphone distance compared to a table microphone as used in the original study(23), therefore we applied a translational factor of -7.5dB on the lowest intensity. Total score was calculated according to the original formula, with a lower score representing a worse voice.(22)

Magnetic resonance imaging protocol

A 30 minute upper airways MRI protocol was developed and performed on a 3T scanner (*Discovery MR750, GE Healthcare, Milwaukee, WI, USA*) using a dedicated and flexible 6 channel carotid coil (*Machnet B.V., Rhoden, The Netherlands* and *Flick Engineering B.V., Winterswijk, The Netherlands)*.(24) The MRI protocol has previously been published.(17) Briefly, the protocol consisted of static two dimensional (2D) morphological sequences with

high in-plane resolution in three planes (0.5 x 0.5 (in plane) x 2 mm (slice thickness)) and 2D and 3D dynamic sequences with a temporal resolution of 330 ms. The dynamic sequences consisted of 2D axial sequences during trained manoeuvres of inspiration and 'AAA' phonation separately, and a 3D cine-MRI during a manoeuvre of two second inspiration followed by six second 'AAA' phonation. These sequences were repeated until at least one of the (2D or 3D) manoeuvres was performed correctly.

Image analysis was done using Advantage Windows Server (*version 2.0, GE Healthcare, Milwaukee, WI, USA*) as follows (figure 1, supplementary material 1):

Morphology assessment consisted of the presence of arytenoid prolapse defined as protrusion of these structures into the airway lumen, altered positioning of the vocal cords defined as deviation from the normal triangular shape between the anterior commissure and the vocal cords and/or vocal cord thickening. Vocal cord thickness was measured as diameters at three consecutive levels from posterior (at the level of the arytenoids) to anterior (at the level of the anterior commissure). Furthermore, the total square area of the vocal cords was measured. Airway lumen area and anterior-posterior and transversal diameters were measured between the vocal cords. Area and diameter measurements were corrected for height in meters.

Tissue characterization assessment consisted of the evaluation of T2 weighted images on the presence of tissue thickening and/or hyperintense signal, as signs of fibrosis, edema or a combination of both.(17)

Dynamic assessment consisted of the evaluation of correct performance of vocal manoeuvres, defined as any form of vocal cord adduction during phonation on 2D dynamic images, and as any vocal cord movement on 3D dynamic images. Images were evaluated by scoring completeness of vocal cord adduction (complete/incomplete) and symmetry (symmetrical/asymmetrical) and by quantitative measurement of the residual area between the vocal cords during phonation. In case 2D dynamic manoeuvres were not performed correctly, no area measurements were done.

The first observer (B.E.) performed measurements twice on 12 randomly selected MRIs to assess intra-observer variability. Inter-observer reproducibility of measurements was tested by reanalysing 12 MRIs by a researcher trained in evaluating upper airways MRI.

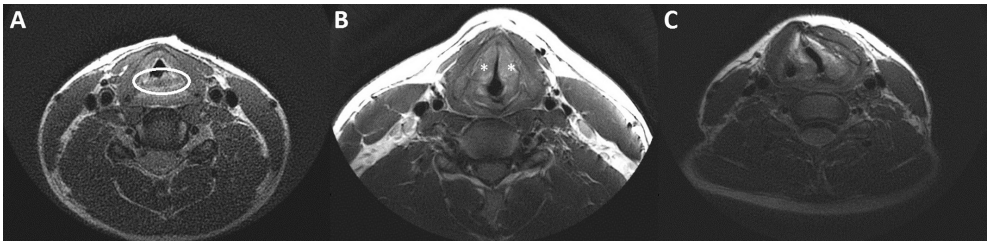

Figure 1: Example of the MRI analysis of the static images showing (a) arytenoid prolapse, (b) vocal cord thickening and (c) vocal cord deviation.

Statistics

Data analysis was done using SPSS Statistics (*version 25, IBM SPSS, Chicago, IL, USA*). Data are presented as mean ± standard deviation or median (range or interquartile range). Patients and healthy volunteers were compared using the parametric t-test for normally distributed data and the Mann Whitney U test for non- normally distributed data. Correlations were tested with the Pearson rho (r) for normally distributed, Spearman's rho (r_s) for not normally distributed data and binary logistic regression for categorical data, for all correlations the uncorrected (p)VHI outcome was used. Intra and inter- correlation was calculated with the intra- class correlation coefficient. Correction for multiple testing was not performed and a significance level of 0.05 is assumed.

Results

Patient and healthy volunteer characteristics are presented in table 1. Forty-eight patients and eleven healthy volunteers were included with a mean age of 14.4 (range 7.5-30.7) and 15.9 (range 8.2-28.8) years.

Total score was higher for the pVHI than the VHI, with highest (most impaired) items scored being the functional and physical subscale for the pVHI and the physical and emotional subscale for the VHI (table 2). Parents of patients younger than 16 years scored significantly worse on the functional and non- significantly worse on the physical sub-scale, compared to patients of 16 years and older.

Patients showed a significantly lower total DSI score than healthy volunteers (-2.6 ± 2.4 versus 0.68 ± 2.9, $p<0.001$), showing a decreased function on all parameters but lowest intensity (supplementary material 2).

Table 1: Patient and healthy volunteer characteristics

	Patients (n= 48)	Volunteers (n=11)	p-value
Age at MRI (years)	14.4 (range 7.5-30.7)	15.9 (range 8.2-28.8)	0.92
Gender (% female)	52.1	36.4	0.37
Weight (kg)	45.2 (IQR 34.5-62.3)	60.8 (IQR 31.6-74.0)	0.34
Height (meter)	1.6 (IQR 1.4-1.7)	1.7 (IQR 1.4-1.8)	0.34
Type of stenosis (%)	Congenital 6.3 Acquired 93.8		
Cotton Myer grade of stenosis (%) Grade I Grade II Grade III Grade IV	 8.3 31.3 56.3 4.2		
Location of stenosis (%)	Posterior glottis 22.9 Subglottis 35.4 Posterior glottis and subglottis 41.7		
Tracheal cannula before repair (%)	79.2		
Type of reconstruction (%)	ss-LTR 87.5 ds- LTR 4.2 CTR 8.3		
Type of graft (%*)	Anterior 4.7 Posterior 9.3 Both 86.0		
Age at reconstruction (years)	2.2 (IQR 1.1-4.5)		
Years since reconstruction	11.5 ± 4.6		

CTR; cricotracheal resection, ds-LTR; double stage laryngotracheal reconstruction, IQR; interquartile range, ss-LTR; single stage laryngotracheal reconstruction. Data are presented as percentage, mean ± standard deviation or median (range or interquartile range). *percentage within the ss- and ds-LTR group.

Table 2: (Pediatric) Voice Handicap Index

	pVHI n=31 64.6%	**VHI n=17** 35.4%	
Talkativeness	4.3 ± 1.9	-	-
Functional	10.6 ± 6.0 *37.9 ± 21.5*	6.6 ± 5.0 *16.5 ± 12.5*	*p<0.001
Physical	12.0 (7.0 – 18.0) *33.3 (19.4 – 50.0)*	6.0 (1.0 – 4.0) *15.0 (2.5 – 35.0)*	0.07
Emotional	4.0 (1.0 – 9.0) *14.3 (3.6 – 32.1)*	5.0 (1.0 – 12.0) *12.5 (2.5 – 30.0)*	0.86
Voice quality (VAS)	3.8 ± 3.0	-	-
Total score	28.2 ± 17.5 *33.7 (16.3 – 41.3)*	21.6 ± 18.0 *14.2 (7.1 – 23.8)*	*p=0.02

The subscales talkativeness and voice quality(VAS) were only scored in the pVHI. VAS; Visual Analogue Scale, VHI; Voice Handicap Index. Data are presented as percentage or mean ± standard deviation, (sub)scores presented as a percentage of maximum amount of points scores are in italic. *p<0.05.

Magnetic resonance imaging

In summary static imaging showed vocal cord thickening in the majority of patients (80.9%). (17) In 12 patients (25.5%) signs of fibrosis located at the vocal cords was seen, in 6 patients (12.8%) signs of edema located at the vocal cords was seen and in 9 patients (19.1%) a combination of fibrosis and edema was seen. Furthermore, impaired vocal cord movement was seen on dynamic MRI in 34 patients (72.3%) and none of the healthy volunteers. The most frequent finding was incomplete adduction of the vocal cords during phonation (n=29, 61.7%). Eleven patients (23.4%) showed unilateral impaired vocal cord movement. Thirty-five patients and nine healthy volunteers had correctly performed 2D dynamic images available for quantitative analyses, showing a non-significant larger residual area between the vocal cords during phonation, and significantly less change in lumen area between inspiration and phonation in patients compared to healthy volunteers.(17)

For the current study we executed additional measurements on vocal cord thickening, showing an increase in vocal cord diameters, but no increase in vocal cord area. Patients showed collapse of the supraglottic and subglottic region in 59.6% and 21.3% respectively during phonation. Conversely, only 30% of healthy volunteers showed collapse of the supraglottic and none showed collapse of the subglottic region during phonation. MRI findings are summarized in supplementary material 3, figure 2 shows a still of a 2D dynamic sequence of a patient.

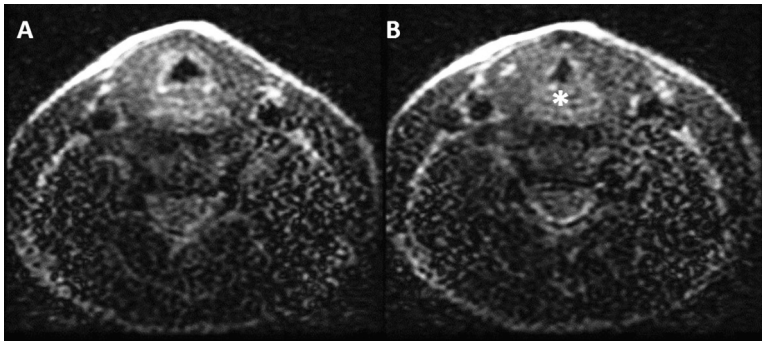

Figure 2: Axial 2D dynamic image of the upper airways of a patient with a history of acquired LTS, post ss-LTR with an anterior and posterior graft during inspiration (a) showing complete abduction of the vocal cords and phonation (b) showing decreased lumen but incomplete closure of the vocal cords with prolapse of the arytenoids (asterisk).

Correlations

Correlations between patient characteristics and the residual lumen area between the vocal cords during phonation as seen on MRI are presented in supplementary material 4. Presence of glottic scarring prior to airway reconstruction did not correlate to the area between the vocal cords during phonation on MRI. Furthermore, vocal cord lumen area during phonation on MRI was not correlated to the type of airway reconstruction. Nor did the type of cartilage

grafts (anterior and/ or posterior) placed have an effect on dynamic MRI findings, however, in our cohort few patients had only one graft.

Correlations between MRI findings and voice outcome are presented in table 3. The presence of vocal cord thickening on MRI was significantly correlated to a decrease in total DSI score but not (p)VHI. No correlations between tissue characterization and DSI nor (p)VHI were found. Presence of incomplete vocal cord adduction on MRI was strongly correlated to a decrease in DSI score. The degree of adduction impairment, expressed as the residual lumen area between the vocal cords during phonation, was significantly correlated to total DSI, but did not have an effect on (p)VHI score. Sub-analyses between the degree of vocal cord adduction and DSI score showed that a bigger area between the vocal cords during phonation was significantly correlated to an increase in jitter sub-score (r=0.31 p=0.04) but none of the other sub-scores (MPT r=--0.09 p=0.58, highest frequency r=-0.16 p=0.30, lowest intensity r=-0.05 r=0.73). The presence of supra- or subglottic collapse during phonation on MRI did not have an effect on DSI or (p)VHI.

Table 3: Correlations between MRI, and (p)VHI and DSI

	pVHI (n=31)	VHI (n=17)	DSI (n=59)
Static MRI			
Vocal cord thickening	1.96 (0.90-1.03) p=0.22	1.00 (0.93-1.06) p=0.88	0.75 (0.58-0.96) **p=0.02**
Abnormal vocal cord positioning	1.01 (0.94-1.09) p=0.73	1.04 (0.98-1.10) p=0.22	0.79 (0.61-1.04) p=0.09
Arytenoid prolapse	1.01 (0.96-1.06) p=0.62	0.98 (0.93-1.04) p=0.49	0.88 (0.71-1.08) p=0.21
Presence of fibrosis	1.04 (0.99-1.09) p=0.17	0.97 (0.92-1.03) p=0.29	0.95 (0.74-1.21) p=0.66
Presence of edema	1.05 (0.99-1.100) p=0.10	1.05 (0.98-1.12) p=0.16	0.90 (0.69-1.17) p=0.42
Dynamic MRI			
Incomplete vocal cord adduction	1.04 (0.98-1.10) p=0.16	0.95 (0.89-1.01) p=0.12	0.65 (0.48-0.88) **p=0.006**
Supraglottic collapse	1.03 (0.98-1.09) p=0.25	0.98 (0.95-1.04) p=0.48	0.93 (0.77-1.13) p=0.48
Subglottic collapse	1.03 (0.97-1.09) p=0.37	1.00 (0.92-1.08) p=0.90	0.91 (0.71-1.17) p=0.46
Unilateral vocal cord movement	1.00 (0.95-1.06) p=0.95	1.00 (0.95-1.07) p=0.12	0.97 (0.71-1.33) p=0.84
Area between the vocal cords during phonation	r=-0.15 p=0.51	r=-0.46 p=0.12	r=-0.31 **p=0.04**

DSI; Dysphonia Severity Index, MRI; Magnetic Resonance Imaging, (p)VHI; pediatric Voice Handicap Index. Data are presented as expected odds (confidence interval) or correlation coefficient (r). P values in bold are significant (<0.05).

Intra- and inter variability analysis showed good to excellent consistency for all static and dynamic MRI measurements, except for the presence of complete abduction or adduction (supplementary material 5).

Discussion

This is the first study correlating MRI of the vocal cords to voice outcome in patients after airway reconstruction for LTS. Our findings show good correlation between MRI and DSI and hereby show the potential of MRI to image the vocal cords in a non- invasive and quantitative matter. In addition, we confirm the impact of consecutive altered anatomy and fibrosis of the vocal tract leading to dysphonia in the post-LTS population.

The gold standard to evaluate the vocal tract is videostroboscopy.(2) An important downside however, is that the data obtained is non- quantified. In the current study, on static images, we were able to quantify both vocal cord thickening correlated to DSI outcome, as well as areas and diameters at the level of the vocal cords. Quantitative analyses revealed increased vocal cord diameters in the majority of patients but no increase in total vocal cord area, implicating thickening and shortening of the vocal cords. This is possibly related to altered laryngeal architecture after surgery, extensive scarring of the larynx or the loss of vocal cord tension following surgery, all leading to dysphonia in LTS patients after airway reconstruction.

We could easily visualize and score impaired vocal cord movement on dynamic MRI in almost all patients from the age of seven years and above. Previous studies have shown MR imaging of non- sedated children to be possible from the age of six years.(12) The vocal cord movement was evaluated by both subjective scoring and quantitative measurements. The quantitative measurements of vocal cord lumen areas were better reproducible than scoring completeness of vocal cord ab- and adduction, since it proved challenging to subjectively score vocal cord movement in combination with thickening and deviation of the vocal cords. Conversely to videostroboscopy, we were not able to visualize vocal cord vibrations with dynamic MRI, since it has a temporal resolution of 330 ms. This is a major downside of the MRI when compared to videostroboscopy. Whether this results in missed diagnosis of clinically relevant dysphonia in this patient population should be focussed on in future research.

An important benefit of imaging methods such as CT and MRI is the ability to visualize the vocal cords in a three-dimensional plane, therefore less influenced by the strongly altered anatomy such as severe supraglottic collapse.(15, 16, 25) Supraglottic constriction during phonation is a common compensatory mechanism in patients with dysphonia, but can also be a sign of architectural distortion after LTS repair.(10, 26, 27) We could identify supraglottic collapse on MRI in the majority of our patients, and in contrast to videostroboscopy, the

presence of supraglottic collapse did not limit the visualization of the vocal cords or the assessment of vocal cord movement.

An imaging modality of the vocal cords that can distinguish between fibrosis, edema and inflammation could aid the airway surgeon greatly. However, to date this is not possible. MRI could possibly overcome this limitation with T1 and T2 weighted imaging, based on water content of tissue, and diffusion weighted imaging (DWI), based on free movement of hydrogen molecules corresponding to cellular swelling or increased tissue density.(28, 29) Although in our previous study tissue alterations on T2 weighted imaging correlated to impaired vocal cord movement on MRI, we did not find a correlation between tissue alterations on and DSI nor (p)VHI in the current study. Therefore MRI seems not yet sensitive enough to identify clinically relevant tissue alterations of the vocal cords. Further protocol refinement is needed to improve MRI capability to detect inflammation and will be the aim of future research.

The majority of imaging studies of the vocal cords has been done using CT.(15, 16, 25) The most important downside of CT compared to MRI is exposure to, albeit low, ionizing-radiation.(16) Comparison studies between dynamic CT and MRI have never been reported, but our MRI study shows excellent identification of the anatomical structures, and thereby closure defects of the vocal cords, comparable to previous CT studies. Besides, MRI is known to be superior over CT in terms of identification of soft tissue structures, and might therefore better identify various structures of the larynx such as the arytenoids and true and false vocal cords.(12) In addition, although vocal cord dynamics have been imaged on MRI before, this has never been done in the current population and this is the first study making a comparison to voice outcome.(13, 14, 25)

In our study population, MRI findings correlated best to voice outcome measured by DSI. The DSI is an objective voice measurement, but can entail limitations in case of severe dysphonia. Examples of this are type II and III voice signals influencing jitter outcome.(30) Although this was also present in our population, our jitter outcomes were within the expected range and the DSI also significantly differed from healthy volunteers on other subscales. Therefore we do not believe that this has impacted the correlations found in the current study.

The limited correlations between MRI findings and voice related quality of life on (p)VHI are most likely because these are subjective measurements investigating only the burden and not the severity of dysphonia. We also found parents reporting a worse voice related quality of life compared to patients. This is in line with previous quality of life research, also in LTS patients, where parents tend to score lower quality of life compared to patients.(31, 32) The difference in voice related quality of life between parents and patients was not observed for the emotional sub-score. Patients reported a high impact of dysphonia on the emotional

quality of life, represented by questions such as “I am tense when talking to others because of my voice” and “People seem irritated by my voice”.(33) These findings are in line with our clinical experience, where patients mainly complain of the increased burden of dysphonia on their social life during adolescence. This emphasizes the importance of long term follow up of dysphonia after airway reconstruction for LTS, and shows that attention should be paid to voice related quality of life and differences between patient and parent reporting.(4)

The most important strength of this study is that it is the first study correlating MRI findings in patients after airway reconstruction for LTS to voice outcome. A weakness of this study is the small study population, with limited patients having undergone a CTR and almost all patients having undergone placement of a posterior cartilage graft during LTR. This might have led to a lack of correlation between voice outcome and MRI findings, and clinical parameters such as type of surgery or type of cartilage grafts placed and MRI findings. However, these findings also emphasize the complex and multifactorial relationship between post- surgical LTS and dysphonia. On one hand, dysphonia is caused by the pre-surgical anatomy such as glottic involvement of the stenosis. On the other hand, both LTR and CTR can cause dysphonia in itself. In LTR the placement of anterior and, more importantly posterior cartilage grafts can prevent complete ab- and adduction of the vocal cords.(2, 10, 20, 27) In CTR the removal of the cricothyroid muscle can cause dysphonia complaints.(2, 10, 34) Another limitation of this study is the lack of comparison between MRI and the current gold standard to image the vocal cords, videostroboscopy. Comparison between these two modalities was not the primary aim of our research but will be the subject of follow-up research. In addition, due to the experimental character of our research, we did not have reference values of our quantitative measurements available.

In conclusion, this is the first study comparing MRI of the vocal cords to voice outcome in patients after airway reconstruction for LTS. Our MRI protocol can safely and feasibly image the vocal cords in children from the age of seven years on and can easily be adopted in all institutions. MRI has the additional benefit of extensive anatomical imaging of the upper airways without ionizing-radiation. Further technical refinements such as protocol improvement will contribute to the usefulness of MRI for imaging of the upper airways. In addition, future research should focus on direct comparison between different modalities to evaluate the voice. Our study suggests MRI, as a tool for extensive imaging of upper airways structure and function in the follow up of LTS patients.

Acknowledgements
We would like to acknowledge E. Rosalina Andrinopoulou for the statistical support on the article and we would like to acknowledge Wytse van den Bosch for his help with the inter-observer analysis.

References

1. Jefferson ND, Cohen AP, Rutter MJ. Subglottic stenosis. Semin Pediatr Surg. 2016;25(3):138-43.
2. Monnier P. Pediatric Airway Surgery Management of Laryngotracheal Stenosis in Infants and Children. Berlin, Heidelberg: Springer Berlin Heidelberg; 2011.
3. Pullens B, Hoeve LJ, Timmerman MK, van der Schroeff MP, Joosten KF. Characteristics and surgical outcome of 98 infants and children surgically treated for a laryngotracheal stenosis after endotracheal intubation: excellent outcome for higher grades of stenosis after SS-LTR. Int J Pediatr Otorhinolaryngol. 2014;78(9):1444-8.
4. Pullens B, Hakkesteegt M, Hoeve H, Timmerman M, Joosten K. Voice outcome and voice-related quality of life after surgery for pediatric laryngotracheal stenosis. Laryngoscope. 2017;127(7):1707-11.
5. Pullens B, Pijnenburg MW, Hoeve HJ, Baatenburg de Jong RJ, Buysse CM, Timmerman MK, et al. Long-term functional airway assessment after open airway surgery for laryngotracheal stenosis. Laryngoscope. 2016;126(2):472-7.
6. Cohen W, Wynne DM, Lloyd S, Townsley RB. Cross-sectional follow-up of voice outcomes in children who have a history of airway reconstruction surgery. Clin Otolaryngol. 2018;43(2):645-51.
7. Baker S, Kelchner L, Weinrich B, Lee L, Willging P, Cotton R, et al. Pediatric laryngotracheal stenosis and airway reconstruction: a review of voice outcomes, assessment, and treatment issues. J Voice. 2006;20(4):631-41.
8. de Alarcon A. Voice outcomes after pediatric airway reconstruction. Laryngoscope. 2012;122 Suppl 4:S84-6.
9. Geneid A, Pakkasjarvi N, Aherto A, Roine R, Sintonen H, Lindahl H, et al. Outcomes of early infancy laryngeal reconstruction on health- and voice-related quality of life. Int J Pediatr Otorhinolaryngol. 2011;75(3):351-5.
10. Kelchner LN, Miller CK. Current research in voice and swallowing outcomes following pediatric airway reconstruction. Curr Opin Otolaryngol Head Neck Surg. 2008;16(3):221-5.
11. Zacharias SR, Weinrich B, Brehm SB, Kelchner L, Deliyski D, Tabangin M, et al. Assessment of Vibratory Characteristics in Children Following Airway Reconstruction Using Flexible and Rigid Endoscopy and Stroboscopy. JAMA Otolaryngol Head Neck Surg. 2015;141(10):882-7.
12. Elders B, Hermelijn SM, Tiddens H, Pullens B, Wielopolski PA, Ciet P. Magnetic resonance imaging of the larynx in the pediatric population: A systematic review. Pediatr Pulmonol. 2019;54(4):478-86.
13. Baki MM, Menys A, Atkinson D, Bassett P, Morley S, Beale T, et al. Feasibility of vocal fold abduction and adduction assessment using cine-MRI. Eur Radiol. 2017;27(2):598-606.
14. Ahmad M, Dargaud J, Morin A, Cotton F. Dynamic MRI of larynx and vocal fold vibrations in normal phonation. J Voice. 2009;23(2):235-9.

15. Bergeron M, Fleck RJ, Middlebrook C, Zacharias S, Tolson S, Oren L, et al. Preliminary Assessment of Dynamic Voice CT in Post-Airway Reconstruction Patients. Otolaryngol Head Neck Surg. 2018;159(3):516-21.
16. Bergeron M, Fleck RJ, Zacharias SRC, Tabangin ME, de Alarcon A. The Value of Dynamic Voice CT Scan for Complex Airway Patients Undergoing Voice Surgery. Ann Otol Rhinol Laryngol. 2019;128(10):885-93.
17. Elders B, Ciet P, Tiddens H, van den Bosch W, Wielopolski P, Pullens B. MRI of the upper airways in children and young adults: the MUSIC study. Thorax. 2021.
18. Myer CM, 3rd, O'Connor DM, Cotton RT. Proposed grading system for subglottic stenosis based on endotracheal tube sizes. Ann Otol Rhinol Laryngol. 1994;103(4 Pt 1):319-23.
19. Zur KB, Cotton S, Kelchner L, Baker S, Weinrich B, Lee L. Pediatric Voice Handicap Index (pVHI): a new tool for evaluating pediatric dysphonia. Int J Pediatr Otorhinolaryngol. 2007;71(1):77-82.
20. Veder L, Pullens B, Timmerman M, Hoeve H, Joosten K, Hakkesteegt M. Reliability and validity of the Dutch pediatric Voice Handicap Index. Int J Pediatr Otorhinolaryngol. 2017;96:15-20.
21. Hakkesteegt MM, Wieringa MH, Gerritsma EJ, Feenstra L. Reproducibility of the Dutch version of the Voice Handicap Index. Folia Phoniatr Logop. 2006;58(2):132-8.
22. Wuyts FL, De Bodt MS, Molenberghs G, Remacle M, Heylen L, Millet B, et al. The dysphonia severity index: an objective measure of vocal quality based on a multiparameter approach. J Speech Lang Hear Res. 2000;43(3):796-809.
23. De Bodt MS, Wuyts FL, Van de Heyning PH, Croux C. Test-retest study of the GRBAS scale: influence of experience and professional background on perceptual rating of voice quality. J Voice. 1997;11(1):74-80.
24. Zhang Q, Coolen BF, van den Berg S, Kotek G, Rivera DS, Klomp DWJ, et al. Comparison of four MR carotid surface coils at 3T. PLoS One. 2019;14(3):e0213107.
25. Faust RA, Remley KB, Rimell FL. Real-time, cine magnetic resonance imaging for evaluation of the pediatric airway. Laryngoscope. 2001;111(12):2187-90.
26. de Alarcon A, Brehm SB, Kelchner LN, Meinzen-Derr J, Middendorf J, Weinrich B. Comparison of pediatric voice handicap index scores with perceptual voice analysis in patients following airway reconstruction. Ann Otol Rhinol Laryngol. 2009;118(8):581-6.
27. Kelchner LN, Weinrich B, Brehm SB, Tabangin ME, de Alarcon A. Characterization of supraglottic phonation in children after airway reconstruction. Ann Otol Rhinol Laryngol. 2010;119(6):383-90.
28. Wang J, Takashima S, Takayama F, Kawakami S, Saito A, Matsushita T, et al. Head and neck lesions: characterization with diffusion-weighted echo-planar MR imaging. Radiology. 2001;220(3):621-30.
29. Chavhan GB, Alsabban Z, Babyn PS. Diffusion-weighted imaging in pediatric body MR imaging: principles, technique, and emerging applications. Radiographics. 2014;34(3):E73-88.
30. Titze IR, Liang H. Comparison of Fo extraction methods for high-precision voice perturbation measurements. J Speech Hear Res. 1993;36(6):1120-33.

31. Eiser C, Varni JW. Health-related quality of life and symptom reporting: similarities and differences between children and their parents. Eur J Pediatr. 2013;172(10):1299-304.
32. Pullens B, Dulfer K, Buysse CM, Hoeve LJ, Timmerman MK, Joosten KF. Long-term quality of life in children after open airway surgery for laryngotracheal stenosis. Int J Pediatr Otorhinolaryngol. 2016;84:88-93.
33. Jacobson BH, Johnson A, Grywalski C, Silbergleit A, Jacobson G, Benninger MS, et al. The Voice Handicap Index (VHI). American Journal of Speech-Language Pathology. 1997;6(3):66-70.
34. Clunie GM, Kinshuck AJ, Sandhu GS, Roe JWG. Voice and swallowing outcomes for adults undergoing reconstructive surgery for laryngotracheal stenosis. Curr Opin Otolaryngol Head Neck Surg. 2017;25(3):195-9.

Supplementary materials

Supplementary material 1: MRI analysis

Static images

Arytenoid prolapse: protrusion of these arytenoids into the airway lumen
Example: circle indication arytenoid prolapse

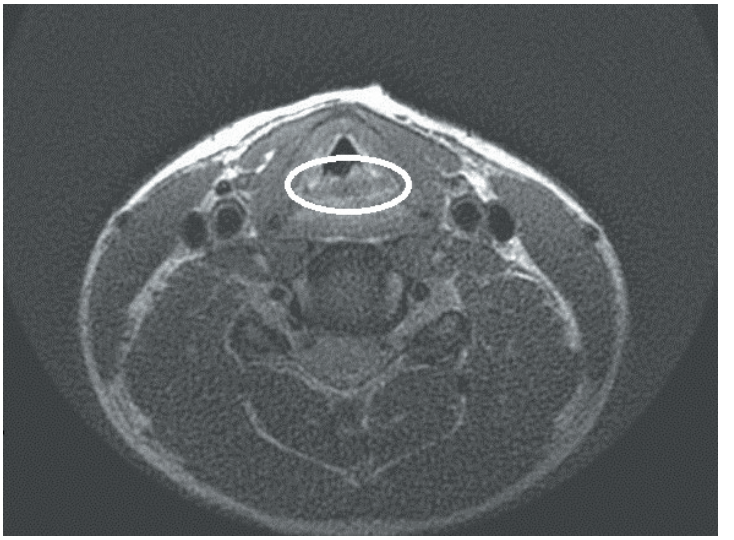

Vocal cord thickening: protrusion of the vocal cords into the airway lumen
Example: asterisk indication vocal cord thickening

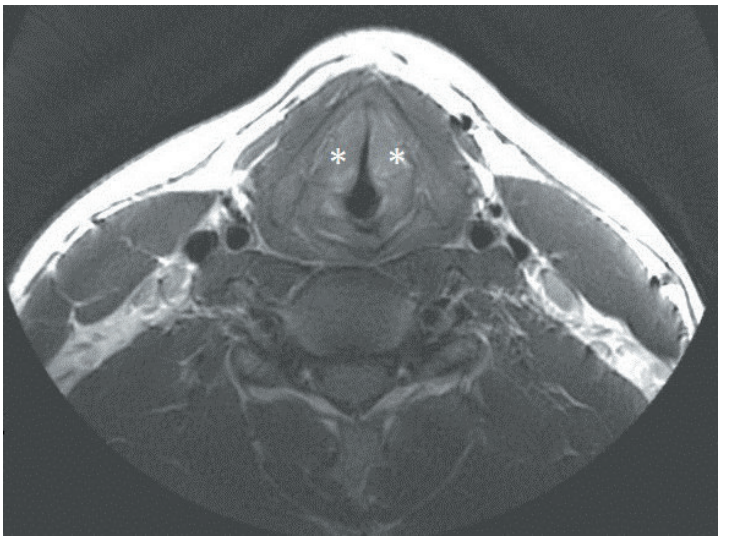

Vocal cord deviation: deviation from the triangular shape between the anterior commissure and the vocal cord

Example: left posterior vocal cord deviation

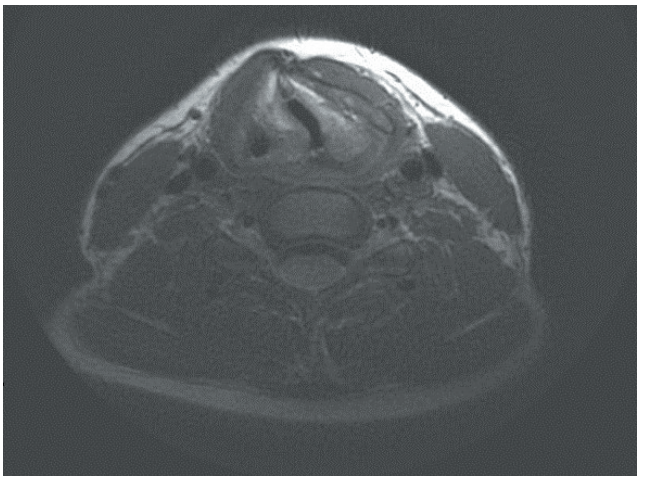

Quantitative measurement of vocal cord thickness: vocal cord thickness measured as diameters at three consecutive levels from posterior (at the level of the arytenoids) to anterior (at the level of the anterior commissure).

Example: vocal cord thickness measured for the level of the arytenoids (1) to the level of the anterior commissure (3)

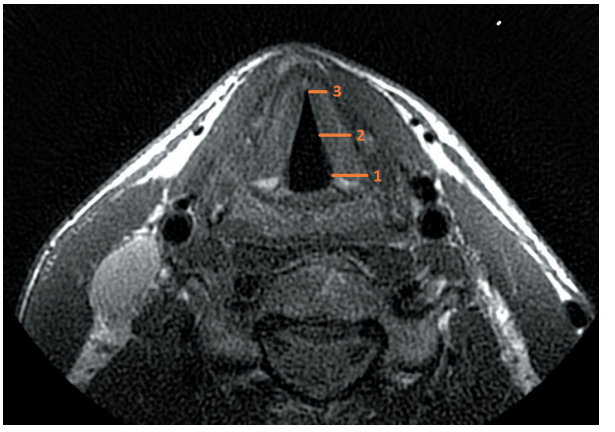

Quantitative measurement of vocal cord lumen area and diameters
Example: measurement of the anterior- posterior (1) and transversal (2) diameter and lumen area (3) at the level of the vocal cords

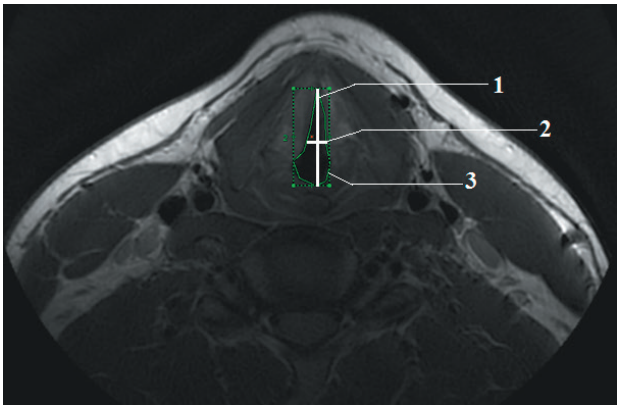

Dynamic images

Quantitative measurement of vocal cord lumen area during inspiration and phonation
Example: measurement of the vocal cord lumen area during inspiration (1) and 'AAA' phonation (2)

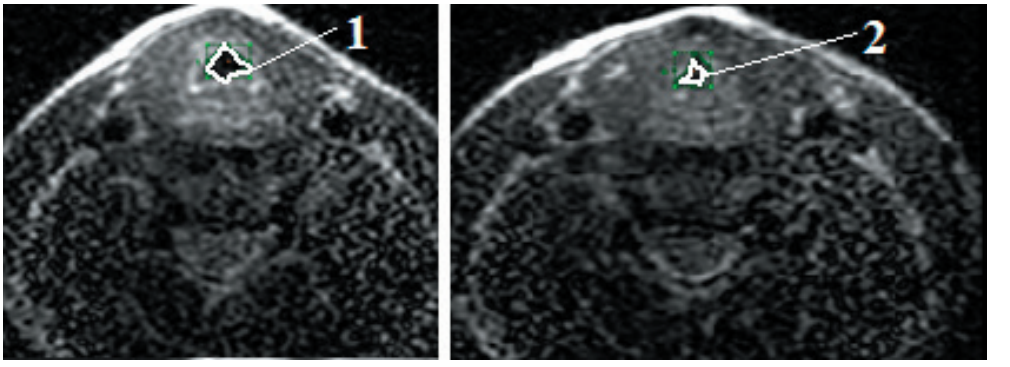

Quantitative measurement of vocal cord lumen area during phonation

Supplementary material 2: Dysphonia Severity Index

	Patients (n= 48)	Volunteers (n=11)	p-value
Maximum phonation time (s)	11.1(8.2-12.9)	17.2(14.3-22.3)	*0.01
Jitter (%)	0.7 (0.5-1.2)	0.4(0.-0.5)	*0.004
Highest frequency (Hz)	599 ± 195	822 ± 217	*0.002
Lowest intensity (dB)	71 ± 6.5	69 ± 6.4	0.55
DSI score	-2.6 ± 2.4	0.68 ± 2.9	*<0.001

DSI; dysphonia severity index. Data are presented as mean ± standard deviation or median (interquartile range), *=p<0.05

Supplementary material 3: Magnetic Resonance Imaging results

	Patients (n= 47)	Volunteers (n=10)	p-value
Static			
Presence of vocal cord thickening (%)	80.9	10	*<0.001
Thickness left vocal cord			
Level 1 (mm)	6.3 ± 1.2	5.0 ± 1.3	*0.002
Level 2 (mm)	4.4 ± 0.9	3.6 ± 0.6	*0.009
Level 3 (mm)	3.0 (2.3-3.5)	2.4 (2.0-2.6)	*0.02
Area (mm²)	76.5 ± 23.0	72.2 ± 23.5	0.60
Thickness right vocal cord			
Level 1 (mm)	6.0 ± 1.3	5.6 ± 0.6	0.43
Level 2 (mm)	4.5 ± 1.1	3.7 ± 0.5	*0.04
Level 3 (mm)	3.0 ± 0.8	2.4 ± 0.5	*0.02
Area (mm²)	77.3 ± 22.1	70.9 ± 29.8	0.44
Abnormal vocal cord positioning (%)	21.3	10	
Arytenoid prolapse (%)	59.6	0	
Area between vocal cords (mm²)	22.0 (17.7-30.3)	35.1 (21.2- 54.7)	*0.03
AP diameter vocal cords (mm)	8.4 ± 2.0	9.0 ± 2.3	0.37
Transversal diameter vocal cords (mm)	2.8 ± 1.0	3.8 ± 1.2	*0.01
Dynamic			
Impaired vocal cord movement (%)	72.3	0	
Impaired abduction during inspiration	42.6	0	
Impaired adduction during phonation	61.7	0	
Area between the vocal cords	**(n=35)**	**(n=9)**	
Inspiration (mm²)	43.7 ± 22.7	72.9 ± 42.3	*0.01
Phonation (mm²)	10.9 ± 9.3	7.2 ± 4.7	0.26
Difference (%)	-72.1 ± 23.7	-88.9 ± 7.3	*0.04
Collapse at other site during phonation(%)			
Supraglottic	59.6	30	
Subglottic	21.3	0	
Unilateral vocal cord movement (%)	23.4	0	

Data are presented as percentage, mean ± standard deviation or median (interquartile range), AP; anterior posterior. All areas are corrected for height in meters. *=p<0.05.

Supplementary material 4: Correlations patient characteristics and impaired vocal cord adduction on MRI

	Area between the vocal cords during phonation on MRI	
Age	r_s= 0.02	p=0.92
Age since reconstruction	r=-0.23	p=0.18
Type of stenosis	1.07 (0.76-1.52)	p=0.69
Posterior glottic involvement of stenosis	1.03 (0.95-1.13)	p=0.46
Type of reconstruction	0.99 (0.84-1.17)	p=0.91
Presence of an anterior graft	0.94 (0.86-1.03)	p=0.16
Presence of a poster graft	1.05 (0.90-1.23)	p=0.53

Data are presented as correlation coefficient (r or rs) expected odds (confidence interval). P values in bold are significant (<0.05).

Supplementary material 5: Intra- and interclass variability

	Intraclass correlation	**Interclass correlation**
Presence of vocal cord thickening	0.92	0.67
Vocal cord area left	0.94	0.83
Vocal cord area right	0.96	0.92
Static vocal cords		
Area	0.99	0.95
AP diameter	0.99	0.91
Transversal diameter	0.98	0.89
Incomplete abduction during inspiration	0.42	0.65
Incomplete adduction during phonation	0.91	0.00
Inspiration area vocal cords	0.91	0.97
Phonation area vocal cords	0.92	0.94

Data are presented as intra class correlation coefficient (ICC). AP; anterior- posterior.

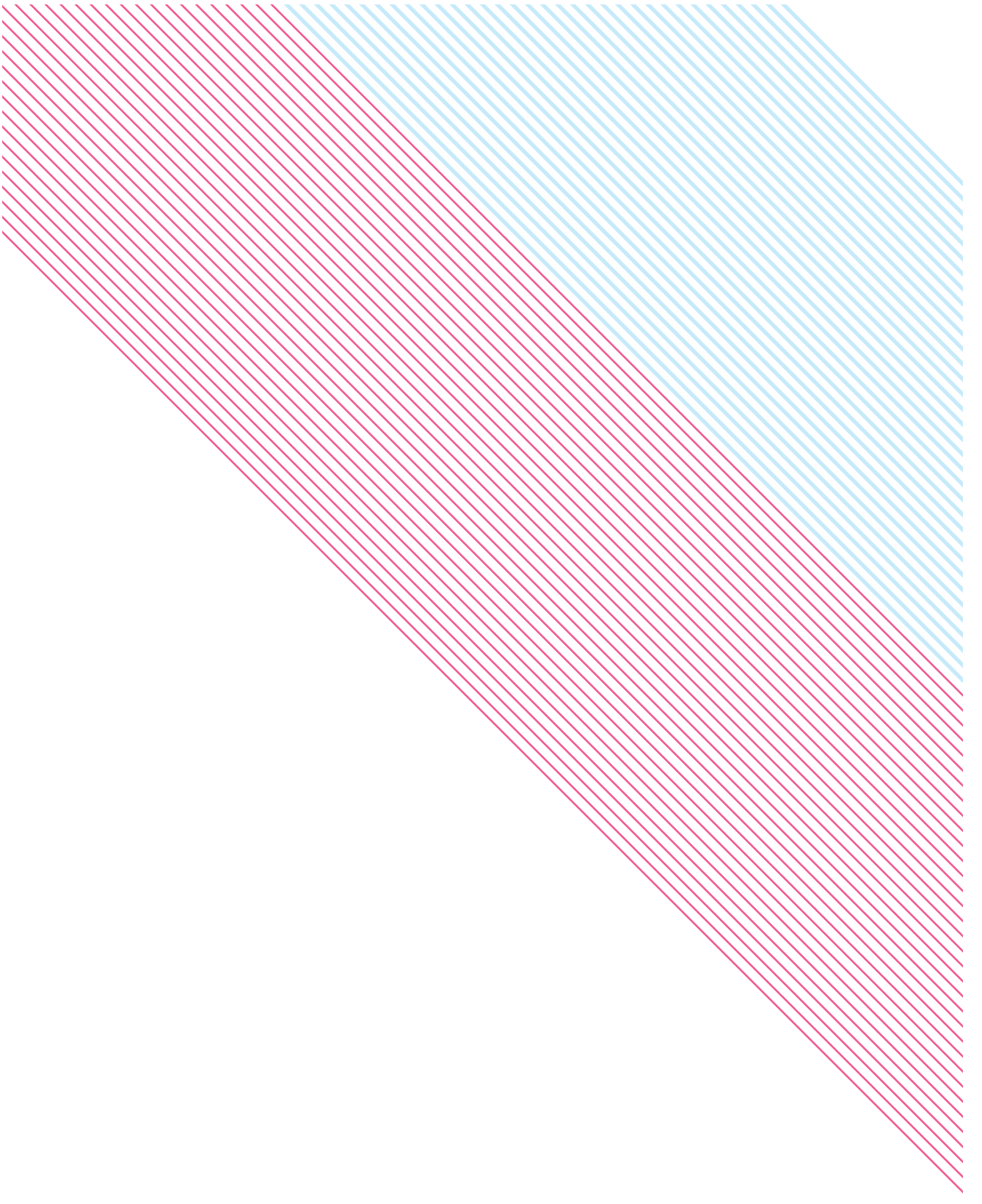

Chapter 5

Computational Fluid Dynamic Modelling of airways after laryngotracheal stenosis

Bernadette BLJ Elders, Hosein Sadafi, Joana Costa, Jan de Backer, Harm AWM Tiddens, Piotr A Wielopolski, Pierluigi Ciet, Bas Pullens

Submitted

Abstract

Purpose: After open airway surgery for laryngotracheal stenosis (LTS) several complex anatomical changes of the airway can remain, leading to altered upper airway airflow patterns and increased airway resistance for which re-operation might be needed. Our aim was to develop an Magnetic Resonance Imaging (MRI) based Computational Fluid Dynamic (CFD) upper airway model allowing digital surgery to predict the effect of surgical interventions on airflow patterns and resistance post LTS repair.

Methods: CFD analyses were performed on free-breathing (FB) and inspiratory (Insp) MRI scans of a healthy volunteer, and two patients post LTS repair. Digital surgery was executed predicting the effect of 1) widening of the vocal cords, 2) removal of the tracheal deformation (TD), 3) both widening of the vocal cords and TD removal.

Results: Patient 1 had a severe vocal cord stenosis and mild TD. Patient 2 had a severe vocal cord stenosis and severe TD. Compared to the healthy volunteer during FB and Insp, patient 1 showed an increased total airway resistance of 269% and 180%, and patient 2 showed an increase of 735% and 1548%. In patient 1, best airway resistance was achieved when just the vocal cords were widened (FB:-20.2 Pa.s/L (45.6%), Insp:-17.9 Pa.s/L (68.8%)). In patient 2, best results were obtained when both the vocal cords were widened and the TD was removed (FB:-71.1 Pa.s/L (71.0%), Insp:-133.9 Pa.s/L (87.3%)).

Conclusion: Our findings suggest that CFD modelling can be used to study the effect of surgical upper airway interventions in patients with complex airway pathology.

Introduction

Changes in upper airway anatomy have a significant effect on overall pulmonary airflow and resistance.(1) This is especially true in children with pediatric laryngotracheal stenosis (LTS).(2) Although LTS can be successfully treated by surgical reconstruction, several anatomical changes to the upper airways mostly remain after surgery, with persistent airflow limitation.(3-6) After surgical repair, persistent respiratory and vocal sequelae are common at long-term follow up, where 70% of LTS patients have an increased flow limitation on spirometry and 75% of LTS patients experience dysphonia.(4, 7-10) In some of these patients additional surgery is needed to relieve symptoms. However, revision surgery especially in cases with multi-level stenosis is more complex with uncertain outcome and possible further worsening of the voice.(11) Therefore, the decision for revision surgery is not taken lightly and is carefully based on expert opinion in combination with extensive assessment of the sequelae. Though, assessment of these post-surgical sequelae is cumbersome with current imaging techniques.(3, 12-15) Direct visualization of the larynx, subglottis and trachea using videolaryngobronchocopy requires general anesthesia, while Computed Tomography (CT) is hampered by high radiation exposure in the sensitive region of the thyroid.(16, 17) For these reasons, a radiation free-technique with dynamic imaging capability, such as Magnetic Resonance Imaging (MRI), is an attractive option, especially in children. Recent studies have shown the ability of MRI to visualize post-surgical anatomical changes in LTS patients.(18, 19) However, the complexity of the anatomy of the reconstructed airways asks for a more in-depth analyses of airflow changes in these patients. Advances in Computational Fluid Dynamic (CFD) modelling of the upper airways make it possible to investigate airflow patterns in LTS patients.(20, 21) CFD provides a detailed analysis of airflow limitation due to airway abnormalities (i.e. airway lumen stenosis), and can simulate the effect of surgical correction on airflow.(22) This technique could be helpful for selecting those patients eligible for further airway surgery to improve respiratory symptoms.

The aim of this study was to develop a CFD model based on MRI of the upper airways and to predict the effect of surgical interventions on airflow patterns and resistance in patients post LTS repair.

Methods

Two patients post-surgical LTS repair, and one healthy volunteer from the **M**agnetic resonance imaging of the **u**pper airways **i**n **c**hildren and young adults (**MUSIC**)- study were selected for CFD analyses.(18) The MUSIC study is a cross-sectional study on structure and function of the upper airways on MRI in a cohort of post-surgical LTS patients, imaging findings were previously reported.(18, 19) Patient selection was based on image quality, and presence of airway stenosis located either at the vocal cords, the cricoid and/or site

of previous tracheostomy. The MUSIC study was approved by the local medical ethics review board (MEC-2018-013), written informed consent was obtained from all study participants.

Magnetic resonance imaging

All study participants underwent upper airways MRI on a 3.0 Tesla scanner (*Discovery MR750, GE Healthcare, Milwaukee, WI, USA*) with a 6 channel carotid coil (*Machnet B.V., Rhoden, The Netherlands* and *Flick Engineering B.V., Winterswijk, The Netherlands).*(23) The protocol consisted, among other sequences, of an axial T2-weighted PROPELLER sequence during free breathing with a resolution of 0.5 x 0.5 x 2 mm^3. In addition, an axial T2-weighted SSFSE sequence was made, during which a trained 7 second manoeuvre of deep inspiration was performed, with a resolution of 1.2 x 0.7 x 2.0 mm^3.(18)

Computational Fluid Dynamic modelling

CFD was performed using the airway geometries on the PROPELLER and SSFSE sequences, acquired in free-breathing and during deep-inspiration respectively. ANSYS Fluent software release 2020 R2 (*ANSYS, Inc., Canonsburg, PA, USA*) was used for CFD modelling.

For the CFD calculation, fluid flow was described according to the Navier-Stokes equations and numerically solved on a computational grid called the mesh.(24) The governing equations were iteratively solved in each grid, and therefore, flow features, such as speed, flow rate, pressure, and density, were determined throughout the model. This allowed to calculate resistance and pressures over the entire lumen trajectory as well as at four specific points of interest: the vocal cords, the cricoid, the tracheal deformation (TD) (if present) and the (normal) trachea.

The Navier-Stokes equations are the basic governing equations for a viscous fluid which also applies to air and are based on the law of conservation of mass (continuity) and momentum (Newton's second law). The continuity equation (equation 1) shows that the sum of the change rate of mass inside a control volume and the net mass flow over the boundaries of the control volume equal to zero.

$$\frac{\partial \rho}{\partial t} + \nabla \cdot (\rho U) = 0 \qquad \text{(Equation 1)}$$

In this equation, ∇ is the divergence, ρ is the density, t the time, and U the velocity vector, which has three components in three coordinates for a 3-dimensional flow.(24) In the CFD analysis of the upper airways, the variation of flow by time was neglected, thus the flow in steady state and the first term in equation 1 was set to zero.

The momentum calculation is described in equation 2. The mass times the acceleration in the Newton's second law is expressed on the left-hand side of the equation, while the right-hand side describes all the possible surface and body forces that can act on air.

$$\frac{\partial(\rho U)}{\partial t} + \nabla \cdot (\rho UU) = -\nabla p + \nabla \cdot (\tau) + S_M \qquad \text{(Equation 2)}$$

In equation 2, the term p is the pressure, and τ is the viscous stress tensor that describes the relationship between viscous stress and strain rate. The term S_M is a source term that can be replaced by the sum of the gravitational body force (ρg) and external body forces.

Each airway was discretized using a Poly-hexcore mesh. To ensure full capturing of near wall features in the turbulence flow, five boundary layers were created on the wall and checked by monitoring the y+ value, the distance from the wall to the first mesh node, and ensuring it is less than one.(25) The average mesh cell number for each airway was approximately 300.000, depending on the complexity and total volume of each upper airway. Based on the grid independence study in this research, fining the mesh beyond this point did not have a significant influence on the results.

The flow regime was turbulent, showing random fluctuations of velocity and pressure in the system. These fluctuations caused a mix of transported quantities such as momentum.(25) To model the turbulence effects, the time-averaged Navier-Stokes equations were solved using the k-ω with Shear Stress Transport (SST) model. This model uses two equations to model the Reynolds stresses in the governing equations.(26) The Semi-Implicit Method for Pressure Linked Equations (SIMPLE) algorithm with staggered grids was used for velocity and pressure couplings. To achieve accurate simulation, a second order discretization was used for turbulent kinetic energy and specific turbulent dissipation rate, and a second order upwind scheme was chosen for solving momentum.

In all simulations, the boundary condition at the vocal cord (inlet) was set to a uniform mass flow inlet of 0.0003 kg/s (15.25 L/min). The boundary condition at the trachea was set to pressure outlet and the pressure was set to the atmospheric value. The flow in the domain was initialized using the velocity and pressure at the inlet. To determine local resistances, the area-weighted average of pressure at planes perpendicular to the flow with 1 mm spacing was considered.

Patient modeling

Mimics Medical 20.0 and 3-Matic Medical Software (*Materialise, Leuven, Belgium*) image processing software tools were used for the construction of 3D airway models based on Hounsfield units (HU). Using MRI landmarks, the region of interest for the segmentation was set to be between the vocal cords and the trachea. A series of image segmentation steps

were applied to isolate and segment the pixels corresponding to the intended anatomical structure. Due to an increase of noise on the SSFSE scan, a set of smoothing image-processing filters were applied to remove sharp edges that would have a negative impact on the CFD simulations.

Digital surgery

For the patient group, three digital surgery options were incorporated into the CFD model. In clinical practice these are the major surgical options in case of severe symptoms, such as dyspnoea and stridor in combination with a diagnosed (re-)stenosis at the level of the vocal cords (posterior glottic stenosis) or upper part of the trachea (at the level of the previous tracheostomy).(3, 11) 1) Widening of the vocal cords i.e. widening of the posterior glottic stenosis by the placement of a cartilage graft in the posterior cricoid plate, was assumed to result in a total widening of 5 mm in the interarytenoid space,(3, 11) 2) Repair of the TD by removal of the tracheal deformity and an end-to-end anastomosis of the trachea,(6) 3) Both widening of the vocal cord stenosis and repair of the TD.

Results

Patient 1 was a 15 year old female patient with a history of acquired LTS for which surgical repair with an anterior and posterior autologous cartilage graft was done 11 years ago. She received a temporary tracheal cannula during surgical repair. The patient had a rigid posterior glottic stenosis, with minimal increase in lumen area (+6%) between free breathing and deep inspiration. In addition, there was collapse of the cricoid region during inspiration (-59%) and a mild TD, with minimal change during inspiration (+7%). The second patient selected was a 14 year old female patient with a history of acquired LTS for which multiple airway reconstructions with posterior cartilage placement were performed. The last revision operation (double stage laryngotracheal reconstruction) was performed three years ago followed by a period of endolaryngeal stenting and tracheal cannula. After 4 months of stenting, the silicone stent was removed and the patient was directly decannulated. The patient had a very severe residual posterior glottic stenosis and a deviation of the vocal cords, with an increase in lumen area during deep-inspiration (+77%). Furthermore, the patient had a severe TD, showing no change during inspiration (0%). Both patients experienced clinical complaints of dysphonia, dyspnea and stridor during the MRI visit.

The healthy volunteer included was a 16 year old male without a history of airway or vocal cord co-morbidities. Table 1 shows the airway lumen areas on MRI for the patients and healthy volunteer at the time of MRI examination, as well as after the digital surgery simulations. Figure 1 shows the MR images at the locations of interest for all study participants.

Table 1: Airway lumen areas of the study participants on MRI

	Areas on MRI (mm^2)							
	Vocal cords		Cricoid		TD		Trachea	
	FB	Insp	FB	Insp	FB	Insp	FB	Insp
Patient 1	44.0	46.6	136.3	56.4	101.5	108.4	103.2	95.9
VC widening	92.1	95.8	133.7	99.9	101.8	108.3	103.0	95.8
TD removal	43.8	46.6	136.0	56.4	109.0	115.5	103.2	95.9
VC widening + TD removal	92.0	95.8	134.4	99.9	109.2	115.5	103.1	95.8
Patient 2	52.0	92.1	162.1	151.1	43.1	37.9	71.6	66.9
VC widening	104.3	130.0	162.4	150.6	44.1	44.1	71.5	68.2
TD removal	52.0	96.2	162.1	150.4	65.0	65.0	71.7	69.1
VC widening + TD removal	104.7	130.0	162.3	150.4	65.1	65.1	71.7	69.1
Healthy volunteer	76.6	101.4	192.4	185.6	-	-	209.0	252.2

FB; free breathing PROPELLER scan, Insp; inspiration SSFE scan, TD; tracheal deformation, VC; vocal cord. Data are presented as area in mm^2.

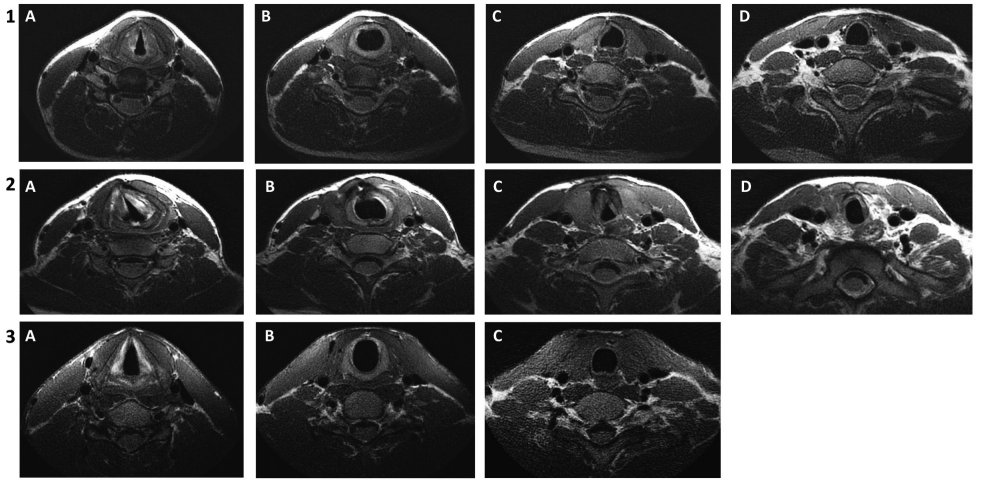

Figure 1: Axial T2 weighted PROPELLER free breathing MR images at the locations of interest for all study participants. 1) Vocal cords (a), cricoid (b), tracheal deformation (c) and trachea (d) of patient 1. 2) Vocal cords (a), cricoid (b) tracheal deformation (c) and trachea (d) of patient 2. 3) Vocal cords (a), cricoid (b) and trachea (c) of the healthy volunteer.

Both patients showed the highest pressure over the upper airways at the location of the vocal cords, with an increase in pressure during inspiration (table 2). While in the healthy volunteer an increase in airway area during inspiration leads to a decrease in airway pressure.

Table 2: Total pressure and resistance at the upper airways

	Airway pressure (Pa)								Resistance (Pa.s/L)	
	Vocal cords		Cricoid		TD		Trachea		Total airway	
	FB	Insp	FB	Insp	FB	Insp	FB	Insp	FB	Insp
Patient 1	16.3	12.1	1.8	10.1	5.3	5.7	5.1	5.5	44.3	26.0
VC widening	10.6	6.8	4.0	6.2	5.0	5.5	4.5	4.7	24.1	8.1
TD removal	19.1	12.3	2.4	10.4	5.5	5.7	5.4	5.5	53.7	27.0
VC widening + TD removal	10.5	6.7	3.7	6.0	4.7	5.3	4.4	4.6	23.6	7.9
Patient 2	39.6	59.7	29.0	58.4	29.8	43.2	14.1	20.7	100.2	153.3
VC widening	35.7	58.4	32.9	56.7	30.8	40.6	14.2	19.8	84.4	152.0
TD removal	20.4	13.7	9.7	12.6	10.9	10.2	9.3	9.6	43.6	16.0
VC widening + TD removal	16.0	14.5	11.4	13.0	10.1	10.2	8.6	9.6	29.1	19.4
Healthy volunteer	4.7	3.6	1.8	1.6	-	-	1.7	1.2	12.0	9.3

FB; free breathing, Insp; inspiration, TD; tracheal deformation, VC; vocal cords. Data are presented as total pressure in Pascal (Pa) for the airway pressure, and Pascal second per liter (Pa.s/L) for the airway resistance.

Total airway resistance during free-breathing, compared to the healthy volunteer, was increased 269% in patient 1 and increased 735% in patient 2. During inspiration the total airway resistance was increased 180% and 1548% for patient 1 and 2 respectively, compared to the healthy volunteer.

In patient 1, with a rigid vocal cord stenosis and a minor TD, widening of the vocal cords leads to a decrease in total airway resistance of 20.2 Pa.s/L (45.6%) during free-breathing and 17.9 Pa.s/L (68.8%) during inspiration compared to the current situation. While during free-breathing this airway resistance is still increased compared to the healthy volunteer, the airway resistance during inspiration resembles that of the healthy volunteer. A combination of widening of the vocal cords and removal of the TD leads to a decrease in total airway resistance of 20.7 Pa.s/L (46.7%) during free-breathing and 18.1 Pa.s/L during inspiration (69.6%), removal of the TD alone does not lead to a change in total airway resistance.

In patient 2, with a severe posterior glottic stenosis in combination with a severe TD, the highest decrease in overall airway resistance was achieved if the vocal cords were widened in combination with removal of the TD (a decrease in overall airway resistance of 71.1 Pa.s/L (71.0%) during free-breathing and 133.9 Pa.s/L (87.3%) during inspiration compared to the current situation). However, significant improvement of the total airway resistance was already seen by only removing the TD (a decrease of 56.6 Pa.s/L (56.5%) during free-breathing and 137.3 Pa.s/L (89.6%) during inspiration). When only the vocal cords were widened, minor improvement was seen (a decrease in airway resistance of 15.8 Pa.s/L (15.8%) during free-breathing and 1.3 Pa.s/L (0.8%) during inspiration). After all the surgical simulations, total airway resistance in patient 2 remained increased compared to the

healthy volunteer during free-breathing as well as inspiration. Figure 2-4 show the pressure distribution in the upper airways obtained by CFD during free-breathing and inspiration of the study participants. Figure 5 represents the airway resistance (y-axis) over the trajectory of the airway from vocal cords to trachea (x-axis). The figure shows peak resistance at the vocal cords in patient 1, with best improvement if the vocal cords are widened (a and b) and peak resistance at the TD in patient 2 with improvement when the TD is removed, also in combination with vocal cord widening (c and d).

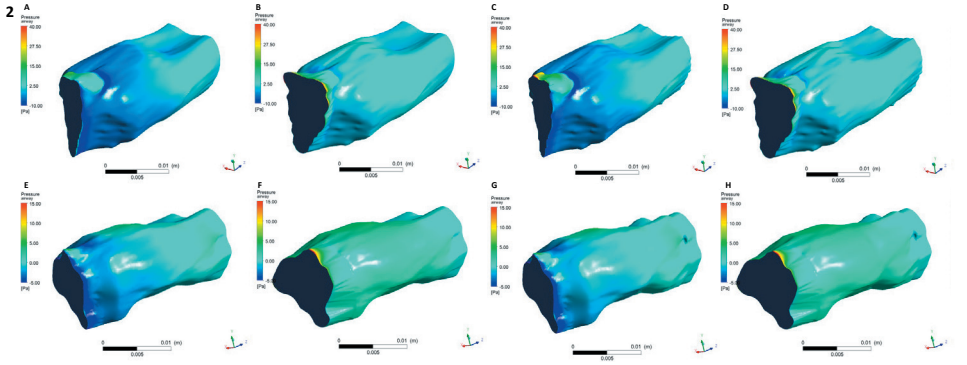

Figure 2: Pressure distribution in the upper airway of patient 1 obtained by CFD during free breathing (a-d) and inspiration (e-h) in the current situation (a and e), after digital surgery in which the vocal cords are widened (b and f), after digital surgery in which the TD is removed (c and g) and after digital surgery in which both the vocal cords are widened and the TD is removed (d and h). Data is presented as pressure in the airway (Pa) shown as a color scale from 40 Pa (red) to -10 Pa (blue).

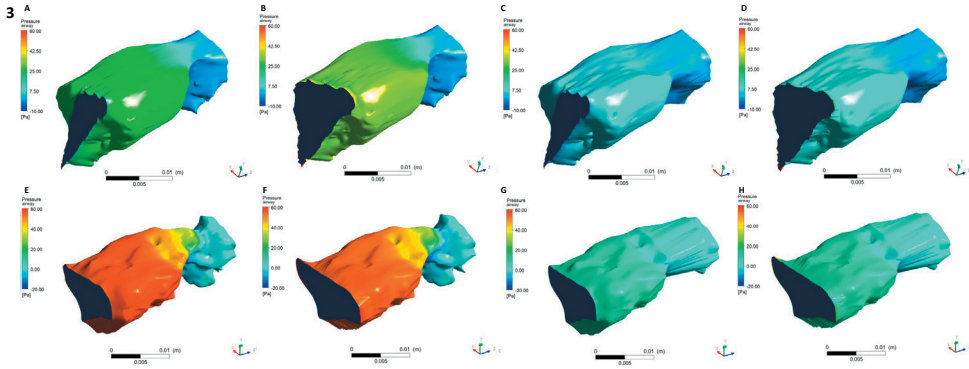

Figure 3: Pressure distribution in the upper airway of patient 2 obtained by CFD during free breathing (a-d) and inspiration (e-h) in the current situation (a and e), after digital surgery in which the vocal cords are widened (b and f), after digital surgery in which the TD is removed (c and g) and after digital surgery in which both the vocal cords are widened and the TD is removed (d and h). Data is presented as pressure in the airway (Pa) shown as a color scale from 40 Pa (red) to -10 Pa (blue).

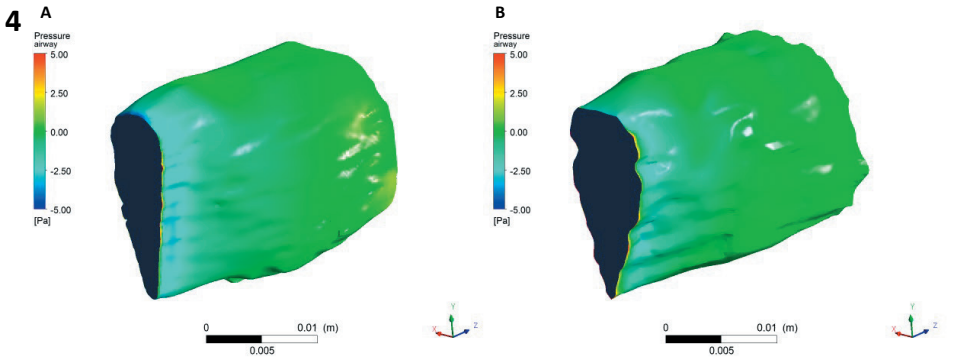

Figure 4: Pressure distribution in the upper airway of the healthy volunteer obtained by CFD during free breathing (a) and inspiration (b). Data is presented as pressure in the airway (Pa) shown as a color scale from 5 Pa (red) to -5 Pa (blue).

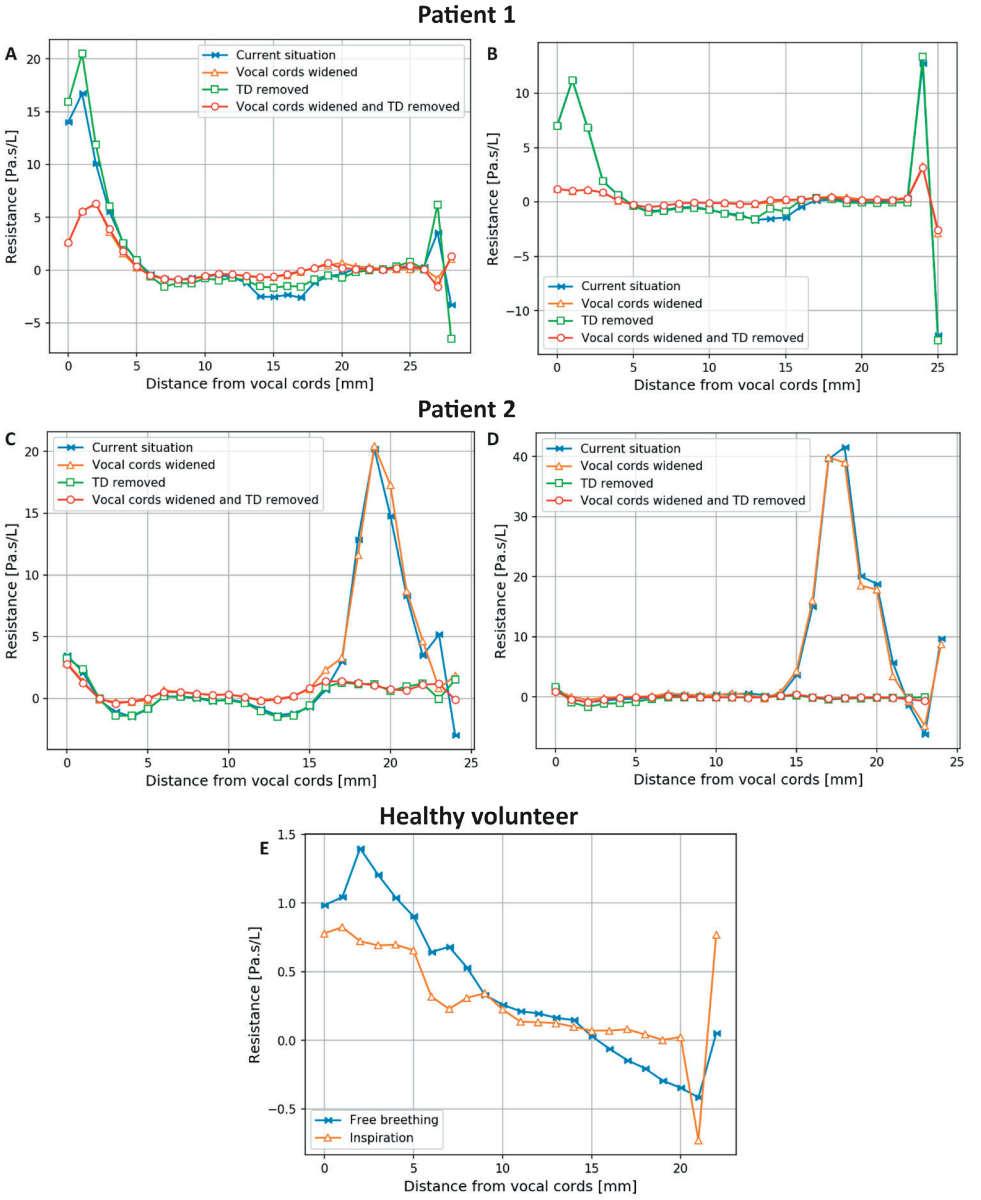

Figure 5: Airway resistance over the total upper airways (x-axis) in patient 1 (A: free breathing, B: inspiration), patient 2 (C: free breathing, D: inspiration) and the healthy volunteer (E) expressed in Pascal second per liter (Pa.s/L) (y-axis). The scales are adapted to fit observed resistance in each study subject. FB; free- breathing, IN; inspiration

Discussion

In this study, we used CFD on dynamic MR images of the upper airways to investigate airflow limitation and resistance on multiple levels in patients post-surgical repair of LTS, and we simulated the effects of further airway surgery on the upper airway airflow. Our findings show the potential of CFD modelling of the upper airways in a group of patients with very complex airway pathologies.

Firstly, we show that in LTS patients airway resistance is not solely related to airway lumen areas. CFD analyses showed a higher total airway resistance in patient 2 compared to patient 1. While patient 1 showed a narrower airway lumen area at the vocal cords and cricoid, patient 2 showed a narrower airway lumen area below the cricoid. In addition, patient 2 had a deviation of the vocal cords, displacing them out of the usual airflow midline, which might explain the increase in airway resistance. As described by Yang *et al.* this misalignment between the glottic and subglottic plane can cause a significant increase in work of breath, due to an increase in airway resistance.(27)

The CFD analyses of our healthy volunteer showed a decrease in airway resistance during inspiration, caused by an increase of the airway areas, such as abduction of the vocal cords. However, this decrease in airway resistance was seen in patient 1, but not in patient 2. While patient 1 showed a higher degree of abduction impairment at the vocal cords (a smaller increase in area during inspiration compared to patient 2), patient 2 showed narrowing of the airway area below the vocal cords during inspiration. This can be explained as a malacic effect, where collapse occurs during inspiration due to the Bernoulli- Venturi effect.(28) Also, these findings show that a-frame deformations of the trachea are often a dynamic airway condition, for which dynamic visualization is vital to diagnose severity.(6, 18)

Secondly, the surgery simulations in our CFD models show that the effect on airflow and resistance of the upper airways is patient specific and consequently surgical repair should be patient-tailored. This is especially true in patients with multi-level stenosis of the airway where it is hard to predict the effect surgery on a single stenotic level has on airflow. In patient 1 with a posterior glottic stenosis, but a mild TD, only widening the vocal cords had a positive effect on total airway resistance. While in patient 2, with both severe posterior glottic stenosis and a severe TD, only widening of the vocal cords did not result in an improvement of airway resistance. In this patient, CFD modeling can aid the clinician in the decision to surgically repair the TD but to refrain from further surgery on the glottic level, which will probably have minimal added effect on airway resistance but probably worsens the patients' voice.

The decision for revision surgery is complex, because revisions are technically more challenging due to local existing scar tissue and possibly need a longer recovery period with stenting and tracheal cannula. In addition, widening the vocal cords comes at the expense of voice quality, and should therefore be performed only when a significant improvement of airflow is expected.(7, 9) The decision for revision surgery is currently based on expert opinion by the otorhinolaryngologist, based on clinical indication and assessment of the anatomy and treatment options. Especially in cases with multiple levels of (re)stenosis, like the posterior glottis, subglottis and (upper) trachea, defining which area to re-operate is challenging. Our findings show that CFD can help identify the area most responsible for airflow limitation and possibly predict the effect that surgery can have on each stenotic area.(3, 11)

Our study has some limitations. First, these pilot simulations were only conducted in one healthy volunteer and two patients. Considering the heterogeneity of the airway anatomy in these patients, simulations in a wider population are needed. However, to perform CFD analyses on the entire patient population, there is need for improved image quality. Many of the MRIs conducted in the MUSIC study, although of sufficient quality for clinical use, were of suboptimal resolution for CFD analyses.(18) To diminish the amount of post-processing of the images to be fit for CFD simulation, the sequences should have a minimum of movement artefacts and noise, therefore dynamic sequences should be made during a slow, controlled inhalation-expiration. This problem could be overcome by using CT. However, conducting CT of the upper airways is contraindicated due to exposure of the thyroid to ionizing radiation.(16, 17) Further refinement of MRI sequences should be performed to solve resolution issues and remove noise artefacts to make MRI more suitable for CFD analyses. Better suited MRI coils around the neck area should also count as part of the enhancement of image quality (signal to noise ratio) and resolution.

Another limitation of our study is that we have used a steady inspiratory flow of 15L/min for both the healthy volunteer, and the two patients. However, it is known that LTS patients have a decreased in- and expiratory pulmonary function due to the stenosis and pulmonary comorbidities, such as bronchopulmonary dysplasia.(4, 18, 29) In addition, during physical exercise higher and less steady airflow rates are expected. This simplification of the model might have led to an underestimation of the effect of airway resistance in our patients. Besides, a study by Kim *et al.* combining CFD of the upper and lower respiratory tract recently showed that altered upper airway airflow can lead to altered flow in the distal airways and can therefore influence ventilation distribution throughout the lungs.(1) This may also be the case for the LTS population, where altered anatomy of the upper airways can lead to an increase in pulmonary problems.

To our knowledge, this is the first study performing CFD analyses in patients post LTS repair using MRI. Previous research performing CFD based on CT in LTS patients only focused on the upper airways before initial repair.(30) Both Lin *et al.* and Mylavarapu *et al.* performed digital surgery on upper airway CT images showing, in line with our findings, the potential of CFD modelling as a clinical decision making tool. However, these studies did not have dynamic images available, while most clinical symptoms present during inspiration and our findings show that anatomical alterations during dynamic maneuvers can substantially influence upper airway airflow and resistance.(21, 22)

In conclusion, our research shows the potential of CFD on (dynamic) MRI of the upper airways to model airflow limitation in patients with complex multilevel stenosis. CFD combined with MRI has the potential to offer patient-tailored management of complex multi-level upper airway stenosis. Future research should focus on performing CFD analyses in a larger group of patients with complex multi-level airway pathology, to investigate whether these results are reproducible in patients with similar pathology and to validate the post-operative improvement with the pre-operative prediction by the CFD modeling.

References

1. Kim M, Collier GJ, Wild JM, Chung YM. Effect of upper airway on tracheobronchial fluid dynamics. Int J Numer Method Biomed Eng. 2018;34(9):e3112.
2. Jefferson ND, Cohen AP, Rutter MJ. Subglottic stenosis. Semin Pediatr Surg. 2016;25(3):138-43.
3. Monnier P. Pediatric Airway Surgery Management of Laryngotracheal Stenosis in Infants and Children. Berlin, Heidelberg: Springer Berlin Heidelberg; 2011.
4. Pullens B, Pijnenburg MW, Hoeve HJ, Baatenburg de Jong RJ, Buysse CM, Timmerman MK, et al. Long-term functional airway assessment after open airway surgery for laryngotracheal stenosis. Laryngoscope. 2016;126(2):472-7.
5. Padia R, Sjogren P, Smith M, Muntz H, Stoddard G, Meier J. Systematic review/meta-analysis comparing successful outcomes after single vs. double-stage laryngotracheal reconstruction. Int J Pediatr Otorhinolaryngol. 2018;108:168-74.
6. Kennedy AA, de Alarcon A, Tabangin ME, Rutter MJ, Myer CMt, Smith MM, et al. Tracheal A-Frame Deformities Following Airway Reconstruction. Laryngoscope. 2021;131(4):E1363-E8.
7. Pullens B, Hakkesteegt M, Hoeve H, Timmerman M, Joosten K. Voice outcome and voice-related quality of life after surgery for pediatric laryngotracheal stenosis. Laryngoscope. 2017;127(7):1707-11.
8. Cohen W, Wynne DM, Lloyd S, Townsley RB. Cross-sectional follow-up of voice outcomes in children who have a history of airway reconstruction surgery. Clin Otolaryngol. 2018;43(2):645-51.
9. Baker S, Kelchner L, Weinrich B, Lee L, Willging P, Cotton R, et al. Pediatric laryngotracheal stenosis and airway reconstruction: a review of voice outcomes, assessment, and treatment issues. J Voice. 2006;20(4):631-41.
10. de Alarcon A. Voice outcomes after pediatric airway reconstruction. Laryngoscope. 2012;122 Suppl 4:S84-6.
11. de Alarcon A, Rutter MJ. Revision pediatric laryngotracheal reconstruction. Otolaryngol Clin North Am. 2008;41(5):959-80, x.
12. van der Pol RJ, Singendonk MM, Konig AM, Hoeve H, Kammeijer Q, Pullens B, et al. Development of the reflux finding score for infants and its observer agreement. J Pediatr. 2014;165(3):479-84.
13. Singendonk MM, Pullens B, van Heteren JA, de Gier HH, Hoeve HL, Konig AM, et al. Reliability of the reflux finding score for infants in flexible versus rigid laryngoscopy. Int J Pediatr Otorhinolaryngol. 2016;86:37-42.
14. Becker M, Burkhardt K, Dulguerov P, Allal A. Imaging of the larynx and hypopharynx. Eur J Radiol. 2008;66(3):460-79.
15. Elders B, Hermelijn SM, Tiddens H, Pullens B, Wielopolski PA, Ciet P. Magnetic resonance imaging of the larynx in the pediatric population: A systematic review. Pediatr Pulmonol. 2019;54(4):478-86.

16. Lubin JH, Adams MJ, Shore R, Holmberg E, Schneider AB, Hawkins MM, et al. Thyroid Cancer Following Childhood Low-Dose Radiation Exposure: A Pooled Analysis of Nine Cohorts. J Clin Endocrinol Metab. 2017;102(7):2575-83.
17. Mazonakis M, Tzedakis A, Damilakis J, Gourtsoyiannis N. Thyroid dose from common head and neck CT examinations in children: is there an excess risk for thyroid cancer induction? Eur Radiol. 2007;17(5):1352-7.
18. Elders B, Ciet P, Tiddens H, van den Bosch W, Wielopolski P, Pullens B. MRI of the upper airways in children and young adults: the MUSIC study. Thorax. 2021.
19. Elders B, Hakkesteegt MM, Ciet P, Tiddens H, Wielopolski P, Pullens B. Structure and Function of the Vocal Cords after Airway Reconstruction on Magnetic Resonance Imaging. Laryngoscope. 2021;131(7):E2402-E8.
20. Faizal WM, Ghazali NNN, Khor CY, Badruddin IA, Zainon MZ, Yazid AA, et al. Computational fluid dynamics modelling of human upper airway: A review. Comput Methods Programs Biomed. 2020;196:105627.
21. Lin EL, Bock JM, Zdanski CJ, Kimbell JS, Garcia GJM. Relationship between degree of obstruction and airflow limitation in subglottic stenosis. Laryngoscope. 2018;128(7):1551-7.
22. Mylavarapu G, Mihaescu M, Fuchs L, Papatziamos G, Gutmark E. Planning human upper airway surgery using computational fluid dynamics. J Biomech. 2013;46(12):1979-86.
23. Zhang Q, Coolen BF, van den Berg S, Kotek G, Rivera DS, Klomp DWJ, et al. Comparison of four MR carotid surface coils at 3T. PLoS One. 2019;14(3):e0213107.
24. Constantin P, Foias C. Navier-stokes equations: University of Chicago Press; 1988.
25. Pope SB. Turbulent flows, Cambridge, 2000. Published; 2017.
26. Batchelor CK, Batchelor GK. An introduction to fluid dynamics: Cambridge university press; 2000.
27. Yang MM, Higano NS, Gunatilaka CC, Hysinger EB, Amin RS, Woods JC, et al. Subglottic Stenosis Position Affects Work of Breathing. Laryngoscope. 2021;131(4):E1220-E6.
28. Freitag L, Ernst A, Unger M, Kovitz K, Marquette CH. A proposed classification system of central airway stenosis. Eur Respir J. 2007;30(1):7-12.
29. Cheng T, Carpenter D, Cohen S, Witsell D, Frank-Ito DO. Investigating the effects of laryngotracheal stenosis on upper airway aerodynamics. Laryngoscope. 2018;128(4):E141-E9.
30. Zdanski C, Davis S, Hong Y, Miao D, Quammen C, Mitran S, et al. Quantitative assessment of the upper airway in infants and children with subglottic stenosis. Laryngoscope. 2016;126(5):1225-31.

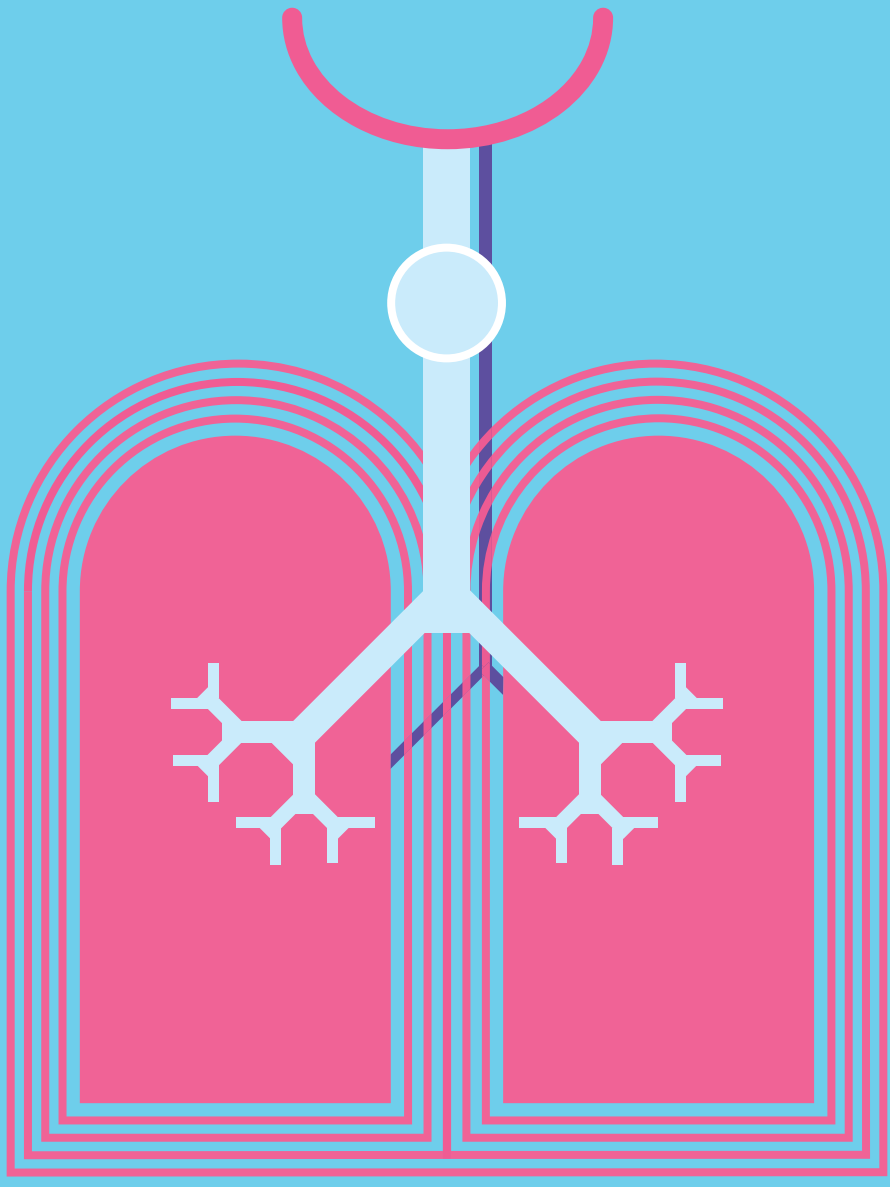

Lower respiratory tract

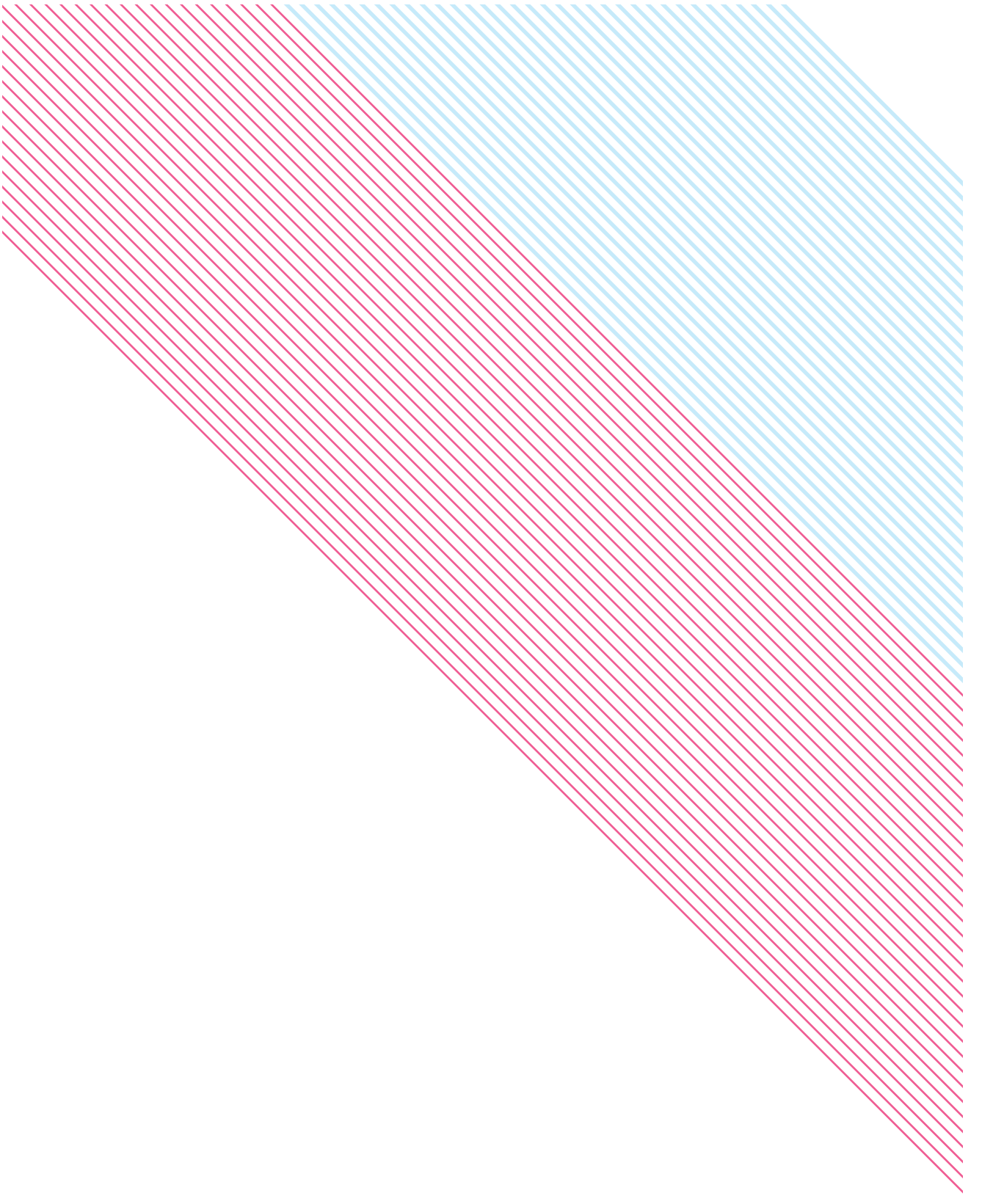

Chapter 6

Lung structure and function on MRI in preterm born school children with and without BPD: a feasibility study

Bernadette BLJ Elders, Harm AWM Tiddens, Mariëlle WH Pijnenburg, Irwin KM Reiss, Piotr A Wielopolski, Pierluigi Ciet

Submitted

Abstract

Rationale: The most common respiratory complication of extreme prematurity is bronchopulmonary dysplasia (BPD), leading to structural lung changes and impaired respiratory outcomes. However, also extremely preterm children without BPD may show similar adverse respiratory outcomes. There is need for a safe imaging modality for preterm children with and without BPD for disease severity and risk stratification assessment.

Objective: To develop a chest Magnetic Resonance Imaging (MRI) protocol in preterm children with and without BPD at school age.

Methods: Nine healthy volunteers (median age 11.6 (range 8.8-12.8) years), eleven preterm children with BPD (11.0 (7.2-15.6) years) and nine without BPD (11.1(10.7-12.6) years) underwent MRI. MR images were scored on hypo- and hyperintense abnormalities, bronchopathy and architectural distortion. MRI data were correlated to spirometry. Ventilation and perfusion defects were analysed using Fourier Decomposition (FD) MRI.

Main results: On MRI, children with BPD had a higher %diseased lung (9.1 (IQR 5.9-11.6)%) compared to preterm children without BPD (3.4 (IQR 2.5-5.4)%, $p<0.001$) and healthy volunteers (0.4 (IQR 0.1-0.8)%, $p<0.001$). %Diseased lung correlated negatively with %predicted FEV_1 ($r=-0.40$, $p=0.04$), FEV_1/FVC ($r=-0.49$, $p=0.009$) and FEF_{75} ($r=-0.63$, $p<0.001$). Ventilation and perfusion defects on FD sequence corresponded to hypointense regions on expiratory MRI.

Conclusion: MRI can identify structural and functional lung damage at school age in preterm children with and without BPD, showing good correlation with spirometry. We propose chest MRI as a sensitive and safe imaging method (without ionising radiation, contrast agents or the use of anaesthesia) for the long-term follow up of preterm children.

Introduction

Respiratory problems related to premature birth can lead to life-long morbidity.(1-3) The most common respiratory complication of extreme prematurity is bronchopulmonary dysplasia (BPD), leading to structural lung changes and impaired respiratory outcomes. However, also patients born extremely preterm without BPD may show similar adverse respiratory outcomes, leading to life-long morbidity.(2-5) To date, little is known about the long term follow up of prematurity related lung disease and the role imaging could play in monitoring children with BPD. Computed Tomography (CT) is the current gold standard to assess structural lung changes seen in children with BPD.(6) Studies have shown that structural lung abnormalities on CT have a high predictive value of short and long-term adverse respiratory outcomes in preterm patients.(7-9) However, the use of CT remains limited for radiation safety reasons, but also because CT imaging does not necessarily change management of BPD. For these reasons, the European Respiratory Society (ERS) Task Force on long-term management of BPD has recently suggested the use of lung imaging only in subgroups of children with clinically severe BPD.(10)

Magnetic resonance imaging (MRI) can overcome the limitation related to radiation exposure, and has the additional benefit of assessing both lung structure and function in a single examination, as shown for several other pediatric lung diseases.(11, 12) The development of MRI as a safe and feasible imaging method for preterm born children has great potential to identify those patients at risk for pulmonary morbidity. However, MRI research in this population is limited. Only two studies have been done in school-age children with BPD, in which hyperpolarized ^{3}He diffusion- weighted MRI was used, showing contradictory results about alveolar enlargement.(13) A disadvantage of ^{3}He diffusion- weighted MRI is the high costs of the technique, related to the hyperpolarized gases and the need of dedicated MRI scanner hardware. In neonatal BPD, multiple studies have been shown good feasibility of MRI without the use of contrast agents to visualize differences in structural lung changes between healthy volunteers, and preterm born children with and without BPD.(14-18) However, these studies focused on short-term outcome and were done on a unique small-footprint MRI scanner using in-house developed sequences, thus making the MRI protocol not easily implementable at other institutions. To date, no studies have been conducted using conventional MRI sequences in older children with BPD, nor in preterm born children without BPD.

In this study, we aimed to develop a chest MRI protocol, on a standard 1.5 Tesla MRI scanner, to assess lung structure and function in preterm born children with and without BPD at school age and to validate MRI findings against spirometry.

Methods

All children followed at the BPD outpatient clinic with severe BPD diagnosed at 36 weeks of gestational age (GA) according to the National Health Institute (NHI) criteria,(19) with an age between 6 and 16 years were approached to participate in the **V**entilation, **I**nflammation, perfusion and structure in **B**ronchopulmonary dysplasia at school ag**e** (**VIBE**) study. Children with BPD were compared to preterm born children (<28 weeks post menstrual age) without BPD or other lung pathology, randomly selected from the general neonatal follow up clinic, and healthy volunteers (born >37 weeks post menstrual age) consisting of siblings or friends of the preterm born children within the same age range. In- and exclusion criteria are shown in supplementary material 1. Approval was obtained from the local medical ethics committee (MEC2018-134 and MEC2018-002) and written informed consent was obtained from parents/ legal representatives of all study participants.

All study participants underwent spirometry and spirometer-controlled chest MRI using the BPD protocol, except for two healthy volunteers included from a different study using the same MRI protocol, in whom only the structural MR imaging was performed. From all preterm born children with and without BPD, clinical data on GA, birth weight and respiratory support during the neonatal period were retrieved from the electronic patient dossier.

Spirometry

Flow volume curves were obtained from all study participants according to ERS/American Thoracic Society (ATS) guidelines.(20, 21) Forced vital capacity (FVC), forced expiratory volume in 1 sec (FEV_1) and forced expiratory flow at 75% of VC (FEF_{75}) are presented as percentage predicted and z-scores as reported by the Global Lung function Initiative (GLI). (22)

Magnetic resonance imaging

A chest MRI protocol was developed on a 1.5T MRI (*Artist, GE Healthcare, Milwaukee, Wisconsin, USA)* using a 32 channels torso coil. The protocol consisted of breath-hold isotropic sagittal 3D proton density (PD) weighted Spoiled Gradient Echo Sequences (SPGR) images during inspiration and expiration, a respiratory navigated axial 2D T2-weighted fat-suppressed (FS) Periodically Overlapping ParalLEL Lines with Enhanced Reconstruction (PROPELLER) and a 3D PD-weighted respiratory navigated axial zero echo time (ZTE) and/ or respiratory gated ultrashort echo time (UTE) sequence during free breathing. In addition, a 2D SPGR multi-phase free-breathing sequence covering the entire thorax with 7 to 10 coronal slabs according to chest size with a slice thickness of 15mm was performed for Fourier Decomposition (FD) imaging. Total protocol duration was 20 to 30 minutes; no sedation was used. Parameters of the MRI protocol are shown in supplementary material 2.

Qualitative MRI analyses

Image quality was assessed using a modified version of the scoring method from Bae *et al.*(23) All sequences were scored on the depiction of fissures, intrapulmonary vessels and bronchi, presence of noise/artifacts and overall acceptability. Artifacts were further classified into blurring, streaking, wrapping and artifacts related to low signal- to-noise ratio (SNR). Supplementary material 3 shows the scoring method, including examples of the artifacts.

Quantitative MRI analyses

For the quantitative analyses of the MR images, a grid based annotation method based on the PRAGMA- BPD method was developed: the bronchopul**M**onary rott**E**rdam m**R**i morpholo**G**y scor**E** (**MERGE**).(9, 24) An in-house developed software was used for the analysis. In this method, a grid is placed over twenty equidistant axial (reconstructed) images. The size of the grid corresponds to the largest airway diameter. Each grid is coloured for BPD related abnormalities or normal lung tissue, in a hierarchical order of clinical relevance as described on previous CT studies.(9) We identified three categories of abnormalities: hypointensity, representing CT hypoattenuation areas of mosaic perfusion, emphysema, trapped air, bullae and cysts; hyperintensity, representing CT hyperattenuation areas of consolidation, atelectasis and lineair/subpleural opacities and bronchopathy, consisting of bronchial wall thickening and bronchiectasis. Each category was expressed as a percentage of the total lung volume. Due to superiority of certain sequences in the identification of specific abnormalities(11), the sequence with the highest percentage per abnormality was chosen for analyses. Figure 1 shows an example of the annotated abnormalities on the MR images from our protocol.

MERGE scoring was done in random order on all anonymized SPGR expiratory, PROPELLER and ZTE/UTE sequences by a trained researcher with 4 years' experience in chest MRI (B.E.). Data are presented as the highest percentage for an abnormality on any of the sequences. The same researcher repeated the MERGE score on the MRIs of seven (n=7; 24% of the MRI data) study participants to assess intra-observer variation of the MRI scoring, with a four week interval to prevent recall bias.

In addition, the degree of anatomical architecture distortion (AAD), defined as abnormal displacement of bronchi, vessels, fissures and/or septa, was scored counting the number of lung segments showing signs of AAD. Considering 10 segments for the right lung and 9 for the left lung.(24, 25) AAD was scored as mild, moderate and severe, when presenting in less than 7, between 7 and 13 and more than 13 lung segments, respectively.

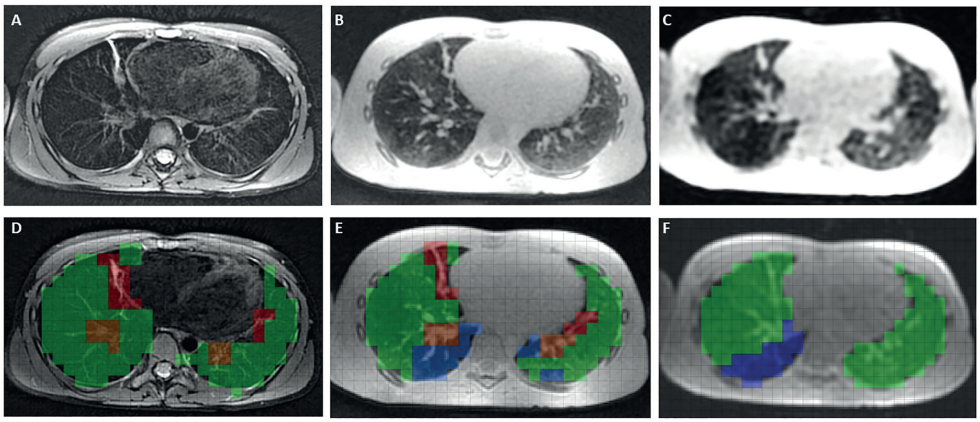

Figure 1: Example of the MERGE score on the MRI of an 8 year old girl with severe BPD. A) the axial PROPELLER, B) ZTE and C) Expiratory SPGR images and corresponding MERGE scoring (D,E,F) showing normal lung tissue (green), hyperintensity (red), hypointensity (blue) and bronchopathy (orange).

Ventilation and perfusion

An in-house developed algorithm based on the work of Voskrebenzev *et al.* was used to analyse the FD images.(26-28) The algorithm first corrects for intensity and registers all the images, after which a spectral decomposition of the signal is applied, separating the components of the signal related to ventilation and perfusion. Then algebraic operations allow to reconstruct ventilation and perfusion maps. This method relays on the periodic variation in signal intensity related to ventilation and perfusion, by detecting the frequency of this variation, the two components can be separated. As exploratory analyses a visual comparison was made between the coronal reformatted SPGR expiration sequence and the ventilation and perfusion maps to classify hypo- and hyper intense regions as ventilation or perfusion defects.

Statistics

Data analysis was done using SPSS Statistics (*version 25, IBM SPSS, Chicago, IL, USA*). Parametric data are presented as mean ± standard deviation and non- parametric data are presented as median (range or interquartile range). Data were compared using the parametric t-test for normally distributed data and the Mann Whitney U test for not normally distributed data. Similarly, Pearson's and Spearman's rho correlations were calculated for normally and not normally distributed data respectively. A 5% significance level was assumed. Intra- observer agreement was calculated with the intra-class correlation coefficient and interpreted as poor (<0.50), moderate (0.50-0.75), good (0.75-0.90) or excellent (>0.90).

Results

Characteristics of study participants, data on respiratory support during the neonatal period and spirometry outcomes are shown in table 1. In total, 11 children with severe BPD, 9 preterm born children without BPD and 9 healthy volunteers were included with a median age of 11.0

(range 7.2-15.6), 11.1 (range 10.7-12.6) and 11.6 (range 8.8-12.8) years, respectively. Children with BPD were born after a mean GA of 27.3 ± 2.4 weeks, and preterm born children after a GA of 28.1 ± 1.4 weeks, which did not differ significantly (p=0.23). In none of the electronic patient files the exact duration of respiratory support was documented, except for the type and amount of respiratory support at time of BPD diagnosis.

Table 1: Characteristics and spirometry outcome of all study participants

	BPD (n= 11)	**Preterm (n=9)**	**Healthy volunteers (n=9/7)**	**p-value**
Age at MRI (years, range)	11.0 (7.2-15.6)	11.1 (10.7-12.6)	11.6 (8.8-12.8)	
Gender (% female)	18.2	66.7	55.6	
PMA (weeks)	27.3 ± 2.4	28.1 ± 1.4		0.23[1]
Birth weight (grams)	910 ± 347	1106 ± 295		**0.02[1]**
Antenatal corticosteroids (n/%)	Complete 5/45 Incomplete 3/27 None 2/18 Unknown 1/9	Complete 7/78 None 2/22		
Surfactant treatment (n/%)	Yes 6/55 No 3/27 Unknown 2/18	Yes 3/33 No 6/66		
Postpartum medication **Diuretics**	Yes 8/73 No 2/18 Unknown 1/9	No 9/100		
Corticosteroids	Yes 4/36 No 5/45 Unknown 2/18	No 9/100		
Oxygen at 6 months GA	Yes 2/18 No 7/64 Unknown 2/18	No 9/100		
FVC				
% predicted	100 (94-104)	99 (95-106)	102 (73-115)	0.77[1], 0.66[2], 0.87[3]
z-score	0.0 (-0.5 -0.3)	-0.1 (-0.5 -0.5)	0.2 (-2.3- 1.3)	0.66[1], 0.66[2], 0.87[3]
FEV_1				
% predicted	87 (70-89)	99 (90-104)	104 (79-109)	**0.003[1],** 0.07[2], 0.52[3]
z-score	-1.1 (-2.4- -1.0)	-0.1 (-0.9- 0.4)	0.3 (-1.8- 0.8)	**0.006[1],** 0.07[2], 0.60[3]
FEV_1/FVC				
% predicted	84 (69-90)	96 (90-105)	99 (89-105)	**0.01[1], 0.006[2],** 0.92[3]
z-score	-2.2 ± 1.1	-0.3 ± 1.4	-0.2 ± 1.1	**0.005[1], <0.001[2],** 0.53[3]
FEF_{75}				
% predicted	52 ± 25	91 ± 21	91 ± 20	**0.002[1], 0.001[2]**, 0.60[3]
z-score	-1.7 (-2.7- -1.2)	-0.2 (-1.0- 0.4)	0.0 (-0.3- 0.3)	**0.002[1], 0.004[2]**, 0.60[3]
VCmax				
% predicted	100 (94-104)	99 (95-107)	102 (73-115)	0.71[1], 0.66[2], 0.87[3]
z-score	0.0 (-0.5- 0.3)	-0.1 (-0.5-0.6)	0.2 (-2.3- 1.3)	0.66[1], 0.66[2], 0.87[3]

BPD; bronchopulmonary dysplasia, FEF_{75}; Forced Expiratory Flow at 75% of expiration, FEV_1; forced expiratory volume in 1 second, FVC; forced vital capacity, GA; gestational age, MRI; magnetic resonance imaging, PMA; post menstrual age, VC max; maximum vital capacity. Data are presented as mean ± standard deviation or median (range or interquartile range), P<0.05 is in bold, 1= children with BPD compared to preterm born children without BPD, 2= children with BPD compared to healthy volunteers, 3= preterm born children without BPD compared to healthy volunteers.

Spirometry

Children with BPD showed a significantly lower FEV_1, FEV_1/FVC and FEF_{75} compared to preterm born children and healthy volunteers (all p<0.01) (table1). No significant difference in spirometry outcomes between preterm born children and healthy volunteers was found.

Qualitative MRI analyses

MRI was successfully performed in 28 out of 29 study subjects (97%). One subject with an age of 7 years was not able to execute the full MRI protocol due to claustrophobia. Qualitative scoring results of the MR scans are shown in table 2. Best overall image quality was achieved for the UTE, T2 weighted PROPELLER and ZTE sequences, with an 'above average' score for all. Visibility of BPD related lung abnormalities, expressed as the disease percentage of total lung volume scored per sequence, was highest on ZTE/UTE for hypointensity and bronchopathy, and on PROPELLER for hyperintensity (supplementary material 4).

The most common image artifacts were blurring for the SPGR inspiration (27.5%) and expiration (37.9%) sequences, streaking for the PROPELLER (34.5%) sequences and low SNR for the ZTE/UTE (20.7%) sequences. However, with a minimal 'satisfactory' acceptability score, these artifacts did not interfere with assessment of MR images, which were all considered of diagnostic quality.

Table 2: Qualitative MRI scoring

	Axial SPGR insp N= 27	Axial SPGR exp n=29	T2- weighted PROPELLER n= 29	ZTE n=26	UTE n =10
Fissures	1 (1-1)	1 (1-2)	2 (2-2)	2 (2-2)	2 (2-2)
Vessels	2 (2-2)	2 (2-3)	4 (3-4)	4 (4-4)	4 (4-4)
Bronchi	2 (2-2)	2 (2-2)	3 (3-4)	4 (4-4)	4 (4-4)
Noise/artifacts	3 (2-3)	3 (2-3)	3 (3-4)	2 (2-4)	3 (3-4)
Overall acceptability	3 (2-3)	3 (2-3)	4 (3-4)	4 (3-4)	4 (4-4)

Qualitative MRI scoring, according to Bae *et al.*. PROPELLER; periodically rotated overlapping parallel lines with enhanced reconstruction, SPGR; spoiled gradient echo, UTE; ultra- short echo time, ZTE; zero- echo time. Data is presented as median (interquartile range). The scores range from 1 representing worst depiction/most artifacts/ worse acceptability and 5 representing best depiction of structures/least artifacts/ superior acceptability (for exact scoring method see supplementary material 3).

Quantitative MRI analyses

MERGE and AAD results are shown in table 3. Figure 2 shows example images of a child with BPD. The most common MRI findings in children with BPD were bronchopathy (mainly bronchial wall thickening) and hyperintensity (mainly linear opacities), while bronchopathy was the most common MRI finding in preterm born children without BPD. Children with BPD showed, compared to preterm born children and healthy volunteers, a significantly higher percentage of hyperintensity (p=0.004 and p<0.001), bronchopathy (p=0.002 and p<0.001) and total diseased lung (p<0.001 and p<0.001) on the free breathing sequences. Hypointensity

on the expiratory images was significantly higher in children with BPD compared to healthy volunteers (p=0.03), but not compared to preterm born children without BPD (p=0.55). On MRI, preterm children without BPD compared to healthy volunteers showed a significantly higher percentage of all abnormalities except for percentage of hypointense regions on free-breathing sequences (p-values all between 0.01 and 0.001). In addition, the expiratory images of preterm born children without BPD scored higher on hypointense regions than healthy volunteers (p=0.01).

Table 3: Quantitative MRI results

	BPD (n= 11)	Preterm (n=9)	Healthy volunteers (n=9)	p-value
Free-breathing				
Diseased lung	9.1 (5.9-11.6)	3.4 (2.5-5.4)	0.4 (0.1-0.8)	**<0.001[1], <0.001[2], 0.001[3]**
Hypointensity	0.0 (0.0-0.8)	0.2 (0.0-0.3)	(0.0-0.0)	0.71[1], 0.18[2], 0.09[3]
Hyperintensity	1.8 (1.4-3.6)	0.5 (0.1-1.4)	(0.0-0.2)	**0.004[1], <0.001[2], 0.01[3]**
Bronchopathy	5.3 (4.5-7.7)	2.6 (1.6-3.7)	0.2 (0.0-0.7)	**0.002[1], <0.001[2], 0.001[3]**
Normal lung	90.9 (88.4-94.1)	96.6 (94.6-97.6)	99.6 (99.3-100.0)	**<0.001[1], <0.001[2], 0.001[3]**
Expiration				
Hypointensity	2.5 (0.0-6.2)	0.9 (0.0-0.9)	0.0 (0.0-0.0)	0.55[1], **0.03[2], 0.01[3]**
Normal lung	97.5 (93.8-100.0)	99.1 (96.5-100.0)	100.0 (100.0-100.0)	0.55[1], **0.03[2], 0.01[3]**
Architectural distortion	2 (1-2)	1 (0-1)	0 (0-0)	**0.002[1], <0.001[2], 0.01[3]**

Quantitative MRI results according to the MERGE scoring and degree of architectural distortion. BPD; bronchopulmonary dysplasia. Data are presented as % of the total lung volume for the MERGE scoring and as a degree for architectural distortion, with 0= none, 1= mild, 2=moderate, 3=severe. All data is presented as median (interquartile range). P<0.05 is in bold, 1= children with BPD compared to preterm born children without BPD, 2= children with BPD compared to healthy volunteers, 3= preterm born children without BPD compared to healthy volunteers.

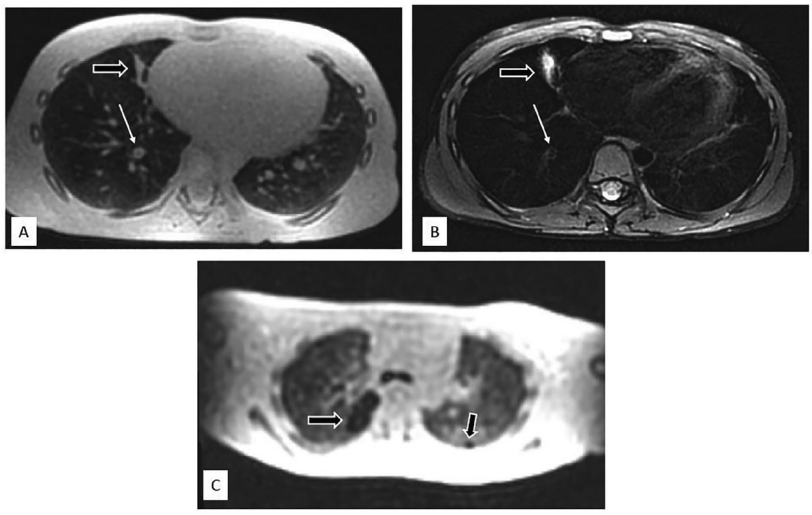

Figure 2: Axial 3D Proton Density weighted (PD-w) Zero echo time with navigator (ZTE vnav) (A) and axial 2D T2-weighted PROPELLER (B) and axial reconstructed 3D PD-w SPGR expiration images in an 8 year old girl with severe BPD. Note the segmental bronchus of the right lower lobe with bronchial wall thickening (A and B, thin arrow), the hyperintense parenchymal abnormality in the middle lobe representing atelectasis/fibrosis (A and B, thick arrow) and the hypointense regions on the expiratory images (C, thick arrow).

Correlations between the quantitative MRI scores and spirometry outcomes are shown in table 4 and supplementary material 5. A significant negative correlation was found between the percentage of diseased lung on MRI and percentage predicted of FEV_1 (p=0.04), FEV_1/FVC (p=0.009) and FEF_{75} (p<0.001), as well as between a higher score of AAD and lower spirometry outcomes (all p<0.001).

Table 4: Correlation analyses between quantitative MRI analyses and spirometry outcomes

	BPD (n= 11)	Preterm (n=9)	Healthy volunteers (n=9)	p-value
Free-breathing				
Diseased lung	9.1 (5.9-11.6)	3.4 (2.5-5.4)	0.4 (0.1-0.8)	**<0.001[1], <0.001[2], 0.001[3]**
Hypointensity	0.0 (0.0-0.8)	0.2 (0.0-0.3)	(0.0-0.0)	0.71[1], 0.18[2], 0.09[3]
Hyperintensity	1.8 (1.4-3.6)	0.5 (0.1-1.4)	(0.0-0.2)	**0.004[1], <0.001[2], 0.01[3]**
Bronchopathy	5.3 (4.5-7.7)	2.6 (1.6-3.7)	0.2 (0.0-0.7)	**0.002[1], <0.001[2], 0.001[3]**
Normal lung	90.9 (88.4-94.1)	96.6 (94.6-97.6)	99.6 (99.3-100.0)	**<0.001[1], <0.001[2], 0.001[3]**
Expiration				
Hypointensity	2.5 (0.0-6.2)	0.9 (0.0-0.9)	0.0 (0.0-0.0)	0.55[1], **0.03[2], 0.01[3]**
Normal lung	97.5 (93.8-100.0)	99.1 (96.5-100.0)	100.0 (100.0-100.0)	0.55[1], **0.03[2], 0.01[3]**
Architectural distortion	2 (1-2)	1 (0-1)	0 (0-0)	**0.002[1], <0.001[2], 0.01[3]**

FEF_{75}; Forced Expiratory Flow at 75% of expiration, FEV_1; forced expiratory volume in 1 second, FVC; forced vital capacity. Data are presented as Pearson (r) or Spearman (r_s) correlation coefficient (95% confidence interval). P<0.05 is in bold.

The intra correlation coefficient for MERGE outcomes on the free- breathing sequences was 0.77 for hypointensity, 0.90 for hyperintensity regions and 0.74 for bronchopathy. Scoring of the hypointense regions on the expiratory sequence resulted in an intra correlation coefficient of 0.94.

Ventilation and perfusion

As exploratory analysis, visual comparison was made between the hypointense regions on the coronal reformatted SPGR expiration sequence and the ventilation and perfusion maps from the FD analyses in the central portion of the lung for preterm born children with and without BPD. Two children with BPD, and one preterm born child without BPD did not have FD images of sufficient quality. In our BPD population, two children showed a ventilation defect, one child showed a combined ventilation and perfusion defect and one child showed two defects, one ventilation and one perfusion defect. In our preterm population without BPD, two children showed a ventilation defect. Five children with BPD and six preterm born children without BPD did not show a defect on the FD maps. However, the FD maps were not able to pick up minor hypointense regions. In addition, since the slice thickness of the FD images was 15mm, movements of the chest wall and heart appeared as signal defects on the FD maps. To prevent wrongful interpretation, these defects in the paramediastinal and peripheral regions of the lungs were left out of the visual comparison. Figure 3 shows examples of the comparison between the coronal reformatted SGPR expiration sequences and FD maps.

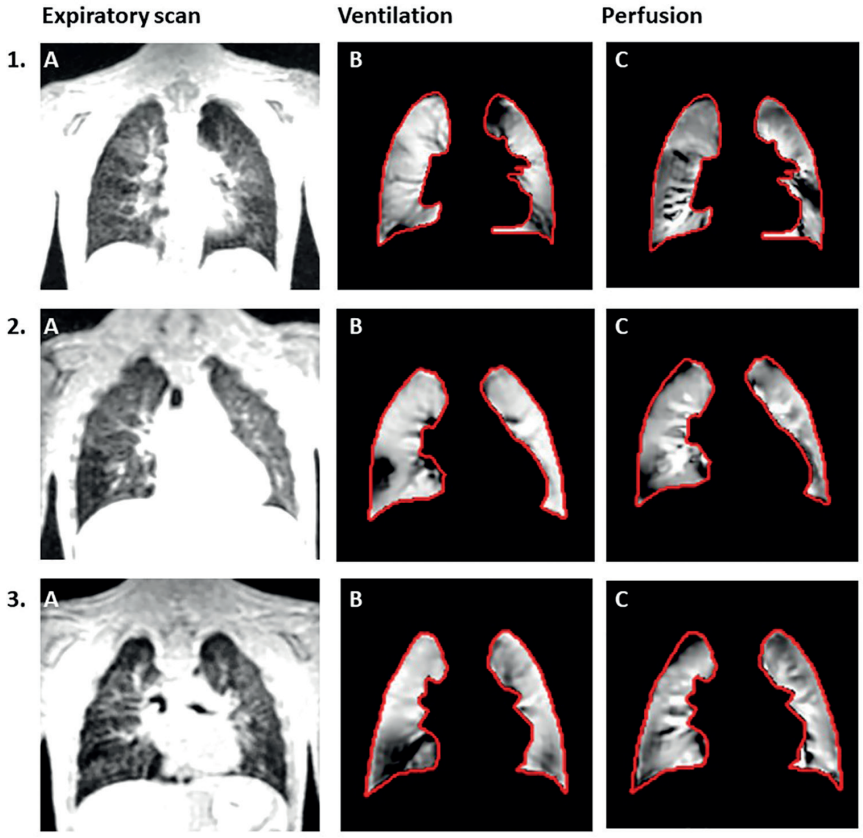

Figure 3: Example images of the comparison between the expiratory MRI scans and FD ventilation and perfusion maps. Black on the FD maps corresponds to a defect. 1) Coronal reformat SPGR expiration image showing hypointense regions in the right lower lobe and apical part of the left lung (a), corresponding FD ventilation map showing a defect in the apical part of the left lung (b) and FD perfusion map showing a defect in the right lower lobe (c) in a child with BPD. 2) Coronal reformat SPGR expiration image showing a hypointense region in the right lower lobe (a), corresponding FD ventilation map showing a defect in the right lower lobe (b) and FD perfusion map showing a defect in the right lower lobe (c) in a child with BPD. 3) Coronal reformat SPGR expiration image showing a hypointense region in the right lower lobe (a), corresponding FD ventilation map showing a defect in the right lower lobe (b) and FD perfusion map showing no defect (c) map in a child with BPD.

Discussion

This is the first study using MRI in the long term follow up of lung abnormalities in preterm born children with and without BPD at school age. Our findings show that MRI is capable to identify clinically relevant changes in lung structure and function in these populations. We propose chest MRI as a sensitive and safe imaging method, without ionising radiation, contrast agents or the use of anaesthesia, for the long-term follow up of preterm born children.

Using a conventional MRI protocol on a standard 1.5 Tesla scanner, we were able to identify the most common structural lung changes related to preterm birth, namely hypo- and hyperintense regions and bronchopathy.(6) Children with BPD showed a higher percentage of hyperintense regions and bronchopathy on free-breathing MRI sequences compared to preterm born children without BPD and healthy volunteers. These findings are in line with previous research using chest CT in this population.(6, 9, 29, 30) We also found a higher percentage of hypointense regions on the expiratory MRI sequence in children with BPD compared to preterm born children without BPD and healthy volunteers, as shown in previous CT studies.(31)

We showed significant correlations between an increase of abnormalities on MRI and lower spirometry outcomes in children with BPD. The strongest correlation was found for FEF_{75}, reflecting airflow in the peripheral airways and thereby representing small airway disease, which in previous studies has been linked to hypoattenuation on CT.(32, 33) It is hypothesized that small airways disease in BPD is caused by both altered development of the alveoli and its vascularization as well as persistent airway inflammation and smooth muscle hypertrophy, and shows the link with the predisposition of developing chronic obstructive pulmonary disease (COPD) later in life for preterm born children.(34, 35)

A unique feature of our study is that we included preterm born children without BPD. Preterm born children without BPD showed significantly better spirometry outcomes compared to preterm children with BPD, but no difference with healthy volunteers. Lower spirometry values in children with BPD compared to preterm born children without BPD have been previously described.(36, 37) In addition, studies show a further decrease in lung function over time in preterm born children with and without BPD and a correlation between this decrease in lung function and increased bronchial wall thickening on CT, suggesting the presence of airway inflammation in this population.(4, 5) Although we did not find a lower spirometry outcome in our cohort of preterm born children without BPD, we did find a significantly higher percentage of abnormalities on MRI compared to healthy volunteers. These findings indicate that MRI might be able to pick up minor changes in lung structure and function that are not detected with spirometry.

Our findings on structural lung changes in both preterm born children with and without BPD brings up the validity and clinical importance of the currently used diagnostic criteria of the severity of BPD, which is based on the amount of oxygen need at 36 weeks PMA.(38) Lung abnormalities in preterm born children are linear and therefore the current diagnostic (severity) criteria, set at one moment in time, and dividing patients into a categorical severity scale does not necessarily identify those children at risk and in need of further follow up. A recent neonatal study showed MRI findings to be a better predictor of short term clinical outcome than BPD severity score according to the NHI criteria.(18) Although

long term follow-up on these findings is necessary, these data indicate that imaging might aid in identifying those preterm patients at risk for respiratory morbidity.

The use of chest CT for the radiological follow-up of lung abnormalities in preterm born children has the advantage that protocols are easier to standardize across centers and vendors compared to MRI and radiation doses are coming down progressively, also thanks to the introduction of photon counting CT technology.(39) Though, the risk for scanning neonatal patients who are more sensitive to radiation should still be taken into consideration. (40, 41) In addition, MRI has the additional benefit of functional imaging. In this study, we explored the use of FD to identify hypointense regions as ventilation or perfusion defects and found this method to be well capable of classifying large hypointense regions. However, our algorithm was not yet sensitive enough to identify minor hypointense regions, such as mosaic perfusion, especially at the periphery of the lung. Distinction between ventilation or perfusion defects on imaging is of special interest in the BPD population, where a simplified development of the alveoli can be associated with pulmonary vascular disease, such as hypoperfusion and pulmonary hypertension.(42) Future research should focus on the improvement of the FD sequence and post processing.

Based on our qualitative scoring, we recommend the use of an MRI protocol consisting of both T2 weighted sequences (such as our PROPELLER sequence) to identify bronchopathy, in combination with a short TE sequence (such as ZTE/UTE) and an end-expiratory SPGR sequence to identify hypointense regions. Some of these short TE sequences have the additional benefit of being silent which makes the MRI less burdensome for (young) children. Hyperintense regions are easily identified on both sequences. We were not able to identify a difference in hypointense regions on free-breathing sequences between all groups, as has been previously described in CT studies.(9, 29-31) However, using end-expiratory breath-hold imaging, children with BPD showed a significant higher amount of hypointense regions compared to healthy volunteers. This can be explained by the better contrast-to-noise (CNR) ratio seen on MRI at residual-volume using expiratory sequences, compared to the functional residual capacity volume obtained in free-breathing sequences. Therefore, we recommend expiratory sequences at residual volume level for the identification of hypointense regions. This implies that in younger children with BPD, who may not be able to perform breath-hold imaging, detection of hypointense region might not be feasible or cumbersome.

Our study has a few limitations. Firstly, being our primary aim to develop the MRI protocol, our study was only conducted in a small population and not all BPD severity groups (mild or moderate BPD) were included, therefore our findings should be validated in a larger group of patients. Secondly, we lacked information on respiratory symptoms to correlate with MRI findings. Finally, we did not have CT available for comparison. Future research should compare these modalities and focus on long term follow up to identify the natural clinical

course of lung abnormalities in preterm born children with and without BPD on imaging in relation to clinical findings, risk assessment and possible treatments.

In conclusion, we show that MRI has the potential to safely image structural and functional abnormalities of the lungs at school-age in preterm born children with and without BPD. An increase in MRI abnormalities correlates with lower spirometry outcomes. These results support the importance of including imaging in the long term follow up of all preterm born children to identify those children at risk for respiratory morbidity and therefore in need of closer monitoring. Larger clinical studies are necessary to investigate the role chest MRI could play in the follow up of the preterm population.

Acknowledgements
We would like to acknowledge G. Colzani with her help on the Fourier Decomposition analyses.

References

1. Kinsella JP, Greenough A, Abman SH. Bronchopulmonary dysplasia. Lancet. 2006;367(9520):1421-31.
2. Islam JY, Keller RL, Aschner JL, Hartert TV, Moore PE. Understanding the Short- and Long-Term Respiratory Outcomes of Prematurity and Bronchopulmonary Dysplasia. Am J Respir Crit Care Med. 2015;192(2):134-56.
3. Voynow JA. "New" bronchopulmonary dysplasia and chronic lung disease. Paediatr Respir Rev. 2017;24:17-8.
4. Simpson SJ, Turkovic L, Wilson AC, Verheggen M, Logie KM, Pillow JJ, et al. Lung function trajectories throughout childhood in survivors of very preterm birth: a longitudinal cohort study. Lancet Child Adolesc Health. 2018;2(5):350-9.
5. Simpson SJ, Logie KM, O'Dea CA, Banton GL, Murray C, Wilson AC, et al. Altered lung structure and function in mid-childhood survivors of very preterm birth. Thorax. 2017;72(8):702-11.
6. van Mastrigt E, Logie K, Ciet P, Reiss IK, Duijts L, Pijnenburg MW, et al. Lung CT imaging in patients with bronchopulmonary dysplasia: A systematic review. Pediatr Pulmonol. 2016;51(9):975-86.
7. Oppenheim C, Mamou-Mani T, Sayegh N, de Blic J, Scheinmann P, Lallemand D. Bronchopulmonary dysplasia: value of CT in identifying pulmonary sequelae. AJR Am J Roentgenol. 1994;163(1):169-72.
8. Sung TJ, Hwang SM, Kim MY, Park SG, Choi KY. Relationship between clinical severity of "new" bronchopulmonary dysplasia and HRCT abnormalities in VLBW infants. Pediatr Pulmonol. 2018;53(10):1391-8.
9. van Mastrigt E, Kakar E, Ciet P, den Dekker HT, Joosten KF, Kalkman P, et al. Structural and functional ventilatory impairment in infants with severe bronchopulmonary dysplasia. Pediatr Pulmonol. 2017;52(8):1029-37.
10. Duijts L, van Meel ER, Moschino L, Baraldi E, Barnhoorn M, Bramer WM, et al. European Respiratory Society guideline on long-term management of children with bronchopulmonary dysplasia. Eur Respir J. 2020;55(1).
11. Ciet P, Tiddens HA, Wielopolski PA, Wild JM, Lee EY, Morana G, et al. Magnetic resonance imaging in children: common problems and possible solutions for lung and airways imaging. Pediatr Radiol. 2015;45(13):1901-15.
12. Hatabu H, Ohno Y, Gefter WB, Parraga G, Madore B, Lee KS, et al. Expanding Applications of Pulmonary MRI in the Clinical Evaluation of Lung Disorders: Fleischner Society Position Paper. Radiology. 2020;297(2):286-301.
13. Flors L, Mugler JP, 3rd, Paget-Brown A, Froh DK, de Lange EE, Patrie JT, et al. Hyperpolarized Helium-3 Diffusion-weighted Magnetic Resonance Imaging Detects Abnormalities of Lung Structure in Children With Bronchopulmonary Dysplasia. J Thorac Imaging. 2017;32(5):323-32.

14. Walkup LL, Tkach JA, Higano NS, Thomen RP, Fain SB, Merhar SL, et al. Quantitative Magnetic Resonance Imaging of Bronchopulmonary Dysplasia in the Neonatal Intensive Care Unit Environment. Am J Respir Crit Care Med. 2015;192(10):1215-22.
15. Walkup LL, Woods JC. Newer Imaging Techniques for Bronchopulmonary Dysplasia. Clin Perinatol. 2015;42(4):871-87.
16. Higano NS, Fleck RJ, Spielberg DR, Walkup LL, Hahn AD, Thomen RP, et al. Quantification of neonatal lung parenchymal density via ultrashort echo time MRI with comparison to CT. J Magn Reson Imaging. 2017;46(4):992-1000.
17. Higano NS, Hahn AD, Tkach JA, Cao X, Walkup LL, Thomen RP, et al. Retrospective respiratory self-gating and removal of bulk motion in pulmonary UTE MRI of neonates and adults. Magn Reson Med. 2017;77(3):1284-95.
18. Higano NS, Spielberg DR, Fleck RJ, Schapiro AH, Walkup LL, Hahn AD, et al. Neonatal Pulmonary Magnetic Resonance Imaging of Bronchopulmonary Dysplasia Predicts Short-Term Clinical Outcomes. Am J Respir Crit Care Med. 2018;198(10):1302-11.
19. Jobe AH, Bancalari E. Bronchopulmonary dysplasia. Am J Respir Crit Care Med. 2001;163(7):1723-9.
20. Miller MR, Crapo R, Hankinson J, Brusasco V, Burgos F, Casaburi R, et al. General considerations for lung function testing. Eur Respir J. 2005;26(1):153-61.
21. Beydon N, Davis SD, Lombardi E, Allen JL, Arets HG, Aurora P, et al. An official American Thoracic Society/European Respiratory Society statement: pulmonary function testing in preschool children. Am J Respir Crit Care Med. 2007;175(12):1304-45.
22. Quanjer PH, Hall GL, Stanojevic S, Cole TJ, Stocks J, Global Lungs I. Age- and height-based prediction bias in spirometry reference equations. Eur Respir J. 2012;40(1):190-7.
23. Bae K, Jeon KN, Hwang MJ, Lee JS, Ha JY, Ryu KH, et al. Comparison of lung imaging using three-dimensional ultrashort echo time and zero echo time sequences: preliminary study. Eur Radiol. 2019;29(5):2253-62.
24. Rosenow T, Oudraad MC, Murray CP, Turkovic L, Kuo W, de Bruijne M, et al. PRAGMA-CF. A Quantitative Structural Lung Disease Computed Tomography Outcome in Young Children with Cystic Fibrosis. Am J Respir Crit Care Med. 2015;191(10):1158-65.
25. Loeve M, van Hal PT, Robinson P, de Jong PA, Lequin MH, Hop WC, et al. The spectrum of structural abnormalities on CT scans from patients with CF with severe advanced lung disease. Thorax. 2009;64(10):876-82.
26. Voskrebenzev A, Gutberlet M, Becker L, Wacker F, Vogel-Claussen J. Reproducibility of fractional ventilation derived by Fourier decomposition after adjusting for tidal volume with and without an MRI compatible spirometer. Magn Reson Med. 2016;76(5):1542-50.
27. Voskrebenzev A, Gutberlet M, Kaireit TF, Wacker F, Vogel-Claussen J. Low-pass imaging of dynamic acquisitions (LIDA) with a group-oriented registration (GOREG) for proton MR imaging of lung ventilation. Magn Reson Med. 2017;78(4):1496-505.
28. Voskrebenzev A, Gutberlet M, Klimeš F, Kaireit TF, Schönfeld C, Rotärmel A, et al. Feasibility of quantitative regional ventilation and perfusion mapping with phase-resolved functional lung

(PREFUL) MRI in healthy volunteers and COPD, CTEPH, and CF patients. Magn Reson Med. 2018;79(4):2306-14.
29. Aukland SM, Rosendahl K, Owens CM, Fosse KR, Eide GE, Halvorsen T. Neonatal bronchopulmonary dysplasia predicts abnormal pulmonary HRCT scans in long-term survivors of extreme preterm birth. Thorax. 2009;64(5):405-10.
30. Wong PM, Lees AN, Louw J, Lee FY, French N, Gain K, et al. Emphysema in young adult survivors of moderate-to-severe bronchopulmonary dysplasia. Eur Respir J. 2008;32(2):321-8.
31. Aquino SL, Schechter MS, Chiles C, Ablin DS, Chipps B, Webb WR. High-resolution inspiratory and expiratory CT in older children and adults with bronchopulmonary dysplasia. AJR Am J Roentgenol. 1999;173(4):963-7.
32. Konstantinos Katsoulis K, Kostikas K, Kontakiotis T. Techniques for assessing small airways function: Possible applications in asthma and COPD. Respir Med. 2016;119:e2-e9.
33. McNulty W, Usmani OS. Techniques of assessing small airways dysfunction. Eur Clin Respir J. 2014;1.
34. McGrath-Morrow SA, Collaco JM. Bronchopulmonary dysplasia: what are its links to COPD? Ther Adv Respir Dis. 2019;13:1753466619892492.
35. Collaco JM, McGrath-Morrow SA. Bronchopulmonary dysplasia as a determinant of respiratory outcomes in adult life. Pediatr Pulmonol. 2021;56(11):3464-71.
36. Verheggen M, Wilson AC, Pillow JJ, Stick SM, Hall GL. Respiratory function and symptoms in young preterm children in the contemporary era. Pediatr Pulmonol. 2016;51(12):1347-55.
37. Broström EB, Thunqvist P, Adenfelt G, Borling E, Katz-Salamon M. Obstructive lung disease in children with mild to severe BPD. Respir Med. 2010;104(3):362-70.
38. Bancalari E, Jain D. Bronchopulmonary Dysplasia: Can We Agree on a Definition? Am J Perinatol. 2018;35(6):537-40.
39. Willemink MJ, Persson M, Pourmorteza A, Pelc NJ, Fleischmann D. Photon-counting CT: Technical Principles and Clinical Prospects. Radiology. 2018;289(2):293-312.
40. Brenner D, Elliston C, Hall E, Berdon W. Estimated risks of radiation-induced fatal cancer from pediatric CT. AJR Am J Roentgenol. 2001;176(2):289-96.
41. Pearce MS, Salotti JA, Little MP, McHugh K, Lee C, Kim KP, et al. Radiation exposure from CT scans in childhood and subsequent risk of leukaemia and brain tumours: a retrospective cohort study. Lancet. 2012;380(9840):499-505.
42. Parker TA, Abman SH. The pulmonary circulation in bronchopulmonary dysplasia. Semin Neonatol. 2003;8(1):51-61.

Supplementary materials

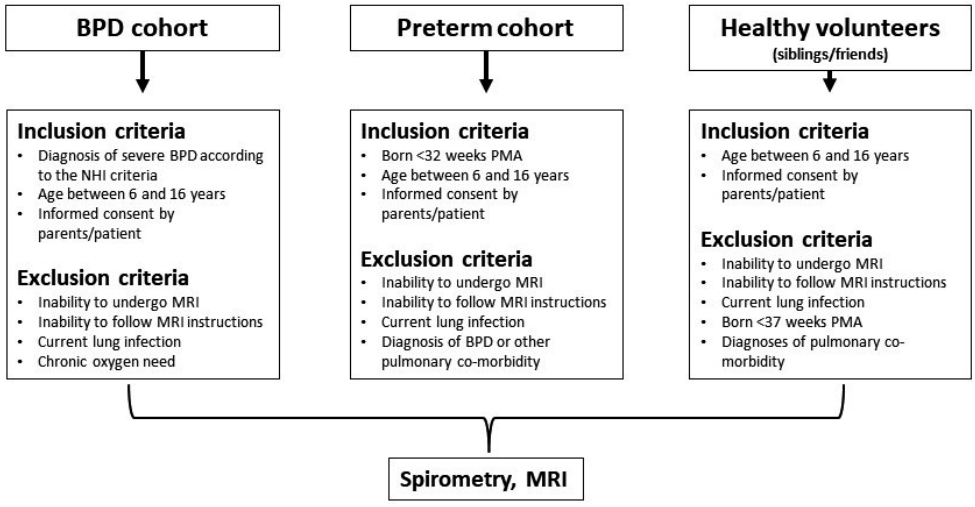

Supplementary material 1: In- and exclusion criteria

Supplementary material 2: MRI protocol

Sequence	SPGR inspiration/ expiration	T2 weighted FS PROPELLER	ZTE	UTE	Fourier Decomposition
Acquisition plane	Sagittal	Axial	Axial	Axial	Coronal
TR/TE (ms)	1.5/0.6	*/73	1.1/0	5.2/0.032	2.3/0.8
Flip angle (°)	2	90/120	2	3	5
RF	Selective	Selective	Non-selective	Selective	Selective
In-plane matrix	120x120	340x340	200x200	228x228	128x128
k-space trajectory	Cartesian	Blades	Radial	Cones	Cartesian
In-plane Field-of-view (FOV)	36	34	30	34	50
RecFOV	0.75	-	-	-	-
Actual voxel resolution (mm^3)	3.0x3.0x3.0	1.0x1.0x3.5	1.5x1.5x1.5	1.5x1.5x1.5	3.9x3.9x15.0
Slices	130	50-70	200	230	7-10
Slice thickness	3.0	3.5	1.5	1.5	15.0
Receiver bandwidth (KHz)	100/90/90	83.33	62.5	125	83.33
Parallel imaging (ARC)	1.5x1.2	3.0	None	None	2.0
Number of averages	1	2.0	2.5	1	1
Number of phases	1	1	1	1	200/186 ms per phase
No. of spokes per segment	-	14	900	-	-
Physiological triggering	BH	Prospective pencil beam navigator	Prospective projection navigator	Prospective pneumo-belt	Free breathing
Scan time (sec) RR=20	+/- 6sec	+/- 5 min	+/- 6 min	+/- 6 min	7-10x 38 sec

FS: fat suppression, FOV; Field Of View, NEX; Number of Excitations, PROPELLER; Periodically Overlapping ParalLEL Lines with Enhanced Reconstruction, RF; radio frequency, SPGR; Spoiled Gradient Echo Sequence, TE; Echo Time, TR; Repetition Time.*TR chosen varied on the respiratory frequency of the patient

A: Qualitative scoring method

Depiction of fissures	1. Unacceptable (invisible interlobar fissure) 2. Fair (blurred interlobar fissure) 3. Good (visible interlobar fissure)
Depiction of intrapulmonary vessels	1. Unacceptable (invisible peripheral pulmonary vessels) 2. Poor (barely visible peripheral pulmonary vessels) 3. Fair (visible peripheral pulmonary vessels) 4. Good (visible peripheral pulmonary vessels with clear margin) 5. Excellent (visible peripheral pulmonary vessels with clear margin)
Depiction of bronchi	1. Unacceptable (indistinguishable lobar bronchial walls) 2. Poor (visible lobar bronchial walls with <10 visible segmental bronchial walls) 3. Fair (visible lobar bronchial walls with >10 visible segmental bronchial walls) 4. Good (visible lobar bronchial walls with >10 visible segmental bronchial walls, with few visible sub/segmental bronchial walls) 5. Excellent (visible sub-subsegmental bronchial walls)
Image noise/artifacts	1. Unacceptable 2. Above average noise/artifacts 3. Average and acceptable 4. Less than average noise/ artifacts 5. Minimum of no noise/artifacts
Overall acceptability	1. Unacceptable 2. Suboptimal 3. Satisfactory 4. Above average 5. Superior

Supplementary material 3A: Qualitative scoring method adjusted from Bae *et al.* (European Radiology 2020)

B: Examples of artifacts

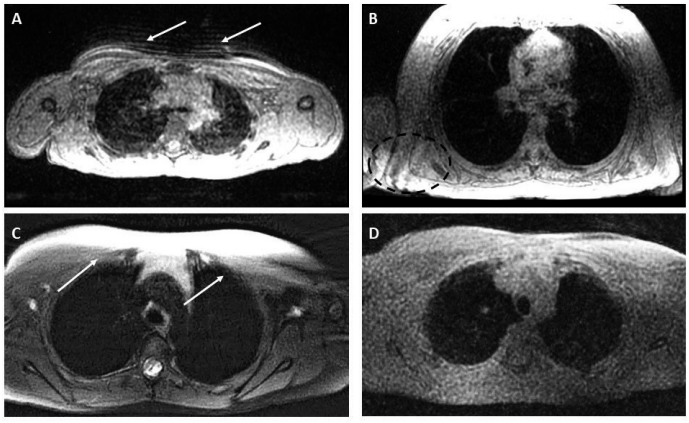

Supplementary material 3B: Examples of artifacts. A) Blurring artifacts (arrows); seen as linear artifacts caused by breathing movement, B) Wrapping artifacts (circle); seen as projection of a body part on the other side of the image, caused by a field-of-view smaller than the thorax imaged, C) Streaking artifacts (arrows); seen as dark or white streaks, these artifacts depend on the field-of-view (FOV) size and K-space reconstruction scheme. PROPELLER acquires K-space in rotating blades, which tend to be displaced within the imaged anatomical region, especially when FOV is small. D) low signal-to-noise ration; seen as a granulated appearance of the image, with poor distinguished structures in grey tones

Supplementary material 4: Disease scoring per MRI sequence

	Propeller	ZTE	UTE
Free-breathing			
Hypointensity	0.0 (0.0-0.2)	0.0 (0.0-0.3)	(0.0-0.0)
Hypointensity	0.5 (0.0-1.8)	0.2 (0.0-1.3)	(0.0-0.2)
Bronchopathy	1.8 (0.0-0.4)	2.6 (0.8-4.7)	0.2 (0.0-1.0)
Diseased lung	3.4 (0.2-6.1)	3.8 (0.8-6.1)	0.6 (0.0-1.5)

Data are presented as median (interquartile range) of the percentage disease of total lung volume. PROPELLER; periodically rotated overlapping parallel lines with enhanced reconstruction, ZTE; zero- echo time, UTE; ultra-short echo time.

Supplementary material 5: Correlations between spirometry function outcome and total percentage of diseased lung on MRI

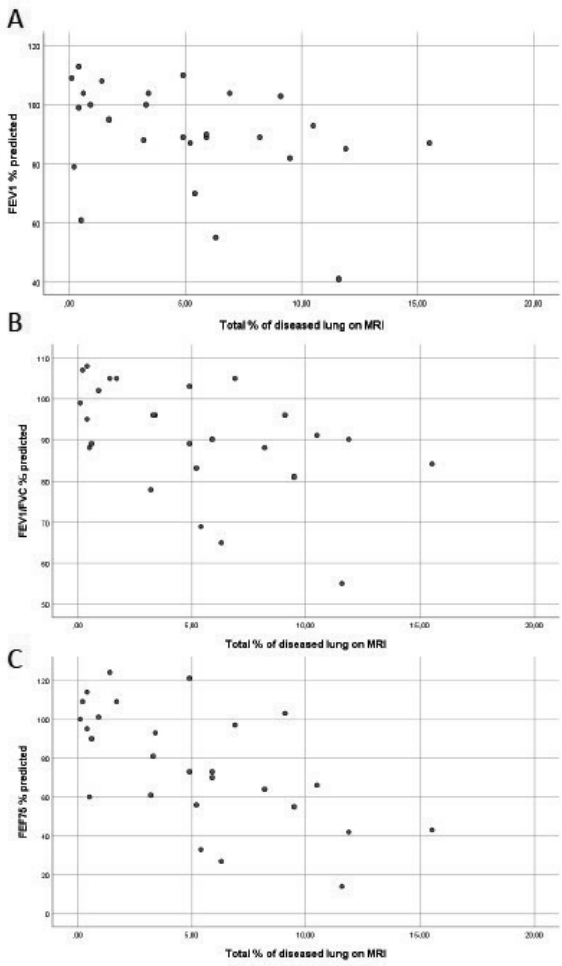

Supplementary material 5: Correlations between spirometry outcome and total percentage of diseased lung on MRI. A) FEV_1 % predicted versus total % of diseased lung on MRI, B) FEV1/FVC % predicted versus total % of diseased lung on MRI, C) FEF_{75} % predicted versus total % of diseased lung on MRI.

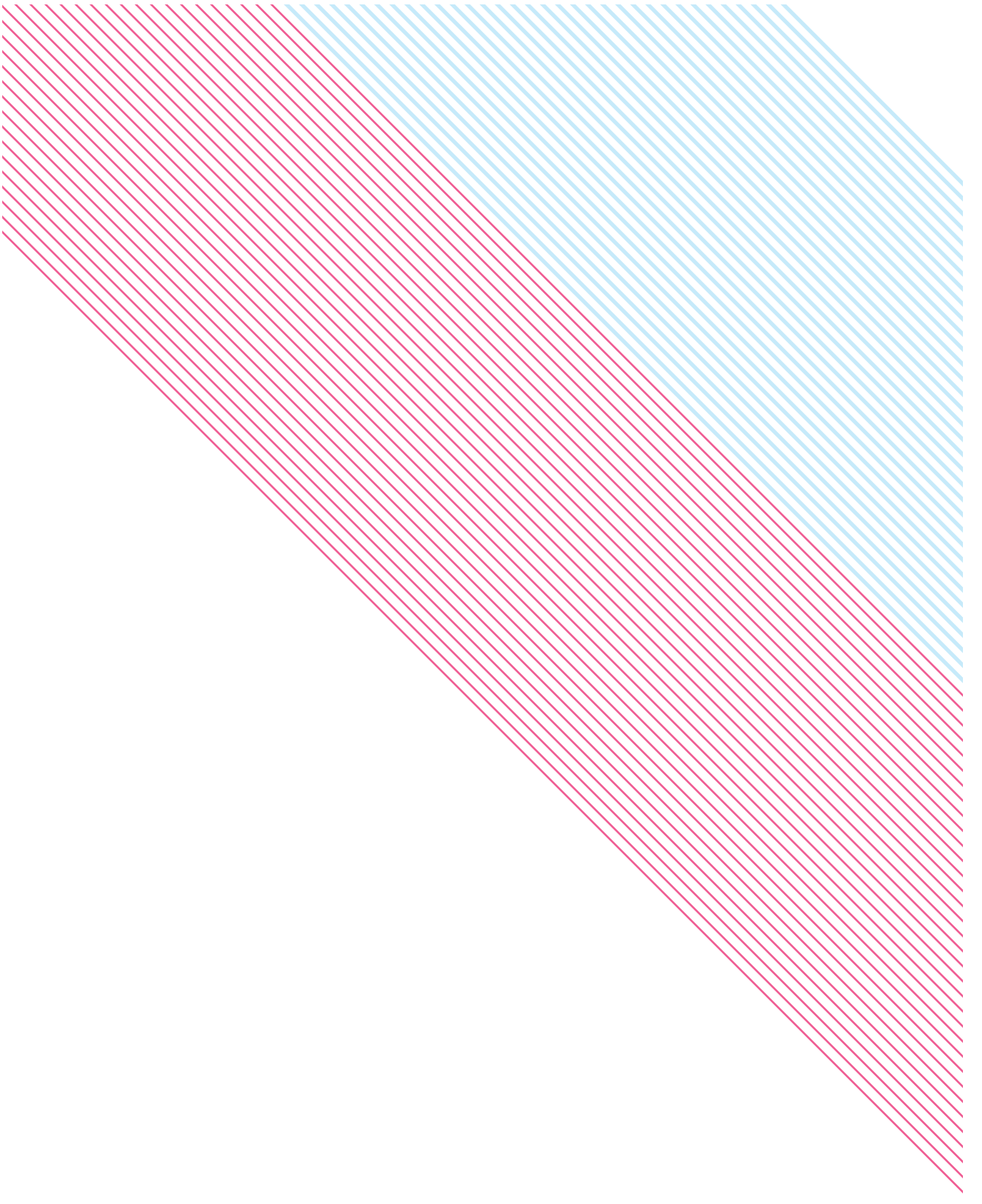

Chapter 7

Lung parenchyma and structure visualization in pediatric chest-MRI: a comparison of different short and ultra-short TE protocols

Dorottya Papp, Bernadette BLJ Elders, Piotr A Wielopolski, Gyula Kotek, Mika Vogel, Harm AWM Tiddens, Pierluigi Ciet, Juan Hernandez-Tamames

Submitted

Abstract

Objectives: MRI has recently emerged as a clinical tool that can produce high resolution images of structural lung changes similar to CT scans, thanks to the use of ultrashort TE readouts. Therefor pediatric patients with chronic lung disease, such as cystic fibrosis (CF) or bronchopulmonary dysplasia (BPD), can undergo routine monitoring with CT like image quality. The aim of this study was to compare image quality acquired with MR sequences of short and ultra-short TE in pediatric patients and in healthy volunteers for lung imaging.

Methods: Scanning and image comparison was performed on 8 CF patients, 7 premature children with or without BPD and 10 healthy volunteers on a 1.5T MRI scanner (*Artist, GE Healthcare, Milwaukee, Wisconsin, USA*) using end-inspiratory and end-expiratory SPGR3D, UTE3D, ZTE3D vnav, ZTE4D and ZTE3D-BH sequences. For quantitative assessment the signal intensity (SI) of the intrathoracic structures was measured, contrast-to-noise ratio (CNR) and signal-to-noise ratio (SNR) values were calculated. To evaluate diagnostic quality, a qualitative analysis was done on all sequences. Images were evaluated on depiction of intrapulmonary vessels, depiction of fissures, depiction of the bronchi, imaging noise and artifacts and overall acceptability.

Results: Based on our results, ZTE3D vnav provides the most reliable output in terms of image quality, although it can be affected by triggering efficiency and irregular respiratory patterns.

Conclusions: Future implementation of ZTE and UTE3D should either focus on improvement of respiratory triggering with a size-specific pneumo-belt or on improved navigator options.

Introduction

Lung Magnetic Resonance Imaging (MRI) with good image quality and high spatial resolution has been a long-desired goal, especially in the pediatric population.(1) To date, Computed Tomography (CT) still prevails as the main imaging tool for the pediatric lung; it is fast, simple to execute and provides the necessary high image quality at any age. However, repeated use of CT in children is limited because of the damage possible from ionizing radiation.(2, 3) Conversely, MRI is an ionizing radiation-free technique that offers superior inherent soft tissue contrast and has therefore a potential for robust structure and function assessment in a single examination.(4)

Unfortunately, obtaining high quality MRI of the thorax has been cumbersome as compared to other anatomical regions.(1) The inherent lung tissue properties and the surrounding magnetic environment and motion during the MRI signal acquisition account for this difficulty. (5) Lung parenchyma has at least a magnitude lower proton density than other tissues, hence the signal received is quite low.(6) Conventional gradient echo based pulse sequences with echo times in the range of milliseconds cannot detect the lung signal because it has already decayed before it can be acquired. Ultrashort echo time (UTE) MRI, first proposed by Bergin *et al*.(7), could attain the necessary short TEs (nearly zero) in order to appreciate parenchymal signal and structure at higher spatial resolution. UTE3D uses radial k-space sampling in order to sample the rapidly decaying signal right after the radiofrequency (RF) excitation and therefore can counteract the signal loss from transverse relaxation time (T_2 decay). Another radial encoding scheme that has recently emerged with zero TE encoding (ZTE) is promising. In this technique, readout gradients are turned on prior to RF excitation so that encoding can start simultaneously upon signal excitation resulting in a nearly zero TE. ZTE has the additional benefit of being nearly silent, and is therefore ideal for neonatal and pediatric imaging.

For pediatric lung MRI, image quality also strongly depends on patient compliance. Short breath-hold (BH) sequences can be successfully performed in children from 6 years and older, reducing motion artifacts from respiratory movements. Unfortunately non-cooperative children and younger ones require free-breathing gated (prospective or retrospective) or ungated strategies.(8) Therefore, recent implementations of retrospectively gated UTE3D and ZTE sequences show promising results in young children.(9, 10) To the best of our knowledge, only one study has been conducted (only in free breathing condition) comparing conventional and novel short TE sequences for lung imaging.(11)

The aim of this study was to compare image quality acquired with MR sequences of short and ultra-short TE with different strategies (breath-hold, prospective and retrospective gating) in pediatric patients and in healthy volunteers for lung imaging.

Materials and methods

Patients and volunteers

The study was approved by the local Institutional Review Board (MEC2018-134, MEC2018-002). Written informed consent was obtained from all subjects or for children from parents or legal guardians before the MR examinations. From March 2019 to May 2020, patients either with cystic fibrosis (CF) or preterm born patients with and without bronchopulmonary dysplasia (BPD) underwent chest MRI. Only healthy male volunteers were recruited in this study to make a standardized comparisons between the different sequence possibilities and scanning scenarios.

Lung MR imaging

MRI scans were performed at 1.5T (*Signa Artist, GE Healthcare, Waukesha, WI, USA*) using a body coil for excitation and a small anterior 16 channels torso array coil and the table embedded spine coil for signal reception. The MRI protocol included several relevant sequences for lung parenchyma and structure visualization: cartesian SPGR3D, breath-hold radial 3D ZTE (ZTE-BH), prospective respiratory pneumo-belt gated cones UTE3D, prospective projection navigated radial ZTE3D (ZTE3D vnav) and a retrospectively reconstructed multi-phasic radial ZTE3D scan (ZTE4D). All sequences were performed with a Proton-Density (PD) weighting. Table 1 shows the acquisition parameters for each sequence. All scans used 3D gradwarping to compensate for gradient non-linearities with the large field-of-views (FOV) acquired and no coil intensity correction was used. The SPGR3D acquisitions were acquired at breath-hold end-inspiration and end-expiration in all patients and healthy volunteers. For patients only these maneuvers were controlled with spirometry using an MRI compatible spirometer (*Masterscreen Pneumo portable spirometer; Carefusion, Houten, NL)*.(12) The standard MRI system pneumo-belt monitoring was used for all subjects. Sixteen different respiratory phases were retrospectively reconstructed from the ZTE4D based on the recorded pneumo-belt signal. To have better comparison with the ZTE4D acquisition a 20s breath-hold ZTE3D was scanned. This sequence was only performed on the healthy participants, who were capable to hold their breath at deep expiration and at full inspiration for 20s.

For each patient, at least one ZTE3D and one UTE3D scan had to be successfully performed to be included in the comparative study.

Table 1: MRI protocol

Sequence	SPGR3D BH (vol/CF/BPD)	UTE3D (vol/CF/BPD)	ZTE3D vnav (vol/CF/BPD)	ZTE4D (vol)	ZTE3D BH (vol)
Acquisition plane	Sagittal	Axial	Axial	Coronal	Coronal
TR/TE (ms)	1.5/0.6	5.2/0.032	1.1/0	1.4/0	1.25/0
Flip angle (º)	2	3	2	1	2
RF	Selective	Selective	Non-selective	Non-selective	Non-selective
In-plane matrix	120x120	228x228	200x200	150x150	150x150
K-space trajectory	Cartesian	Cones	Radial	Radial	radial
In-plane FOV	36	34	30	34	34
Rec FOV	0.75	-	-	-	-
Actual voxel resolution (mm^3)	3.0x3.0x3.0	1.5x1.5x1.5	1.5x1.5x1.5	2.2x2.2x2.2	2.2x2.2x2.2
Slices	130/130/80-100	230	200	110	110
Slice thickness (mm)	3.0	1.5	1.5	2.2	2.2
Receiver bandwidth (KHz)	100/90/90	125	62.5	50	62.5
Parallel imaging (ARC)	None/1.5x1.2/1.5x1.2	None	None	None	None
Number of averages	1	1	2.5	7	1
Number of phases	1	1	1	16	1
Number of spokes per segment	-	-	900	64	200
Physiological triggering	BH	Prospective pneumo-belt	Prospective projection navigator	Retrospective pneumo-belt	BH
Scan time (sec) RR=20	13s/8s/5-6s	4 min 48s	9 min 50s	3 min 10s	20s

Parameters of the used MRI sequences: In volunteers a ZTE3D acquisition was included. Scan time was set for a respiratory rate of 20 breaths/minute. BPD; bronchopulmonary dysplasia, BH; breath-hold, CF; cystic fibrosis, FOV; field of view, RF; radiofrequency, RR; respiratory rate, SPGR; Spoiled Gradient Echo Sequence TE; echo time, TR; repetition time, UTE; ultrashort echo time, vol; volunteer, ZTE; zero echo time,

Image analysis

All non-axially acquired scans were reformatted into the axial plane for comparison, and anonymized and randomized for image analysis. Images were reviewed on the Advantage Window Server platform (*AWS 2.0, GE Healthcare, Waukesha, WI, USA*).

Quantitative assessment

To compare the ability of the different sequences to detect lung parenchyma signal and depict normal structures, the signal intensity (SI) of the intrathoracic structures was measured. Additionally, contrast to noise ratio (CNR) and signal to noise ratio (SNR) values were calculated. Regions of interest (ROIs) were drawn in the background air, lung parenchyma and oblique muscles. The ROI in the lung parenchyma was carefully positioned and sized on the SPGR3D expiration scans, so it did not contain a major vascular component/fissure; the ROIs were subsequently copied to all the different sequences evaluated per subject. The location of the ROI in the lung parenchyma was adjusted in case of motion artifacts due to breathing. The mean of these six ROIs was used for assessment of the SNR of the lung parenchyma (see figure 1).

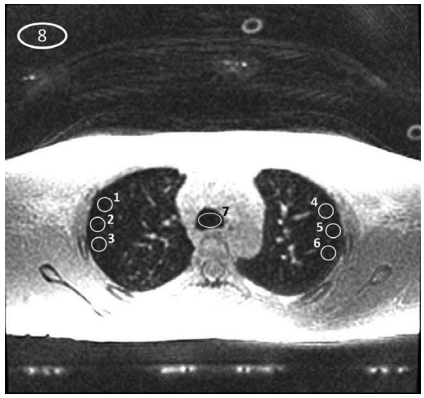

Figure 1. Example of the placement of the ROIs for the SNR calculation in a UTE3D sequence. Circles 1-6 provide the mean value for the signal intensity. Standard deviation of ROI 8 was used for the calculation of $\mathrm{SNR}_{\mathrm{out}}$ and the standard deviation of ROI 7 was used for the calculation of $\mathrm{SNR}_{\mathrm{trachea}}$.

To evaluate the ability of the different sequences to provide lung parenchymal signal, the SI of the background air and lung parenchyma were compared within each sequence. The SNR of the lung parenchyma was compared between all used sequences. SNR was calculated as the mean SI of the measured structure divided by the standard deviation (STD) of the background.

$$SNR = \frac{SI_{lung\ parenchyma}}{STD_{background}}.$$

For ZTE and UTE3D sequences artifactual signal/noise from the frame of the coils can appear in the background outside the chest. Because of this, the SNR calculation was performed with two different background noise computations. One was taken from an area from the background (this we refer to as $\mathrm{SNR}_{\mathrm{out}}$) where we could avoid any artefacts and the other was taken from the trachea ($\mathrm{SNR}_{\mathrm{trachea}}$).

CNRs of the lung parenchyma and pulmonary artery (CNR Lung- Blood, $\mathrm{CNR}_{\mathrm{LB}}$), the lung parenchyma and oblique muscle (CNR Lung-Muscle, $\mathrm{CNR}_{\mathrm{LM}}$) and the pulmonary artery and oblique muscle (CNR Blood-Muscle, $\mathrm{CNR}_{\mathrm{BM}}$) were also measured. The calculations of the CNR values were as follows:

$$\mathrm{CNR}_{\mathrm{LB}} = \frac{\mathrm{mean(SI\ (pulmonary\ artery\ ))} - \mathrm{mean\ (SI\ (lung))}}{\mathrm{STD(noise)}}.$$

$$\mathrm{CNR}_{\mathrm{LM}} = \frac{\mathrm{mean(SI\ (oblique\ muscles\ ))} - \mathrm{mean\ (SI\ (lung))}}{\mathrm{STD(noise)}},$$

and the CNR of the pulmonary artery-muscle as

$$\mathrm{CNR}_{\mathrm{BM}} = \frac{\mathrm{mean(SI\ (pulmonary\ artery))} - \mathrm{mean\ (SI\ (oblique\ muscles))}}{\mathrm{STD(noise)}}.$$

Qualitative assessment

To evaluate diagnostic quality, a qualitative analysis was done on end-inspiratory and end-expiratory SPGR3Ds, UTE3D, ZTE3D vnav, ZTE4D and ZTE3D-BH sequences. All sequences were evaluated on depiction of intrapulmonary vessels, depiction of fissures, depiction of the bronchi, imaging noise and artifacts and overall acceptability using a modified version of the scoring system used by Bae *et al.*(Table 2).(11) Modification took into account the assessment of bronchi visibility, which was scored by calculation of the amount of lobar, segmental and sub-segmental bronchi visible in each sequence. All scans were scored in random order by an independent reviewer (B.E) with 3 years of experience in lung MRI. To test intra- and inter observer reproducibility, the scoring was repeated 3 months after the original measurements, and all scans were also scored by a second reviewer (P.C.) with 10 years of experience in lung MRI.

Table 2: Method of the qualitative MRI assessment

Depiction of the intrapulmonary vessels
1. unacceptable (invisible peripheral pulmonary vessels and interlobar fissure) 2. poor (barely visible peripheral pulmonary vessels/invisible interlobar fissure) 3. fair (visible peripheral pulmonary vessels/invisible interlobar fissure) 4. good (visible peripheral pulmonary vessels with clear margin/blurred interlobar fissure) 5. excellent (visible peripheral pulmonary vessels with clear margin/sharp interlobar fissure)
Depiction of fissures
1. Unacceptable (invisible interlobar fissure) 2. Fair (blurred lobar fissure) 3. Good (visible interlobar fissure)
Depiction of the bronchus
1. unacceptable (indistinguishable lobar bronchial walls) 2. poor (visible lobar bronchial walls with <10 visible segmental bronchial walls) 3. fair (visible lobar bronchial walls with >10 visible segmental bronchial walls) 4. good (visible lobar bronchial walls with >10 visible segmental bronchial walls, with few visible sub/segmental bronchial walls) 5. excellent (visible sub-subsegmental bronchial walls)
Image noise/ artifacts (cardiac, respiratory and streaking)
1. unacceptable; 2. above-average noise/artifacts; 3. average and acceptable; 4. less than average; 5. minimum or nothing
Overall acceptability
1. unacceptable; 2. suboptimal; 3. satisfactory; 4. above average; 5. superior

Qualitative assessment of MRI sequences, adapted and modified from Bae *et al.*.(11)

Statistical analyses

Differences between sequences in CNR and SNR were compared with a paired T-test. Image quality was assessed with descriptive statistics. Intra- and inter- observer agreement was assessed using the intra-class correlation coefficient and Bland-Altman plots. Statistical tests were performed using SPSS Statistics (*version 25, IBM SPSS, Chicago, IL, USA*).

Results

We included 8 CF patients (age range 13-17 years, median 14 years), 7 premature children with or without BPD (age range 10-11 years, median 10 years) and 10 volunteers (age range 20-52 years, median 32 years).

Examples of all different acquisitions in a healthy volunteer are shown in figure 2 and 3. SPGR3D expiration and inspiration, UTE3D, ZTE3D vnav were performed on volunteers and patients (n=25), ZTE4D were performed on all volunteers but due to time limitations not on all patients (n=15) and ZTE3D breath-hold expiration and inspiration were only performed on volunteers (n=10).

In some scenarios we noticed an artifactual brightening of lung parenchyma in ZTE3D vnav and ZTE4D. This artifact is not present either on UTE3D or breath-hold SPGR3D scanning (there is signal from lung parenchyma that is not real). UTE3D has some artifactual increases in the lung parenchyma if not calibrated correctly. The ZTE4D sequence which is able to capture both inspiratory and expiratory phases (maximum of 16) typically captures images with adequate sharpness and without artifacts for a very limited number of phases around the end-expiratory period.

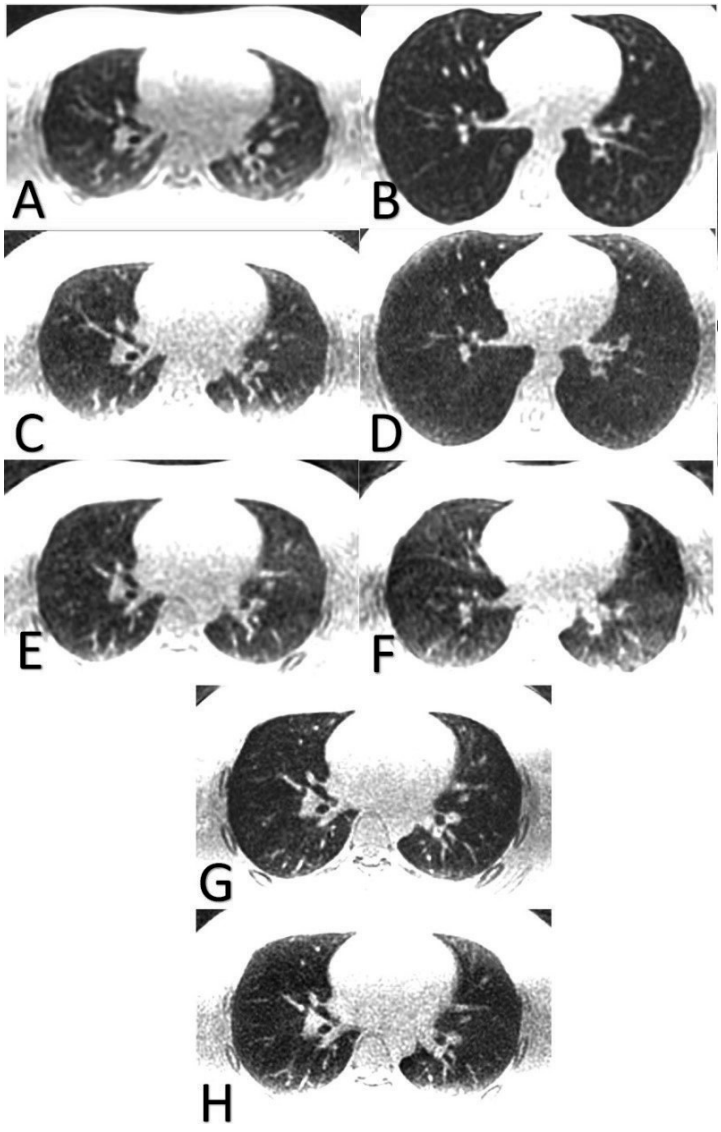

Figure 2. Axial MR images obtained using SPGR3D expiration (A) and inspiration (B), ZTE3D breath-hold expiration (C) and inspiration (D), ZTE4D expiratory phase (E) and inspiratory phase (F), UTE3D (G) and ZTE3D vnav (H) sequences in a healthy 29- year-old male.

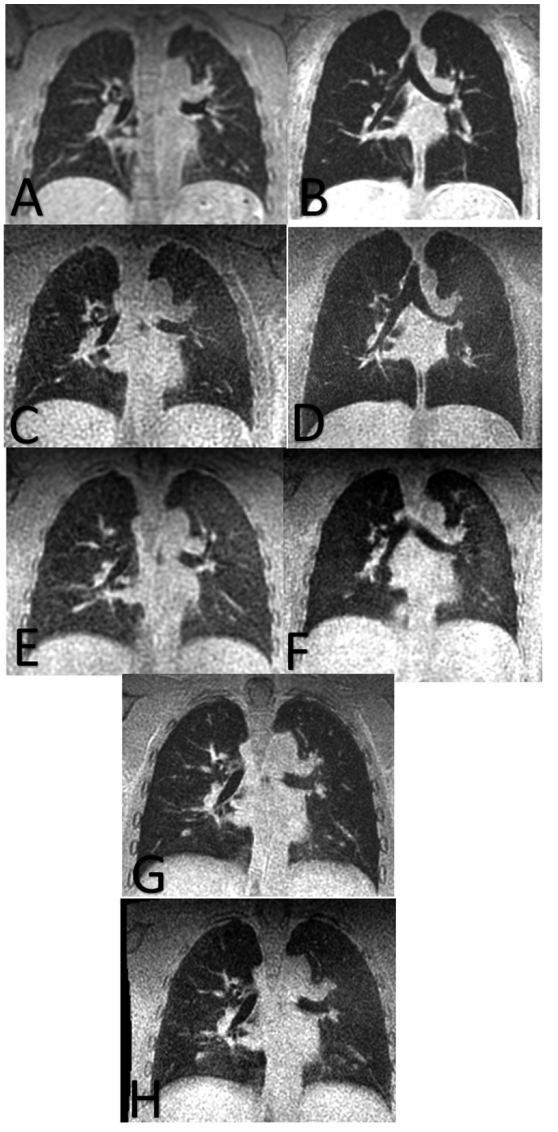

Figure 3. Coronal MR images obtained using SPGR3D expiration (A) and inspiration (B), ZTE3D breath-hold expiration (C) and inspiration (D), ZTE4D expiratory phase (E) and inspiratory phase (F), UTE3D (G) and ZTE3D vnav (H) sequences in a healthy 29- year-old male.

Quantitative assessment

The results of the quantitative analyses are shown in table 3. The SNR_{out} had the highest value for SPGR3D in expiration, followed by ZTE4D (p=0.4391). UTE3D and SPGR3D in inspiration had the lowest SNR values.

CNR_{LB} was significantly higher for SPGR3D in inspiration and in expiration than for ZTE3D BH in both conditions (all p<0.001). CNR_{LM} was significantly higher in SPRG inspiration than expiration (p=0.0085). SPGR3D inspiration had the highest CNR, followed by ZTE3D BH inspiration (p=0.2960). The CNR of blood-muscle was highest on the two inspiratory breath-hold sequences, and significantly lower on UTE3D (UTE3D vs ZTE3D BH: p<0.0001, UTE3D vs SPGR3D: p=0.0003).

Table 3: Comparison of SNR and CNR between sequences

	SPGR3D inspiration	SPGR3D expiration	ZTE3D vnav	UTE3D	ZTE4D	ZTE3D BH Inspiration	ZTE3D BH expiration
SNR_{out}	8.66±2.49	17.74±8.26	14.06±4.41	8.23±3.79	15.51±5.38	9.74±3.48	12.74±4.17
$SNR_{trachea}$			13.18±5.50	9.26±3.29	13.80±5.05	11.77±2.20	10.64±3.32
CNR_{LB}	17.91±6.80	16.39±5.31	15.86±5.87	12.56±5.59	10.22±3.95	8.46±3.18	9.11±2.58
CNR_{LM}	40.25±19.64	27.58±11.13	29.92±13.42	20.79±9.55	28.80±17.80	33.09±12.42	26.71±10.31
CNR_{BM}	22.03±16.33	12.76±9.83	14.06±10.73	8.14±5.88	18.59±15.25	23.80±10.68	18.43±9.22

Comparison of SNR of the lung parenchyma and CNR of the lung parenchyma-blood (LB), lung parenchyma and muscle (LM) and blood muscle (BM) between sequences (mean± standard deviation.

Qualitative assessment

Image quality assessment is shown in table 4. Image quality was highest for UTE3D for noise and overall acceptability, and highest for ZTE3D vnav for fissures and bronchus depiction. Both sequences showed similar scores for vessel depiction (table 4). Depiction of vessels was significantly better on UTE3D/ZTE3D compared to SPGR3D inspiration (p<0.001), SPGR3D expiration (p<0.001) and ZTE4D (p=0.025). Overall, fissure depiction was poor on all sequences, with a best depiction on ZTE3D vnav (2.06 out of 5.00). The depiction of the bronchi on UTE3D/ZTE3D was significantly better than on SPGR3D inspiration (p=0.035) and SPGR3D expiration (p=0.001). The noise level was acceptable for UTE3D and ZTE3D vnav, with significantly less noise on UTE3D than all other sequences (p=0.012 for SPGR3D inspiration, p=0.009 for SPGR3D expiration, p=0.003 for ZTE3D vnav, p=0.022 for ZTE3D BH and p=0.041 for ZTE4D).

Table 4: Qualitative MRI assessment outcomes

	SPGR3D insp.	SPGR3D Exp.	UTE3D	ZTE3D vnav	ZTE4D	ZTE3D BH
vessels	2.25±0.61	2.21±0.66	3.24±0.77	3.24±0.56	2.36±0.63	2.22±0.67
fissures	1.13±0.34	1.25±0.34	2.05±0.49	2.06±0.25	1.60±0.63	1.22±0.44
bronchus	2.00±0.41	1.88±0.45	3.47±0.87	3.56±0.63	2.27±0.70	2.33±0.86
noise/artifacts	2.83±0.82	2.67±0.70	3.52±1.03	3.0±0.61	2.36±0.74	2.44±0.53
acceptability	2.38±0.77	2.33±0.64	3.81±0.98	3.71±0.69	2.79±0.58	2.44±0.53

Qualitative assessment of all sequences. Data are presented as mean ± standard deviation.

Intra and inter correlation are shown in table 5 and figure 4, where good agreement between readers was considered if $\kappa_{inter} \geq 0.6$. Moderate to good agreement was found for most sequences, except for SPGR3D inspiration and expiration. In addition, very low agreement was found for the scoring of the fissures on all sequences. The best inter- observer agreement was found for UTE3D. The lowest agreement appeared for the detection of fissure on all sequences.

Table 5: Intra and inter correlation coefficients

Intra CC values						
	SPGR3D insp.	**SPGR3D Exp.**	**UTE3D**	**ZTE3D vnav**	**ZTE4D**	**ZTE3D BH**
vessels	0.302	0.291	0.684	0.529	0.533	0.391
fissures	0.286	0.156	0.231	0.091	0.345	0.273
bronchus	0.114	0.243	0.624	0.607	0.675	0.600
noise/artifacts	0.650	0.721	0.859	0.586	0.395	0.111
acceptability	0.269	0.284	0.910	0.463	0.717	0.429
Inter CC values						
vessels	0.230	0.659	0.837	0.566	0.128	0.333
fissures	0.150	0.156	0.674	0.119	0.276	0.500
bronchus	0.491	0.419	0.756	0.655	0.368	0.562
noise/artifacts	0.791	0.639	0.762	0.264	0.551	0.444
acceptability	0.497	0.455	0.740	0.552	0.513	0.250

Intra and inter correlation coefficients for all the sequences. Data are presented as intra correlation coefficient (ICC)

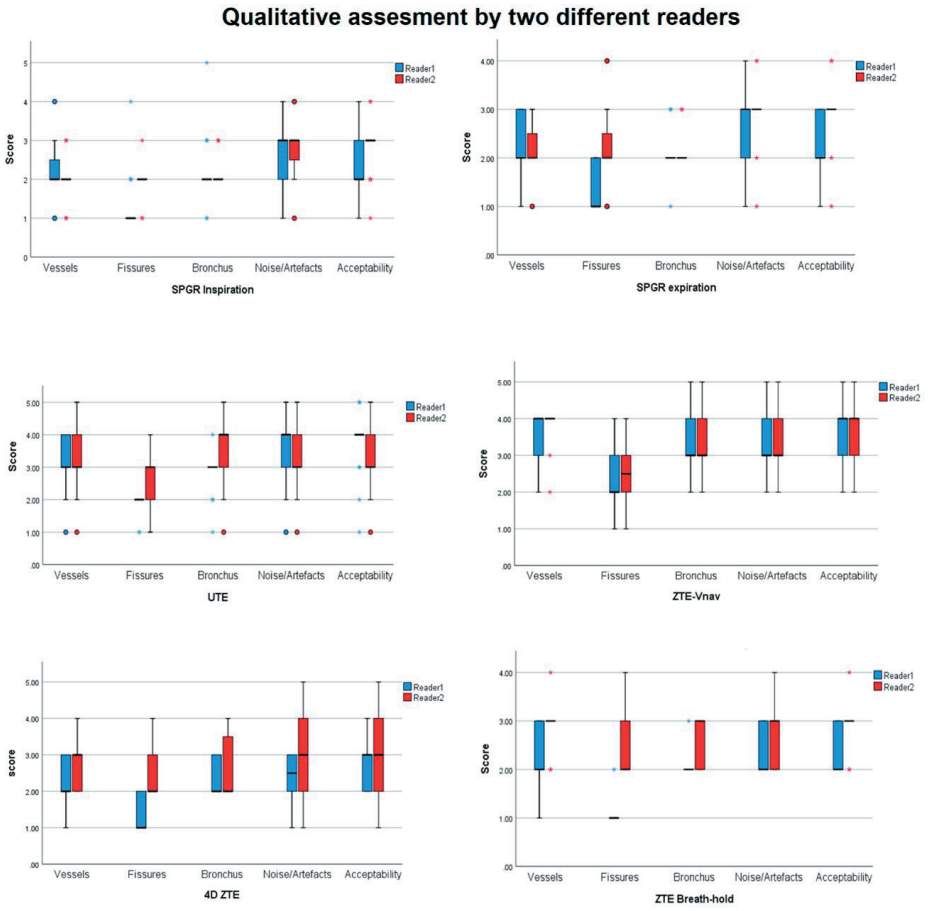

Figure 4. Boxplots for visualization of the qualitative assessment

Discussion

In this study different short and ultra-short TE sequences were compared in healthy volunteers and pediatric patients during free breathing and BH conditions to determine the most suitable clinical setting for future pediatric lung MRI examinations. Currently, SPGR3D sequences can cover the complete lung anatomy in reasonable breath-hold times (5 – 8 sec), and are able to visualize gross anatomic features and air trapping due to its high CNR. Unfortunately, spatial resolution is low in order to maintain a short TE, and SNR and CNR may be compromised with high acceleration parallel imaging factors.

UTE3D showed the highest overall acceptability score from both observers. UTE3D sequences were applied with prospective gating using a pneumo-belt. According to the

statistical analyses SNR and CNR values were not the highest for UTE3D, although qualitative assessment showed the highest agreement between the readers.

ZTE3D vnav provided good image quality for the bronchi, giving high-resolution structural information with better SNR for intrapulmonary structures. Better depiction of bronchi with ZTE3D was achieved by overall higher SNR than the other sequences and with the same spatial resolution as UTE3D. ZTE3D vnav had 12.5% of the voxel size compared to SPGR3D, while voxel size reduction for ZTE3D BH was 25%. This voxel size was still larger than standard CT voxel size, which is usually 1 mm isotropic.(13, 14) The smaller voxel size of ZTE had less dephasing across the voxel than the larger voxel of SPGR3D and therefore, the signal decay could have been more pronounced. However this can be difficult to prove because it depends on the amount of air present in a voxel.(11, 14, 15)

Breath-hold ZTE3D offered the same advantages as the navigated version, with an enhanced SI of the lung parenchyma. A major limitation of ZTE3D BH was the long scan time. The tested combination of 20 second breath hold scan time was not feasible in small children, who cannot hold their breath longer than 12 seconds. In our study, the scan time of the ZTE3D BH sequence could be reduced to less than 10s, however this led to insufficient SNR and therefore the data could not be reconstructed effectively to view the entire lung. The breath-hold scans were collected in deep inspiration and full expiration. During free-breathing these phases are not present, the amount of air in the lungs is different from what we are able to see on ZTE4D scans.

As an alternative to ZTE3D BH, we also tested ZTE4D, which is able to capture both inspiratory and expiratory phases (maximum of 16 respiratory phases during free breathing reconstructed retrospectively based on the physiologic signal provided by the pneumo-belt) and has a high spatial resolution, making it suitable to capture smaller vessels and peripheral bronchial walls, also in children. Throughout acquisition the respiration has to be constant to correctly reconstruct images with ZTE4D. Our study showed that even in subjects with a constant respiratory pattern and rate during the entire acquisition, the reconstructed images often showed considerable ghosting/blurring/streaking artifacts in most of the reconstructed phases (between inspiration and the more stable expiratory phase). We also observed artifactual increased brightness (figure 5 and 6) appearing in the lung parenchyma when using ZTE4D and ZTE3D vnav. This artifactual brightness was also seen in UTE3D sequences, but only when calibrated incorrectly. This artifact may be problematic in the assessment of lung disease because it can be wrongly interpreted as ground glass opacity, therefore as sign of pathology. The ground truth or parenchymal enhancement can only be trusted on the SPGR3D breath-hold scans.

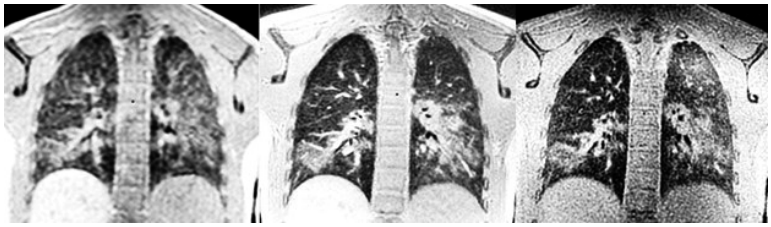

Figure 5. Example of imaging artifacts per sequence on a patient. (left - Breath-hold SPGR3D (8s) (NEX=7), middle - UTE3D, right - ZTE4D single phase). Demonstrating the limitations of the different sequences. UTE3D has some artifactual increases in the lung parenchyma if not calibrated correctly. For ZTE3D vnav and ZTE4D parenchyma signal in the left upper lobe (arrow) has the same brightening effects.

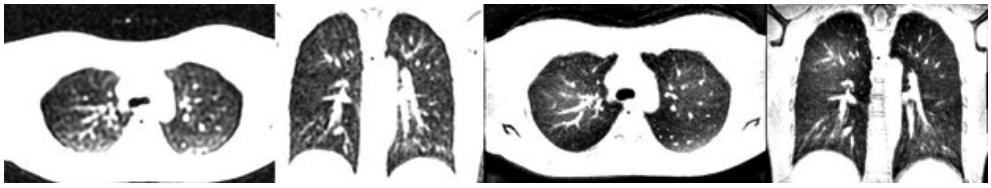

Figure 6. Example of imaging artifacts on a ZTE3D vnav sequence compared to SPGR3D scan on a patient (left two images - Breath-hold SPGR3D (8s), right two images - ZTE3D vnav). ZTE3D vnav has the same brightening effects in the parenchyma; likewise other regions around in the parenchyma seem artificially darkened. (Signa Explorer 1.5T, *GE Healthcare, Waukesha, WI, USA*)

Due to appearance of artifactual signal from the coils in the background outside of the chest both for ZTE and UTE3D sequences, the SNR calculation was performed with two different background noise ROIs. One was taken from an area of the background where we could avoid any artifacts and the other was taken from the trachea. This double approach on SNR measurements was influenced by FOV size of the ZTE sequence. For ZTE sequences, the scan time depends on the FOV. To keep scan time as short as possible at the desired resolution, the FOV was kept small, therefore ROIs taken from the background could have included artifactual signal/noise coming from the coil elements. It is unclear how to deal with the right standard deviation on noise inside the trachea because of possible artifacts. The mean background intensity of the trachea on both UTE3D and ZTE was lower than outside the chest.

For the qualitative measurements, intra and inter observer variability were tested. Intra reader agreement was moderate to good for most sequences, except for SPGR3D in- and expiration. The most difficult structures to assess were lung fissures, which were very poorly identified on all MRI sequences by both readers.

Our study has limitations. Firstly, we did not perform all sequences in the pediatric cohort, mainly because of the available scan time. Secondly, we did not standardize lung volume acquisitions in healthy volunteers, as we did for patients using an MRI compatible spirometer. This could have improved image quality of breath-hold scans and enhanced visualization of

low intensity regions (LIR) in expiration, representing hypoperfusion or hypoventilation of the lung parenchyma. This comparison would have been important for ZTE3D and UTE3D scans compared to SPGR3D expiration, which currently remains our reference standard to detect LIR.

Conclusions

We aimed to test feasibility and image quality of different ZTE and UTE3D lung MRI sequences for pediatric lung imaging. Based on our results, ZTE3D vnav provides the most reliable output in terms of image quality, although it can be affected by triggering efficiency and irregular respiratory patterns. UTE3D also provides high image quality, but pneumo-belt respiratory triggering is currently inadequate in small children, where the fitting of the pneumo-belt is poor. Current implementation of ZTE4D does not provide diagnostic image quality and can introduce artifacts mimicking lung pathology. Future implementation of ZTE and UTE3D should either focus on improvement of respiratory triggering with a size-specific pneumo-belt or on improved navigator options.

References

1. Zucker EJ, Cheng JY, Haldipur A, Carl M, Vasanawala SS. Free-breathing pediatric chest MRI: Performance of self-navigated golden-angle ordered conical ultrashort echo time acquisition. J Magn Reson Imaging. 2018;47(1):200-9.
2. Macdougall RD, Strauss KJ, Lee EY. Managing radiation dose from thoracic multidetector computed tomography in pediatric patients: background, current issues, and recommendations. Radiol Clin North Am. 2013;51(4):743-60.
3. Pearce MS, Salotti JA, Little MP, McHugh K, Lee C, Kim KP, et al. Radiation exposure from CT scans in childhood and subsequent risk of leukaemia and brain tumours: a retrospective cohort study. Lancet. 2012;380(9840):499-505.
4. Tiddens HA, Stick SM, Wild JM, Ciet P, Parker GJ, Koch A, et al. Respiratory tract exacerbations revisited: ventilation, inflammation, perfusion, and structure (VIPS) monitoring to redefine treatment. Pediatr Pulmonol. 2015;50 Suppl 40:S57-65.
5. Bergin CJ, Glover GH, Pauly JM. Lung parenchyma: magnetic susceptibility in MR imaging. Radiology. 1991;180(3):845-8.
6. Wild JM, Marshall H, Bock M, Schad LR, Jakob PM, Puderbach M, et al. MRI of the lung (1/3): methods. Insights Imaging. 2012;3(4):345-53.
7. Bergin CJ, Pauly JM, Macovski A. Lung parenchyma: projection reconstruction MR imaging. Radiology. 1991;179(3):777-81.
8. Puderbach M, Hintze C, Ley S, Eichinger M, Kauczor HU, Biederer J. MR imaging of the chest: a practical approach at 1.5T. Eur J Radiol. 2007;64(3):345-55.
9. Gibiino F, Sacolick L, Menini A, Landini L, Wiesinger F. Free-breathing, zero-TE MR lung imaging. Magma. 2015;28(3):207-15.
10. Higano NS, Hahn AD, Tkach JA, Cao X, Walkup LL, Thomen RP, et al. Retrospective respiratory self-gating and removal of bulk motion in pulmonary UTE MRI of neonates and adults. Magn Reson Med. 2017;77(3):1284-95.
11. Bae K, Jeon KN, Hwang MJ, Lee JS, Ha JY, Ryu KH, et al. Comparison of lung imaging using three-dimensional ultrashort echo time and zero echo time sequences: preliminary study. Eur Radiol. 2019;29(5):2253-62.
12. Salamon E, Lever S, Kuo W, Ciet P, Tiddens HA. Spirometer guided chest imaging in children: It is worth the effort! Pediatr Pulmonol. 2017;52(1):48-56.
13. Niwa T, Nozawa K, Aida N. Visualization of the airway in infants with MRI using pointwise encoding time reduction with radial acquisition (PETRA). J Magn Reson Imaging. 2017;45(3):839-44.
14. Yu J, Xue Y, Song HK. Comparison of lung T2* during free-breathing at 1.5 T and 3.0 T with ultrashort echo time imaging. Magn Reson Med. 2011;66(1):248-54.
15. Hatabu H, Alsop DC, Listerud J, Bonnet M, Gefter WB. T2* and proton density measurement of normal human lung parenchyma using submillisecond echo time gradient echo magnetic resonance imaging. Eur J Radiol. 1999;29(3):245-52.

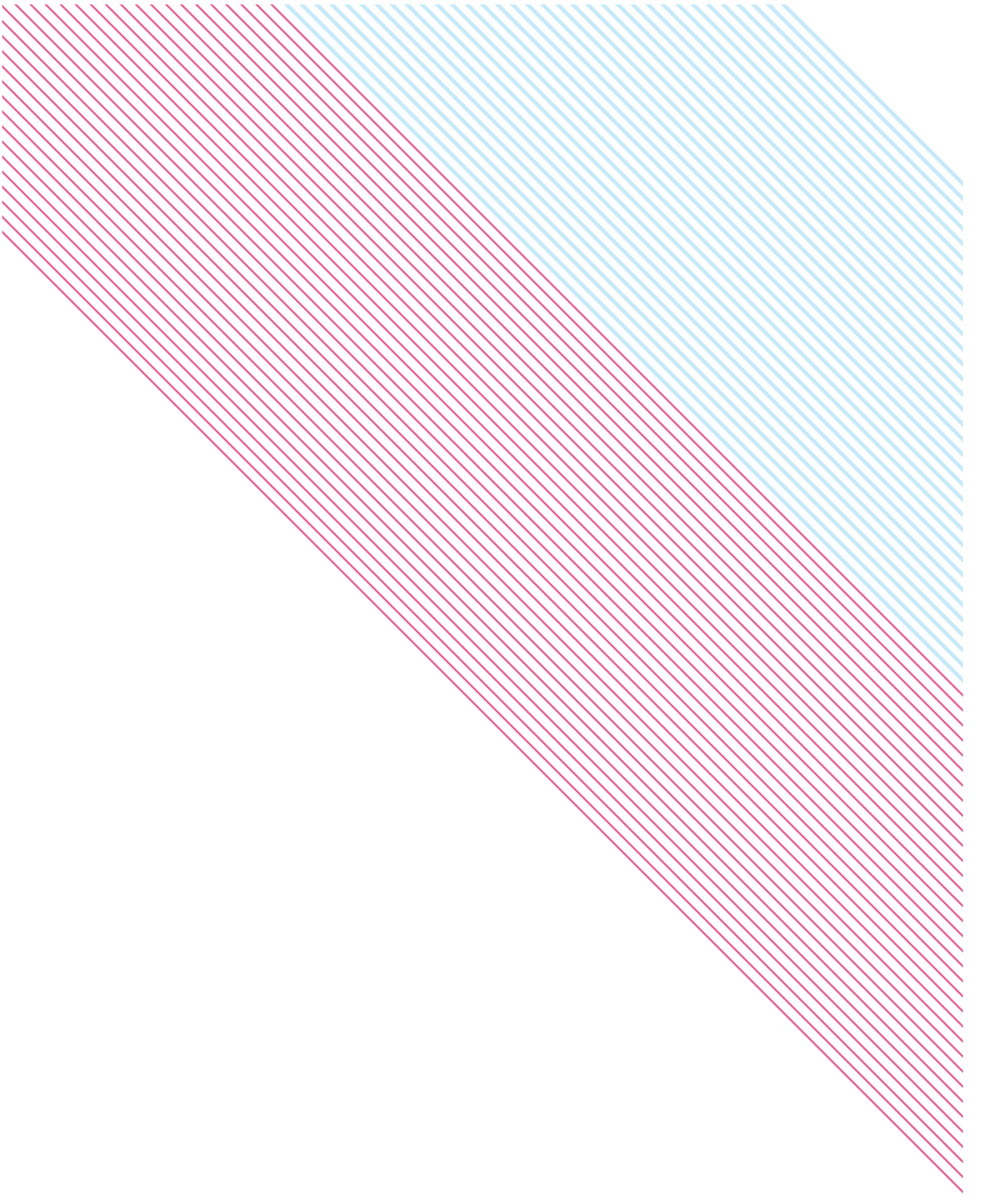

Chapter 8

Development of a neonatal chest magnetic resonance imaging protocol for bronchopulmonary dysplasia patients: a preliminary report

Bernadette BLJ Elders, Piotr A Wielopolski, André A Kroon,
Harm AWM Tiddens, Mariëlle WH Pijnenburg, Irwin KM Reiss, Pierluigi Ciet

Work in progress

Abstract

Rationale: There is need for an accurate imaging method to monitor neonates with bronchopulmonary dysplasia (BPD), to assess severity and identify neonates with increased risk for respiratory morbidity. Chest Magnetic Resonance Imaging (MRI), as ionizing radiation free technique and with the option of silent scanning, shows potential for this.

Objective: To develop and test a chest MRI protocol to image the lungs of neonates with BPD in their first year of life.

Methods: An MRI protocol was developed on a 1.5T system and tested on preterm neonates born <28 weeks of gestation with severe BPD and healthy term neonates >37 weeks of gestation. MRIs were scored on image quality, hypo- and hyperintense regions and bronchopathy and amount of anatomical architectural distortion (AAD). Structural changes are expressed as % of total lung volume. This preliminary report describes our findings of the first two study participants included.

Main results: MRI was feasible without anaesthesia by using the feed-and-swaddle method. Images showed minimal movement artefacts. Best image quality was obtained on T2-w PROPELLER sequence. Best image resolution was obtained with the ZTE sequence (1.0x1.0x1.0 mm^3). Patient 1, born at 26+3 weeks scanned at 43+6 weeks postmenstrual age (PMA), showed 22% structural lung changes and a severe AAD score. Patient 2 born at 26+4 weeks PMA, scanned at 40+2 weeks PMA, showed 15% structural lung changes and a moderate AAD score.

Conclusion: Our BPD-MRI protocol is a feasible and promising diagnostic tool to image the lungs of neonates with BPD without need for anaesthesia and without exposure to ionising radiation.

Introduction

The most common lung disease in preterm born neonates is bronchopulmonary dysplasia (BPD).(1) BPD is caused by altered development of the alveoli and accompanying vasculature associated with premature birth and thereby leads to ventilation and perfusion defects, inflammation and structural changes of the lungs. Assessment of the severity of BPD is currently based on the National Health Institute (NHI) criteria and depends on the need of oxygen at 36 weeks post menstrual age (PMA).(2, 3) The knowledge on BPD is rapidly evolving, significantly improving perinatal care.(4, 5) Nonetheless, there is currently no established and validated imaging method for the short and long term follow up of neonates with BPD which is needed to assess severity and identify those neonates at risk for chronic respiratory morbidity.

Recent technical developments have made Magnetic Resonance Imaging (MRI) a feasible modality to image several paediatric lung diseases.(6, 7) In particular the lack of exposure to ionising radiation makes MRI an attractive alternative to Computed Tomography (CT).(8) Besides, MRI offers the possibility of dynamic imaging of central airways and lungs(9, 10) and has superior tissue characterization compared to CT. MRI also includes novel functional techniques, such as Fourier Decomposition (FD), which can visualize lung ventilation and perfusion without using intravenous or gaseous contrast agents.(11-13) So, MRI shows great potential especially for neonates, who are most sensitive to ionising radiation, and should therefore be considered as imaging technique to assess neonates with BPD.

Several recent studies on chest MRI in neonates with BPD have shown the feasibility of MRI to image BPD associated pathology. MRI findings correlated well with short term clinical outcome, such as respiratory support at hospital discharge.(14-17) Although these results are promising, nevertheless these studies were conducted on a modified small-footprint MRI system, originally designed for adult orthopaedic use and non-commercially available. However, for MRI to be introduced in clinical practice of BPD follow-up, these results need to be available for conventional MRI systems. For this reason the **V**entilation, **I**nflammation, perfusion and structure in **B**ronchopulmonary dysplasia at school ag**e** (**VIBE**) study was recently conducted, where we have developed and tested a chest MRI protocol for the follow up of school age children with BPD, showing promising results (Elders *et al*, submitted data). In our current study, we describe the **V**entilation, **I**nflammation, perfusion and structure in **N**eonatal **L**ung patients (**VINyL**) study, which aims to implement and test our chest MRI protocol to image neonates with BPD, using a conventional 1.5 Tesla MRI system. This preliminary report describes our findings from the first two patients included in the VINyL study.

Methods

A flowchart of the development and testing of our neonatal chest MRI protocol is shown in figure 1. First, findings from the VIBE study were analysed to define the best sequences to image BPD related lung abnormalities. Then, the selected sequences were incorporated into a neonatal chest MRI protocol for the VINyL study, and tested and optimized in healthy neonates and neonates with BPD. The study was approved by the local medical ethics committee (MEC2019-0378).

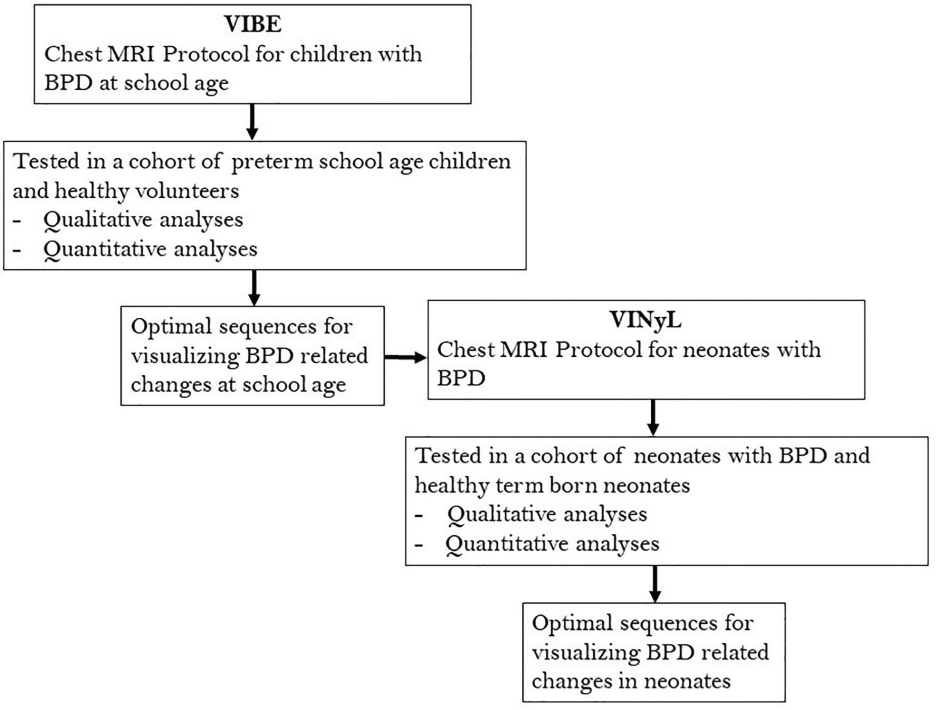

Figure 1: Flowchart of the development of an optimal chest MRI protocol for neonates with BPD in the VINyL study. BPD; bronchopulmonary dysplasia, MRI; magnetic resonance imaging, VIBE; ventilation, inflammation, perfusion and structure in bronchopulmonary dysplasia at school age, VINyL; ventilation, inflammation, perfusion and structure in neonates with lung disease.

Protocol development

Recent findings from the VIBE study on the development and implementation of a chest MRI protocol in school age children with BPD was used to select the best sequences for the neonatal BPD-MRI protocol (Elders *et al.* submitted data). We concluded that the BPD-MRI protocol should at least consist of a T2-w PROPELLER sequence to image hyper intense regions and a short echo time (UTE or ZTE) sequence to image hypo intense regions and airway abnormalities. In addition, our VIBE findings showed Fourier Decomposition (FD) sequences to be promising to visualize ventilation and perfusion defects in this population.

These findings led to the development of a neonatal chest BPD-MRI test- protocol on a 1.5T scanner (*SIGNA Explorer, GE Healthcare, Milwaukee, Wisconsin, USA)*, with the use of a dedicated neonatal chest coil (*LMT Medical Systems GmbH, Lubeck, Germany)*. The protocol consisted of an axial T2-weigthed (T2-w) PROPELLER sequence and axial Proton Density-weighted (PD-w) ZTE sequences (tested at several resolutions). In addition, a single 2D SPGR multi-phase free-breathing sequence in the centre of the thorax was added for FD analyses. Sequence parameters are shown in table 1.

Table 1: Chest BPD-MRI protocol

Sequence	T2-w PROPELLER	PD-w ZTE	FD
Acquisition plane	Axial	Axial	Coronal
TR/TE (ms)	7500/54	1.8/0	2.6/0.9
Flip angle (°)	90/120	2	5
RF	Selective	Non-selective	Selective
In-plane matrix	192 x 192	180 x 180	128 x 128
k-space trajectory	blades	Radial	Cartesian
In-plane FOV	23	18	50
Actual voxel resolution (mm^3)	1.2 x 1.2 x 1.2	1.0 x 1.0 x 1.0	3.0 x 3.0 x 10.0
Slices	64	100	4-6
Slice thickness	1.2	1.0	10.0
Receiver bandwidth (kHz)	50.0	31.3	83.33
Parallel imaging	3.0	None	2.5
Number of averages	6	4	1
Number of phases	-	-	190/145 ms per phase
Number of spokes per segment	16	512	-
Physiological triggering	None Free breathing	None Free breathing	None Free Breathing
Scan time	+/- 9 min	+/- 4 min	38 sec

Final chest BPD-MRI protocol as concluded for the first two patients included in the VINyL study. FD; Fourier Decomposition, FOV; Field Of View, PROPELLER; PD-w; proton density weighted, Periodically Overlapping ParalLEL Lines with Enhanced Reconstruction, RF; radio frequency, SPGR; Spoiled Gradient Echo Sequence, T2-w; T2 weighted, TE; Echo Time, TR; Repetition time, ZTE; zero echo time

Protocol testing

We aim to test the neonatal BPD-MRI protocol in a cohort of neonates with BPD and neonatal controls. Preterm neonates admitted at the neonatal intensive care unit (NICU), born before 28 weeks gestational age with the diagnosis of severe BPD according to the NHI criteria, are approached to participate in this study. Exclusion criteria are contraindication for MRI or congenital cardiovascular or pulmonary abnormalities that could hamper the imaging. Neonates with BPD will be compared to neonates born after 37 weeks gestational age, who did not obtain mechanical ventilation, and without cardiovascular or pulmonary abnormalities. We aim to include 12 neonates with BPD and 6 controls. Written informed consent is obtained from the parents of all study participants before participation.

Clinical data on gender, gestational age, birth weight and pulmonary condition is obtained from the electronic patient file. All study participants will undergo cardiovascular echocardiography and chest MRI without sedation, children will be fed, swaddled and immobilized with the use of a vacuum matrass during the MRI. Study participants can be soothed with a pacifier and sucrose in between the MRI sequences.

The protocol will be tested for up to 60 minutes, or until the study participant shows signs of discomfort, as judged by the healthcare giver present at the MRI examination. Our aim is to develop a clinical neonatal BPD-MRI protocol of maximum 30 minutes.

Qualitative and quantitative analyses

For the two study subjects included to date qualitative analyses were performed on all sequences according to Bae *et al*. qualitative scoring method (table 2).(18) Then, we assessed the presence of artifacts, namely blurring, wrapping, streaking or low signal-to-noise (SNR) artifacts.

Table 2: Qualitative MRI scoring

Depiction of fissures	1. Unacceptable (invisible interlobar fissure) 2. Fair (blurred interlobar fissure) 3. Good (visible interlobar fissure)
Depiction of intrapulmonary vessels	1. Unacceptable (invisible peripheral pulmonary vessels) 2. Poor (barely visible peripheral pulmonary vessels) 3. Fair (visible peripheral pulmonary vessels) 4. Good (visible peripheral pulmonary vessels with clear margin) 5. Excellent (visible peripheral pulmonary vessels with clear margin)
Depiction of bronchi	1. Unacceptable (indistinguishable lobar bronchial walls) 2. Poor (visible lobar bronchial walls with <10 visible segmental bronchial walls) 3. Fair (visible lobar bronchial walls with >10 visible segmental bronchial walls) 4. Good (visible lobar bronchial walls with >10 visible segmental bronchial walls, with few visible sub/segmental bronchial walls) 5. Excellent (visible sub-subsegmental bronchial walls)
Image noise/artefacts	1. Unacceptable 2. Above average noise/artifacts 3. Average and acceptable 4. Less than average noise/ artifacts 5. Minimum of no noise/artifacts
Overall acceptability	1. Unacceptable 2. Suboptimal 3. Satisfactory 4. Above average 5. Superior

Qualitative scoring method adjusted from Bae *et al*. (European Radiology 2020)

In addition, a quantitative analysis is performed to calculate the volume and percentage of BPD related lung abnormalities on MRI. For this a grid based scoring system, based on the PRAGMA-BPD scoring system, is used: the bronchopul**M**onary rott**E**rdam m**R**i morpholo**G**y scor**E** (**MERGE**) scoring system (Elders *et al.* submitted data).(19-21) For this method a grid is placed over twenty equidistant axial MR images, with a grid-size corresponding to the average airway size. These grids are coloured in a hierarchical order for all BPD related abnormalities as hypo-intense regions, such as mosaic perfusion, emphysema, trapped air, bullae and cysts; hyper-intense regions, such as consolidations, atelectasis and linear/sub plural opacities; bronchopathy and normal lung tissue. Data are presented as a percentage of total lung volume. An in-house developed software is used for the MERGE analysis. Figure 2 shows an example of the grid-based scoring system on a neonatal MR image.

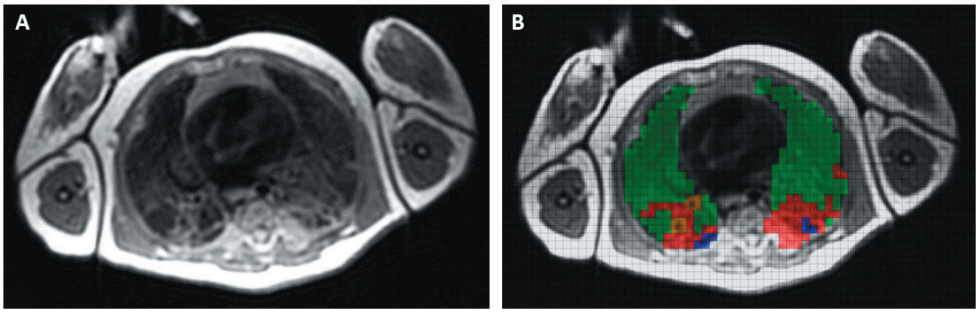

Figure 2: axial T2- weighted PROPELLER sequence of patient 1 (A) and corresponding grid-based scoring system showing hypo intense regions (blue), hyper intense regions (red), bronchopathy (orange) and normal lung tissue (green) (B).

In addition, the amount of anatomical architectural distortion (AAD) defined as abnormal displacement of bronchi, vessels, fissures and/or septa, is scored as mild (<7 lung segments involved), moderate (7-13 lung segments involved) or severe (>13 lung segments involved). (20) For the FD analyses we use an in-house developed algorithm based on the work of Voskrebenzev *et al.*(22-24) This algorithm applies a spectral decomposition on the intensity corrected ventilation and perfusion images, thereby reconstructing ventilation and perfusion maps.

Results

In this preliminary report we present our findings on the first two neonates with BPD included in the VINyL study.

The first patient was a girl born at 26+3 weeks PMA with a birth weight of 815 grams. She was intubated and ventilated for nine weeks, after which she received oxygen via continuous positive airway pressure (CPAP) until a PMA of 43 weeks, and oxygen via low flow up until

the study MRI. At 36 weeks PMA the diagnosis of severe BPD according to the NHI criteria was made.(3) Echocardiography showed a small patent foramen ovale with a left-to-right shunt and a mild tricuspid insufficiency without signs of increased pressure on the right heart. No persistent ductus arteriosus (PDA) or signs of pulmonary hypertension were seen.

Chest MRI was conducted at 43+6 weeks PMA.

The second patient was a boy born at 26+4 weeks gestational age with a birth weight of 790 grams. He was intubated and ventilated for six days after which he received oxygen via CPAP and nasal intermittent positive pressure ventilation (NIPPV) for more than 28 days. At 36 weeks PMA the diagnosis of severe BPD according to the NHI criteria was made.

Echocardiography showed no PDA, no signs of pulmonary hypertension and no other abnormalities.

Chest MRI was conducted at 40+2 weeks PMA.

Qualitative analyses

During MRI no anaesthesia or sedation was used, both neonates were fed, swaddled and immobilised with a vacuum mattress to prevent patient movement. Both neonates were kept calm with a pacifier and sucrose in between the sequences multiple times. Protocol duration was 44 minutes in patient 1 and 37 minutes in patient 2. In patient 2 the scanning was terminated early and not all sequences were tested because of discomfort, therefore this patient has only one ZTE sequence available.

The qualitative scores of the MRI sequences is shown in table 3. Depiction of fissures was best on the T2-w PROPELLER sequence. Depiction of vessels was best on the PD-w ZTE sequences. No difference was found between the sequences for the depiction of bronchi. The T2-w PROPELLER sequences showed less artefacts compared to the PD-w ZTE sequences, which showed low SNR, and in patient 2, blurring artefacts due to general movement. Overall acceptability of the images was ‘acceptable’ for the PD-w ZTE sequences and above average for the T2-w PROPELLER sequences. The ZTE sequence with a resolution of 1.0x1.0x1.0mm^3 scored better than the ZTE sequence with a resolution of 1.3x1.3x1.3mm^3 mainly due to better depiction of bronchi.

Table 3: Qualitative MRI scoring

	Patient 1			Patient 2	
	PROPELLER (1.2 x 1.2 x 1.2mm^3)	**ZTE (1.3 x 1.3 x 1.3 mm^3)**	**ZTE (1.0 x 1.0 x 1.0 mm^3)**	**PROPELLER (1.2 x 1.2. x 1.2 mm^3)**	**ZTE (1.3 x 1.3 x 1.3 mm^3)**
Fissures	2	2	2	3	2
Vessels	2	3	3	2	3
Bronchi	3	2	3	2	2
Artefacts	4	3	3	4	2
Acceptability	4	3	3	4	3
Type of artefacts	-	Low SNR	Low SNR	-	Low SNR, blurring

PROPELLER; Periodically Overlapping ParalLEL Lines with Enhanced Reconstruction, ZTE; zero-echo time. Scoring method according to Bae *et al.(18)* Data are presented as unacceptable (1) to good (3) for the depiction of fissures, unacceptable (1) to excellent (5) for the depiction of vessels and bronchi, unacceptable (1) to minimum of noise/ artefacts (5) for artefacts and unacceptable (1) to superior (5) for overall acceptability.

Quantitative analyses

The MERGE scoring results are summarized in table 4. The MERGE scoring was applied on the sequences with best image quality: on the T2-w PROPELLER sequence and the PD-w ZTE sequence with a resolution of 1.0x1.0x1.0 mm^3 for patient 1, and on the T2-w PROPELLER and PD-w ZTE sequence for patient 2.

Figure 3 shows the MR images of patient 1. The MERGE scoring showed an average percentage disease of 21.7% of total lung volume, with the most seen abnormality being hyper intense regions (16.6% of total lung volume). The highest percentage of hypo intense regions and bronchopathy was scored on the T2-w PROPELLER sequence, the percentage of hyper intense regions was scored equal on both the ZTE and T2-w PROPELLER sequence. The total number of affected lung segments with AAD was 15, resulting in a score of severe AAD.

The exploratory FD analyses are visualized in figure 4, showing a hypo intense region in the left upper lope on the ZTE image corresponding to a mixed ventilation/ perfusion defect on the FD maps and a hypo intense region on the ZTE image in the right lower lobe corresponding to a perfusion defect on the FD maps.

Table 3: MERGE scoring

	Patient 1		Patient 2	
	ZTE	PROPELLER	ZTE	PROPELLER
	ml/%	ml/%	ml/%	ml/%
Diseased lung	23.6/20.7	25.4/22.6	9.8/14.1	11.6/14.8
Hypo intense regions	4.0/3.5	5.5/4.9	1.4/2.0	2.2/2.8
Hyper intense regions	18.8/16.5	18.7/16.6	8.4/12.1	9.4/12.0
Bronchopathy	0.8/0.7	1.2/1.1	0.0/0.0	0.0/0.0
Normal lung tissue	90.5/79.3	87.1/77.4	59.7/85.9	66.8/85.2
AAD	15 (severe)		10 (moderate)	

AAD; anatomical architecture distortion, MRI; magnetic resonance imaging, PROPELLER; Periodically Overlapping ParalLEL Lines with Enhanced Reconstruction, ZTE; zero-echo time. Data are presented as volume in ml and percentage of the total lung volume for the lung abnormalities and normal lung tissue, and as the number of affected lung segments (severity score) for the anatomical architecture distortion. Architectural distortion is presented as the number of lung segments involved.

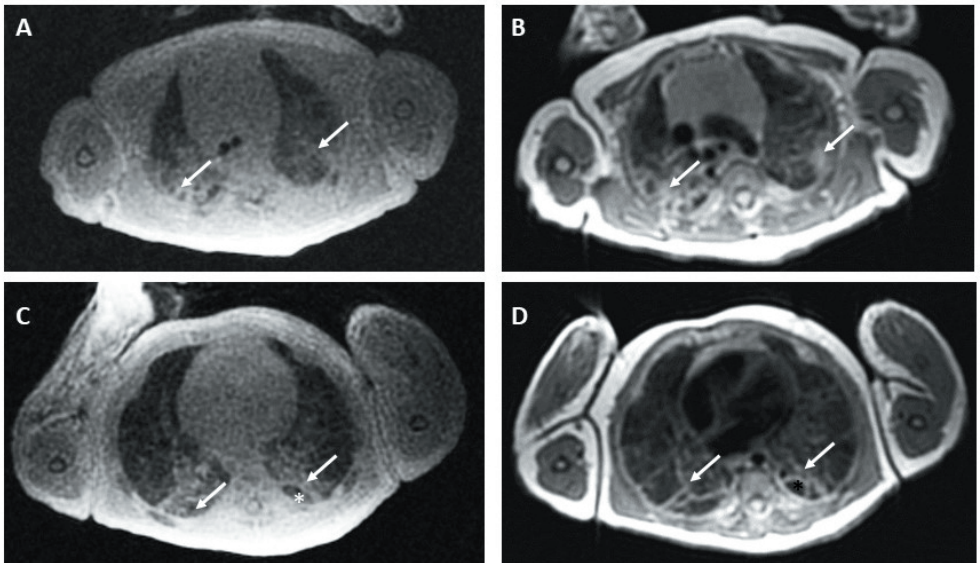

Figure 3: Axial PD-weighted ZTE (A and C) and axial T2-weighted PROPELLER sequences of patient 1 at corresponding locations showing hypo intense regions: atelectasis and linear opacities (arrows) and hypo intense regions (asterisk).

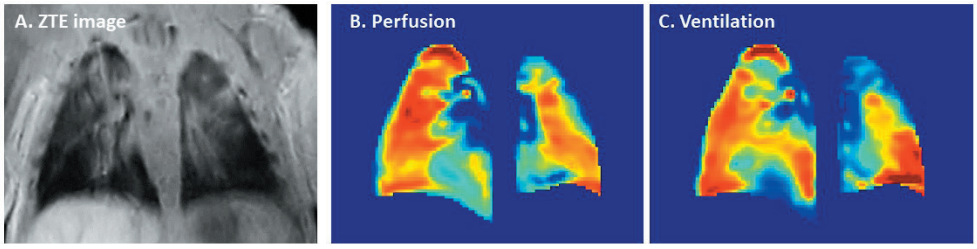

Figure 4: Fourier decomposition (FD) analyses of patient 1. Showing a coronal reformat zero echo time (ZTE) sequence (A) and the corresponding perfusion and ventilation maps in a colour scale representing low (blue) to high (red) perfusion and ventilation (B and C). The ZTE image shows a hypo intense region in the left upper lobe corresponding to a mixed ventilation/ perfusion defect on the FD maps and a hypo intense region on the ZTE image in the right lower lobe corresponding to a perfusion defect on the FD maps.

Figure 5 shows the MR images of patient 2. The MERGE scoring showed an average percentage of diseased lung of 14.5% of total lung volume. The most frequent abnormality was hyper intense regions (12.1% of total lung volume). No bronchopathy was seen in this patient. The percentage of hypo intense regions was scored highest on the T2-w PROPELLER sequence, hyper intense regions and bronchopathy were scored equal on both the T2-w PROPELLER and PD-w ZTE sequence. The total number of affected lung segments with AAD was 10, resulting in a score of moderate AAD. Patient 2 did not have FD images of sufficient quality available for analyses.

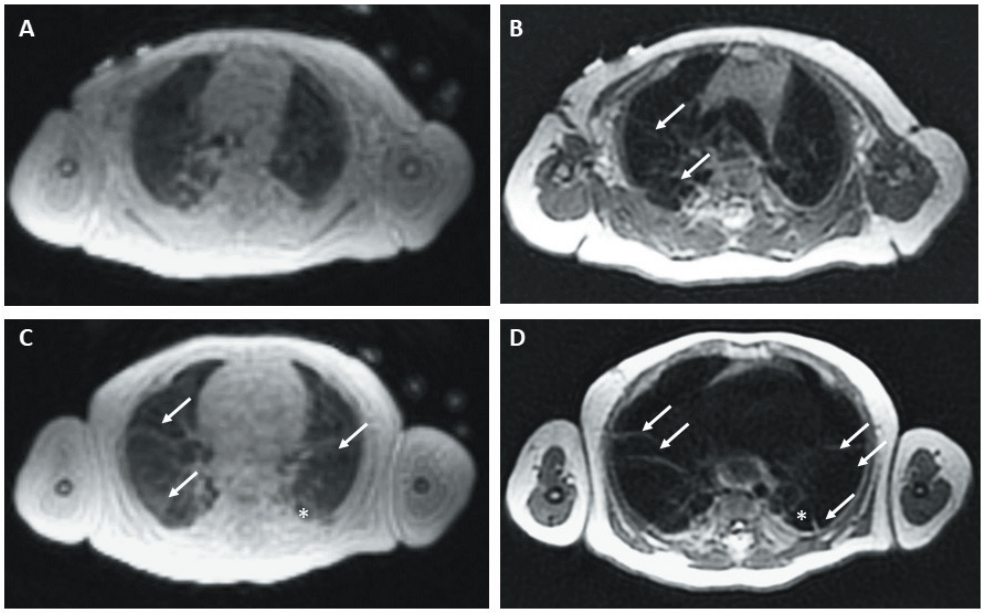

Figure 5: Axial ZTE (A and C) and axial T2-weighted PROPELLER sequences of patient 2 at corresponding locations showing hypo intense regions: linear opacities (arrows) and hypo intense regions (asterisk). Note that on the top left image (A) the hypo intense regions are not easily identified due to a low signal-to-nose ratio

Discussion

In this study we have developed and tested a neonatal chest MRI protocol to image BPD on a conventional 1.5 T MRI system. Our preliminary report shows the results from testing the protocol in two neonates with BPD.

We demonstrate that chest MRI is feasible in neonates without using anaesthesia, by using the feed and swaddle method. Both patients remained comfortable in the MRI scanner for up to 37 minutes. Although, in the second patient scanning had to be terminated preliminary due to discomfort, these findings show that a clinical BPD-MRI protocol of 30 minutes will be feasible. Movement artifacts were only seen in one sequence of the second patient. We had a researcher present at both MRIs, who was able to soothe the patients in between sequences with a pacifier and sucrose in case of discomfort. Such dedicated guidance during the MRI examination is recommended to facilitate compliance and to minimize the burden on the neonate.(25) In addition, having a fully silent MRI protocol will most likely omit the consoling of the neonate during the examination, improve compliance and reduce the chance of movement artifacts. Another option is retrospective removal of those images with movement artifacts by repeated k-space sampling.(14, 16)

Results from our qualitative analyses show the T2-w PROPELLER sequence having the best image quality, followed by the ZTE sequence. Conversely the ZTE sequence was superior for the depiction of lung vessels. The images obtained from our chest MRI protocol showed minimal artifacts. One sequence showed artifacts related to low SNR and one sequence showed artifacts related to low SNR and general movement of the patient. However, besides these artifacts the diagnostic quality of all sequences was acceptable. The best resolution obtained was 1.0x1.0x1.0 mm^3 for the ZTE sequence in patient one, comparable to previous chest MRI research in the neonatal population.(14-16, 26) And albeit not comparable yet, this image resolution is approaching the resolution of chest CT in this population (± 0.5x0.5x1 mm^3).

Findings from our quantitative analyses show that chest MRI is able to identify the most important BPD related lung abnormalities in this neonatal population. Hypo intense regions and bronchopathy were scored highest on the T2-w PROPELLER sequence, while the hyper intense regions were scored equal on both the T2-w PROPELLER and PD-w ZTE sequence. These findings are in line with previous research describing excellent lung parenchyma visualization on T2-w and superior identification of hypo intense regions on ultra-short echo time (UTE) sequences in the neonatal population.(14, 16, 26) However, our imaging results from chest MRI in school age children with BPD, showed a better visualization of most BPD related abnormalities on the short echo time sequence instead of the T2-w sequence. We speculate that the better identification of abnormalities on T2-w sequences in neonates

might be caused by a higher water content and density of the lungs seen in the neonatal population compared to school age, and therefore better contrast to noise obtained by T2 weighting.(27)

Using the MERGE scoring, we were able to calculate the percentage of lung showing structural changes related to BPD. Interestingly, both patients described in this preliminary report meet the NHI criteria of severe BPD, but the patient having received the most respiratory support shows a higher percentage of disease on MRI and a higher AAD severity score. This is in line with a recent study that suggests MRI findings to better correlate to short term clinical outcome compared to the BPD severity score.(17) The remaining participants in this study cohort should be included and analysed to confirm this finding.

The highest percentage of disease according to the MERGE scoring was found for hyper intense regions, a combined scoring of linear and sub pleural opacities and atelectasis. The hyper intense regions in our patients were primarily seen in the dorsal parts of the lungs. Dorsal atelectasis is a common finding on radiological imaging of neonates, which could be fibrosis, physiological atelectasis or fluid accumulation due to the supine position of the neonate. A study by Adams *et al.* confirmed the presence of these hyper intense regions on MRI in neonates, and showed them to be position dependant.(28) These hyper intense regions are increasingly pronounced in the (severe) BPD population and it is therefore hypothesized that this represents alveolar flooding, as seen in acute lung disease.(29) Comparison to the healthy neonatal population should be conducted to further investigate this hypothesis and long term follow up is needed to study how these abnormalities develop over time.

Our study has some specific strengths for further development of neonatal chest MRI . First, we have explored the use of MRI for functional imaging, i.e. the visualization of ventilation and perfusion, in the neonatal BPD population. Previous studies have used hyperpolarized gasses for this purpose, but this technique has high costs related to the need for a dedicated MRI system, polarizer and hyperpolarized gases.(30-33) Our exploratory results look promising for the use of FD, however, further validation in a large cohort is needed.

Second, we have developed a chest MRI protocol to be used on conventional MRI systems, in contrast to the research group of Cincinnati Children's Hospital, that uses a non- conventional MRI system.(14) Our findings also show that short echo time sequences, such as ZTE, are an asset for chest MRI protocols for neonates, because these sequences show best image resolution, are superior to depict vessels and ideal to identify hypo intense regions in the BPD population. Most importantly, the ZTE sequence can be a silent sequence, and therefore makes MRI less burdensome for neonates, limiting the chance of movement artifacts. This

sequence, which is nowadays only available as a research product on most MRI systems, should be made available for clinical practice.

In conclusion, chest MRI is a promising technique to image neonates with BPD, as it is a safe and possibly feasible method, without the need for anaesthesia or sedation and without exposure to ionising radiation. This ongoing study will be focused on refining the BPD-MRI protocol and comparing the lung abnormalities seen in neonates with BPD to findings in term born neonates. Next our findings should be validated in a larger cohort and correlated to clinical outcomes.

References

1. Kinsella JP, Greenough A, Abman SH. Bronchopulmonary dysplasia. Lancet. 2006;367(9520):1421-31.
2. Morty RE. Recent advances in the pathogenesis of BPD. Semin Perinatol. 2018.
3. Jobe AH, Bancalari E. Bronchopulmonary dysplasia. Am J Respir Crit Care Med. 2001;163(7):1723-9.
4. Bancalari E, Jain D. Bronchopulmonary Dysplasia: 50 Years after the Original Description. Neonatology. 2019;115(4):384-91.
5. Ibrahim J, Bhandari V. The definition of bronchopulmonary dysplasia: an evolving dilemma. Pediatr Res. 2018;84(5):586-8.
6. Ciet P, Tiddens HA, Wielopolski PA, Wild JM, Lee EY, Morana G, et al. Magnetic resonance imaging in children: common problems and possible solutions for lung and airways imaging. Pediatr Radiol. 2015;45(13):1901-15.
7. Hatabu H, Ohno Y, Gefter WB, Parraga G, Madore B, Lee KS, et al. Expanding Applications of Pulmonary MRI in the Clinical Evaluation of Lung Disorders: Fleischner Society Position Paper. Radiology. 2020;297(2):286-301.
8. Sodhi KS, Lee EY. What all physicians should know about the potential radiation risk that computed tomography poses for paediatric patients. Acta Paediatr. 2014;103(8):807-11.
9. Ciet P, Wielopolski P, Manniesing R, Lever S, de Bruijne M, Morana G, et al. Spirometer-controlled cine magnetic resonance imaging used to diagnose tracheobronchomalacia in paediatric patients. Eur Respir J. 2014;43(1):115-24.
10. Hysinger EB, Bates AJ, Higano NS, Benscoter D, Fleck RJ, Hart C, et al. Ultrashort Echo-Time MRI for the Assessment of Tracheomalacia in Neonates. Chest. 2019.
11. Veldhoen S, Weng AM, Knapp J, Kunz AS, Stäb D, Wirth C, et al. Self-gated Non-Contrast-enhanced Functional Lung MR Imaging for Quantitative Ventilation Assessment in Patients with Cystic Fibrosis. Radiology. 2017;283(1):242-51.
12. Bauman G, Scholz A, Rivoire J, Terekhov M, Friedrich J, de Oliveira A, et al. Lung ventilation- and perfusion-weighted Fourier decomposition magnetic resonance imaging: in vivo validation with hyperpolarized 3He and dynamic contrast-enhanced MRI. Magn Reson Med. 2013;69(1):229-37.
13. Sodhi KS, Ciet P, Vasanawala S, Biederer J. Practical protocol for lung magnetic resonance imaging and common clinical indications. Pediatr Radiol. 2021:1-17.
14. Hahn AD, Higano NS, Walkup LL, Thomen RP, Cao X, Merhar SL, et al. Pulmonary MRI of neonates in the intensive care unit using 3D ultrashort echo time and a small footprint MRI system. J Magn Reson Imaging. 2017;45(2):463-71.
15. Higano NS, Fleck RJ, Spielberg DR, Walkup LL, Hahn AD, Thomen RP, et al. Quantification of neonatal lung parenchymal density via ultrashort echo time MRI with comparison to CT. J Magn Reson Imaging. 2017;46(4):992-1000.

16. Higano NS, Hahn AD, Tkach JA, Cao X, Walkup LL, Thomen RP, et al. Retrospective respiratory self-gating and removal of bulk motion in pulmonary UTE MRI of neonates and adults. Magn Reson Med. 2017;77(3):1284-95.
17. Higano NS, Spielberg DR, Fleck RJ, Schapiro AH, Walkup LL, Hahn AD, et al. Neonatal Pulmonary Magnetic Resonance Imaging of Bronchopulmonary Dysplasia Predicts Short-Term Clinical Outcomes. Am J Respir Crit Care Med. 2018;198(10):1302-11.
18. Bae K, Jeon KN, Hwang MJ, Lee JS, Ha JY, Ryu KH, et al. Comparison of lung imaging using three-dimensional ultrashort echo time and zero echo time sequences: preliminary study. Eur Radiol. 2019;29(5):2253-62.
19. Rosenow T, Oudraad MC, Murray CP, Turkovic L, Kuo W, de Bruijne M, et al. PRAGMA-CF. A Quantitative Structural Lung Disease Computed Tomography Outcome in Young Children with Cystic Fibrosis. Am J Respir Crit Care Med. 2015;191(10):1158-65.
20. van Mastrigt E, Kakar E, Ciet P, den Dekker HT, Joosten KF, Kalkman P, et al. Structural and functional ventilatory impairment in infants with severe bronchopulmonary dysplasia. Pediatr Pulmonol. 2017;52(8):1029-37.
21. van Mastrigt E, Logie K, Ciet P, Reiss IK, Duijts L, Pijnenburg MW, et al. Lung CT imaging in patients with bronchopulmonary dysplasia: A systematic review. Pediatr Pulmonol. 2016;51(9):975-86.
22. Voskrebenzev A, Gutberlet M, Becker L, Wacker F, Vogel-Claussen J. Reproducibility of fractional ventilation derived by Fourier decomposition after adjusting for tidal volume with and without an MRI compatible spirometer. Magn Reson Med. 2016;76(5):1542-50.
23. Voskrebenzev A, Gutberlet M, Kaireit TF, Wacker F, Vogel-Claussen J. Low-pass imaging of dynamic acquisitions (LIDA) with a group-oriented registration (GOREG) for proton MR imaging of lung ventilation. Magn Reson Med. 2017;78(4):1496-505.
24. Voskrebenzev A, Gutberlet M, Klimeš F, Kaireit TF, Schönfeld C, Rotärmel A, et al. Feasibility of quantitative regional ventilation and perfusion mapping with phase-resolved functional lung (PREFUL) MRI in healthy volunteers and COPD, CTEPH, and CF patients. Magn Reson Med. 2018;79(4):2306-14.
25. Mastro KA, Flynn L, Preuster C, Summers-Gibson L, Stein MH. The Effects of Anesthesia on the Pediatric Developing Brain: Strategies to Reduce Anesthesia Use in Pediatric MRI and Nursing's Role in Driving Patient Safety. J Perianesth Nurs. 2019;34(5):900-10.
26. Walkup LL, Tkach JA, Higano NS, Thomen RP, Fain SB, Merhar SL, et al. Quantitative Magnetic Resonance Imaging of Bronchopulmonary Dysplasia in the Neonatal Intensive Care Unit Environment. Am J Respir Crit Care Med. 2015;192(10):1215-22.
27. Stein JM, Walkup LL, Brody AS, Fleck RJ, Woods JC. Quantitative CT characterization of pediatric lung development using routine clinical imaging. Pediatr Radiol. 2016;46(13):1804-12.
28. Adams EW, Harrison MC, Counsell SJ, Allsop JM, Kennea NL, Hajnal JV, et al. Increased lung water and tissue damage in bronchopulmonary dysplasia. J Pediatr. 2004;145(4):503-7.

29. Adams EW, Counsell SJ, Hajnal JV, Cox PN, Kennea NL, Thornton AS, et al. Magnetic resonance imaging of lung water content and distribution in term and preterm infants. Am J Respir Crit Care Med. 2002;166(3):397-402.
30. Walkup LL, Woods JC. Newer Imaging Techniques for Bronchopulmonary Dysplasia. Clin Perinatol. 2015;42(4):871-87.
31. Higano NS, Thomen RP, Quirk JD, Huyck HL, Hahn AD, Fain SB, et al. Alveolar Airspace Size in Healthy and Diseased Infant Lungs Measured via Hyperpolarized 3He Gas Diffusion Magnetic Resonance Imaging. Neonatology. 2020;117(6):704-12.
32. Flors L, Mugler JP, 3rd, Paget-Brown A, Froh DK, de Lange EE, Patrie JT, et al. Hyperpolarized Helium-3 Diffusion-weighted Magnetic Resonance Imaging Detects Abnormalities of Lung Structure in Children With Bronchopulmonary Dysplasia. J Thorac Imaging. 2017;32(5):323-32.
33. Kruger SJ, Nagle SK, Couch MJ, Ohno Y, Albert M, Fain SB. Functional imaging of the lungs with gas agents. J Magn Reson Imaging. 2016;43(2):295-315.

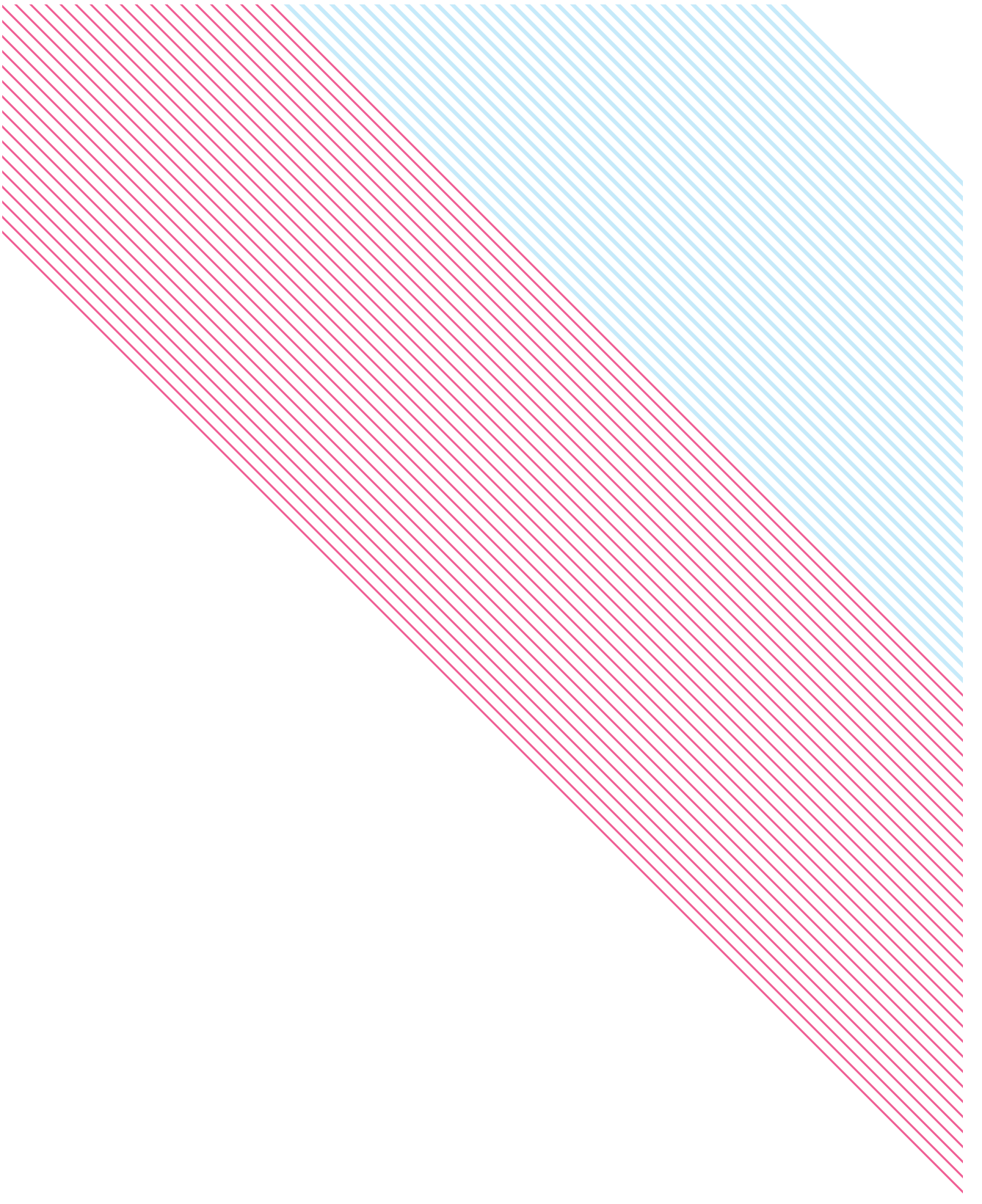

Chapter 9

A clinical guideline for structured assessment of CT-imaging in Congenital Lung Abnormalities

Sergei M Hermelijn, Bernadette BLJ Elders, Pierluigi Ciet,
René MH Wijnen, Harm AWM Tiddens, J Marco Schnater

Paediatric Respiratory Review 2021;37:80-88

Abstract

Objectives: To develop a clinical guideline for structured assessment and uniform reporting of congenital lung abnormalities (CLA) on Computed Tomography (CT)-scans.

Materials and Methods: A systematic literature search was conducted for articles describing CT-scan abnormalities of congenital pulmonary airway malformation(CPAM), bronchopulmonary sequestration(BPS), congenital lobar emphysema(CLE) and bronchogenic cyst(BC). A structured report using objective features of CLA was developed after consensus between a paediatric pulmonologist, radiologist and surgeon

Results: Of 1581 articles identified, 158 remained after title-abstract screening by two independent reviewers. After assessing full-texts, we included 28 retrospective cohort-studies. Air-containing cysts and soft tissue mass are described in both CPAM and BPS while anomalous arterial blood supply is only found in BPS. Perilesional low-attenuation areas, atelectasis and mediastinal shift may be found in all aforementioned abnormalities and can also be seen in CLE as a cause of a hyperinflated lobe. We have developed a structured report, subdivided into five sections: Location & Extent, Airway, Lesion, Vascularization and Surrounding tissue.

Conclusions: CT-imaging findings in CLA are broad and nomenclature is variable. Overlap is seen between and within abnormalities, possibly due to definitions often being based on pathological findings, which is an unsuitable approach for CT imaging. We propose a structured assessment of CLA using objective radiological features and uniform nomenclature to improve reporting.

Introduction

Structured prenatal screening and technical advances in prenatal ultrasound imaging have led to an increase in the detection of congenital lung abnormalities (CLA).(1) Postnatally, computed tomography (CT) is the gold standard for diagnosis in pre-operative patients due to its high spatial resolution and short acquisition times. Yet, the diagnosis can be challenging due to overlapping features and inconsistent use of nomenclature.(2)

The most common CLA in order of prevalence are congenital pulmonary airway malformation (CPAM), bronchopulmonary sequestration (BPS), congenital lobar emphysema (CLE) and bronchogenic cyst (BC).

CPAM is a cystic malformation with aberrant connection to the tracheobronchial tree caused by overgrowth of terminal bronchioles. Its appearance on postnatal imaging is dependent on the subtype (type 0 - 4) of CPAM, and varies from a mass consisting of multiple small cysts to large air-filled cysts (figure 1-2).(3). BPS is an afunctional lung mass without a connection to the bronchial tree, and vascularized by systemic arteries (figure 3-4). A distinction is made between intralobar sequestration (ILS), which is located within the pleura of the lung, and extralobar sequestration (ELS) which is contained within its own pleura. Both types receive systemic arterial blood supply and often differ in venous drainage as ILS commonly drain to the pulmonary vein, while ELS often drain to the azygos system. A hybrid BPS is reported when a sequestration is seen in conjunction with CPAM.(4) CLE is a hyperinflation of lung tissue that usually occupies a whole lobe and is caused by abnormal bronchial wall development or external compression on an airway (figure 5).(5) Some prefer the term hyperinflation instead of emphysema as overdistention of intact alveoli is found on pathology opposed to destructed alveoli in emphysema.(6) We encourage the use of the newer term Congenital Lobar Overinflation (CLO) as this more accurately describes this disease, but will use CLE throughout this paper to prevent confusion in the literature review. BC is a fluid-filled cyst, typically located in the mediastinum near the carina, but also occurring within the lung parenchyma.(7) Contents may have a mucoid substance or appear milky due to calcium depositions within the cyst.(7, 8)

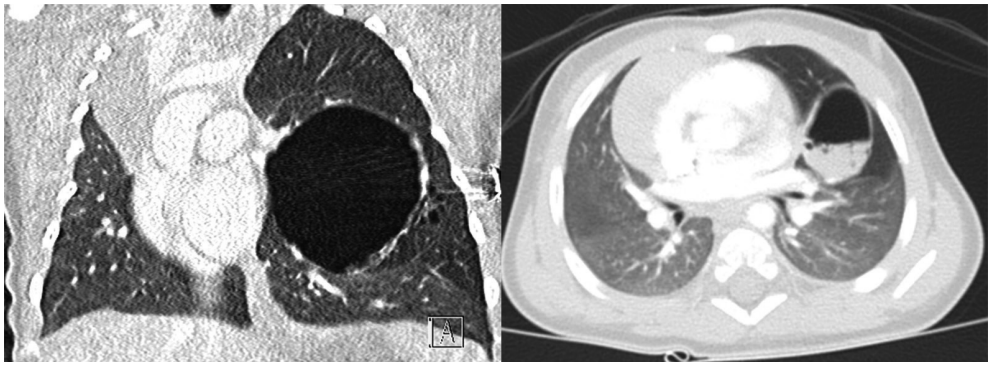

Figure 1. Pathology diagnosis: Congenital Pulmonary Airway Malformation type 1. Radiological diagnosis according to standardized report: Left image: coronal CT-image depicting an air-filled dominant cyst with a well-defined border, with adjacent smaller cysts, comprising up to 2/3 of the left upper lobe. Normal pulmonary arterial and venous vascularization. Some mass effect with slight rightward mediastinal shift.

Right image: Axial CT-image depicting a dominant cyst with a well-defined thickened border and air-fluid level, comprising up to 1/3 of the left upper lobe. Normal pulmonary arterial and venous vascularization and adjacent low-attenuation region of 2/3 of the left upper lobe. Some mass effect with slight rightward mediastinal shift.

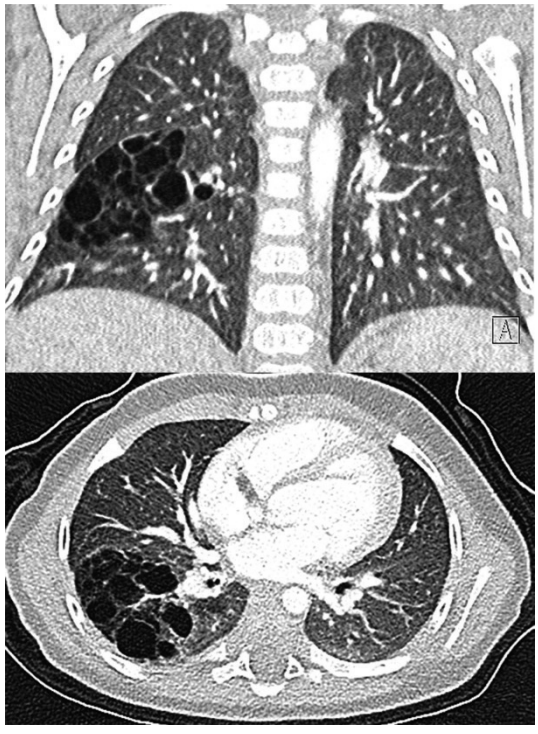

Figure 2. Pathology diagnosis: Congenital Pulmonary Airway Malformation type 2. Radiological diagnosis according to standardized report: Coronal and axial CT-image depicting a cluster of multiple air-filled cysts with a well-defined border, comprising up to 2/3 of the right middle lobe. Normal pulmonary arterial and venous vascularization and no abnormalities of adjacent lung tissue.

Figure 3. Pathology diagnosis: Bronchopulmonary Sequestration. Radiological diagnosis according to standardized report: Coronal CT-image depicting a homogeneous lesion with a well-defined border, comprising the whole right lower lobe. Arterial blood supply from the descending thoracic aorta by a single blood vessel and normal pulmonary venous drainage. No abnormalities of adjacent lung tissue in this image.

Figure 4. Pathology diagnosis: Hybrid Bronchopulmonary Sequestration. Radiological diagnosis according to standardized report: Coronal and axial CT-images depicting a homogeneous lesion with a well-defined border and adjacent cluster of multiple cysts, comprising up to 2/3 of the right lower lobe. Arterial blood supply from the descending thoracic aorta by a single blood vessel and pulmonary venous drainage by enlarged pulmonary veins . No abnormalities of adjacent lung tissue in this image.

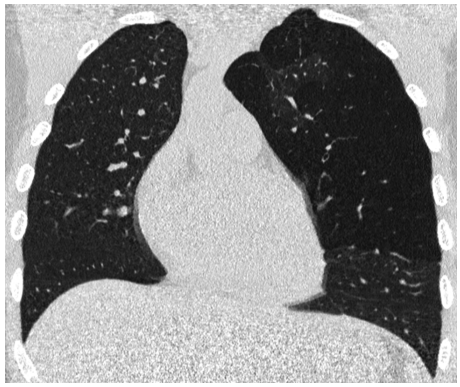

Figure 5. Pathology diagnosis: Congenital Lobar Emphysema. Radiological diagnosis according to standardized report: Coronal CT-image depicting a hyperinflated region of the whole left upper lobe, with slight rightward mediastinal shift. No abnormalities of the central and peripheral airways depicted in this image.

Most CLA are asymptomatic and thus are often missed if not detected prenatally. In some cases they may be an incidental finding, such as BC, which may cause dysphagia, persistent cough or retrosternal chest pain.(8) ELS and CPAM type 2 may be diagnosed in association with other congenital anomalies such as congenital diaphragmatic hernia, vertebral anomalies and congenital heart disease.(9, 10) However, most BPS remain asymptomatic, especially ELS.(6, 11, 12) In contrast, CLE usually causes respiratory distress within the first 6 months and earlier presentation is associated with worse distress.(13) More recently, bronchial atresia is increasingly being reported in conjunction with CPAM and CLE as a diagnosis depicting an abrupt interruption of the airway with a distal mucus plug. However, this is more likely a feature which may be found in combination with the underlying CLA rather than a diagnosis on its own.(14, 15)

While surgical resection is the generally accepted treatment in symptomatic patients, the management in asymptomatic patients is still under debate.(16) Standardized guidelines for describing radiological CLA-related features on chest CT are lacking, although a clear pathological classification exists.(10) We aimed to summarize the radiological appearance of parenchymal abnormalities in CLA on chest CT and devised a standardized, objective manner of assessing and reporting them.

Materials and Methods

Systematic literature search

To assess current descriptions in the literature we conducted a systematic literature search in accordance with PRISMA guidelines.(17) A search of all published reports on postnatal CT-imaging of CLA was carried out in the PubMed, EmBase, Medline, Web of Science, Cochrane and Google Scholar database in August 2017 and updated in July 2019. The search strategy is summarized in figure 6 and search terms are supplied in the supplementary materials.

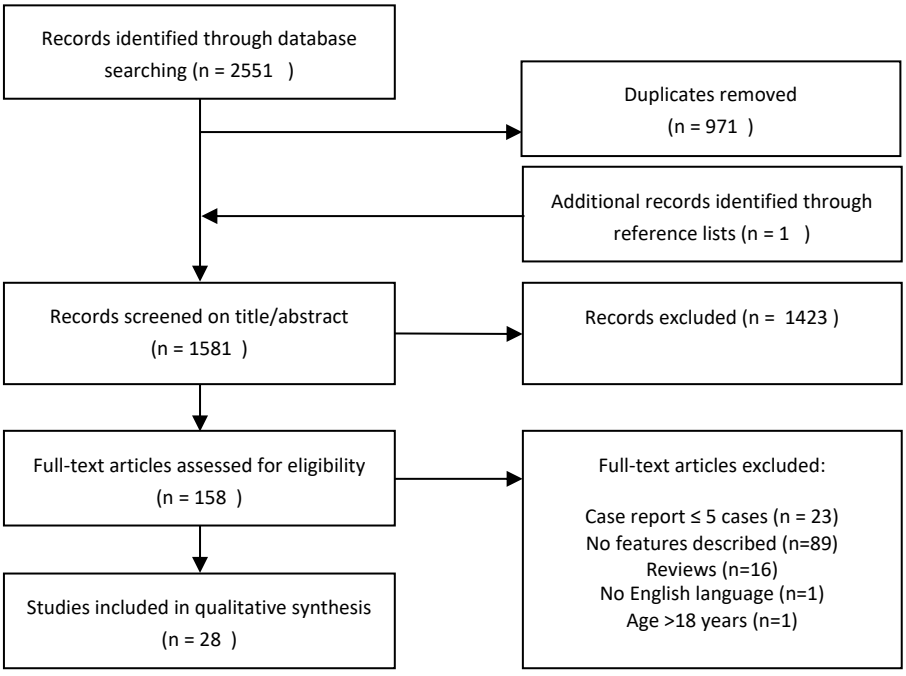

Figure 6. Article selection process flow chart

All articles published in English until August 2018 and describing a paediatric cohort with a median/mean age ≤ 18 years were included. Articles and case-series exceeding 5 cases, describing parenchymal CT-abnormalities of CPAM, BPS, CLE and BC, were studied in detail. Articles with a cohort consisting of multiple CLA and < 5 cases for each individual diagnosis were included as well. Articles that only described prenatal imaging and articles reporting findings of other than the aforementioned CLA were excluded. Articles reporting only confirmation of diagnosis by means of CT-imaging without describing specific parenchymal abnormalities in detail were excluded as well.

Data extraction & construction of guide

From each article we extracted all CT-imaging descriptions for the CLA concerned, and based our approach on distinctive features which may be useful in diagnosis and clinical decision-making. The pediatric surgeon and pulmonologist screened for clinically relevant features with implications for further management and the pediatric radiologist added essential features for diagnosis. Using the information extracted from these articles, a structured way of reporting was developed by consensus (Figure 7). Reporting of these features was translated into objective radiological terms with help of the Fleischner Society lexicon.(18)

Structured radiology report Congenital Lung Abnormalities

Scan protocol:
□ Inspiration □ Volumetric Slice thickness: mm
□ Expiration □ Volumetric Slice thickness: mm

Contrast enhancement:
□ None
□ Venous phase
□ Arterial phase

A. Findings:

Location & extent:

	RUL	RML	RLL	LUL	LLL
Extent					

1= ⅓ lobe 2= ⅔ lobe 3=complete lobe

Airway:
□ Normal connection
□ Bronchomalacia
□ Atresia

B. Lesion:

Cystic tissue:
- Structure:
  □ Dominant cyst □ Cluster of multiple uniform cysts
- Average cyst size: mm
- Size of largest cyst: mm
- Content:
  □ Air-filled
  □ Fluid-filled
  □ Air-Fluid levels

Solid tissue:

	RUL	RML	RLL	LUL	LLL
Extent					

1= ⅓ lobe 2= ⅔ lobe 3=complete lobe

- Density:
  □ Homogeneous
  □ Heterogeneous

C. Border:

□ Well-defined □ Ill-defined

D. Vascularization:

Arterial:
□ Normal pulmonary
□ Aberrant:
Number & Size: Origin:

Venous:
□ Normal pulmonary
□ Aberrant:
Number & Size: Origin:

E. (Surrounding) tissue:

	RUL	RML	RLL	LUL	LLL
Atelectasis					
Low-attenuation					
Hyperinflation					

1= ⅓ lobe 2= ⅔ lobe 3=complete lobe

□ Mass effect
□ Mediastinal shift
□ Mediastinal herniation

Remarks:

Figure 7. Structured radiologic report Congenital Lung Abnormalities

Results

The updated literature search resulted in 1581 citations of which 158 remained after title/abstract screening and 28 after assessing full texts (figure 6). Articles were independently assessed by two reviewers (SH, BE) and discordant selections were discussed to reach a consensus. All 28 articles reported a retrospective study; no randomized controlled trials were found.

Article characteristics and CT-imaging features can be found in tables 1a-d; bar charts visualizing the weighted prevalence of each feature are displayed in figure 8. The prevalence of features for each abnormality alongside corresponding bar charts are shown in descending order in the supplementary materials.

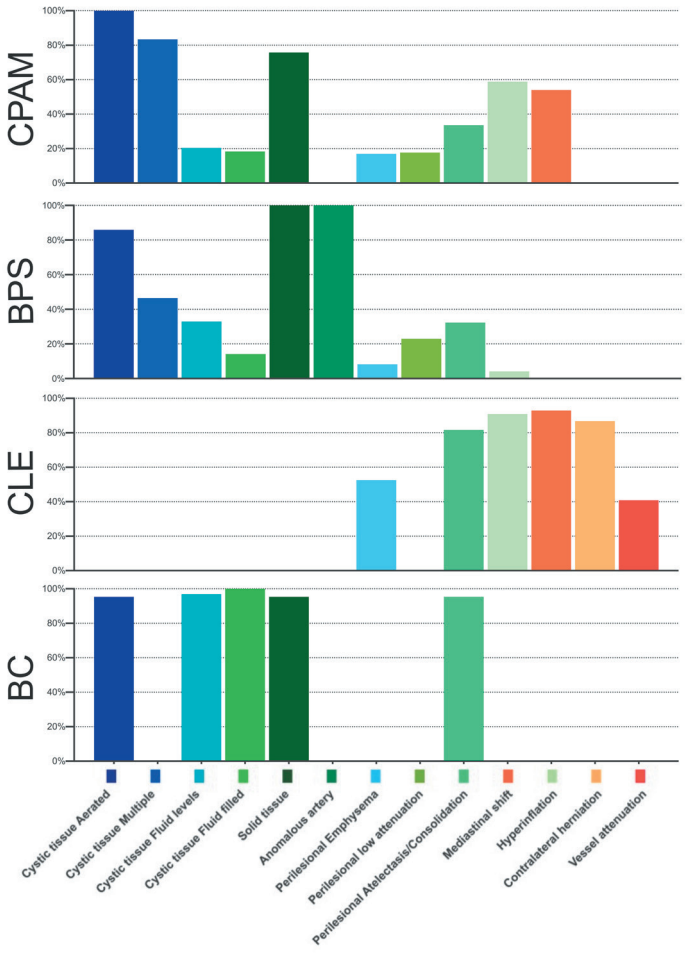

Figure 8. Proportion of CT-imaging abnormalities found in the articles divided by type of Congenital Lung Abnormality

CPAM was described in 16 articles and identified as air-containing cysts in all 16.(6, 19-33) Thirteen of these articles distinguish between a single cyst and multiple cysts (6, 19-30); four also describe fluid-filled cysts (6, 23, 26, 29) and four describe air-fluid levels.(20, 23, 29, 32) Ten articles describe a soft tissue mass which is dependent on the type of CPAM.(6, 19-21, 25, 28-31, 33) Perilesional low-attenuating lung parenchyma (four articles).(22-24, 33) emphysema (four articles) (20, 25, 26, 32), atelectasis (six articles) (20, 22, 23, 25, 31, 32) and hyperinflation (five articles) (21, 22, 29-31) are described, as well as mediastinal shift (six articles).(21, 22, 27, 29, 31, 32)

BPS was described in ten articles and identified as a soft-tissue mass with an anomalous arterial blood supply in all ten.(4, 6, 11, 12, 19, 22, 26, 33-35) Aerated cysts are described in six articles (11, 12, 19, 22, 34, 35) and three articles distinguish between a single cyst and multiple cysts (12, 22, 34). Two articles describe air-fluid levels (11, 34) and one article describes fluid filled cysts.(12) Perilesional emphysema is described in two articles (4, 11) and perilesional low-attenuating lung parenchyma in four.(6, 12, 22, 33) Two articles describe atelectasis (22, 34) and one described mediastinal shift.(22) Low-attenuation (4) and air within the mass (11) are each described in one article.

CLE was described in ten articles and identified as hyperinflation of the affected segment in nine of the ten articles.(5, 6, 13, 19, 27, 33, 36-38) One article describes only emphysematous changes in the lung parenchyma (39), whereas five describe this in addition to hyperinflation. (5, 6, 13, 33, 37) These abnormalities are variably reported in combination with mediastinal shift (eight articles) (5, 6, 13, 27, 36-39), herniation of lung through the mediastinum (seven articles) (5, 13, 27, 36-39), atelectasis of neighbouring lobes (six articles) (5, 13, 36-39) and decreased lung vessel attenuation (five articles).(6, 19, 27, 36, 39) A bronchial stenosis is described in six articles.(5, 13, 33, 36, 37, 39) One described a normal bronchial tree (38) and three did not report these findings.(6, 19, 27)

Mediastinal and parenchymal BC was described in four articles (6, 7, 19, 26) and identified as a solitary, round or ovoid cystic structure in three articles.(6, 7, 19) Two describe a soft tissue mass (7, 26), two a well-defined, smooth border (6, 19) and one article describes atelectasis of neighbouring structures.(7)

Anomalous artery in BPS, contralateral herniation and vessel attenuation in CLE were the only exclusive features.

We assessed all the features described in our literature search, categorized them based on anatomical distribution as is customary in lung CT imaging (40) and selected features relevant for radiological diagnosis and/or surgical planning. These features were divided into five clinically important main categories: the location and extent, airway connection, characterization of the lesion, vascularization and aspect of surrounding lung tissue.

Discussion

Our results show a broad range of CT- imaging findings in CLA and inconsistent use of nomenclature. Imaging features clearly overlap between and within various abnormalities. This is partly due to definitions being based on pathological findings, which might not be the best approach for CT-imaging.(2, 33, 41, 42) A glossary of terms for thoracic imaging is provided by the Fleischner Society, but it is not uniformly used and not specifically developed for CLA.(18)

Overlap in CT-imaging features

In CPAM, various cystic abnormalities corresponding to the respective subtypes are seen. Depending on the composition of the cohort, either single aerated cysts are described (31-33) or multiple cysts.(6, 19-30) In CPAM type 3, a soft tissue mass can be seen, also one of the most common features in BPS. The systemic arterial blood supply to the lung mass in BPS distinguishes this entity from a CPAM although this is not always easily discernible. Perilesional features such as low-attenuation, mediastinal shift, and atelectasis may be seen in all CLA due to mass effect and are dependent on the size and location of the lesion. (29, 43) In both BPS and CPAM the terms hypodense area and emphysema are variably used to describe an area of low attenuation although emphysema suggests structural lung damage. Similarly, in CLE the terms hyperinflation or overinflation are sometimes preferred instead of emphysema because pathological examination shows overdistended but intact alveoli in contrast to the destructed alveoli seen in emphysema.(6) Previous studies assessing correlations between CT findings and pathology show a good correlation and accurate diagnosis of the type of CLA on CT. Yet, distinguishing CPAM subtypes and hybrid lesions proved to be more difficult.(7, 22-24, 28, 33) Previous studies suggested different classification systems for the various CLA based on either clinical relevance, pathological appearance or pathogenesis.(2, 42, 44-46) Each classification system has its merits and limitations and, so far, no consensus has been reached on the optimal classification of these CLA.

In our opinion, a more objective description depending on the most relevant findings is needed. This will ensure that future studies use the same parameters, which facilitates comparison of study findings. In order to achieve this, we have constructed a structured radiologic report which can be used as a guide for structured assessment and uniform reporting of CT-imaging findings in CLA. We have subdivided this into five sections (Location & Extent, Airway, Lesion, Vascularization and Surrounding tissue) and explain the relevance of the features.

Location & Extent (figure 7, section A)

The location and extent of the CLA is essential for the clinical management and potential surgical plan.(33) For instance, it is known that upper lobe involvement is associated with

more severe symptoms.(13, 36, 37) Similar to reporting CT-imaging of cystic fibrosis, we suggest reporting the affected lobes as well as the extent in each lobe expressed as the affected volume in thirds (up to ⅓ lobe, up to ⅔ lobe, complete lobe; see figure 7, section A).(47) This lobe-oriented approach is clinically relevant as a lobectomy is preferred over a wedge resection, due to more frequent postoperative complications such as persistent air leakage, residual disease in up to 15% of cases (48) and risk of malignancy in the residual tissue.(49, 50)

Airway (figure 7, section B)

Different CLA can be distinguished by looking at the connection to the bronchial tree. In BPS and BC no airway connection with the bronchial tree is found whereas in CPAM and CLE an aberrant connection may be identified.(51) An aberrant connection can either be a bronchomalacia or bronchial atresia, both of which can be diagnosed with bronchoscopy, inspiratory and expiratory CT-scan, cine-CT, dynamic MRI and on pathology.(52, 53) On CT-imaging, bronchomalacia can be diagnosed in cooperative children by computing the change in cross-sectional area between inspiration and expiration.(6, 52) In non-cooperative children, CT is performed in cine-mode or by changing lung volume under anaesthesia.(54) Atresia is an abrupt complete interruption of the bronchus which can be identified on CT-imaging as a mucus plug distal from the atresia and a local hypodense region distally. The mucus plug is formed due to accumulated mucus produced in the patent distal bronchus (mucocèle).(14, 15, 55) The hypodense region is a result of hyperinflation of the excluded lung parenchyma by collateral ventilation through the pores of Kohn.(56) Especially in smaller children, atresia may be difficult to diagnose due to the small diameter of distally located airways in relation to the resolution of the CT-scanner.(52)

Lesion (figure 7, section C)

CLA lesions are variable in appearance and can be characterized as cystic, solid or hybrid lesions. Cystic lesions can be seen in CPAM, BPS and BC and can be distinguished by number, size and content of the cyst(s). Hybrid lesions exhibit features of both CPAM and BPS.

In CPAM, the average cyst size and size of the largest cyst are used to determine the subtype. A cut off at 2 cm for largest cyst size is suggested for distinguishing CPAM types 1 and 4 from type 2, while a soft tissue mass is seen in CPAM types 0 and 3.(6, 19, 22-24, 26, 29, 30, 32, 33) Classification on the basis of cyst size and aspect showed a good correlation with final histological diagnosis (22-24, 29, 33), although cyst size may be dependent on age and growth of the child and the cut-off values are arbitrarily chosen. Due to the association between CPAM type 4 and pleuropulmonary blastoma (PPB), classification is desirable to determine treatment and follow-up. PPB is a rare, aggressive, pediatric lung tumor which appears as a distally located cystic or solid mass.(57, 58) The risk of PPB type 1 is significantly increased in CPAM type 4; still it is often thought to be the same entity.(59, 60) Distinction

on imaging is difficult, although cystic PPB lesions seem to have a bigger largest cyst, are septated and more often contain solid components.(21, 22)

In BPS, the appearance of ILS ranges from aerated cystic lesions to homogeneous or heterogeneous solid lesions. This variation may be the result of collateral airflow to the homogeneous solid lesion through the 'pores of Kohn'. Depending on the degree of this airflow, the appearance might become heterogeneous with hypodense areas or air-filled cysts.(12, 61-65) In contrast, ELS rarely contains air as it is separated from the normal lung parenchyma by its own pleura. Thus, the presence or absence of air may be used to distinguish ELS from ILS.(4, 6, 11, 12)

In BC, the common mediastinal localization makes it difficult to characterize the cyst and to distinguish it from malignant neoplasms and lymphadenopathy.(6) However, BC may occur in the lung parenchyma as well and present with a smooth well-defined cyst wall, opposed to a thick irregular wall. Contrast agents usually enhance surrounding tissue rather than the BC. Furthermore, opposed to homogeneous BC, a heterogeneous mass with central contrast-enhancement is more suggestive for a mediastinal neoplasm.(6, 7)

BC are commonly fluid filled and as such can objectively be distinguished from a soft tissue mass if the region of interest measurement is lower than the cut-off value of 20 Hounsfield units (22) or by comparing content to fluid in the gall bladder or spinal canal.(6, 7, 19, 26) An internal air-fluid level and enhanced thick cyst wall are signs of infection.(3)

Vascularization (figure 7, section D)

Abnormal vascularization is an important distinctive feature of BPS and is often the only difference between BPS and CPAM type 3 on CT imaging. Particularly for planning surgery or interventional radiology, the number, size and origin of abnormal vessels is important. Spontaneous regression of ELS is more likely with arterial blood supply by multiple small arteries opposed to a large feeding artery.(66) Venous drainage to the pulmonary vein is common in ILS, while ELS often drain to the azygos system. This may help distinguishing between different types of BPS.(34) Hypervascularity is often seen in BPS and is caused by a high systemic blood pressure in the low-resistance lung circulation.(4, 12, 35)

Surrounding tissue (figure 7, section E)

Surrounding lung tissue may be affected by the lesion and show abnormalities as well. Mediastinal shift and atelectasis may be seen in large lesions and increase the risk of becoming symptomatic.(29) Growth and increasing solid appearance are other concerning features.(43, 67) In PPB , mediastinal shift, hyperdensity and lack of hypodensity (22) is seen more often as well as pleural effusion and right side predominance.(68) Hyperinflation is seen in both CPAM and PPB, although studies contradict each other on its predictive value.(21, 22)

Perilesional low-attenuation areas indicate poorly perfused or ventilated regions.(69) It is hypothesized these regions may be CLE alongside CPAM, which would support the hypothesis that all CLA share a common pathogenesis.(14, 15, 33, 44)

Worsening of symptoms may occur after chest tube insertion when CPAM or CLE is misdiagnosed as a pneumothorax. Although commonly misdiagnosed as such, a pneumothorax is rarely associated with CLE.(21, 23, 36, 37, 39, 59) Vascular markings and low-attenuation surrounding the cyst suggest a CPAM (27), while cranial or caudal lung compression is seen in CLE opposed to lung collapse towards the hilum.

Conclusion

Due to the wide variety of CT-imaging features in CLA, assessment and reporting can be difficult. Distinction may be hard and depends on the quality and type of scan. The inconsistent nomenclature when describing these abnormalities leads to confusing, non-uniform and incomplete reports.(33) Radiological appearances should not be categorized using a pathological classification as the overlap between abnormalities in both imaging features and pathology make distinction on CT-imaging difficult and unreliable.(2) When a structured approach is used, uniform and complete reports with well-defined terms are made, which is beneficial in clinical decision-making.(70, 71) In our structured report we have captured key features of structural changes required for diagnosing the different CLA and clinical decision-making . Structured assessment and reporting of objective radiologic features utilizing uniform nomenclature is time-efficient and could improve the diagnostic accuracy. Using this method and avoiding subjective interpretation could lead to better quality of reports in CT- imaging of CLA. We aim to test the proposed structured report in a large multi-centre longitudinal study.

Acknowledgements
We would like to acknowledge W.M. Bramer, from the Erasmus MC- medical library, for his assistance in the literature search.

References

1. Stocker LJ, Wellesley DG, Stanton MP, Parasuraman R, Howe DT. The increasing incidence of foetal echogenic congenital lung malformations: an observational study. Prenat Diagn. 2015;35(2):148-53.
2. Bush A. Congenital lung disease: a plea for clear thinking and clear nomenclature. Pediatr Pulmonol. 2001;32(4):328-37.
3. Lee EY, Boiselle PM, Cleveland RH. Multidetector CT evaluation of congenital lung anomalies. Radiology. 2008;247(3):632-48.
4. Hang JD, Guo QY, Chen CX, Chen LY. Imaging approach to the diagnosis of pulmonary sequestration. Acta Radiol. 1996;37(6):883-8.
5. Karnak I, Şenocak ME, Ciftci AO, Büyükpamukçu N. Congenital lobar emphysema: Diagnostic and therapeutic considerations. J Pediatr Surg. 1999;34(9):1347-51.
6. El-Medany S, El-Noueam K, Sakr A, Galal A. Role of multi slice computed tomography in the evaluation of congenital anomalies of tracheobronchial tree and lungs. Egypt J Radiol Nucl Med. 2011;42(3):315-25.
7. McAdams HP, Kirejczyk WM, Rosado-de-Christenson ML, Matsumoto S. Bronchogenic cyst: imaging features with clinical and histopathologic correlation. Radiology. 2000;217(2):441-6.
8. Sarper A, Ayten A, Golbasi I, Demircan A, Isin E. Bronchogenic cyst. Tex Heart Inst J. 2003;30(2):105-8.
9. Durell J, Lakhoo K. Congenital cystic lesions of the lung. Early Hum Dev. 2014;90(12):935-9.
10. Stocker JT. Congenital pulmonary airway malformation - a new name for and an expanded classification of congenital cystic adenomatoid malformation of the lung. Histopathology. 2002(41):424-31.
11. Kang M, Kh, elwal N, Ojili V, Rao KLN, Rana SS. Multidetector CT angiography in pulmonary sequestration. J Comput Assisted Tomogr. 2006;30(6):926-32.
12. Ikezoe J, Murayama S, Godwin JD, Done SL, Verschakelen JA. Bronchopulmonary sequestration: CT assessment. Radiology. 1990;176(2):375-9.
13. Choudhury SR, Chadha R, Mishra A, Kumar V, Singh V, Dubey NK. Lung resections in children for congenital and acquired lesions. Pediatr Surg Int. 2007;23(9):851-9.
14. Kunisaki SM, Fauza DO, Nemes LP, Barnewolt CE, Estroff JA, Kozakewich HP, et al. Bronchial atresia: the hidden pathology within a spectrum of prenatally diagnosed lung masses. J Pediatr Surg. 2006;41(1):61-5; discussion -5.
15. Riedlinger WF, Vargas SO, Jennings RW, Estroff JA, Barnewolt CE, Lillehei CW, et al. Bronchial atresia is common to extralobar sequestration, intralobar sequestration, congenital cystic adenomatoid malformation, and lobar emphysema. Pediatr Dev Pathol. 2006;9(5):361-73.
16. Morini F, Zani A, Conforti A, van Heurn E, Eaton S, Puri P, et al. Current Management of Congenital Pulmonary Airway Malformations: A “European Pediatric Surgeons’ Association” Survey. Eur J Pediatr Surg. 2018;28(1):1-5.

17. Moher D, Liberati A, Tetzlaff J, Altman DG, Group P. Preferred reporting items for systematic reviews and meta-analyses: the PRISMA statement. BMJ. 2009;339:b2535.
18. Hansell DM, Bankier AA, MacMahon H, McLoud TC, Muller NL, Remy J. Fleischner Society: glossary of terms for thoracic imaging. Radiology. 2008;246(3):697-722.
19. Bondioni MP, Gatta D, Lougaris V, Palai N, Signorelli M, Michelini S, et al. Congenital cystic lung disease: prenatal ultrasound and postnatal multidetector computer tomography evaluation. Correlation with surgical and pathological data. Radiol Med. 2014;119(11):842-51.
20. Chow PC, Lee SL, Tang MHY, Chan KL, Lee CP, Lam BCC, et al. Management and outcome of antenatally diagnosed congenital cystic adenomatoid malformation of the lung. Hong Kong Med J. 2007;13(1):31-9.
21. Feinberg A, Hall NJ, Williams GM, Schultz KAP, Miniati D, Hill DA, et al. Can congenital pulmonary airway malformation be distinguished from Type i pleuropulmonary blastoma based on clinical and radiological features? J Pediatr Surg. 2016;51(1):33-7.
22. Griffin N, Devaraj A, Goldstraw P, Bush A, Nicholson AG, Padley S. CT and histopathological correlation of congenital cystic pulmonary lesions: a common pathogenesis? Clin Radiol. 2008;63(9):995-1005.
23. Kim WS, Lee KS, Kim IO, Suh YL, Im JG, Yeon KM, et al. Congenital cystic adenomatoid malformation of the lung: CT-pathologic correlation. AJR Am J Roentgenol. 1997;168(1):47-53.
24. Lanza C, Bolli V, Galeazzi V, Fabrizzi B, Fabrizzi G. Cystic adenomatoid malformation in children: CT histopathological correlation. Radiol Med. 2007;112(4):612-9.
25. Lee HJ, Song MJ, Cho JY, Lee YH. Echogenic fetal lung masses: Comparison of prenatal sonographic and postnatal CT findings. J Clin Ultrasound. 2003;31(8):419-24.
26. Mata JM, Caceres J, Lucaya J, Garcia-Conesa JA. CT of congenital malformations of the lung. Radiographics. 1990;10(4):651-74.
27. Prabhu S, Choudhury S, Solanki R, Shetty G, Agarwala S. Inadvertent chest tube insertion in congenital cystic adenomatoid malformation and congenital lobar emphysema-highlighting an important problem. Indian J Radiol Imaging. 2013;23(1):8-14.
28. Shimohira M, Hara M, Kitase M, Takeuchi M, Shibamoto Y, Kurono K, et al. Congenital pulmonary airway malformation: CT-pathologic correlation. J Thorac Imaging. 2007;22(2):149-53.
29. Tawil MI, Pilling DW. Congenital cystic adenomatoid malformation: Is there a difference between the antenatally and postnatally diagnosed cases? Pediatr Radiol. 2005;35(1):79-84.
30. Winters WD, Effmann EL, Nghiem HV, Nyberg DA. Disappearing fetal lung masses: Importance of postnatal imaging studies. Pediatr radiol. 1997;27(6):535-9.
31. Lima JS, Camargos PAM, Aguiar RALP, Campos AS, Aguiar MJB. Pre and perinatal aspects of congenital cystic adenomatoid malformation of the lung. J Matern -Fetal Neonatal Med. 2014;27(3):228-32.
32. Zhang ZJ, Huang MX. Children with congenital cystic adenomatoid malformation of the lung CT diagnosis. Int J Clin Exp Med. 2015;8(3):4415-9.

33. Kyncl M, Koci M, Ptackova L, Hornofova L, Ondrej F, Snajdauf J, et al. Congenital bronchopulmonary malformation: CT histopathological correlation. Biomed Pap Med Fac Univ Palacky Olomouc Czech Repub. 2016;160(4):533-7.
34. Ou J, Lei X, Fu Z, Huang Y, Liu E, Luo Z, et al. Pulmonary sequestration in children: A clinical analysis of 48 cases. Int J Clin Exp Med. 2014;7(5):1355-65.
35. Ren JZ, Zhang K, Huang GH, Zhang MF, Zhou PL, Han XW, et al. Assessment of 64-row computed tomographic angiography for diagnosis and pretreatment planning in pulmonary sequestration. Radiol Med. 2014;119(1):27-32.
36. Thakral CL, Maji DC, Sajwani MJ. Congenital lobar emphysema: experience with 21 cases. Pediatr Surg Int.17(2):88-91.
37. Özçelik U, Göçmen A, Kiper N, Doğru D, Dilber E, Yalçin EG. Congenital lobar emphysema: Evaluation and long-term follow-up of thirty cases at a single center. Pediatr Pulmonol. 2003;35(5):384-91.
38. Cataneo DC, Rodrigues OR, Hasimoto EN, Schmidt Jr AF, Cataneo AJM. Congenital lobar emphysema: 30-year case series in two university hospitals. J Bras Pneumol. 2013;39(4):418-26.
39. Song ZW, Ge W, Xu CY, Fang BD, Yang CY, Zhang HL, et al. The diagnostic value of multislice computed tomography in children with congenital lobar emphysema. Expert Rev Med Devices. 2011;8(4):435-9.
40. Raju S, Ghosh S, Mehta AC. Chest CT Signs in Pulmonary Disease: A Pictorial Review. Chest. 2017;151(6):1356-74.
41. Epelman M, Kreiger PA, Servaes S, Victoria T, Hellinger JC. Current imaging of prenatally diagnosed congenital lung lesions. Semin Ultrasound CT MR. 2010;31(2):141-57.
42. Newman B. Congenital bronchopulmonary foregut malformations: concepts and controversies. Pediatr Radiol. 2006;36(8):773-91.
43. van Leeuwen K, Teitelbaum DH, Hirschl RB, Austin E, Adelman SH, Polley TZ, et al. Prenatal diagnosis of congenital cystic adenomatoid malformation and its postnatal presentation, surgical indications, and natural history. J Pediatr Surg. 1999;34(5):794-8; discussion 8-9.
44. Langston C. New concepts in the pathology of congenital lung malformations. Semin Pediatr Surg. 2003;12(1):17-37.
45. Seear M, Townsend J, Hoepker A, Jamieson D, McFadden D, Daigneault P, et al. A review of congenital lung malformations with a simplified classification system for clinical and research use. Pediatr Surg Int. 2017;33(6):657-64.
46. Lee ML, Tsao LY, Chaou WT, Yang AD, Yeh KT, Wang JK, et al. Revisit on congenital bronchopulmonary vascular malformations: a haphazard branching theory of malinosculations and its clinical classification and implication. Pediatr Pulmonol. 2002;33(1):1-11.
47. Brody AS, Klein JS, Molina PL, Quan J, Bean JA, Wilmott RW. High-resolution computed tomography in young patients with cystic fibrosis: distribution of abnormalities and correlation with pulmonary function tests. J Pediatr. 2004;145(1):32-8.

48. Stanton M, Njere I, Ade-Ajayi N, Patel S, Davenport M. Systematic review and meta-analysis of the postnatal management of congenital cystic lung lesions. J Pediatr Surg. 2009;44(5):1027-33.
49. Baird R, Puligandla PS, Laberge JM. Congenital lung malformations: informing best practice. Semin Pediatr Surg. 2014;23(5):270-7.
50. Muller CO, Berrebi D, Kheniche A, Bonnard A. Is radical lobectomy required in congenital cystic adenomatoid malformation? J Pediatr Surg. 2012;47(4):642-5.
51. Correia-Pinto J, Gonzaga S, Huang Y, Rottier R. Congenital lung lesions--underlying molecular mechanisms. Semin Pediatr Surg. 2010;19(3):171-9.
52. Ciet P, Wielopolski P, Manniesing R, Lever S, de Bruijne M, Morana G, et al. Spirometer-controlled cine magnetic resonance imaging used to diagnose tracheobronchomalacia in paediatric patients. Eur Respir J. 2014;43(1):115-24.
53. Ngerncham M, Lee EY, Zurakowski D, Tracy DA, Jennings R. Tracheobronchomalacia in pediatric patients with esophageal atresia: comparison of diagnostic laryngoscopy/bronchoscopy and dynamic airway multidetector computed tomography. J Pediatr Surg. 2015;50(3):402-7.
54. Lee EY, Zucker EJ, Restrepo R, Daltro P, Boiselle PM. Advanced large airway CT imaging in children: evolution from axial to 4-D assessment. Pediatr Radiol. 2013;43(3):285-97.
55. Gipson MG, Cummings KW, Hurth KM. Bronchial atresia. Radiographics. 2009;29(5):1531-5.
56. Desir A, Ghaye B. Congenital abnormalities of intrathoracic airways. Radiol Clin North Am. 2009;47(2):203-25.
57. Papaioannou G, Sebire NJ, McHugh K. Imaging of the unusual pediatric 'blastomas'. Cancer Imaging. 2009;9:1-11.
58. Feinberg A, Hall NJ, Williams GM, Schultz KA, Miniati D, Hill DA, et al. Can congenital pulmonary airway malformation be distinguished from Type I pleuropulmonary blastoma based on clinical and radiological features? J Pediatr Surg. 2016;51(1):33-7.
59. MacSweeney F, Papagiannopoulos K, Goldstraw P, Sheppard MN, Corrin B, Nicholson AG. An assessment of the expanded classification of congenital cystic adenomatoid malformations and their relationship to malignant transformation. Am J Surg Pathol. 2003;27(8):1139-46.
60. Hill DA, Dehner LP. A cautionary note about congenital cystic adenomatoid malformation (CCAM) type 4. Am J Surg Pathol. 2004;28(4):554-5; author reply 5.
61. Mirza B, Raza AB, Ijaz I, Ijaz L, Naz F, Sheikh A. Intralobar pulmonary sequestration masquerading as congenital lobar emphysema. J Indian Assoc Pediatr Surg. 2011;16(1):15-7.
62. Kim M, Woo JJ, An JK, Jung YY, Choi YS. A Pulmonary Sequestered Segment with an Aberrant Pulmonary Arterial Supply: A Case of Unique Anomaly. Korean Journal of Radiology. 2016;17(2):302-5.
63. Ferretti GR, Jouvan FB, Coulomb M. MDCT Demonstration of Intralobar Pulmonary Sequestration of the Right Upper Lobe in an Adult. American Journal of Roentgenology. 2005;185(6):1663-4.
64. Stern EJ, Webb WR, Warnock ML, Salmon CJ. Bronchopulmonary sequestration: dynamic, ultrafast, high-resolution CT evidence of air trapping. AJR Am J Roentgenol. 1991;157(5):947-9.
65. Cooke CR. Bronchopulmonary sequestration. Respir Care. 2006;51(6):661-4.

66. Yoon HM, Kim EAR, Chung SH, Kim SO, Jung AY, Cho YA, et al. Extralobar pulmonary sequestration in neonates: The natural course and predictive factors associated with spontaneous regression. Eur Radiol. 2017;27(6):2489-96.
67. Cook J, Chitty LS, De Coppi PD, Ashworth M, Wallis C. The natural history of prenatally diagnosed congenital cystic lung lesions: Long-term follow-up of 119 cases. Arch Dis Child. 2017.
68. Naffaa LN, Donnelly LF. Imaging findings in pleuropulmonary blastoma. Pediatr Radiol. 2005;35(4):387-91.
69. Tiddens HA, Rosenow T. What did we learn from two decades of chest computed tomography in cystic fibrosis? Pediatr Radiol. 2014;44(12):1490-5.
70. Larson DB, Towbin AJ, Pryor RM, Donnelly LF. Improving consistency in radiology reporting through the use of department-wide standardized structured reporting. Radiology. 2013;267(1):240-50.
71. Ganeshan D, Duong PT, Probyn L, Lenchik L, McArthur TA, Retrouvey M, et al. Structured Reporting in Radiology. Acad Radiol. 2018;25(1):66-73.

Supplementary materials

Supplementary material 1: Search strategy

Database	Search query
Embase	('lung malformation'/de OR 'congenital lung disease'/de OR 'cystic adenomatoid malformation'/de OR 'lung sequestration'/de OR 'lung disease'/exp/dm_cn OR 'lung emphysema'/exp/dm_cn OR 'lung lesion'/exp/dm_cn OR ('congenital malformation'/de AND ('lung disease'/de OR airway/exp OR 'lower respiratory tract'/de OR 'lung'/de)) OR (((lung OR pulmon* OR extrapulmon* OR intrapulmon* OR bronch* OR 'cyst* adenomat*' OR cystadenomat* OR airway* OR lobe OR extralob* OR intralob* OR lobar) NEAR/3 (malform* OR abnormal* OR anomal* OR congenital* OR lesion* OR sequestrat*)) OR (respirator* NEAR/3 cyst* NEAR/3 dysplasia*)):ab,ti) AND ('infant'/exp OR 'infancy'/exp OR 'perinatal period'/exp OR (infan* OR newborn* OR neonat* OR postnatal* OR perinatal*):ab,ti) AND ('computer assisted tomography'/de OR 'computed tomography scanner'/de OR (((cat) NEXT/1 (scan)) OR ct OR (compute* NEAR/3 tomograph*)):ab,ti) NOT ([animals]/lim NOT [humans]/lim) NOT ([Conference Abstract]/lim OR [Letter]/lim OR [Note]/lim OR [Editorial]/lim) AND [english]/lim
Medline Ovid	(Cystic Adenomatoid Malformation of Lung, Congenital/ OR Bronchopulmonary Sequestration/ OR Bronchogenic Cyst/ OR Lung Diseases/co OR Pulmonary Emphysema/co OR (Congenital Abnormalities/ AND (Lung Diseases/ OR lung/)) OR (((lung OR pulmon* OR extrapulmon* OR intrapulmon* OR bronch* OR cyst* adenomat* OR cystadenomat* OR airway* OR lobe OR extralob* OR intralob* OR lobar) ADJ3 (malform* OR abnormal* OR anomal* OR congenital* OR lesion* OR sequestrat*)) OR (respirator* ADJ3 cyst* ADJ3 dysplasia*)).ab,ti.) AND (exp infant/ OR (infan* OR newborn* OR neonat* OR postnatal* OR perinatal*).ab,ti.) AND (Tomography, X-Ray Computed/ OR (((cat) ADJ (scan)) OR ct OR (compute* ADJ3 tomograph*)).ab,ti.) NOT (exp animals/ NOT humans/) NOT (letter OR news OR comment OR editorial OR congresses OR abstracts).pt. AND english.la.
Web of science	TS=(((((lung OR pulmon* OR extrapulmon* OR intrapulmon* OR bronch* OR "cyst* adenomat*" OR cystadenomat* OR airway* OR lobe OR extralob* OR intralob* OR lobar) NEAR/2 (malform* OR abnormal* OR anomal* OR congenital* OR lesion* OR sequestrat*)) OR (respirator* NEAR/2 cyst* NEAR/2 dysplasia*))) AND ((infan* OR newborn* OR neonat* OR postnatal* OR perinatal*)) AND ((((cat) NEAR/1 (scan)) OR ct OR (compute* NEAR/2 tomograph*)))) AND DT=(article) AND LA=(english)
Cochrane	((((lung OR pulmon* OR extrapulmon* OR intrapulmon* OR bronch* OR 'cyst* adenomat*' OR cystadenomat* OR airway* OR lobe OR extralob* OR intralob* OR lobar) NEAR/3 (malform* OR abnormal* OR anomal* OR congenital* OR lesion* OR sequestrat*)) OR (respirator* NEAR/3 cyst* NEAR/3 dysplasia*)):ab,ti) AND ((infan* OR newborn* OR neonat* OR postnatal* OR perinatal*):ab,ti) AND ((((cat) NEXT/1 (scan)) OR ct OR (compute* NEAR/3 tomograph*)):ab,ti)
Google scholar	"lung | pulmonary | bronchopulmonary | bronchogenic | airway | lobe | loba | adenomatoid malformation | abnormalities | anomalies | lesions | sequestration" infant | infancy | newborn | neonatal|postnatal|perinatal "computed | computer tomography" | "computed | computer*tomography"

Supplementary material 2: Most common CLA related CT features

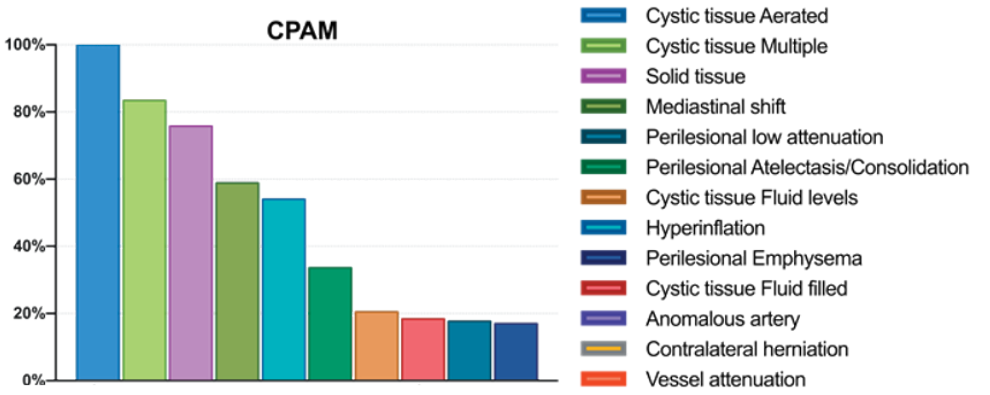

CT-features		
Cystic tissue Aerated	100	%
Cystic tissue Multiple	83	%
Solid tissue	76	%
Mediastinal shift	59	%
Hyperinflation	54	%
Perilesional Atelectasis/Consolidation	34	%
Cystic tissue Fluid levels	20	%
Cystic tissue Fluid filled	18	%
Perilesional low attenuation	18	%
Perilesional Emphysema	17	%
Anomalous artery	0	%
Contralateral herniation	0	%
Vessel attenuation	0	%

Chart & Table 2a Proportion CPAM features

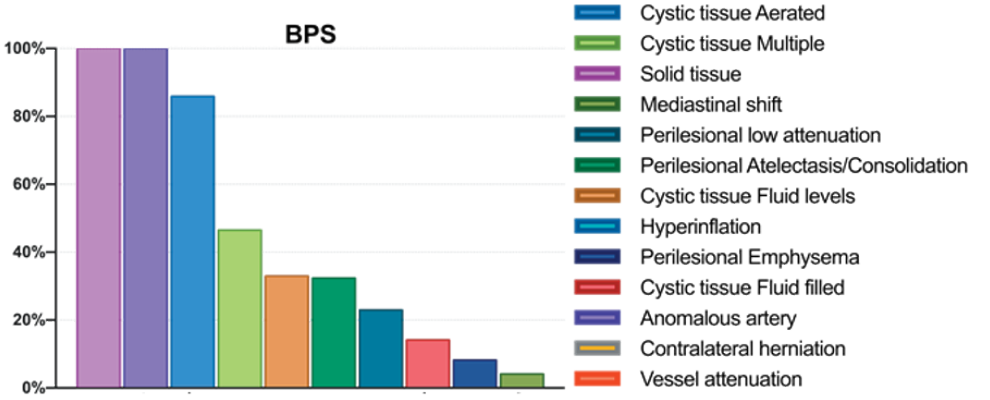

CT-features		
Solid tissue	100	%
Anomalous artery	100	%
Cystic tissue Aerated	86	%
Cystic tissue Multiple	46	%
Cystic tissue Fluid levels	33	%
Perilesional Atelectasis/Consolidation	32	%
Perilesional low attenuation	23	%
Cystic tissue Fluid filled	14	%
Perilesional Emphysema	8.2	%
Mediastinal shift	4.1	%
Hyperinflation	0	%
Contralateral herniation	0	%
Vessel attenuation	0	%

Chart & Table 2b Proportion BPS features

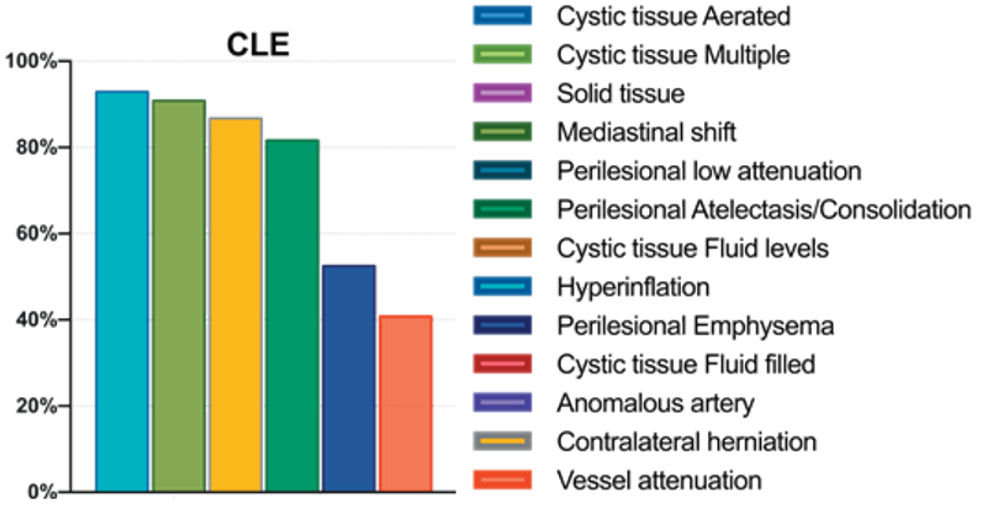

CT-features		
Hyperinflation	100	%
Mediastinal shift	83	%
Contralateral herniation	76	%
Perilesional Atelectasis/Consolidation	59	%
Perilesional Emphysema	54	%
Vessel attenuation	34	%
Cystic tissue Aerated	20	%

Cystic tissue Multiple	18	%
Cystic tissue Fluid levels	18	%
Cystic tissue Fluid filled	17	%
Solid tissue	0	%
Anomalous artery	0	%
Perilesional low attenuation	0	%

Chart & Table 2c Proportion CLE features

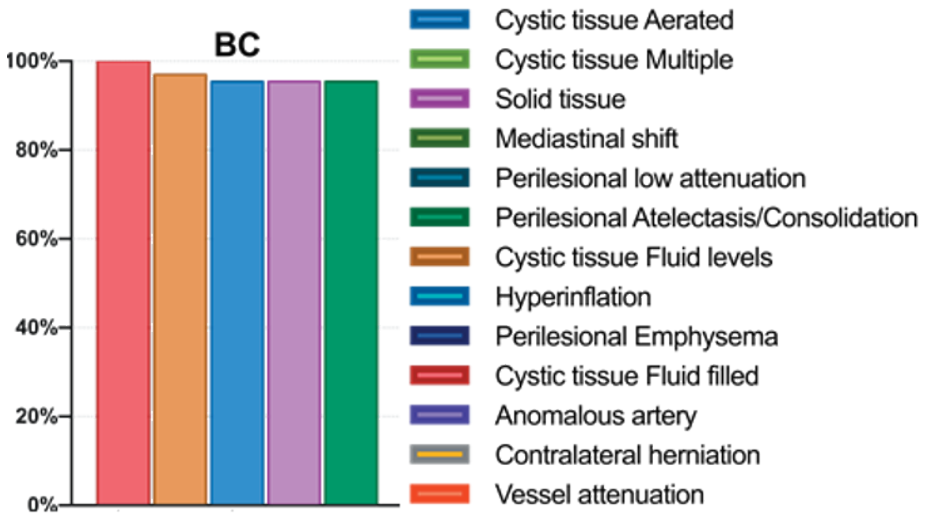

CT-features		
Cystic tissue Fluid filled	100	%
Cystic tissue Fluid levels	83	%
Cystic tissue Aerated	76	%
Solid tissue	59	%
Perilesional Atelectasis/Consolidation	54	%
Cystic tissue Multiple	34	%
Anomalous artery	20	%
Perilesional Emphysema	18	%
Perilesional low attenuation	18	%
Mediastinal shift	17	%
Hyperinflation	0	%
Contralateral herniation	0	%
Vessel attenuation	0	%

Chart & Table 2d Proportion BC features

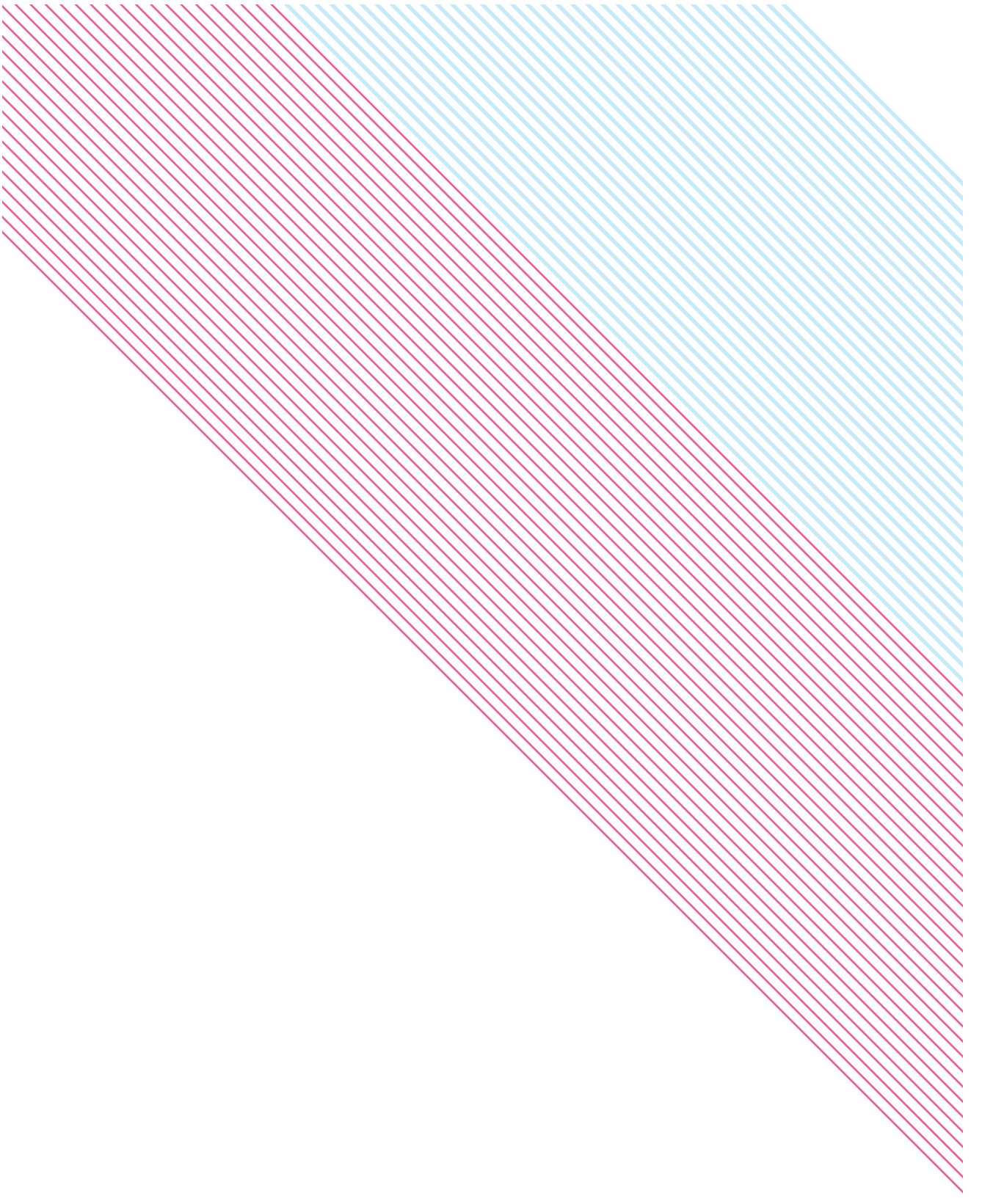

Chapter 10

Congenital lung abnormalities on magnetic resonance imaging: the CLAM study

Bernadette BLJ Elders, Casper M Kersten, Sergei M Hermelijn,
Piotr A Wielopolski, Harm AWM Tiddens, J Marco Schnater, Pierluigi Ciet

Submitted

Abstract

Rationale: Follow up of Congenital Lung Abnormalities (CLA) is currently done with chest Computer Tomography (CT). Major disadvantages of CT are exposure to ionizing radiation and need for contrast enhancement to visualize vascularization. Chest Magnetic Resonance Imaging (MRI) could be a safe alternative to image CLA without using contrast agents.

Objective: To develop a non-contrast MRI protocol for the follow up of paediatric CLA patients, and to compare findings on MRI to postnatal CT in school age CLA patients.

Methods: Twenty-one CLA patients, four after surgical resection and 17 unoperated, with a mean age of 12.8 (range 9.4-15.9) years, underwent spirometry and chest MRI. Chest MRI was compared to postnatal CT on appearance and size of the lesion, and lesion associated abnormalities, such as hyperinflation and atelectasis.

Results: By comparing school age chest MRI to postnatal CT, radiological appearance and diagnostic interpretation of the type of lesion changed in 7(41%) of the 17 unoperated patients. In unoperated patients, the relative size of the lesion in relation to the total lung volume remained stable (0.9% ((range -6.2- +6.7%),p=0.3) and the relative size of lesion associated parenchymal abnormalities decreased (-2.2% ((range -0.8- +2.8%),p=0.005)).

Conclusion: Non-contrast enhanced chest MRI was able to identify all CLA related lung abnormalities. Changes in radiological appearance between MRI and CT were related to CLA changes, patient' growth and differences between imaging modalities. Further validation is needed for MRI to be introduced as a safe imaging method for the follow up of paediatric CLA patients.

Introduction

In recent years, the incidence of prenatally diagnosed congenital lung abnormalities (CLA) has increased fourfold up to 4 cases per 10 000 life-births, mostly due to improved prenatal screening.(1) Different types of CLA can be distinguished: congenital pulmonary airway malformation (CPAM), bronchopulmonary sequestration (BPS), hybrid lesion (i.e. features of both CPAM and BPS), congenital lobar overinflation (CLO), bronchogenic cyst (BC) and bronchial atresia (BA).(2-4) CLA can cause symptoms, such as respiratory distress, recurrent infections and failure to thrive, but are asymptomatic in around 70-80% of the cases.(2, 5) While symptomatic CLA are treated with surgical resection, controversy exists on the correct management of asymptomatic CLA, as highlighted by several surveys carried out in Europe, the United Kingdom and Canada.(5-9) These different approaches create management dilemmas. In case a wait-and-see management is preferred, it remains unclear how and when these patients should undergo imaging to monitor changes in the CLA configuration or to detect possible malignant degeneration.(3, 10) The current gold standard for postnatal CLA imaging is chest Computed Tomography (CT), but this has disadvantages, such as exposure to ionizing radiation and need for a contrast agent to visualize vascularization of the lesion.(11-13) Magnetic Resonance Imaging (MRI) could be a safe alternative, being free of ionizing radiation and comparable at showing lung structure, as recently seen in a postnatal cohort of CLA patients.(14, 15) To date no studies on the long term follow up of CLA using MRI have been reported.

Therefore, the aim of this study was to develop and test a non-contrast chest MRI protocol for the follow up of paediatric CLA patients, and to compare MRI to postnatal CT findings in a cohort of school age CLA patients.

Methods

A flowchart of the study design and patient inclusions is shown in figure 1. Patients from the surgical long term follow up program with a radiologically or histologically (in case of surgical resection) confirmed CLA, aged between 8 and 18 years were approached to participate in this study.(16) Patients with associated thoracic anomalies which could alter imaging results (e.g. interstitial lung diseases, cystic fibrosis, bronchopulmonary dysplasia or pulmonary hypertension), and patients with contraindications to undergo MRI or unable to follow instruction during the MRI were excluded from participation. The study was approved by the local medical ethics committee (MEC2018-107), written informed consent was obtained from all patients and/or legal representatives.

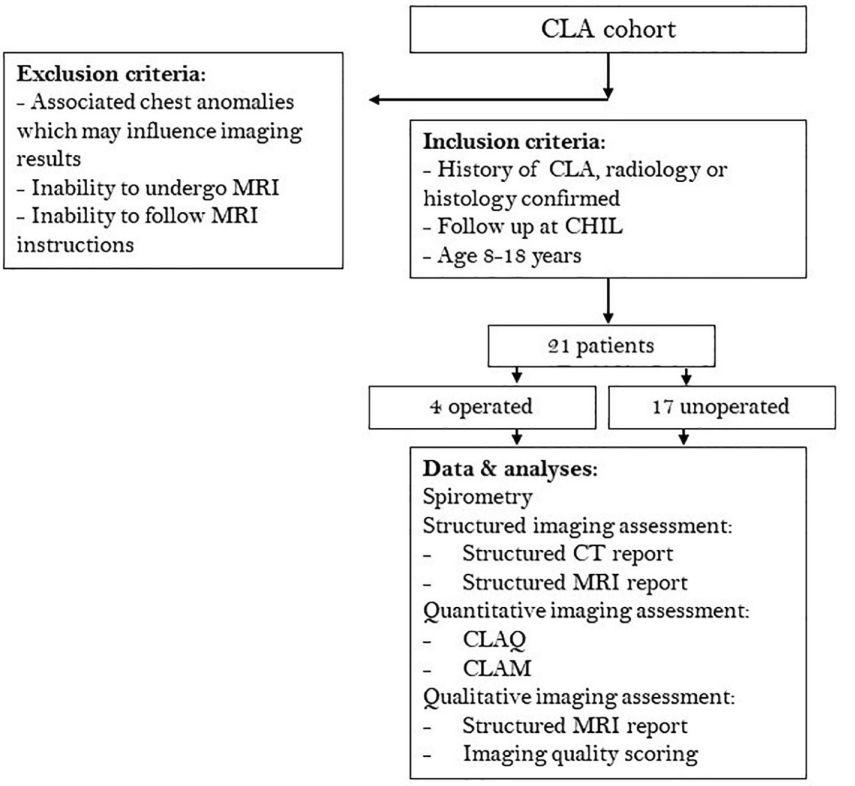

Figure 1: Flowchart of the study design and included patients. CHIL; surgical long term follow up outpatient clinic, CLA; congenital lung abnormality, CT; computed tomography, MRI; magnetic resonance imaging.

Data on primary diagnosis, symptoms and surgical resection were retrieved from the electronic patient dossier. All patients underwent spirometry and chest MRI. Postnatal CTs were collected to compare with the MRIs.

Spirometry

Spirometry was completed in all patients according to European Respiratory Society (ERS)/ American Thoracic Society (ATS) guidelines and data are presented as percentage predicted and z-scores as reported by the General Lung function Institute (GLI).(17-19)

CT

A free breathing contrast enhanced chest CT scan was acquired within the first year of life using a standardized protocol. The majority of scans (18/21) were acquired on an Emotion 6 CT scanner (*Siemens Healthcare, Forchheim, Germany*), 2/21 were acquired on a SOMATOM Definition CT scanner (*Siemens Healthcare, Forchheim, Germany*) and 1/21 was acquired on a Lightspeed QX/i CT scanner (*GE Healthcare, Milwaukee, Wisconsin, USA)*. The following range of parameters applies, with differences caused by changes in CT protocols over

the years: tube load 20-101 mAs, kilovoltage peak 80-120 kV, field-of-view 103-214 mm, slice thickness 0.75-2.5 mm, kernel B30s-B75f. In 90% of patients, a split bolus contrast enhancement protocol was used with both arterial and venous contrast enhancement.

MRI

All patients underwent a spirometry-guided chest MRI on a 1.5 Tesla scanner (*Artist, GE Healthcare, Milwaukee, Wisconsin, USA*). The MRI protocol consisted of sagittal 3D SPGR Proton Density weighted (PD-w) sequences during end- inspiratory and expiratory breath-hold, an axial 2D PROPELLER fat suppressed (FS) T2 weighted (T2-w) sequence during free-breathing and a 3D axial ZTE PD-w sequence during free breathing. To minimalize scan time, only in those patients with known vascular abnormalities on postnatal CT, a coronal non-contrast enhanced MR Angiography (MRA) 3D FIESTA T2/T1-w sequence was added (supplementary material 1). Total scan time was 30 minutes.

Structured imaging assessment

Structured radiological reports describing findings on postnatal CTs and school age MRIs (supplementary material 2) were completed.(3) CLA types were defined as: CPAM; cystic abnormality without systemic arterial blood supply, BPS; solid lesion with systemic arterial blood supply, hybrid lesion; combination of CPAM and BPS, BC; (partial) fluid-filled cyst near the mediastinum, CLO; overinflated hypodense lung lobe, BA; a focal interruption of a lobar, segmental, or subsegmental bronchus with associated peripheral mucus impaction (bronchocèle, mucocèle) and associated hyperinflation of the obstructed lung segment. (3) All scans were anonymized and randomly ordered, after which they were assessed by an observer with 10 years' experience in thoracic radiology (P.C.). There was a four week interval between the CT and MRI scoring to prevent recall bias. A comparison was made between the abnormalities seen on postnatal CT and school age MRI, and their diagnostic interpretation.

Quantitative imaging assessment

To compare the relative volume of the lesion between postnatal CT and school age MRI, we computed the volume of CLA lesion and associated parenchymal abnormalities, and the volume of normal lung tissue in relation to total lung volume. Volume quantification was done with a morphometry based quantitative grid system using an in-house developed software.(20-22) A simplified version of the previously published Congenital Lung Abnormalities Quantification on CT (CLAQ) scoring method was used to score postnatal CTs.(20) For the school age MRIs, a similar scoring method was used: the Congenital Lung Abnormalities quantification on MRI (CLAM) scoring method. For both the CLAQ and the CLAM scoring methods equidistant axial images with a maximum distance of 3 mm between the slices, were overlaid with a grid and each grid was scored hierarchically according to the abnormality within. Three categories were scored in which highest hierarchy was

assigned to lesional abnormalities followed by lesion associated parenchymal abnormalities defined as parenchymal hypo- or hyperdensity and normal lung tissue. In addition, on the axial reconstructed MR images in end- expiration, grids were hierarchically scored for hypo intense regions and normal lung tissue. From the grid scoring, the software calculates a volume and relative percentage of the lesion, lesion associated parenchymal abnormalities and normal lung tissue. Figure 2 shows an example of both the CLAQ and CLAM scoring methods. The CLAQ and CLAM were scored on anonymized and randomly ordered scans by two certified observers (S.H. and B.E.) with 2 and 4 years' experience in thoracic imaging, respectively. Both observers completed a standardized training module that included scoring four practice batches of five CT-scans each, including all types of CLA to assess performance. For the CLAM scoring, the highest percentage of either the lesion or lesion associated parenchymal abnormalities as seen on any of the sequences is presented, since not all abnormalities are equally visualized on each sequence due to different MR weighting. (23)

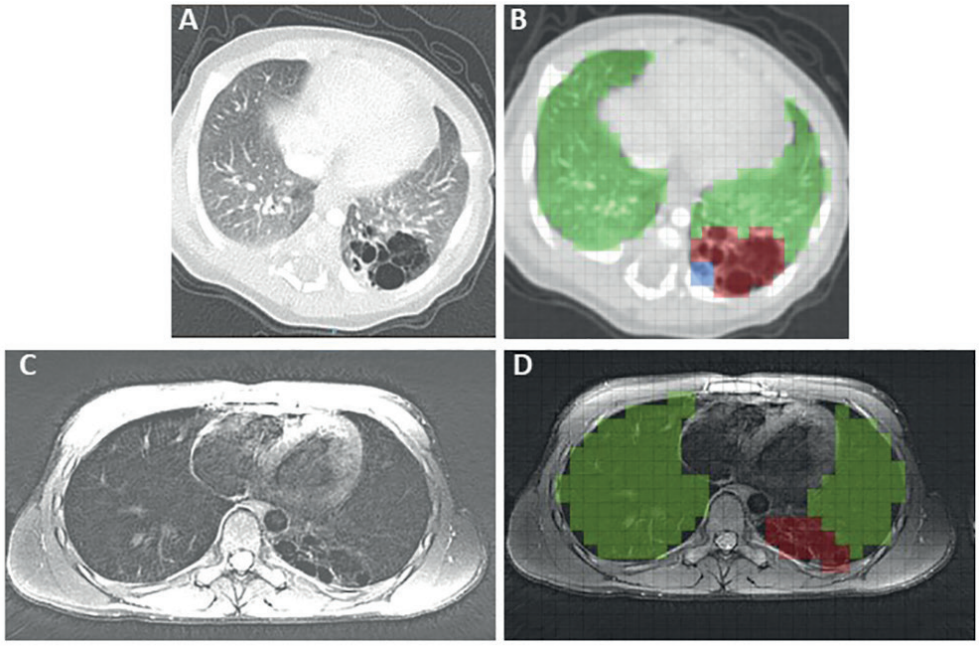

Figure 2: Example of an axial postnatal CT (a) and school age MRI (c) in a patient with a CPAM of the left lower lobe, showing a multi cystic lesion. Both images show a multicystic, air filled lesion. CLAQ scoring (b) shows normal lung tissue (green), lesion associated parenchymal abnormalities (atelectasis, blue) and the lesion (red), the CLAM scoring (d) shows normal lung tissue (green) and the lesion (red).

The CLAQ and CLAM outcomes were compared to evaluate change in the relative size of the CLA lesion, lesion associated parenchymal abnormalities and normal lung tissue between postnatal CT and school age MRI.

Qualitative imaging assessment

To assess whether MRI is able to visualize all CLA related abnormalities and to determine which sequences are best for this aim, a qualitative imaging assessment was performed. Firstly, the structured MRI report contained questions on whether certain CLA related abnormalities were visible on MRI. Secondly, the structured MRI report contained questions on which sequence was best to visualize certain abnormalities (supplementary material 2B). Thirdly, a qualitative scoring was applied on all MR images according to an adjusted version of the scoring method proposed by Bae *et al.* (supplementary material 3).(24) In short, all MRI sequences were scored on the depiction of fissures, intrapulmonary vessels and bronchi, the presence of noise/artifacts and overall acceptability, grading from unacceptable to superior on a five point scale.

Statistics

Data are presented as mean ± standard deviation for parametric data and median (range or interquartile range) for non-parametric data. SPSS Statistics (*version 25, IBM SPSS, Chicago, IL, USA*) was used for the data analysis. Data comparison was done using the parametric t-test for normally distributed data and the Mann Whitney U test for not normally distributed data. We assumed a 5% significance level.

Results

Patient inclusions are shown in figure 1, characteristics and spirometry outcomes of all study participants are shown in table 1. In total 21 CLA patients were included with a mean age of 12.8 (range 9.4 – 15.9) years. The most common CLA was CPAM (n=10, 48%). Four patients underwent surgical resection of whom two patients with a CPAM were operated because of development of symptoms (respiratory distress and/or cardiac volume overload). Furthermore, two patients with a BPS were operated because of respiratory distress and recurrent infection, respectively.

All patients successfully completed the MR examination. Median interval between postnatal CT and school age MRI was 12.1 (range 10.0-14.7) years.

Table 1: Characteristics of all study participants

	All patients (n= 21)	Unoperated (n=17)	Operated (n=4)
Age at MRI (years)	12.8 (9.4-15.9)	12.6 (9.4-15.9)	13.8 (11.3-15.9)
Gender (% female)	52	47	75
Type of CLA (%)			
CPAM	48		50
BPS	33	47	50
Hybrid lesion	10	29	0
Bronchial atresia	19	12	0
		24	
Age at surgery (months)	-	-	2 (1-30)
Reason for surgery (n)			
Respiratory distress	-	-	3
Infection	-	-	1
Volume overload	-	-	1
Type of surgery (n)			
Pneumonectomy	-	-	1
Lobectomy	-	-	1
Lesion resection	-	-	2
FVC			
% predicted	95.6 ± 12.9	98.8 ± 10.7	82.0 ± 13.8
z-score	-0.38 ± 1.1	-0.10 ± 0.9	-1.58 ± 1.2
FEV_1			
% predicted	91.2 ± 15.6	94.7 ± 12.5	76.8 ± 21.3
z-score	-0.74 ± 1.3	-0.45 ± 1.0	-1.94 ± 1.7
FEV_1/FVC			
% predicted	95.0 ± 8.9	95.7 ± 7.9	92.0 ± 13.6
z-score	-0.69 ± 1.0	-0.65 ± 0.9	-0.87 ± 1.5
PEF			
% predicted	94.9 ± 17.9	98.0 ± 15.5	81.8 ± 23.9
z-score	-0.44 ± 1.1	-0.24 ± 0.9	-1.30 ± 1.7
FEF_{25}			
% predicted	94.5 ± 20.7	98.9 ± 16.7	76.0 ± 28.6
z-score	-0.50 ± 1.4	-0.24 ± 0.9	-1.73 ± 2.1
FEF_{50}			
% predicted	81.5 ± 23.7	83.4 ± 21.8	73.8 ± 33.6
z-score	-1.41 ± 1.6	-1.29 ± 1.5	-1.95 ± 2.5
FEF_{75}			
% predicted	81.7 ± 29.1	84.5 ± 28.4	69.8 ± 33.6
z-score	-0.73 ± 1.1	-0.61 ± 1.0	-1.23 ± 1.4
$MEF_{75/25}$			
% predicted	81.2 ± 23.8	84.2 ± 22.2	68.5 ± 30.0
z-score	-0.95 ± 1.2	-0.79 ± 1.1	-1.61 ± 1.6
VCmax			
% predicted	96.7 ± 12.6	99.2 ± 10.5	82.7 ± 16.9
z-score	-0.30 ± 1.1	-0.08 ± 0.9	-1.55 ± 1.5

Characteristics and spirometry results of all study participants. BPS; bronchopulmonary sequestration, CPAM; congenital pulmonary airway malformation, CLA; congenital lung abnormality, $FEF_{25,50,75}$; forced expiratory flow at 25, 50 and 75% of expiration, FEV_1; forced expiratory volume in 1 second, FVC; forced vital capacity, MEF; mean expiratory flow, MRI; magnetic resonance imaging, PEF; peak expiratory flow, VCmax; maximum vital capacity. Data are presented as mean ± standard deviation or median (range)

Spirometry

Spirometry was within the normal range for all patients (z-score for all measurements between -1.41 and -0.30). Patients with a history of surgical resection had lower z-scores on spirometry (z scores for all measurements between -1.95 and -0.87). However, this was mostly caused by one patient with a history of a left pneumonectomy with spirometry z-scores of -2.15 (FVC), -3.77 (FEV_1) and -2.98 (FEV_1/FVC).

Structured qualitative assessment

Results from the structured CT and MRI reports are shown in table 2 and 3. Between postnatal CT and school age MRI, the appearance and diagnostic interpretation of the type of CLA changed in 7 patients of the unoperated group (41%). In three patients the lesion was classified as a CPAM on postnatal CT and as a BA on school age MRI, and in one patient a mixed lesion (CPAM and BA) was seen on postnatal CT, and only a BA was found on school age MRI. In addition, in three patients the solid component of the lesion classified as a hybrid lesion (n=1) or BPS (n=2) appeared as cystic tissue on school age MRI. Example images of changing appearances of CLA between postnatal CT and school age MRI are shown in figure 3.

Table 2: CLAQ and CLAM scoring per patient

	CLAQ				CLAM				
							Free- breathing MRI		Expiratory MRI
Patient	**Diagnostic interpretation**	**Lesion**	**Lesion associated parenchymal abnormalities**	**Normal lung tissue**	**Diagnostic interpretation**	**Lesion**	**Lesion associated parenchymal abnormalities**	**Normal lung tissue**	**Hypo intense regions**
	Unoperated								
1	CPAM	9.5	1.0	89.5	CPAM	3.3	0	96.7	7.2
2	Hybrid lesion	7.9	3.5	88.6	Hybrid lesion	3.1	1.2	95.7	5.7
3	BA	6.4	0.5	93.1	BA	0.8	0.4	98.8	0
4	CPAM +BA	7.3	7.5	85.2	BA	1.2	1.7	97.1	24.3
5	CPAM	1.9	6.3	91.8	CPAM	2.4	0.6	97.0	0.2
6	CPAM	9.7	3.1	87.2	CPAM	8.6	0	91.4	11.8
7	Hybrid lesion	3.2	0.2	96.6	CPAM	4.3	1.0	94.7	7.3
8	BPS + BA	0.5	0.9	98.6	CPAM + BA	1.8	0	98.2	0
9	CPAM	1.8	1.3	96.9	BA	0.9	0	99.1	3.3
10	BPS	13.4	3.1	83.5	BPS	10.5	0	89.5	17.9
11	BPS	1.6	12.6	85.8	BPS	2.5	2.8	94.7	10.7
12	CPAM	3.2	4.3	92.5	CPAM	4.0	0	96.0	5.3
13	CPAM	3.2	0.3	96.5	BA	0.2	3.0	96.8	5.0
14	CPAM	7.0	5.7	87.3	BA	5.3	0	94.7	7.7
15	BPS	1.1	0	98.9	CPAM	1.6	0	98.4	0
16	BA	3.4	0	96.6	BA	8.0	0	92.0	17.2
17	BPS	6.7	2.2	91.1	BPS	13.3	0	86.7	12.5
	Operated								
18	BPS	41.4	18.1	40.5	-	0	0.7	99.3	4.5
19	BPS	2.3	0.5	97.2	-	0	0.2	99.8	0
20	CPAM	58.8	8.1	33.1	-	0	0.6	99.4	0
21	CPAM	49.3	0.8	49.9	-	0	0.5	99.5	23.8

Overview of the quantitative scoring of the postnatal CT and school age MRI per patient. BA; bronchial atresia, BPS; bronchopulmonary sequestration, CLAQ; congenital lung abnormalities quantification on computed tomography, CLAM; congenital lung abnormalities quantification on magnetic resonance imaging, CPAM; congenital pulmonary airway malformation. Data are presented as % of total lung volume.

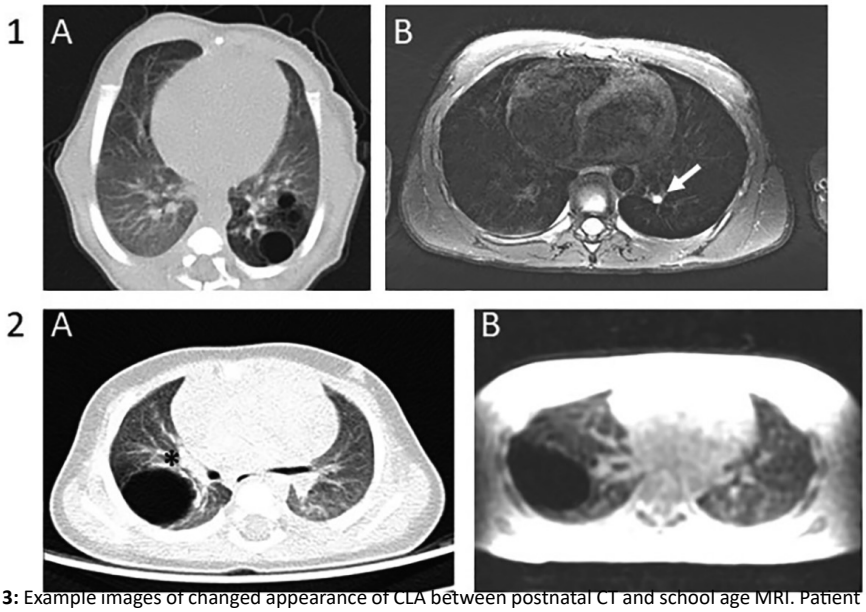

Figure 3: Example images of changed appearance of CLA between postnatal CT and school age MRI. Patient 1) axial postnatal CT showing an air-filled multi- cystic CPAM and BA in the left lower lobe (A) and an axial T2- weighted PROPELLER image at school age showing only BA in the left lower lobe (arrow) (B). Patient 2) axial postnatal CT showing an air-filled CPAM with surrounded by lesion associated parenchymal atelectasis (asterisk) (A) and an axial SPGR expiratory image at school age showing an air-filled CPAM without lesion associated parenchymal abnormalities(B).

Quantitative imaging assessment

Results from the CLAQ and CLAM scoring are shown in table 2 and 3. Figure 4A shows an overview of the change in size of the CLA in relation to total lung volume between the CLAQ on postnatal CT and the CLAM on school age MRI. Comparing the CLAQ and CLAM outcomes in unoperated patients the median size of the lesion relative to total lung volume remained stable (-0.9% ((range -6.2% - +6.7%), p=0.3)).

Table 3: CLAQ and CLAM scoring

	CLAQ (n=17)	CLAM (n=17)	Change in abnormalities	p-value
Age (years)	0.3 (0.0-0.8)	12.3 (9.4-15.9)	11.9 (9.1-15.9)	-
Free breathing				
Lesion	3.4 (0.5-13.4)	3.1 (0.2-13.3)	-0.9 (-6.2- +6.7)	0.29
Lesion associated parenchymal abnormalities	2.2 (0.0-12.6)	0.0 (0.0-3.1)	-2.2 (-0.8- +2.8)	**0.005**
Normal lung tissue	91.8 (83.5-98.9)	96.0 (86.7-99.1)	+4.2 (-4.6- +11.9)	**0.02**
End- expiration				
Hypointensity regions	-	7.1 (0.0-24.3)	-	-
Normal lung tissue	-	92.9 (75.7-100.0)	-	-

CLAQ and CLAM scoring results from all unoperated patients. Data are presented as median (range) of the percentage (%) of the total lung volume. P values <0.05 are in bold.

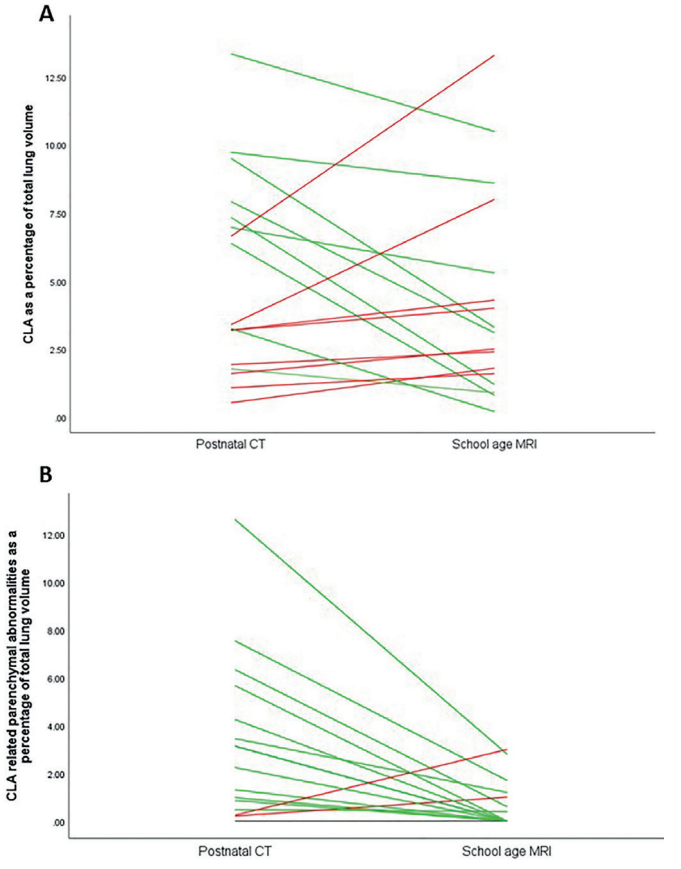

Figure 4: Plot of the changes in (A) size of the CLA lesion in relation to total lung volume between postnatal CT and school age MRI and (B) size of lesion associated parenchymal abnormalities between postnatal CT and school age MRI. Lines in green indicate a decrease in relative size, lines in red indicate an increase in relative size.

Figure 4B show the changes in lesion associated parenchymal abnormalities in relation to total lung volume between postnatal CT and school age MRI. In 7/17 (41%) patients the associated parenchymal abnormalities were no longer visible on MRI, in most of these patients this concerned atelectasis seen during the postnatal period which was absent at school age. One patient had an increase in lesion associated parenchymal abnormalities. This was a patient with a CPAM on postnatal CT which was scored as BA with associated surrounding parenchymal hypointensity on school age MRI, hence this change in classification resulted in a decrease of the volume occupied by the lesion and an increase in the volume of lesion associated parenchymal abnormalities. Overall, in unoperated patients, the median size of lesion associated parenchymal abnormalities in relation to total lung tissue decreased (-2.2% ((range -0.8- +2.8%), p=0.005)).

On MRI, the most common associated parenchymal abnormality was hypointense lung parenchyma seen on free-breathing images in 35% (6/17) and on expiratory images in 82% (14/17).

In all patients in whom the CLA was surgically resected, only minor scar tissue was observed. One of these patients had a pneumonectomy of the left lung at the age of one week and showed diffuse hypointense lung parenchyma on expiratory MRI (24% of the total lung volume), representing hyperinflation of the remaining right lung.

Qualitative imaging assessment

According to the qualitative imaging assessment included on the structured MRI report, CLA related abnormalities were best seen on ZTE (airway), PROPELLER (vascularization) and SPGR expiration (hypointense structures such as cysts, low attenuation regions and hyperinflation) sequences. Six patients had an MRA FIESTA sequence available, this sequence was rated best to depict abnormal vascularization in five patients. In one patient the MRA FIESTA was insufficient due to severe movement artifacts. In two patients with a vascular component of the CLA, no MRA FIESTA sequence was made, however abnormal vascularization was sufficiently visualized on the T2-w PROPELLER sequence. An example of the visualization of lesion vascularization on postnatal CT compared to school age MRI is shown in figure 5. Qualitative scoring showed acceptable quality for the ZTE sequence, with a median score of 'above average' for the visualization of all lung structures (table 4). The T2 weighted PROPELLER sequence scored 'satisfactory' but did show less noise/artifacts compared to the ZTE sequence.

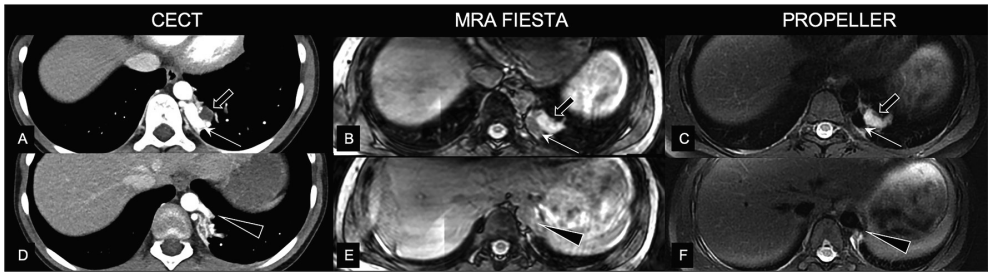

Figure 5: Visualization of lesion vascularization on axial contrast-enhanced postnatal CT (A and D), MRA FIESTA (B and E) and T2-w PROPELLER (C and F) in a patient with a BPS. Images show venous drainage of the lesion into the hemiazigos vein (thin arrow on A,B,C) and a bronchocèle (thick arrow on A,B,C) and arterial supply from the aorta descendens (arrow on D,E,F). BPS; bronchopulmonary sequester, CECT; contrast enhanced Computed Tomography, MRA FIESTA; Magnetic Resonance Angiography , PROPELLER; PROPELLER; Periodically Overlapping ParalLEL Lines with Enhanced Reconstruction.

Table 4: Qualitative MRI scoring

	Axial SPGR insp	Axial SPGR exp	T2- weighted FS PROPELLER	ZTE	MRA FIESTA
A. Qualitative scoring according to Bae *et al.*					
Fissures	1 (1-1)	1 (1-1)	2 (2-2)	2 (2-2)	*
Vessels	2 (2-2)	2 (2-2)	3 (3-3)	3.5 (3-4)	*
Bronchi	2 (2-2)	2 (2-2)	3 (3-3)	4 (3-4)	*
Noise/artifacts	3 (2-3)	3 (2-3)	3 (3-4)	3 (2-4)	*
Overall acceptability	2 (2-3)	2 (2-3)	3 (3-4)	4 (3-4)	*
B. Best sequence to depict CLA related abnormalities, according to structured MRI report					
Airway	-	-	2	19	-
Cystic lesion	-	2	3	5	-
Solid/emphysematous lesion	-	11	5	1	-
Lesion border	-	1	6	10	-
Vascularization	-	-	15	3	5
Atelectasis	-	1	8	3	-
Low attenuation	-	15	-	1	-
Hyperinflation	-	8	-	-	-

FS; fat suppressed, PROPELLER; periodically rotated overlapping parallel lines with enhanced reconstruction, SPGR; spoiled gradient echo, UTE; ultra- short echo time, ZTE; zero- echo time. Table 3A shows qualitative scoring of the MRI sequences according to Bae *et al*. (European Radiology 2020). * no qualitative scoring was performed on the MRA FIESTA sequence. Data is presented as median (interquartile range). Table 3B shows the qualitative score according to the structured MRI report, data are presented as the number of patients in whom this sequence was scored as best depicting CLA related abnormalities (note, not all structures were present in all patients).

Discussion

In this study we have used non-contrast MRI for the long term follow up of CLA patients and describe our findings in a cohort of school age CLA patients in comparison to postnatal CT. We show that MRI is able to identify all CLA related lung structures. In addition, we show the development of unoperated CLA over time.

In 41% of the unoperated patients the radiological appearance, and therefore radiological diagnostic interpretation of the CLA, was different between postnatal and school age. The different appearance of the CLA found in this study has multiple possible explanations. First, this could be related to an actual change in the CLA. Examples are the disappearance of cystic tissue or the accumulation of mucus in a BA changing its appearance into a bronchocèle, which increases visibility on an MRI image compared to an airway without mucus, as we saw in two patients.(25) Second, the change in appearance can be related to age related growth of body size making certain lung structures, such as the airways, better visible on MRI images. Furthermore, growth related changes in the appearance of CLA can also be related to progressive hyperinflation of lung parenchyma due to collateral ventilation, appearing as hypo intense regions on MRI which were not initially identified on postnatal CT.(26-28)

A third explanation for the different appearance of some of the CLA, is the different imaging modalities used between postnatal and school age follow-up. On one hand, CT has a higher image resolution compared to MRI. On the other hand, our MRI protocol in cooperative school age children offers the possibility to perform end in-and expiratory scans, showing the lung at residual volume (RV) with a superior contrast-to-noise ratio compared to images taken at functional residual capacity (FRC), as is the case in postnatal CT imaging. These RV images are more sensitive to visualize hypo- intense regions, such as CLO and BA, than CT.

On average, in unoperated patients, the size of the lesion in relation to total lung volume did not change between postnatal and school age follow-up. Although this finding corresponds to our experience from clinical practice, no long term follow up studies have reported on the development of CLA over time. The stable relative size of the lesion, in combination with spirometry outcomes within the normal range, could justify the wait-and-see approach in asymptomatic CLA patients.(6) These findings are in line with a study describing normal lung function in CLA patients that did not undergo surgery.(29) In addition, studies comparing prenatal screening to postnatal follow up frequently describe regression of CLA. But our findings show that this regression of CLA does not occur after the postnatal period.(30)

We also found a decrease in lesion associated parenchymal abnormalities in relation to total lung volume between postnatal and school age follow up. The relative decrease was most often related to atelectasis seen on postnatal CT that decreased or disappeared on school age MRI. This atelectasis seen on postnatal CT could be related to either local compression of the primary lesion on the surrounding parenchyma that decreases over time, indicating possible decreased impact of the CLA on the normal lung tissue over time. In addition, this could also be related to the young age of the patients and thereby prolonged periods of supine position, or anaesthesia.(31, 32) Both reasons show that atelectasis on postnatal imaging may not be related to the clinical condition of the patient

Our qualitative scoring revealed which MRI sequences are best suitable for the visualization of CLA. First, best structural visualization of the CLA was achieved with the ZTE and SPGR expiratory sequences. Second, hyper dense regions, such as atelectasis, were best visualized on the T2-w PROPELLER sequence. Third, vascularization was best visualized on the MRA sequence, but could also be visualized on T2-w PROPELLER sequences. These findings show that contrast enhancement is not needed for the follow up of CLA when using MRI. Thereby patient compliance to the examination could be increased by omitting the need for intravenous access and possible concerns related to gadolinium deposition.(33)

To our knowledge this is the first study using non-contrast MRI for the long term follow up of CLA. A recent study by Zirpoli *et al.* compared postnatal contrast enhanced CT to postnatal non-contrast MRI. MRI was found to be comparable to CT for the visualization of all CLA related lung structures, expect for vascularization.(14) A study by Kellenberger *et al.* compared postnatal contrast-enhanced CT to contrast-enhanced MRI, and although this study describes comparable findings on the two modalities, contrast-enhancement is described as indispensable.(15) In contrast, we found that MRI was able to identify CLA related vascular abnormalities in all patients. However, our study was spirometer- controlled, conducted in an older population and an MRA sequence was added to our MRI protocol, specifically to image the vasculature. Both studies also did not include an ultra-short echo time sequence in their MRI protocol, which from our qualitative analyses proved best for CLA visualization. In addition, recent studies have shown these ultra-short echo time sequences to be ideal for postnatal imaging due to superior image resolution and the additional benefit of these sequences being silent on some MRI systems and therefore less burdensome for young children.(34-36) Further research is needed to standardize postnatal MRI protocols for CLA between MRI vendors, including the addition of the most recently developed sequences.

Our study has some limitations. First, this was a single- centre study with a small number of study participants. Second, we did not have school age CT available for direct comparison. Another point that is not addressed in our study is the ability of MRI to detect possible development of malignancy within CLA, for which our population size is too small considering the extremely low incidence.(10, 37) As a matter of fact, the radiological characteristics of malignant deterioration of CLA are not well defined.(38)

In conclusion, this is the first study describing the use of non-contrast MRI for the follow up of CLA. Based on our study, MRI is able to identify the most important CLA related lung abnormalities without the use of contrast-enhancement or sedation. We also show that the radiological appearance of a large proportion of the unoperated CLA changes over time, related to actual changes in the CLA, growth of the patient and imaging modalities used. Further research is needed to validate our results in a larger cohort and to compare school age MRI to school age CT. Such a study will allow introduction of MRI as safe imaging method alternative for chest CT for the long term follow up of paediatric CLA patients.

References

1. Stocker LJ, Wellesley DG, Stanton MP, Parasuraman R, Howe DT. The increasing incidence of foetal echogenic congenital lung malformations: an observational study. Prenat Diagn. 2015;35(2):148-53.
2. Stanton M, Njere I, Ade-Ajayi N, Patel S, Davenport M. Systematic review and meta-analysis of the postnatal management of congenital cystic lung lesions. J Pediatr Surg. 2009;44(5):1027-33.
3. Hermelijn SM, Elders B, Ciet P, Wijnen RMH, Tiddens H, Schnater JM. A clinical guideline for structured assessment of CT-imaging in congenital lung abnormalities. Paediatr Respir Rev. 2021;37:80-8.
4. Wong KKY, Flake AW, Tibboel D, Rottier RJ, Tam PKH. Congenital pulmonary airway malformation: advances and controversies. Lancet Child Adolesc Health. 2018;2(4):290-7.
5. Morini F, Zani A, Conforti A, van Heurn E, Eaton S, Puri P, et al. Current Management of Congenital Pulmonary Airway Malformations: A "European Pediatric Surgeons' Association" Survey. Eur J Pediatr Surg. 2018;28(1):1-5.
6. Stanton M. The argument for a non-operative approach to asymptomatic lung lesions. Semin Pediatr Surg. 2015;24(4):183-6.
7. Singh R, Davenport M. The argument for operative approach to asymptomatic lung lesions. Semin Pediatr Surg. 2015;24(4):187-95.
8. Peters RT, Burge DM, Marven SS. Congenital lung malformations: an ongoing controversy. Ann R Coll Surg Engl. 2013;95(2):144-7.
9. Lo AY, Jones S. Lack of consensus among Canadian pediatric surgeons regarding the management of congenital cystic adenomatoid malformation of the lung. J Pediatr Surg. 2008;43(5):797-9.
10. MacSweeney F, Papagiannopoulos K, Goldstraw P, Sheppard MN, Corrin B, Nicholson AG. An assessment of the expanded classification of congenital cystic adenomatoid malformations and their relationship to malignant transformation. Am J Surg Pathol. 2003;27(8):1139-46.
11. Baez JC, Ciet P, Mulkern R, Seethamraju RT, Lee EY. Pediatric Chest MR Imaging: Lung and Airways. Magn Reson Imaging Clin N Am. 2015;23(2):337-49.
12. Miglioretti DL, Johnson E, Williams A, Greenlee RT, Weinmann S, Solberg LI, et al. The use of computed tomography in pediatrics and the associated radiation exposure and estimated cancer risk. JAMA Pediatr. 2013;167(8):700-7.
13. Young JR, Orosz I, Franke MA, Kim HJ, Woodworth D, Ellingson BM, et al. Gadolinium deposition in the paediatric brain: T1-weighted hyperintensity within the dentate nucleus following repeated gadolinium-based contrast agent administration. Clin Radiol. 2018;73(3):290-5.
14. Zirpoli S, Munari AM, Primolevo A, Scarabello M, Costanzo S, Farolfi A, et al. Agreement between magnetic resonance imaging and computed tomography in the postnatal evaluation of congenital lung malformations: a pilot study. Eur Radiol. 2019;29(9):4544-54.

15. Kellenberger CJ, Amaxopoulou C, Moehrlen U, Bode PK, Jung A, Geiger J. Structural and perfusion magnetic resonance imaging of congenital lung malformations. Pediatr Radiol. 2020;50(8):1083-94.
16. IJsselstijn H, Gischler SJ, Wijnen RMH, Tibboel D. Assessment and significance of long-term outcomes in pediatric surgery. Semin Pediatr Surg. 2017;26(5):281-5.
17. Miller MR, Crapo R, Hankinson J, Brusasco V, Burgos F, Casaburi R, et al. General considerations for lung function testing. Eur Respir J. 2005;26(1):153-61.
18. Beydon N, Davis SD, Lombardi E, Allen JL, Arets HG, Aurora P, et al. An official American Thoracic Society/European Respiratory Society statement: pulmonary function testing in preschool children. Am J Respir Crit Care Med. 2007;175(12):1304-45.
19. Quanjer PH, Hall GL, Stanojevic S, Cole TJ, Stocks J, Global Lungs I. Age- and height-based prediction bias in spirometry reference equations. Eur Respir J. 2012;40(1):190-7.
20. Hermelijn SM, Dragt OV, Bosch JJ, Hijkoop A, Riera L, Ciet P, et al. Congenital lung abnormality quantification by computed tomography: The CLAQ method. Pediatr Pulmonol. 2020;55(11):3152-61.
21. van Mastrigt E, Kakar E, Ciet P, den Dekker HT, Joosten KF, Kalkman P, et al. Structural and functional ventilatory impairment in infants with severe bronchopulmonary dysplasia. Pediatr Pulmonol. 2017;52(8):1029-37.
22. Rosenow T, Oudraad MC, Murray CP, Turkovic L, Kuo W, de Bruijne M, et al. PRAGMA-CF. A Quantitative Structural Lung Disease Computed Tomography Outcome in Young Children with Cystic Fibrosis. Am J Respir Crit Care Med. 2015;191(10):1158-65.
23. Ciet P, Tiddens HA, Wielopolski PA, Wild JM, Lee EY, Morana G, et al. Magnetic resonance imaging in children: common problems and possible solutions for lung and airways imaging. Pediatr Radiol. 2015;45(13):1901-15.
24. Bae K, Jeon KN, Hwang MJ, Lee JS, Ha JY, Ryu KH, et al. Comparison of lung imaging using three-dimensional ultrashort echo time and zero echo time sequences: preliminary study. Eur Radiol. 2019;29(5):2253-62.
25. Morikawa N, Kuroda T, Honna T, Kitano Y, Fuchimoto Y, Terawaki K, et al. Congenital bronchial atresia in infants and children. J Pediatr Surg. 2005;40(12):1822-6.
26. Gipson MG, Cummings KW, Hurth KM. Bronchial atresia. Radiographics. 2009;29(5):1531-5.
27. Matsushima H, Takayanagi N, Satoh M, Kurashima K, Kanauchi T, Hoshi T, et al. Congenital bronchial atresia: radiologic findings in nine patients. J Comput Assist Tomogr. 2002;26(5):860-4.
28. Kawamoto S, Yuasa M, Tsukuda S, Heshiki A. Bronchial atresia: three-dimensional CT bronchography using volume rendering technique. Radiat Med. 2001;19(2):107-10.
29. Hijkoop A, van Schoonhoven MM, van Rosmalen J, Tibboel D, van der Cammen-van Zijp MHM, Pijnenburg MW, et al. Lung function, exercise tolerance, and physical growth of children with congenital lung malformations at 8 years of age. Pediatr Pulmonol. 2019;54(8):1326-34.
30. Griggs C, Schmaedick M, Gerall C, Fan W, Orlas C, Price J, et al. Vanishing congenital lung malformations: What is the incidence of true regression? J Neonatal Perinatal Med. 2021.

31. Mahmoud M, Towe C, Fleck RJ. CT chest under general anesthesia: pulmonary, anesthetic and radiologic dilemmas. Pediatric Radiology. 2015;45(7):977-81.
32. Sodhi KS, Ciet P, Vasanawala S, Biederer J. Practical protocol for lung magnetic resonance imaging and common clinical indications. Pediatr Radiol. 2021:1-17.
33. Gulani V, Calamante F, Shellock FG, Kanal E, Reeder SB, International Society for Magnetic Resonance in M. Gadolinium deposition in the brain: summary of evidence and recommendations. Lancet Neurol. 2017;16(7):564-70.
34. Walkup LL, Woods JC. Newer Imaging Techniques for Bronchopulmonary Dysplasia. Clin Perinatol. 2015;42(4):871-87.
35. Higano NS, Hahn AD, Tkach JA, Cao X, Walkup LL, Thomen RP, et al. Retrospective respiratory self-gating and removal of bulk motion in pulmonary UTE MRI of neonates and adults. Magn Reson Med. 2017;77(3):1284-95.
36. Tiddens H, Kuo W, van Straten M, Ciet P. Paediatric lung imaging: the times they are a-changin'. Eur Respir Rev. 2018;27(147).
37. Hall NJ, Stanton MP. Long-term outcomes of congenital lung malformations. Semin Pediatr Surg. 2017;26(5):311-6.
38. Nasr A, Himidan S, Pastor AC, Taylor G, Kim PC. Is congenital cystic adenomatoid malformation a premalignant lesion for pleuropulmonary blastoma? J Pediatr Surg. 2010;45(6):1086-9.

Supplementary materials

Supplementary material 1: MRI protocol

Sequence	SPGR inspiration/ expiration	FS T2 weighted PROPELLER	ZTE	MRA Fiesta
Acquisition plane	Sagittal	Axial	Axial	Coronal
TR/TE (ms) flip angle (°) RF	1.5/0.6 2 Selective	*/73 90/120 Selective	1.1/0 2 Non-selective	3.6/1.1 50 Selective
In-plane matrix	120x120	340x340	200x200	220x220
k-space trajectory	Cartesian	BLADES	Radial	Cartesian
In-plane Field-of-view (FOV) RecFOV Actual voxel resolution (mm^3) Slices Slice thickness	36 0.75 3.0x3.0x3.0 90 (as in VIBE) 3.0	34 - 1.0x1.0x3.5 50-70 3.5	30 - 1.5x1.5x1.5 200 1.5	40 - 1.8x1.8x1.8 60-80 1.8
Receiver bandwidth (KHz)	90	83.33	62.5	100
Parallel imaging	ARC (1.5x1.2)	3.0	None	Asset (2.0)
Number of average	1	2.0	2.5	1
No. of spokes per segment	-	14	512	150-180 ms
Physiological triggering	BH	Prospective pencil beam navigator	Prospective projection navigator	Respiratory gated and cardiac triggered
Scan time (sec) RR=20	+/- 6sec	+/- 5 min	+/- 6 min	+/- 6 min

FOV; Field Of View, FS: fat suppressed, NEX; Number of Excitations, PROPELLER; Periodically Overlapping ParalLEL Lines with Enhanced Reconstruction, RF; radio frequency, SPGR; Spoiled Gradient Echo Sequence, TE; Echo Time, TR; Repetition Time. * TR chosen depended on the respiratory frequency of the patient.

Supplementary material 2: Structured radiological reports

A: Structured CT report

Structured CT report Congenital Lung Abnormalities

Scan protocol:
□ Inspiration □ Volumetric Slice thickness: mm
□ Expiration □ Volumetric Slice thickness: mm

Contrast enhancement:
□ None
□ Venous phase
□ Arterial phase

A. Findings:

Location & extent:

	RUL	RML	RLL	LUL	LLL
Extent					
1= ¼ lobe 2= ½ lobe 3=complete lobe					

Airway:
□ Normal connection
□ Bronchomalacia
□ Atresia

B. Lesion:

Cystic tissue:
- Structure:
  □ Dominant cyst □ Cluster of multiple uniform cysts
- Average cyst size: mm
- Size of largest cyst: mm
- Content:
  □ Air-filled
  □ Fluid-filled
  □ Air-Fluid levels

Solid tissue:

	RUL	RML	RLL	LUL	LLL
Extent					
1= ¼ lobe 2= ½ lobe 3=complete lobe					

- Density:
  □ Homogeneous
  □ Heterogeneous

C. Border:

□ Well-defined □ Ill-defined

D. Vascularization:

Arterial:
□ Normal pulmonary
□ Aberrant:
Number & Size: Origin:

Venous:
□ Normal pulmonary
□ Aberrant:
Number & Size: Origin:

E. (Surrounding) tissue:

	RUL	RML	RLL	LUL	LLL
Atelectasis					
Low-attenuation					
Hyperinflation					
1= ¼ lobe 2= ½ lobe 3=complete lobe					

□ Mass effect
□ Mediastinal shift
□ Mediastinal herniation

F. Conclusion :

□ CPAM
□ BPS
□ Hybrid lesion
□ CLO
□ BA
□ BC

B: Structured MRI report

Structured MRI report Congenital Lung Abnormalities

A. Findings:

Location & extent:

	RUL	RML	RLL	LUL	LLL
Extent					
1= ⅓ lobe 2= ⅔ lobe 3=complete lobe					

Airway:
- □ Normal connection
- □ Bronchomalacia
- □ Atresia
- □ Not clearly visible

On which sequence was the airway best visualized:
- □ SPGR inspiration
- □ SPGR expiration
- □ T2-w PROPELLER
- □ ZTE
- □ Other, namely…

B. Lesion:

Cystic tissue:
- Structure:
  - □ Dominant cyst
  - □ Cluster of multiple uniform cysts
  - □ Not clearly visible
- Average cyst size: mm
- Size of largest cyst: mm
- Content:
  - □ Air-filled
  - □ Fluid-filled
  - □ Air-Fluid levels
  - □ Not clearly visible

On which sequence was the airway best visualized:
- □ SPGR inspiration
- □ SPGR expiration
- □ T2-w PROPELLER
- □ ZTE
- □ Other, namely…

Solid tissue:

	RUL	RML	RLL	LUL	LLL
Extent					
1= ⅓ lobe 2= ⅔ lobe 3=complete lobe					

- Density:
  - □ Homogeneous
  - □ Heterogeneous

On which sequence was the airway best visualized:
- □ SPGR inspiration
- □ SPGR expiration
- □ T2-w PROPELLER
- □ ZTE
- □ Other, namely…

C. Border:

□ Well-defined □ Ill-defined □ Not clearly visible

On which sequence was the airway best visualized:
- □ SPGR inspiration
- □ SPGR expiration
- □ T2-w PROPELLER
- □ ZTE
- □ Other, namely…

D. Vascularization:

- □ Normal pulmonary
- □ Aberrant:
  Number & Size: Origin:

On which sequence was the airway best visualized:
- □ SPGR inspiration
- □ SPGR expiration
- □ T2-w PROPELLER
- □ ZTE
- □ Other, namely…

E. (Surrounding) tissue:

	RUL	RML	RLL	LUL	LLL
Atelectasis					
Low-attenuation					
Hyperinflation					
1= ⅓ lobe 2= ⅔ lobe 3=complete lobe					

□ Mass effect
□ Mediastinal shift
□ Mediastinal herniation

On which sequence was atelectasis best visualized:
□ SPGR inspiration
□ SPGR expiration
□ T2-w PROPELLER
□ ZTE
□ Other, namely…

On which sequence was low-attenuation best visualized:
□ SPGR inspiration
□ SPGR expiration
□ T2-w PROPELLER
□ ZTE
□ Other, namely…

On which sequence was hyperinflation best visualized:
□ SPGR inspiration
□ SPGR expiration
□ T2-w PROPELLER
□ ZTE
□ Other, namely…

F. Conclusion :

□ Post- surgical CLA
□ CPAM
□ BPS
□ Hybrid lesion
□ CLO
□ BA
□ BC

Supplementary materials 3: Qualitative scoring method

Depiction of fissures	4. Unacceptable (invisible interlobar fissure) 5. Fair (blurred interlobar fissure) 6. Good (visible interlobar fissure)
Depiction of intrapulmonary vessels	6. Unacceptable (invisible peripheral pulmonary vessels) 7. Poor (barely visible peripheral pulmonary vessels) 8. Fair (visible peripheral pulmonary vessels) 9. Good (visible peripheral pulmonary vessels with clear margin) 10. Excellent (visible peripheral pulmonary vessels with clear margin)
Depiction of bronchi	6. Unacceptable (indistinguishable lobar bronchial walls) 7. Poor (visible lobar bronchial walls with <10 visible segmental bronchial walls) 8. Fair (visible lobar bronchial walls with >10 visible segmental bronchial walls) 9. Good (visible lobar bronchial walls with >10 visible segmental bronchial walls, with few visible sub/segmental bronchial walls) 10. Excellent (visible sub-subsegmental bronchial walls)
Image noise/artifacts	6. Unacceptable 7. Above average noise/artifacts 8. Average and acceptable 9. Less than average noise/ artifacts 10. Minimum of no noise/artifacts
Overall acceptability	6. Unacceptable 7. Suboptimal 8. Satisfactory 9. Above average 10. Superior

Qualitative scoring method adjusted from Bae et al. (European Radiology 2020)

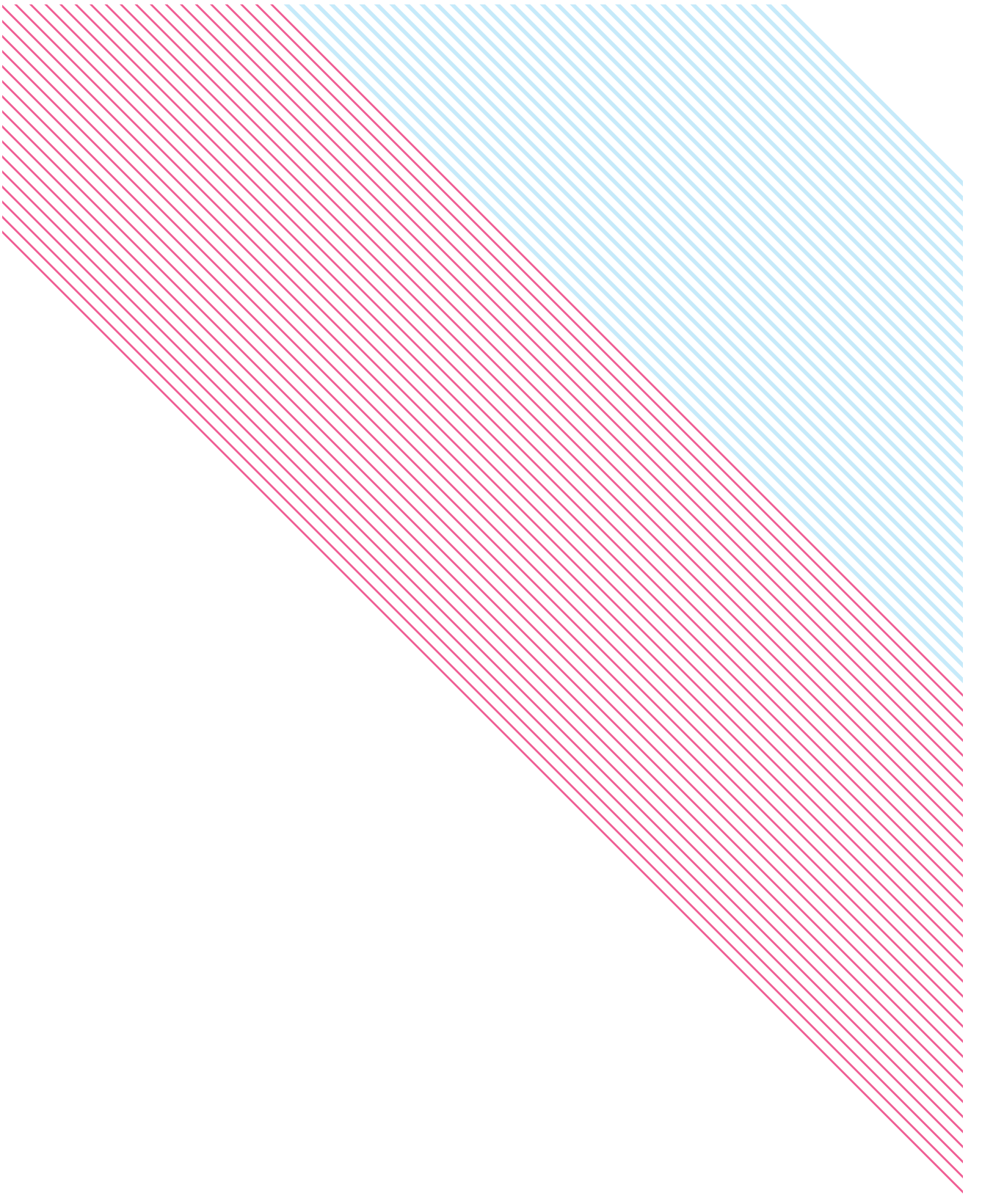

Chapter 11

General discussion

The aim of this thesis is to contribute to the development and validation of Magnetic Resonance Imaging (MRI) protocols to image structure and function of the paediatric respiratory tract, with the ultimate goal to allow these MRI techniques to be applied in clinical practice.

In this final chapter our most important findings will be discussed in light of the current literature. In addition, we will make suggestions for the next steps that are needed before these MRI techniques can be implemented for the diagnosis and management of paediatric respiratory tract diseases.

Attributions to MRI of paediatric respiratory tract diseases

The upper respiratory tract

We succeeded to develop a high resolution static and dynamic MRI protocol to image the upper airways of children with laryngotracheal stenosis (LTS) (in chapter 3,4 and 5 of this thesis). Our current protocol is of sufficient image quality to image the most important respiratory and vocal structures in this patient population. As a result of our study this upper airway protocol has been implemented in clinical practice at our institution and is used for extensive structural and functional imaging of children before and after LTS repair.

For the static upper airways imaging, we make use of conventional T2 weighted (T2-w) and proton density weighted (PD-w) sequences and for dynamic imaging of two (2D) and three-dimensional (3D) dynamic sequences. All these sequences can be implemented in any MRI system of different MRI vendors and could therefore be implemented in other hospitals.

In our studies, we used a dedicated carotid coil, which is not commercially available. However, regular body coils can also be used, as they have shown comparable image quality. Depending on patient's size the current clinical protocol uses two different set-ups: a small flexible coil for neonates and a head-neck-spine coil for older children.

In this thesis, we have shown that this protocol can be used in children and adults from the age of 7 years on. More recently we have also implemented the protocol for children below this age including neonates, who require anaesthesia, showing good image quality. However, the best image quality was achieved in older and more cooperative patients. For our study we had a dedicated researcher available, who could took care of the required extensive preparation and support during the MRI. For successful implementation of the MRI protocol and correct execution of dynamic sequences we advise clinics to organize such dedicated guidance. Future studies should focus on direct comparison with the gold standard, laryngotracheoscopy, in a larger population of patients after LTS.

The lower respiratory tract

We succeeded to develop and test an MRI protocol for the long term follow up of structural and functional lung changes in premature born children, with and without bronchopulmonary dysplasia (BPD) and children with congenital lung abnormalities (CLA) (in chapter 6,7 and 10 of this thesis). Chapter 8 of this thesis shows the preliminary results of the implementation of these sequences to image neonatal lung patients. The studies in this thesis show that this protocol is able to detect clinically relevant abnormalities in paediatric lung diseases. The protocol consists of conventional T2-w and spirometry guided Steady State Free Precession T2/T1-w (SSFP) in- and expiratory sequences, and novel short echo time (ZTE and UTE) sequences to image structural lung changes for the imaging of functional lung changes, such as ventilation and perfusion. In addition, Magnetic Resonance Angiography (MRA) sequences were used to image the vascular component in CLA without the use of contrast enhancement (chapter 10). The conventional sequences (T1/T2-w) are available on MR scanners from multiple vendors and can therefore be implemented at different centres. However, our qualitative analyses (in chapter 6,7,8 and 10 of this thesis) shows that the best diagnostic quality is achieved with the short TE sequences. These sequences are not available on every scanner and are still being provided as research product by several MR brands.

Future studies on our BPD-MRI protocol should focus on the comparison between MRI and Computed Tomography (CT), and the identification of the natural clinical course of BPD on imaging, in both our school-age as well as our neonatal premature population. In addition, our CLA MRI protocol should be validated in a larger cohort of patients.

Steps towards the implementation of MRI for paediatric respiratory tract diseases

Clinical need for imaging

The most important question for new radiological imaging techniques, such as MRI, is what the added value over conventional follow up methods like spirometry, chest radiography or CT is. This thesis contributes to the knowledge on the added value of MRI of the respiratory tract, by showing that MRI is better at reflecting the complexity and heterogeneity of the upper airways in children post LTS repair than conventional follow up methods, namely spirometry and voice tests. And although no direct comparison was made, our findings suggest that MRI provides more quantifiable data than direct videolaryngoscopy. This thesis contributes to the knowledge on the added value of MRI to image the lower respiratory tract by showing that MRI can detect possible clinically relevant lung changes in preterm born patients which are not detected on spirometry. In addition, MRI is as good or better than CT in diagnosing pulmonary and vascular abnormalities and hypo-attenuation related to CLA, without having to use contrast enhancement.

However, for the implementation of MRI in clinical practice, more studies should be conducted to investigate the sensitivity of MRI to track structural changes in long term follow up. In addition, for further implementation of MRI, a cost-benefit analysis has to be performed, where the clinical usefulness of the examination is not only balanced against the burden on the patient. But also the burden on the healthcare system should be taken into account, with MRI having a high demand on healthcare personnel and costs.(1) The average costs of a thoracic MRI are around 300 euros, but with this investment we hope to identify patients in need of treatment and to increase patient' quality adjusted life years (QUALY). Importantly, reduced scan times, improved sequences, a standardized protocol, quantitative analyses methods and better patient compliance will all contribute to this higher value of MRI.(1) A recent introduction of a low-field MR system in the market might fulfil all these requirements by providing a significant improvement in image quality for the respiratory tract and a reduction in costs.(2, 3)

CT versus MRI

There are new imaging modalities on the rising that might make MRI irrelevant. Photon-counting CT decreases the exposure of radiation by 30 to 70% and offers a five-fold increase in imaging resolution.(4, 5) Therefore, MRI would most likely be outweighed with regards to structural imaging. Hence, future research should focus on the added benefit of MRI over CT, namely the possibilities for tissue characterization, dynamic and functional imaging.

Besides, a hybrid monitoring model for the use of MRI could be incorporated, in which CT and MRI are alternated to follow up those changes seen on CT. In our institution for instance, all patients with cystic fibrosis (CF) get a biennial CT scan to look at structural lung changes, and in the year in between an MRI is made. This hybrid model was also applied in our CLA population (in chapter 10 of this thesis), where the time consuming non-contrast MRA sequence was only made in case abnormal vascularization was seen on contrast- enhanced postnatal CT, showing the joint value of the two imaging techniques.

Protocol standardization

A major hurdle for the implementation of MRI in clinical practice is protocol standardization and implementation. Reproducible MRI outcomes depend on many predictable and unpredictable variables related to MRI scanner hardware and software, which differ between MRI vendors and centres. Among the predictable variables lie the different sequences available, small twitches in echo time (TE), repetition time (TR) and flip angle which can be applied within sequences by the MR technician, coil selection and placement, and respiratory triggering. But also less predictable variables may hamper protocol outcome, such as updates to the MRI system and adherence to protocols.(6, 7)

A recent study in children with CF has shown the ability to implement standardized MRI protocols at multiple centres with scanners from multiple vendors. In this study they make use of central training, standard operating procedures, a standard protocol, continuous supervision and a central MRI analyses centre.(8) Though this was done within an already existing trial network with over 10 years' experience in thoracic MRI, of which validation in a broader network will likely be more challenging. We are currently conducting a study that aims to standardize and implement a multivendor- multicentre MRI protocol to image Ventilation, Inflammation, Perfusion and Structure (VIPS)-changes in CF lung disease.(6) The short TE sequences used in our studies are part of this protocol. Therefore, once validated in the VIPS study, our protocol could be of great importance for MR imaging of a variety of paediatric lung diseases and implementation in clinical practice is to be expected.

Protocol refinement

To increase clinical implementation of MRI, it would be important to reduce the burden on the patient and health care professionals, and to increase availability of the scanners. For instance, if MRI protocols would become shorter, this would significantly improve patient's compliance, especially in young children, and simultaneously will increase scanner availability. The same advantage is achieved by proper training and coaching of children. As a result, increasing image quality and thereby the chance of having a scan of sufficient diagnostic quality could become a clinical reality. This can be done by increasing the resolution (and thereby making it easier to identify lung structures and pathology) and by decreasing the chance of artefacts. Technical advances to increase image quality are the development of superior hardware and the broad implication of novel short-echo time sequences, such as UTE and ZTE. The latter having the additional benefit of being silent and thereby decreasing the burden on children and increasing the likelihood of a successful MR examination. Protocol refinements that decrease the chance of artefacts are mostly post-processing tools, such as repeated k-space sampling, making it possible to eliminate those images with artefacts due to patient movement during reconstruction.(9) More recently, deep learning enhancing filters have been applied to improve image quality, by reducing noise and artifacts.(10) In addition, respiratory gating for the paediatric population could be improved by increasing the sensitivity of self-gating sequences or the development of a size appropriate respiratory belt.(11) On the field of tissue characterization, further development of Positron Emission Tomography (PET)-MRI will likely further improve diagnostic quality of MRI.(12, 13)

Image analysis

Last decade has clearly seen a shift from qualitative to quantitative radiological imaging, where post-processing tools for the extraction of quantitative biomarkers have been developed and validated in several studies.(14) For instance, scoring methods for CT have been developed, like the CF-CT scoring system and the grid based scoring systems for CF

and BPD.(15-17) In addition, scoring methods have been developed to asses airway-artery ratios for the assessment of bronchiectasis in patients.(18) Besides its use in clinical studies, these scoring methods are currently used in clinical practice in the follow up of CF and BPD. However, these scoring methods are very time consuming: up to half an hour per patient for the grid based scoring system and up to a week per patient for the airway-artery ratios. This has led to the development of automatic artificial intelligence (AI) based analyses for CT, which is currently underway.(19-21) Post-processing tools for chest-MRI are at an early stage of development. As matter of fact there is no commercially available software for chest-MRI, with most of the publications using in-house developed solutions. Also, in this thesis we have adapted CT software to be used for quantitative scoring of MRIs. We used manual area measurements on the upper airway (in chapter 3, 4 and 5 of this thesis) as well as grid-based scoring of the lung (in chapter 6,8 and 10 of this thesis). The latter being even more time consuming than for CT, because the scoring had to be conducted on multiple sequences included in the MRI protocol, resulting in long scoring sessions up to an hour per patient. It is of outmost importance to develop more sophisticated MRI analyses tools, possibly fully automated, to increase clinical utility of chest-MRI. The main challenge remains the paucity of large dataset of chest-MRI scans of sufficient image quality and from a standardized protocol. Therefore, a next step for the development of automatic MRI analyses tools would be protocol standardization to increase clinical implementation and consequently the creation of a large dataset.

How to make MRI child friendly

Our studies show a high success rate of the MRIs up to 97-100%, without the use of anaesthesia. Important downsides to the use of anaesthesia are the side effects of the agents used, which include negative effects on brain development, increased tendency to atelectasis in the dorsal parts of the lungs mimicking pathology, inability to perform breathing manoeuvres, higher costs and fear related to the anaesthetic procedure (intravenous access).(22, 23) All our studies were conducted with the same researcher present at the MRI preparation phase and during the MRI scan. There was enough time for extensive preparation, such as visiting a mock MRI. In addition, a child friendly environment was created by offering the parents to stay with their child during the MRI scan and asking study participants to bring their favourite music to comfort them during the MRI. In our neonatal study, we successfully used the feed and swaddle technique, and offered a pacifier and sucrose to comfort the neonate during the MRI so that the use of sedation could be avoided (in chapter 8 of this thesis). And again, during these MRI scans, a researcher was present to safeguard the patients and to comfort them in between sequences if necessary. At our institution, there is an MRI compatible incubator available to further minimize the burden of the procedure on the neonate, but this is only used in patients that are in need of temperature support, which was not the case for our study participants. Multiple studies have reported on the positive effect of extensive patient preparation, such as mock MRI

visits and a patient and family centred approach of the MRI, and distraction via audio-visual systems on the amount of sedation used during paediatric MRI.(22-25) As well as the positive effect of comforting neonatal patients during MRI investigations with the feed and swaddle method.(22, 23)

However, in clinical practice the MRIs are often made by multiple MRI technicians, who are more focussed on operating the MRI system than on comforting the patient. At our institution, we already have a lung function technician available for patient preparation and coaching with relation to the spirometry manoeuvres during the MRI. We would however recommend hiring a dedicated MRI research nurse to create a patient- and family-centred experience during the MRI scan, making children and parents at ease and ensuring correct execution of the MRI protocols.(23) An MRI research nurse will most likely also be cost-effective by enhancing image quality and reducing scan time. The development of shorter and silent sequences, such as ZTE, will also aid in making MRI more child friendly.

An age group not included in our research, most challenging for MRI without the use of sedation, are patients between 6 months and 6 years of age. In this age group a patient tailored decision should be made on whether to undergo the MRI, based on patient risk factors, compliance and need for imaging. In addition, attention should be paid to the least possible burden of anaesthesia. For instance, at our institution we are currently testing a moderate sedation protocol during MRI scan using light sedation via Fentanyl nasal spray, showing promising results and good success rate of the examinations.

Teach the doctor

A recent study among newly graduated American paediatric radiologists showed 70% not feeling confident about setting up MR sequences.(26) The training of radiological residents is mostly focussed on the interpretation of imaging results, but limited attention is paid to the technical aspects, especially of the most complex techniques, such as MRI. Not to mention other medical specialists, such as pulmonologists and neonatologists who work with MRI in daily practice, but have even less knowledge on its interpretation and technical aspects. For MRI to be implemented in clinical practice, these knowledge gaps have to be bridged by adding radiology to standard clinical training for medical specialists. Clinicians have to comprehend some technical aspects of MRI to realize the added value of MRI for paediatric respiratory tract diseases but also of its challenges, which will help its broader use in clinical practice.

Conclusion

This thesis has contributed to the development and implementation of MRI for the imaging of the paediatric upper and lower respiratory tract. Our findings show that MRI is well

suitable to image changes in the anatomy and function after complex airway stenosis. In addition, we show that MRI can be used for the follow up of structural and functional lung changes in a variety of lower respiratory tract diseases, such as BPD and CLA. Findings in this thesis can be used to set up future studies on the long term follow up of respiratory tract diseases, as well as the implementation of MRI for the neonatal population.

References

1. Pipe JG. High-Value MRI. J Magn Reson Imaging. 2019;49(7):e12-e3.
2. Campbell-Washburn AE, Ramasawmy R, Restivo MC, Bhattacharya I, Basar B, Herzka DA, et al. Opportunities in Interventional and Diagnostic Imaging by Using High-Performance Low-Field-Strength MRI. Radiology. 2019;293(2):384-93.
3. Campbell-Washburn AE, Suffredini AF, Chen MY. High-Performance 0.55-T Lung MRI in Patient with COVID-19 Infection. Radiology. 2021;299(2):E246-E7.
4. Willemink MJ, Persson M, Pourmorteza A, Pelc NJ, Fleischmann D. Photon-counting CT: Technical Principles and Clinical Prospects. Radiology. 2018;289(2):293-312.
5. Tagliati C, Lanza C, Pieroni G, Amici L, Carotti M, Giuseppetti GM, et al. Ultra-low-dose chest CT in adult patients with cystic fibrosis using a third-generation dual-source CT scanner. Radiol Med. 2021;126(4):544-52.
6. Tiddens HA, Stick SM, Wild JM, Ciet P, Parker GJ, Koch A, et al. Respiratory tract exacerbations revisited: ventilation, inflammation, perfusion, and structure (VIPS) monitoring to redefine treatment. Pediatr Pulmonol. 2015;50 Suppl 40:S57-65.
7. Biederer J, Beer M, Hirsch W, Wild J, Fabel M, Puderbach M, et al. MRI of the lung (2/3). Why … when … how? Insights Imaging. 2012;3(4):355-71.
8. Wielpütz MO, von Stackelberg O, Stahl M, Jobst BJ, Eichinger M, Puderbach MU, et al. Multicentre standardisation of chest MRI as radiation-free outcome measure of lung disease in young children with cystic fibrosis. J Cyst Fibros. 2018;17(4):518-27.
9. Hahn AD, Higano NS, Walkup LL, Thomen RP, Cao X, Merhar SL, et al. Pulmonary MRI of neonates in the intensive care unit using 3D ultrashort echo time and a small footprint MRI system. J Magn Reson Imaging. 2017;45(2):463-71.
10. Li Y, Wang Y, Qi H, Hu Z, Chen Z, Yang R, et al. Deep learning-enhanced T(1) mapping with spatial-temporal and physical constraint. Magn Reson Med. 2021;86(3):1647-61.
11. Higano NS, Hahn AD, Tkach JA, Cao X, Walkup LL, Thomen RP, et al. Retrospective respiratory self-gating and removal of bulk motion in pulmonary UTE MRI of neonates and adults. Magn Reson Med. 2017;77(3):1284-95.
12. Gatidis S, Bender B, Reimold M, Schafer JF. PET/MRI in children. Eur J Radiol. 2017;94:A64-A70.
13. Lillington J, Brusaferri L, Kläser K, Shmueli K, Neji R, Hutton BF, et al. PET/MRI attenuation estimation in the lung: A review of past, present, and potential techniques. Med Phys. 2020;47(2):790-811.
14. Tiddens H, Kuo W, van Straten M, Ciet P. Paediatric lung imaging: the times they are a-changin'. Eur Respir Rev. 2018;27(147).
15. Rosenow T, Oudraad MC, Murray CP, Turkovic L, Kuo W, de Bruijne M, et al. PRAGMA-CF. A Quantitative Structural Lung Disease Computed Tomography Outcome in Young Children with Cystic Fibrosis. Am J Respir Crit Care Med. 2015;191(10):1158-65.

16. Caudri D, Zitter D, Bronsveld I, Tiddens H. Is sweat chloride predictive of severity of cystic fibrosis lung disease assessed by chest computed tomography? Pediatr Pulmonol. 2017;52(9):1135-41.
17. van Mastrigt E, Logie K, Ciet P, Reiss IK, Duijts L, Pijnenburg MW, et al. Lung CT imaging in patients with bronchopulmonary dysplasia: A systematic review. Pediatr Pulmonol. 2016;51(9):975-86.
18. Kuo W, Andrinopoulou ER, Perez-Rovira A, Ozturk H, de Bruijne M, Tiddens HA. Objective airway artery dimensions compared to CT scoring methods assessing structural cystic fibrosis lung disease. J Cyst Fibros. 2017;16(1):116-23.
19. Perez-Rovira A, Kuo W, Petersen J, Tiddens HA, de Bruijne M. Automatic airway-artery analysis on lung CT to quantify airway wall thickening and bronchiectasis. Med Phys. 2016;43(10):5736.
20. Garcia-Uceda A, Selvan R, Saghir Z, Tiddens H, de Bruijne M. Automatic airway segmentation from computed tomography using robust and efficient 3-D convolutional neural networks. Sci Rep. 2021;11(1):16001.
21. Dournes G, Hall CS, Willmering MM, Brody AS, Macey J, Bui S, et al. Artificial intelligence in CT for quantifying lung changes in the era of CFTR modulators. Eur Respir J. 2021.
22. Edwards AD, Arthurs OJ. Paediatric MRI under sedation: is it necessary? What is the evidence for the alternatives? Pediatr Radiol. 2011;41(11):1353-64.
23. Mastro KA, Flynn L, Preuster C, Summers-Gibson L, Stein MH. The Effects of Anesthesia on the Pediatric Developing Brain: Strategies to Reduce Anesthesia Use in Pediatric MRI and Nursing's Role in Driving Patient Safety. J Perianesth Nurs. 2019;34(5):900-10.
24. Lemaire C, Moran GR, Swan H. Impact of audio/visual systems on pediatric sedation in magnetic resonance imaging. J Magn Reson Imaging. 2009;30(3):649-55.
25. Harned RK, 2nd, Strain JD. MRI-compatible audio/visual system: impact on pediatric sedation. Pediatr Radiol. 2001;31(4):247-50.
26. Reid JR, Delgado J, Hailu TA, Dayneka JS, Back SJ, Gokli A. Pediatric magnetic resonance imaging training versus job-readiness: using education research tools to re-align. Pediatr Radiol. 2021;51(9):1732-7.

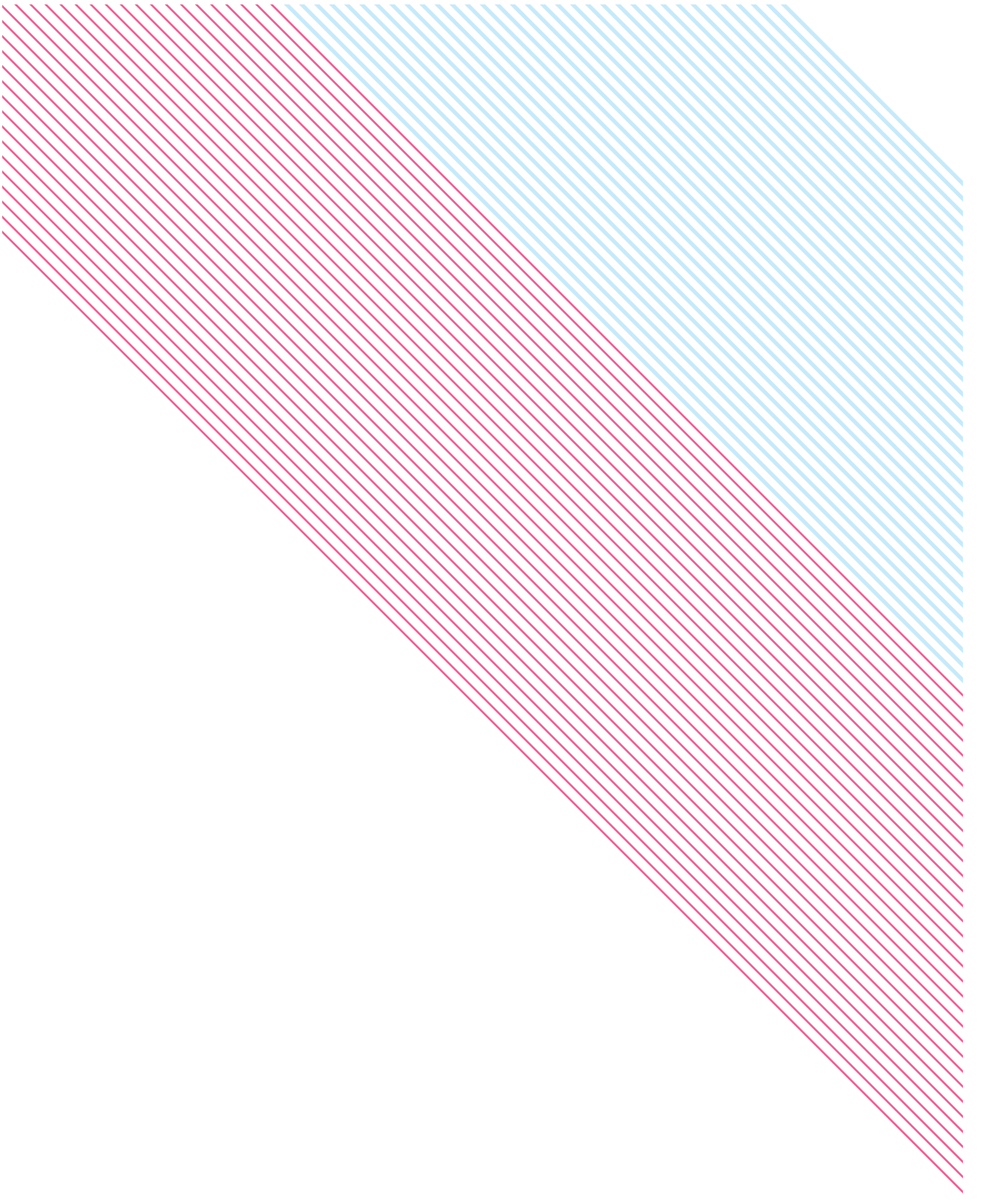

Appendices

Summary

This thesis focuses on Magnetic Resonance Imaging (MRI) of the paediatric respiratory tract. In **chapter 1** an introduction is given to the paediatric respiratory tract which is divided into the upper respiratory tract (part 1 of this thesis), in which we discuss our research on laryngotracheal stenosis (LTS), and the lower respiratory tract (part 2 of this thesis). The diseases discussed in the latter part are bronchopulmonary dysplasia (BPD) and congenital lung abnormalities (CLA). We discuss the methods that are currently used for the follow up of paediatric respiratory tract diseases and explain why a safe imaging method is needed to visualize structure and function in these patients. Next, the opportunities and challenges of MRI for the follow up of paediatric respiratory tract diseases are explained and the aims of this thesis are introduced.

Part 1 The upper respiratory tract

Chapter 2 describes a systematic literature research done about MRI of the paediatric upper respiratory tract. We describe that although MRI has hardly been used to visualize the paediatric larynx, studies show its potential as an imaging modality relatively insensitive to motion artefacts (due to limited movement of the larynx during respiration), with good imaging quality and excellent tissue characterisation. Furthermore, we describe that MRI has the possibility of dynamic imaging of the vocal cords.

In **chapter 3 and 4** the results from the ''Magnetic resonance imaging of the upper airways in children and young adults'' (MUSIC) study are presented. In this study, we have developed an MRI protocol to image the upper respiratory tract after LTS repair. We show that MRI is able to visualize important anatomical changes in this patient population, such as vocal cord thickening, displacement of autologous cartilage grafts placed during surgical repair and the frequent presence of tracheal deformations at previous site of tracheostomy. We also show that our MRI findings correlate to spirometry outcomes. In addition, using the dynamic sequences in our protocol, we were able to detect impaired movement of the vocal cords, which was present in the majority of this population and which was correlated to poor voice outcome and low voice related quality of life.

In **chapter 5,** we describe how we used a Computational Fluid Dynamic (CFD) model to calculate pressure and resistance patterns in the complex upper airways after LTS repair, and show that digital surgery can be performed to predict the outcome of further surgery helping preoperative planning.

Part 2 The lower respiratory tract

In **chapter 6,7 and 8** we describe the development of a thoracic MRI protocol to image structure and function in paediatric lower respiratory tract diseases. **Chapter 6** describes our findings in preterm born children with and without BPD at school age. MRI allowed us to identify the most common BPD-related abnormalities, being hypo intense regions, hyper intense regions and bronchopathy. We found that children with BPD have more lung abnormalities on MRI compared to children without BPD, and that these abnormalities were associated with lower spirometry outcomes. Importantly, we also observed lung abnormalities in preterm children without BPD. In addition, we describe our exploratory analyses using Fourier Decomposition (FD) to image ventilation and perfusion defects in this population. In **chapter 7,** we describe further improvements of the MRI protocol. We tested sequences with different echo times (TE) to identify the best sequence to visualize the paediatric lower respiratory tract. The lower respiratory tract was best visualized with the navigator trigged ZTE (ZTE vnav) sequence. This sequence showed the best signal-to-noise (SNR) and contrast-to-noise (CNR) ratios. A downside to the ZTE vnav sequence is its sensitivity to irregular breathing patterns. The UTE sequence was scored second best on the qualitative analyses, but also this sequence has an important downside which is the need for a respiratory belt that currently does not fit in the youngest patients.

Chapter 8 is a report on the current status of the development of a chest MRI protocol to image structure and function in neonatal lung patients. We present a preliminary report on the successful implementation of MRI in two neonatal patients. The images obtained were free from movement artefacts, without the use of sedation, by using the feed and swaddle method. In addition, we were able to identify relevant lung changes, with an isotropic resolution up to 1.0x1.0x1.0 mm^3.

In **chapter 9 and 10,** we describe our findings on the imaging of CLA. **Chapter 9** describes a literature research into the reporting of structural lung changes on imaging of CLA. We conclude that imaging findings are broad and have variable nomenclature. Therefore, we propose a structured report for the assessment of CLA. **Chapter 10** describes the development of a chest MRI protocol for the long term follow up of CLA and its implementation in a cohort of school age CLA patients. We show that we are able to identify all CLA related structures including vascularization without the use of contrast- enhancement. By comparing school age MRI to postnatal CT in a cohort of non-operated CLA patients, we show that the relative size of the CLA lesion remains stable, and the relative size of the lesion associated parenchymal abnormalities decreases. However, we also found that the radiological appearance of the CLA changed in 41% of the patients. This change in appearance is caused by actual changes in the CLA, growth of the patient and by the comparison of different imaging modality. Further research is needed to validate these results.

In **chapter 11** the findings of these studies are discussed in light of current literature. We conclude that the studies in this thesis show the ability of MRI to image diseases of the paediatric respiratory tract. This thesis can be used for the setup of future research into the validation of our findings as well as further development of MRI for the neonatal population.

Nederlandse samenvatting

Het onderwerp van dit proefschrift is Magnetic Resonance Imaging (MRI) van het ademhalingsstelsel bij kinderen. In **hoofdstuk 1** wordt een inleiding gegeven over het ademhalingsstelsel bij kinderen, die is onderverdeeld in de bovenste luchtwegen (deel 1 van dit proefschrift), waarin we ons onderzoek naar laryngotracheale stenose (LTS) bespreken, en de onderste luchtwegen (deel 2 van dit proefschrift). De ziekten die in het tweede deel worden besproken zijn bronchopulmonale dysplasie (BPD) en congenitale longafwijkingen (CLA). We bespreken de huidige follow up methoden van aandoeningen aan het ademhalingsstelsel bij kinderen en leggen uit waarom een veilige beeldvormingsmethode nodig is om de structuur en functie bij deze patiënten in beeld te brengen. Vervolgens worden de mogelijkheden en uitdagingen van MRI voor de follow up van aandoeningen aan het ademhalingsstelsels bij kinderen toegelicht en worden de doelstellingen van dit proefschrift geïntroduceerd.

Deel 1 De bovenste luchtwegen

In **hoofdstuk 2** wordt een systematisch literatuuronderzoek beschreven dat gedaan is naar MRI van de bovenste luchtwegen bij kinderen. We beschrijven dat, hoewel MRI nog nauwelijks is gebruikt om de larynx van kinderen in beeld te brengen, studies de potentie ervan aantonen als een beeldvormingsmodaliteit die relatief ongevoelig is voor bewegingsartefacten (als gevolg van de beperkte beweging van de larynx tijdens de ademhaling), met een goede beeldkwaliteit en uitstekende weefselkarakterisering. Verder beschrijven we dat MRI de mogelijkheid biedt tot dynamische beeldvorming van de stembanden.

In **hoofdstuk 3 en 4** worden de resultaten gepresenteerd van de ''Magnetic resonance imaging of the upper airways in children and young adults'' (MUSIC) studie. In deze studie hebben wij een MRI protocol ontwikkeld om de bovenste luchtwegen na LTS chirurgie in beeld te brengen. Wij tonen aan dat MRI in staat is om belangrijke anatomische veranderingen in deze patiëntenpopulatie in beeld te brengen, zoals stembandverdikking, verplaatsing van autologe kraakbeentransplantaten geplaatst tijdens de chirurgische reparatie en de frequente aanwezigheid van tracheale deformaties op de plaats van de tracheacanule. Wij tonen ook aan dat onze MRI-bevindingen correleren met spirometrie-uitkomsten. Bovendien waren we in staat om, met behulp van dynamische sequenties in ons protocol, verminderde bewegelijkheid van de stembanden te detecteren, wat aanwezig was in de meerderheid van deze populatie en die gecorreleerd was met een slechte uitslag op de stemtest en een lagere stemgerelateerde kwaliteit van leven.

In **hoofdstuk 5** beschrijven we hoe we een Computational Fluid Dynamic (CFD) model hebben gebruikt om druk- en weerstandspatronen te berekenen in de complexe bovenste

luchtwegen na LTS reparatie, en laten we zien dat digitale chirurgie kan worden uitgevoerd om de uitkomst van verdere chirurgie te voorspellen, wat kan helpen bij de preoperatieve planning.

Deel 2 De onderste luchtwegen

In **hoofdstuk 6,7 en 8** beschrijven we de ontwikkeling van een thorax MRI protocol om structuur en functie in beeld te brengen bij aandoeningen van de onderste luchtwegen bij kinderen. **Hoofdstuk 6** beschrijft onze bevindingen bij prematuur geboren kinderen met en zonder BPD op de schoolleeftijd. MRI stelde ons in staat om de meest voorkomende BPD-gerelateerde afwijkingen te identificeren, zijnde hypo intense regio's, hyper intense regio's en bronchopathie. Wij zagen dat kinderen met BPD meer longafwijkingen hebben op MRI in vergelijking met kinderen zonder BPD, en dat deze afwijkingen geassocieerd waren met lagere spirometrie uitkomsten. Belangrijk is dat we ook longafwijkingen hebben waargenomen bij premature kinderen zonder BPD. Daarnaast beschrijven we onze verkennende analyses met behulp van Fourier Decompositie (FD) om ventilatie- en perfusieafwijkingen in deze populatie in beeld te brengen. In **hoofdstuk 7** beschrijven we verdere verbeteringen van het MRI protocol. We hebben sequenties met verschillende echotijden (TE) getest om de beste sequentie te identificeren voor het visualiseren van de onderste luchtwegen bij kinderen. De onderste luchtwegen werden het best gevisualiseerd met de navigator triggered ZTE (ZTE vnav) sequentie. Deze sequentie vertoonde het beste signal-to-noise ratio (SNR) en contrast-to-noise ratio (CNR). Een nadeel van de ZTE vnav sequentie is de gevoeligheid voor een onregelmatig ademhalingspatroon. De UTE sequentie kwam als één na beste uit de kwalitatieve analyses, maar ook deze sequentie heeft een belangrijk nadeel, namelijk de noodzaak van een ademhalingsgordel die momenteel niet past bij de jongste patiënten.

In **hoofdstuk 8** bespreken wij de huidige status van de ontwikkeling van een thorax MRI protocol om structuur en functie in neonatale longpatiënten in beeld te brengen. Dit hoofdstuk is een tussentijds verslag van de succesvolle toepassing van MRI bij twee neonatale patiënten. De MRI beelden waren vrij van bewegingsartefacten, zonder gebruik van sedatie, door gebruik te maken van de "feed and swaddle" methode. Bovendien waren we in staat om relevante longafwijkingen te identificeren, met een isotrope resolutie tot 1.0x1.0x1.0 mm^3.

In **hoofdstuk 9 en 10** beschrijven wij onze bevindingen met betrekking tot de beeldvorming van CLA. **Hoofdstuk 9** beschrijft een systematisch literatuur onderzoek naar de rapportage van structurele longveranderingen op beeldvorming van CLA. Wij concluderen dat bevindingen op beeldvorming divers zijn en dat variabele nomenclatuur wordt gebruikt. Daarom stellen wij voor om een gestructureerd rapport te gebruiken bij de radiologische beoordeling van CLA. **Hoofdstuk 10** beschrijft de ontwikkeling van een thorax MRI protocol

voor de lange termijn follow-up van CLA en de implementatie hiervan in een cohort van CLA patiënten op de schoolleeftijd. We laten zien dat we in staat zijn om alle CLA gerelateerde structuren inclusief vascularisatie te identificeren zonder gebruik te maken van contrast. Door MRI op schoolleeftijd te vergelijken met postnatale CT in een cohort van niet-geopereerde CLA-patiënten, tonen we aan dat de relatieve grootte van de CLA-laesie stabiel blijft, en dat de relatieve grootte van de laesie geassocieerde parenchymale afwijkingen afneemt. Wij vonden echter ook dat de radiologische verschijning van de CLA veranderde bij 41% van de patiënten. Deze verandering in verschijningsvorm wordt veroorzaakt door feitelijke veranderingen in de CLA, groei van de patiënt en door dat wij verschillende beeldvormingsmodaliteiten hebben vergeleken. Verder onderzoek is nodig om deze resultaten te valideren.

In **hoofdstuk 11** worden de bevindingen van deze studies besproken in het licht van de huidige literatuur. We concluderen dat de studies in dit proefschrift het vermogen van MRI aantonen om ziekten aan het ademhalingsstelsel bij kinderen in beeld te brengen. Dit proefschrift kan worden gebruikt voor het opzetten van toekomstig onderzoek naar de validatie van onze bevindingen, alsmede voor de verdere ontwikkeling van MRI voor de neonatale populatie.

List of abbreviations

2D	Two dimensional
3D	Three dimensional
AAD	Anatomical architecture distortion
ADC	Apparent diffusion coefficient
AI	Artificial intelligence
AP	Anterior- posterior
ATS	American Thoracic Society
BA	Bronchial atresia
BC	Bronchogenic cyst
BH	Breath hold
BM	Blood- muscle
BPD	Bronchopulmonary dysplasia
BPS	Bronchopulmonary sequestration
BW	Bandwidth
CF	Cystic fibrosis
CFD	Computational Fluid Dynamic
CI	Confidence interval
CLA	Congenital Lung Abnormality
CLAQ	Congenital Lung Abnormalities Quantification on CT
CLAM	Congenital Lung Abnormalities quantification on MRI
CLE	Congenital lobar emphysema
CLO	Congenital Lobar Overinflation
CM	Cotton Myer
CNR	Contrast to noise ratio
CPAM	Congenital pulmonary airway malformation
CPAP	Continuous positive airway pressure
CT	Computed Tomography
CTR	Cricotracheal reconstruction
DSI	Dysphonia Severity Index
Ds-LTR	Double stage laryngotracheal reconstruction
DWI	Diffusion Weighted Imaging
EDI	Expiratory Disproportion Index
ELS	Extalobar sequestration
EMA	European Medicines Agency
ERS	European Respiratory Society
ETL	Echo Train Length
FB	Free breathing

FD	Fourier Decomposition
FEF_{25-75}	Forced Expiratory Flow at 25-75% of expiration
FEV_1	Forced expiratory volume in 1 sec
FIV_1	Forced inspiratory volume in 1 sec
FOV	Field of View
FRC	Functional residual capacity
FVC	Forced Vital Capacity
FVC in	Forced vital inspiratory capacity
FS	Fat suppressed
FSE	Fast spin echo
GA	Gestational age
GLI	Global Lung function Initiative
HU	Hounsfield units
ICC	Intraclass correlation coefficient
ILS	Intralobar sequestration
Insp	Inspiration
IQR	Interquartile range
LB	Lung parenchyma- blood
LIR	Low intensity region
LM	Lung parenchyma - muscle
LTS	Laryngotracheal stenosis
MEF	Mean Expiratory Flow
MERGE	bronchopulMonary rottErdam mRi morpholoGy scorE
MPT	Maximum phonation time
MRA	Magnetic resonance angiography
MRI	Magnetic Resonance Imaging
MUSIC	Magnetic resonance imaging of the upper airways in children and young adults
NEX	Number of excitations
NHI	National Health Institute
NICU	Neonatal intensive care unit
NIPPV	Nasal intermittent positive pressure ventilation
OSAS	Obstructive sleep apnoea syndrome
Pa	Pascal
PCC	Paediatric Chest Centre
PDA	Patent ductus arteriosus
PD-w	Proton density weighted
PEF	Peak Expiratory Flow
PET- MRI	Positron Emission Tomography- Magnetic resonance imaging
PI	Principal investigator
PMA	Post menstrual age

PMR	Psychomotor retardation
PPB	Pleuropulmonary blastoma
PRISMA	Preferred Reporting Items for Systematic Reviews and Meta- Analysis
PROPELLER	Periodically Overlapping ParalLEL Lines with Enhanced Reconstruction
(p)VHI	(pediatric) Voice Handicap Index
QUALY	Quality adjusted life year
RF	Radio frequency
RGE	Rapid gradient echo
ROI	Region of interest
RR	Respiratory rate
RV	Residual volume
SIMPLE	Semi-Implicit Method for Pressure Linked Equations
SE	Spin echo
SNR	Signal to noise ratio
SPGR	Spoiled Gradient Echo Sequence
SI	Signal intensity
SS	Single stage laryngotracheal reconstruction
SSFSE	Single Shot Fast Spin Echo
SSFP	Steady State Free Precession
SST	Shear Stress Transport
STD	Standard deviation
T	Tesla
T1-w	T1 weighted
T2-w	T2 weighted
TD	Tracheal deformation
TE	Echo time
TR	Repetition time
TRICKS	Time Resolved Imaging of Contrast Kinetics
UTE	Ultra short echo time
VAS	Visual analogue scale
VC	Vocal cord
VIPS	Ventilation, inflammation, perfusion and structure
VINyL	Ventilation, Inflammation, perfusion and structure in Neonatal Lung patients
Vmax	Maximal vital capacity
ZTE	Zero echo time

List of publications

This thesis

1. **Magnetic Resonance Imaging of the larynx in the paediatric population: a systematic review**
   Bernadette BLJ Elders, Sergei M Hermelijn, Harm AWM Tiddens, Bas Pullens, Piotr A Wielopolski, Pierluigi Ciet
   Pediatric Pulmonology 2019;54(4):478-486
2. **Magnetic resonance imaging of the paediatric upper airways: the MUSIC study**
   Bernadette BLJ Elders, Pierluigi Ciet, Harm AWM Tiddens, Wytse B van den Bosch, Piotr A Wielopolski, Bas Pullens
   Thorax 2021;76:44-51
3. **Structure and function of the vocal cords after airway reconstruction on magnetic resonance imaging**
   Bernadette BLJ Elders, Marieke M Hakkesteegt, Pierluigi Ciet, Harm AWM Tiddens, Piotr A Wielopolski, Bas Pullens
   Laryngoscope 2021;131:E2402-E2408
4. **Computational Fluid Dynamic Modelling of airways after laryngotracheal stenosis**
   Bernadette BLJ Elders, Hosein Sadafi, Joana Costa, Jan De Backer, Harm AWM Tiddens, Piotr A Wielopolski, Pierluigi Ciet, Bas Pullens
   Submitted
5. **Lung structure and function on MRI in preterm born school children with and without BPD: a feasibility study**
   Bernadette BLJ Elders, Harm AWM Tiddens, Mariëlle WH Pijnenburg, Irwin KM Reiss, Piotr A Wielopolski, Pierluigi Ciet
   Submitted
6. **Lung parenchyma and structure visualization in pediatric chest-MRI: a comparison of different short and ultra-short TE protocols**
   Dorottya Papp, Bernadette BLJ Elders, Piotr A Wielopolski, Gyula Kotek, Mika Vogel, Harm AWM Tiddens, Pierluigi Ciet, Juan Hernandez-Tamames
   Submitted
7. **A clinical guideline for structured assessment of CT-imaging in Congenital Lung Abnormalities.**
   Sergei M Hermelijn, Bernadette BLJ Elders, Pierluigi Ciet , René MH Wijnen, Harm AWM Tiddens, J Marco Schnater
   Paediatric Respiratory Review 2021;37:80-88
8. **Congenital Lung Abnormalities on Magnetic resonance imaging: the CLAM study**
   Bernadette BLJ Elders, Casper M Kersten, Sergei M Hermelijn, Piotr A Wielopolski, Harm AWM Tiddens, J Marco Schnater, Pierluigi Ciet
   Submitted

Publications not included in this thesis

1. **Atrioventricular septal defect: From embryonic development to long-term follow-up**
   Emmeline E Calkoen, Mark G Hazekamp, Nico A Blom, Bernadette BLJ Elders, Adri C Gittenbergen – de Groot, Monique C Haak, Margot M Bartelings, Arno A Roest, Monique RM Jongbloed
   International Journal of Cardiology 2016;202:784-95
2. **Increased left ventricular myocardial extracellular volume is associated with longer cardiopulmonary bypass times, biventricular enlargement and reduced exercise intolerance in children after repair of Tetralogy of Fallot**
   Eugenie Reissenkampff, Wietske Luining, Mike Seed, Paweena Chungsomprasong, Cedric Manlhiot, Bernadette BLJ Elders, Brian W McCrindle, Shi-Joon Yoo, Lars Grosse-Wortmann
   Journal of cardiovascular magnetic resonance imaging 2016;18(1):75
3. **Altered ascending aortic wall shear stress in patients with corrected atrioventricular septal defect: a comprehensive cardiovascular magnetic resonance and 4D flow MRI evaluation**
   Bernadette BLJ Elders, Jos Westenberg, Pieter van den Boogaard, Emmeline Calkoen, Nico Blom, Lucia Kroft, Alfred de Roos, Arno A Roest
   Cardiology in the Young 2019;29(5):637-642
4. **The modified history of Tetralogy of Fallot during childhood and adolescence**
   Tamadir F Gazzaz, Bernadette BLJ Elders, Chun-Po Ste Fan, Cedric Manlhiot, Shi-Joon Yoo, Glen van Arsdell, Lars- Grosse Wortmann
   JACC Cardiovascular imaging 2021;14(7):1478-14780
5. **Aspergillus related lung disease in people with cystic fibrosis: Can imaging help us to diagnose disease?**
   Qianting Lv, Bernadette BLJ Elders, Adilia Warris, Daan Caudri, Pierluigi Ciet, Harm A.W.M. Tiddens
   European Respiratory Reviews 2021 Nov 17;30(162):210103

Affiliations of co-authors

Author	Affiliations
De Backer, Jan	Fluidda, NV, Kontich, Belgium
Van den Bosch, Wytse	Department of Paediatric Pulmonology and Allergology, Erasmus MC - Sophia Children's Hospital, University Medical Centre Rotterdam, The Netherlands Department of Radiology and Nuclear Medicine, Erasmus MC, University Medical Centre Rotterdam, The Netherlands
Ciet, Pierluigi	Department of Paediatric Pulmonology and Allergology, Erasmus MC - Sophia Children's Hospital, University Medical Centre Rotterdam, The Netherlands Department of Radiology and Nuclear Medicine, Erasmus MC, University Medical Centre Rotterdam, The Netherlands
Costa, Joana	Fluidda, NV, Kontich, Belgium
Hakkesteegt, Marieke	Department of Otorhinolaryngology, Erasmus MC, University Medical Centre Rotterdam, The Netherlands
Hermelijn, Sergei	Department of Paediatric Surgery, Erasmus MC - Sophia Children's Hospital, University Medical Centre Rotterdam, The Netherlands
Hernandez- Tamames, Juan	Department of Radiology and Nuclear Medicine, Erasmus MC, University Medical Centre Rotterdam, The Netherlands
Kersten, Casper	Department of Paediatric Surgery, Erasmus MC - Sophia Children's Hospital, University Medical Centre Rotterdam, The Netherlands
Kotek, Gyula	Department of Radiology and Nuclear Medicine, Erasmus MC, University Medical Centre Rotterdam, The Netherlands
Kroon, André	Department of Neonatology, Erasmus MC - Sophia Children's Hospital, University Medical Centre Rotterdam, The Netherlands
Papp, Dorottya	Department of Radiology and Nuclear Medicine, Erasmus MC, University Medical Centre Rotterdam, The Netherlands
Pijnenburg, Marielle	Department of Paediatric Pulmonology and Allergology, Erasmus MC - Sophia Children's Hospital, University Medical Centre Rotterdam, The Netherlands
Pullens, Bas	Department of Otorhinolaryngology, Erasmus MC - Sophia Children's Hospital, University Medical Centre Rotterdam, The Netherlands
Reiss, Irwin	Department of Neonatology, Erasmus MC - Sophia Children's Hospital, University Medical Centre Rotterdam, The Netherlands
Sadafi, Hosein	Fluidda, NV, Kontich, Belgium
Schnater, Marco	Department of Paediatric Surgery, Erasmus MC - Sophia Children's Hospital, University Medical Centre Rotterdam, The Netherlands
Tiddens, Harm	Department of Paediatric Pulmonology and Allergology, Erasmus MC - Sophia Children's Hospital, University Medical Centre Rotterdam, The Netherlands
Vogel, Mika	General Electric Healthcare, Waukesha, WI, USA
Wielopolski, Piotr	Department of Radiology and Nuclear Medicine, Erasmus MC, University Medical Centre Rotterdam, The Netherlands
Wijnen, René	Department of Paediatric Surgery, Erasmus MC - Sophia Children's Hospital, University Medical Centre Rotterdam, The Netherlands

PhD portfolio

	Year	Workload
Conferences		
ESPO (Congress of the European Society of Paediatric Otorhinolaryngology), poster presentation	2018	1
Sophia Research Day	2018	0.3
ECR (European Congress of Radiology), poster presentation	2019	1
ERS (European Respiratory Society), poster presentation	2019	1
Paediatric Chest Centre Symposium	2019	0.5
ERC (European Radiology Conference), two oral presentations	2020	1
ESPO (Congress of the European Society of Paediatric Otorhinolaryngology), two oral presentations	2021	1
Courses		
Literature research	2017	0.4
Basic introduction course SPSS	2017	1
Basic course in applied MR techniques (ESMRMB)	2017	0.5
CF-CT course	2017	0.5
PRAGMA-CF course	2017	0.5
Basic course on regulations and organisation for clinical investigations (BROK)	2018	1
Research integrity	2018	0.3
PRAGMA-BPD course	2018	0.5
The European Course in Paediatric Radiology (ECPR) on Chest imaging	2018	0.5
Open Clinica course	2019	0.3
English writing	2019	2
MRI in practice	2019	1
Castor course	2021	0.5
Medical Leadership	2021	1.5
Scientific meetings		
Clinical meeting department of paediatric pulmonology and & allergology and department of radiology and nuclear medicine	2017-2021	5
Research meeting department of paediatric pulmonology & allergology	2017-2021	4
Research meeting Lung Analysis research group	2017-2021	3
Other scientific activities		
TULIPS PhD Curriculum	2018-2020	4
Organizing committee Sophia Research Day 2019, 2020, 2021	2018-2021	2
Sophia Onderzoekers Vertegenwoordiging, board member	2019- 2021	1
Outpatient clinical paediatric pulmonology	2017-2021	3
Peer review for articles for scientific journals	2017-2021	3
Total ECTS		**41.9**

About the author

Bernadette Elders was born on the 1st of March 1991 in Amsterdam and grew up in Hoofddorp. In 2009 she finished her secondary school at the Atheneum College Hageveld in Heemstede. After this she obtained her propaedeutic degree in Law and Business Administration at the Leiden University. In 2010 she started her medical school at the Leiden University Medical Centre. During her medical school she did various clinical internships abroad: at the Kanti Chilren's Hospital in Kathmandu, Nepal and at the Groote Schuur Hospital in Cape Town, South Africa. In addition, she did research at the department of paediatric cardiology at the Leiden University Medical Centre under supervision of dr. Arno Roest and a research internship at the Hospital for Sick Children in Toronto, Canada under supervision of dr. Lars Grosse- Wortmann, both on cardiac MRI. After her graduation from medical school in 2016 she worked as a paediatric resident (ANIOS) at the Juliana Children's Hospital in The Hague.

In 2017 she started the research project described in this thesis at the Erasmus MC- Sophia Children's Hospital under supervision of prof. dr. Harm Tiddens and dr. Pierluigi Ciet.

Besides her research project, Bernadette was a member of the Sophia Onderzoekers Vereniging board and part of the Sophia Research Days Organizing Committee. In 2019 and 2020 she participated in the Skate4AIR Daylight Challenge and Alternatieve Elfstedentocht, with which she raised money for research into Cystic Fibrosis.

Bernadette is currently working as a resident (AIOS) in paediatrics at the Amsterdam University Medical Centre- Emma Kinderziekenhuis.

She lives in Amsterdam together with her partner Gijs, dog Jip and daughter Otte.

Dankwoord

In één van de stellingen van dit proefschrift schrijf ik dat muziek ervoor zorgt dat kinderen een prettigere ervaring hebben in de MRI, waardoor de MRI vaker een succes is. Ik geloof dat muziek dit effect ook op andere vlakken kan hebben: getuige dit proefschrift. Allereerst gaat mijn dank dan ook uit naar de muziek die dit proefschrift mogelijk heeft gemaakt: aan **Bjørn, Benny, Agnetha en Anni-Frid** dat jullie er altijd voor mij waren die uren dat ik naar MRI's heb gestaard, aan **Elton** dat je er was om mij te steunen bij alle tegenslagen en aan **Freddie**, dat je er altijd voor mij was om de hoogtepunten binnen dit promotietraject te vieren.

Daarna uiteraard allereerste hartelijk dank aan **alle studiedeelnemers en hun familie** die vaak vanuit verre uithoeken van het land naar Rotterdam zijn gekomen om deel te nemen aan dit wetenschappelijke onderzoek.

Mijn promotor, **professor dokter Tiddens, beste Harm,** dankjewel dat je in mij geloofd hebt en mij de mogelijkheid hebt geboden om dit promotietraject binnen Lung Analysis te starten. Dank voor jouw begeleiding de afgelopen vier jaar!

Mijn co-promotor, **dr. Ciet**, beste Pier. De start van mijn promotie viel samen met de hectische start van jouw fellowship bij de kinderradiologie. Dit zorgde voor de nodige hindernissen en leidde vaak tot besprekingen laat in de avond in een donkere radiologie verslagruimte. Daarom ben ik extra trots dat wij dit promotietraject tot een succesvol einde hebben gebracht. Dankjewel dat je mij een kijkje hebt gegeven in het werk van een radioloog en mij enkele kneepjes van het vak hebt weten te leren.

Tevens dank aan de overige leden van mijn kleine promotiecommissie, **prof. Dr. Aerts, Prof. dr. Schaefer-Prokop** en **Dr. Merkus**, dank jullie wel voor de beoordeling van mijn proefschrift.

Lieve **Els**, de steun en toeverlaat van Lung Analysis, dankjewel voor alles wat je voor mij gedaan hebt. Dank voor alle motiverend gesprekken, de gezellige koffietjes en voor de vele keren dat jij 'de heren achter de broek aan hebt gezeten'.

Iedereen binnen de Lung Analysis research group, dank jullie wel voor de fijne samenwerking: **Merlijn, Sergei, Casper, Hamed, Jorien, Badies, David, Lisa en Elrozy**. Gracie mile to all of the Italian visitors: **Alice, Valentina, Giuseppe, Giulia and Federico** thank you very much for the nice Italian dinners. And 謝謝 to **Yuxin and Qianting**, for introducing me to hot pot.

Binnen Lung Anaysis in het bijzonder nog een woord gericht aan **Jennifer**, collega en kamergenoot vanaf mijn begintijd in het Sophia, en dan ook nog samen ons grote schaatsavontuur aan gegaan. Dankjewel voor jouw aanstekelijke enthousiasme.

Mariette, dank voor al jouw hulp bij technische moeilijkheden, maar toch met name dank dat jij al die jaren zo'n gezellig kamergenoot bent geweest.

Angelina, wij hebben maar een deel van mijn promotie samengewerkt, maar je was direct een frisse wind in de groep. Dankjewel voor de gezelligheid en voor de vrolijke noot in de groep.

Daarnaast heb ik de afgelopen jaren veel tijd gespendeerd met mijn collega's van de **Sophia Onderzoekers Vereniging**. Zowel het bestuur: Saranda, Renate en Denise, als mijn collega's bij het organiseren van de **Sophia Research Days**: Berthe, Marije, Imke en Lotte. We hebben aardig wat (technische) tegenslagen moeten verduren in tijden van COVID, maar ondanks dat ben ik trots op wat wij gezamenlijk neer hebben gezet, dank jullie wel voor jullie tomeloze inzet en enthousiasme.

Mijn lieve vrienden van het **TULIPS curriculum**, wat heb ik een heerlijke tijd met jullie gehad. Dank dat jullie voor mij een veilige plek zijn geweest om mijn verhaal kwijt te kunnen en om mij te inspireren mijn dromen na te jagen binnen de kindergeneeskunde.

Aan mijn collega's van de **afdeling Kinderlongziekten**: Johan, Hettie, Liesbeth, Daan, Esmé, Monique, Marije en Sanne en de arts-onderzoekers Evelien, Rosalie, Esmee, Antonio, Shelly en Stephanie dank voor de fijne samenwerking en de leerzame tijd. Hierbij in het bijzonder dank aan **Mariëlle**, als hoofd van de afdeling heb jij mij door jouw vriendelijke berichtjes en kaartjes, ook in tijden van persoonlijke hoogtepunten, altijd welkom doen voelen binnen de afdeling. **Irma**, dank voor jouw grote hulp met alle administratieve vraagstukken en alle gezellig kletsmomenten. En natuurlijk mijn collega's van de **kinderlongfunctie**, dank voor al jullie hulp bij mij onderzoek, en in het specifiek voor Darreck, dankjewel voor alle lange maar gezellige avonden samen naast de MRI.

Dr. Pullens, best Bas, dank voor al jouw hulp bij het MUSIC project, voor alles wat je mij geleerd hebt over de luchtweg en met name voor jouw frisse, nuchtere en doortastende houding binnen het onderzoek.

Beste **Marieke**, dankjewel voor al jouw hulp bij het artikel over de stem en voor alles wat jij mij hebt geleerd over de stem.

Piotr, Senior Wielopolski, over the past four years we must have spent hours behind the MRI together. You call me Don Bernadette for a reason, because most of these hours spend behind the MRI meant you raging on about all of the possibilities and me trying to temper your enthusiasm to keep track of the scan time and to protect my brain from the information overload. Thank you for the massive amount of MRI knowledge you have passed on to me.

Dear colleagues from **Fluidda** thank you for your help on the Computational Fluid Dynamic manuscript.

Prof. Dr. Reiss, beste Irwin, dankjewel voor de brainstrom sessies over de BPD projecten en voor jouw inspirerende gesprekken over het onderzoek.

Dr. Schnater, beste Marco, dank voor jouw betrokkenheid bij de CLAM studie.

Lieve collega's uit het **Emma Kinderziekenhuis** en in het bijzonder beste dr. Bosman en beste dr. de Bie, Diederik en Brigitte, dank jullie wel voor het warme welkom in het Amsterdamse en dat jullie mij de kans hebben gegeven om mijn droom na te jagen.

Mijn lieve Fabulous Five vriendinnen: **Thyrza, Liefke, Sophia en Fieke**. Al ruim 15 jaar zijn jullie mijn steun en toeverlaat, dank jullie wel dat jullie er in deze tijd voor mij zijn geweest als luisterend oor. Ik hoop dat we nog samen op de tafel blijven dansen tot wij oud en kreupel zijn.

Cordial Taxi, **Strijders en oud-huisgenoten van de Oude Singel** bedankt voor de mooie avonden en hoognodige afleiding de afgelopen vier jaar.

Mijn vriendinnen uit Canada: **Chris, Inez, Wietske en Mick**. Mijn allereerste kennismaking met wetenschappelijk onderzoek was met jullie in Sickkids in Toronto. Mede door deze mooie tijd ben ik met enthousiasme aan mijn promotieonderzoek begonnen. In het bijzonder lieve **Chris**, ik hoop dat wij nog jaren samen lange wandelingen blijven maken en zullen dromen en plannen voor de toekomst.

Mijn paranimfen **Wytse en Anu**. Wytse: van de (kortdurende) hoogtijden in ons privékantoor met 12 maanden per jaar kerstverlichting tot aan dieptepunten in onze onderzoekstijd. Ik heb van jou geleerd het leven altijd minstens een 9/10 te geven en dat het altijd een goed moment is voor taart. Dank voor jouw steun en dat je het aandurft mijn paranimf te zijn.
En lieve **Anu**: mijn jaarclub-genootje, dispuutsgenoot, huisgenoot, collega en nu ook paranimf. Ik vind het ontzettend bijzonder dat we allebei onze droom om kinderarts te worden waar aan het maken zijn en ben heel blij dat ik dit met jou als goed vriendinnetje aan

mijn zijde heb kunnen doen. We gaan uiteraard regelen dat we later in hetzelfde ziekenhuis komen te werken!

Lieve schoonfamilie, **Wim-Jan, Caroline, Anne en Mats** dank jullie wel voor het warme welkom in de familie. Dank dat jullie er altijd voor ons zijn geweest, welke idiote ideeën Gijs en ik ons ook in ons hoofd haalden, en dat jullie altijd open staan voor een lange duinwandeling in de Panne om mijn hoofd leeg te maken. En ook nog in het bijzonder dank aan Anne voor jouw hulp en creatieve brein bij het ontwerp van dit proefschrift.

Één van mijn favoriete uitspraken uit de Tao Te Ching is ‘’*If you teach your children to achieve, they will never be content. If you teach them contentment, they will naturally achieve everything*’’. Bij deze uitspraak moet ik altijd denken aan mijn eigen opvoeding en de normen en waarden die ik van mijn ouders mee heb gekregen. Lieve **papa en mama,** ik wil jullie dan ook bedanken voor het warme gezin waarin ik op ben gegroeid, de ruimte die mij geboden is om te worden wie ik ben en jullie steun de afgelopen jaren.

Lieve **Daan, Tamieck en kleine Jimme** of het nu vanuit Brussel, Tokyo of Den Haag is, ik ben ontzettend blij dat we zoveel contact hebben en dat we zo’n hechte band hebben. Dank voor de telefonische hotline waarbij ik altijd bij jullie terecht kan.

Lieve **Gijs**, ik ben nog iedere dag zo dankbaar dat ik jou op het Zweedse ijs tegen het lijf ben gelopen. Dankjewel dat jij mijn rots in de branding bent en dat je mij stimuleert het beste uit mijzelf te halen. Ik kijk nu al uit naar ons volgende avontuur.

Jip, dankjewel voor jouw gezelschap op de lange dagen werkend vanuit huis en dat jij altijd een goed excuus was om tijdens lange wandelingen mijn hoofd leeg te maken.

Lieve **Otte**, kleine Otje, dankjewel voor de blijdschap die je ons hebt gebracht. Ik hoop dat je, als je later groot bent, door dit boekje bladert en dan ontzettend trots bent op je mama. En dat je beseft dat, net als dat ik van kinds af aan graag kinderarts wilde worden, je later alles kunt worden waar je van droomt.